OVEREXPLOITATION OF GROUNDWATER AND ITS IMPACT ON QUALITY OF WATER IN WINDER BALOCHISTAN: AN ENVIRONMENTAL GEOPHYSICAL APPROACH

Muhammad Irfan
02-283161-004

A thesis submitted in fulfilment of the

requirements for the award of the degree of

Doctor of Philosophy (Geophysics)

Department of Earth and Environmental Sciences

BAHRIA UNIVERSITY KARACHI CAMPUS

October 2023

Approval for Examination

Scholar's Name: Muhammad Irfan

Registration No: 9904

Programme of Study: Geophysics (Department: Earth and Environmental Sciences).

Thesis Title: "Overexploitation of Groundwater and Its Impact on Quality of Water in Winder Balochistan: An Environmental Geophysical Approach"

It is to certify that the above scholar's thesis has been completed to my satisfaction and, to my belief, its standard is appropriate for submission for examination. I have also conducted plagiarism test of this thesis using HEC prescribed software and found similarity index 17% that is within the permissible limit set by HEC for the PhD degree thesis. I have also found the thesis in a format recognized by the BU for the PhD thesis.

Principal Supervisor

Dr. Salma Hamza
HOD/Associate Professor
Department of Earth & Environmental Sciences

Signature:

Date:

AUTHOR'S DECLARATION

I, Muhammad Irfan hereby state that my Ph.D. thesis titled "Overexploitation of Groundwater and Its Impact On Quality of Water in Winder Balochistan: An Environmental Geophysical Approach" is my own work and has not been submitted previously by me for taking any degree from Bahria University (Karachi Campus) or anywhere else in the country/world. At any time if my statement is found to be incorrect even after my graduation, the University has the right to withdraw/cancel my Ph.D. degree.

Name of Scholar: Muhammad Irfan

Date: 02 August 2023

PLAGIARISM UNDERTAKING

I, solemnly declare that research work presented in the thesis titled "Overexploitation of Groundwater and Its Impact on Quality of Water in Winder Balochistan: An Environmental Geophysical Approach" is solely my research work with no significant contribution from any other person. Small contribution / help wherever taken has been duly acknowledged and that complete thesis has been written by me.

I understand the zero tolerance policy of the HEC and Bahria University towards plagiarism. Therefore, I as an Author of the above titled thesis declare that no portion of my thesis has been plagiarized and any material used as reference is properly referred / cited.

I undertake that if I am found guilty of any formal plagiarism in the above titled thesis even after award of PhD degree, the university reserves the right to withdraw / revoke my PhD degree and that HEC and the University has the right to publish my name on the HEC / University website on which names of scholars are placed who submitted plagiarized thesis.

Scholar / Author's Sign:
Name of the Scholar: Muhammad Irfan

DEDICATION

My teachers, friends, students and family who encourage and support me

ACKNOWLEDGEMENT

Firstly, I am very thankful to Allah Almighty for the completion of my research work. I acknowledge the generous and intellectual support of my supervisor Associate Professor & Head of the Department Earth & Environmental Sciences, Dr. Salma Hamza for her support, motivation and immense knowledge. Her guidance helped us in all the time of research and writing of this thesis.

I would also like to acknowledge and give my warmest thanks to my Co-Supervisor Dr. Anwar Qadir who made this work possible through his guidance and advice and carried me through all the stages of writing my research paper and thesis. I would also like to thank Principal BSMAS Dr. Asif Inam, for his brilliant comments and suggestions. I sincerely appreciate the guidance of Dr. Sohaib Ahmed, Principal BSEAS throughout the PhD Project.

I would also like to give special thanks to my Parents and family as a whole for their continuous support and understanding when undertaking my research and writing my thesis. Your prayer for me was what sustained me this far. Finally, I would like to thank Ms. Shaista Iftikhar, Mr. Ahsan Majeed, Mr. Ejaz Ahmed and Dr. Syed Nawaz ul Huda, Dawn Group for letting me through all the difficulties. Finally, I would like to acknowledge the Higher Education Commission NRPU-5250 funded project and the support of the Director General and Director of Bahria University Karachi for providing lab facilities at Digital Geophysical Lab.

ABSTRACT

In Winder Town District Lasbela, Balochistan, groundwater is at a vulnerable stage due to overexploitation mainly for irrigation activities. It is situated 80 km in the north-west of Karachi city near the Makran Coast. The research was conducted through integrated geophysical and hydro-geochemical approach to map the subsurface groundwater and estimate the aquifer parameters. The study also highlighted the spatial variation for hydro-geophysical parameters integrated with hydrochemistry and hydrogeology to assess the overexploitation impact and groundwater quality of study area. There have been no integrated scientific studies conducted and documented for sustainable groundwater development of the area. Previous research on hydro-geochemistry of groundwater and data analysis were used for comparison and to develop temporal variation in the quality of water. The geophysical electrical resistivity method was selected; utilizing vertical electrical sounding (VES), and Schlumberger electrode arrangement to map the potential aquifer and other hydrogeological parameters. PASI 16-GLN earth resistivity meter was utilized to acquire 27 points, of vertical electrical sounding (VES). The maximum lateral spacing of current electrode has been kept at 300 meters (AB), to delineate electrical properties up to 150 meters' depth. The resistance values acquired in the study area were multiplied with the Geometrical Factor (K) to estimate apparent resistivity. Finally, obtained field data from the geophysical survey was processed using computer inversion program IPI2Win developed by Moscow State University, Russia. The geophysical results delineate five layer of variable resistivity; layer 1 (1.5-3.5 m) resistivity ranges from 2-38 Ωm and an average value is 17.5 Ωm. This shows that the resistivity is higher toward the western side of the RCD highway due to dry and unsaturated sand dunes deposits. The lower

resistivity pattern in east and the central part near the Winder River of the study area depict sandy clay and clay. In layer 2 (3.2-14.2 m) resistivity ranges from 6.32-42 Ωm and the average value is 23 Ωm. The range in the north-east of study area shows higher resistivity interpreted as sandy gravel whereas the south-west & north-west comprise sand deposits. The layer 3 (13-51 m) resistivity varies from 14-50.4 Ωm and the mean value is 29 Ωm. Layer 4 (50.4-114 m) resistivity ranges from 13.5-51.6 Ωm and an average value is 31.5 Ωm. Layer 5 resistivity value ranges from 14.1-51.4 Ωm and an average value is 27.35 Ωm. Layer 3,4 and 5 show higher resistivity in central and eastern region where as the western side shows low resistivity zones. The layer 4 and 5 are saturated and low resistivity depicts the brackish water condition toward the western side, the higher resistivity closure along the Winder River is delineated as the high potential of low TDS water zone. Due to over-pumping of groundwater in Winder Balochistan the water table declined from 15 to 45 meters. The freshwater hand pump near the coastal belt is abandoned and deeper water is more saline. In the vicinity of agriculture farm groundwater, TDS ranges from 1000-2800 ppm. The sample of groundwater from the tube well in the study area provides the spatial distribution of groundwater quality. The analysis of 94 groundwater samples were carried out for physiochemical parameters. Trace elements for the selected samples were also assessed for comparative analysis with published research of 2013. The hydrochemical analysis shows that the dominant hydro facies type is NaCl, Ca-Cl and $MgSO_4$. The HEF-D plot, Gibbs diagram, Stiff plot, Piper diagram, Ionic ratio and statistical analysis of physiochemical analysis suggest that seawater intrusion plays a vital part in groundwater recharge due to aquifer overexploitation. The physiochemical analysis shows that the $Na^+ > Ca^{2+} > Mg^{2+} > K^+$ (meq/l) for the cation and $Cl^- > HCO_3^- > SO_4^{2-}$ (meq/l) for anions in groundwater of study area. The nitrate contamination >50 mg/l concentration was observed in the samples of Winder which can be the result of livestock activity, agriculture activity and some extent to domestic use of water. The results of the present study also compared with the previous research on groundwater which represents, decline in groundwater quality. The hydro-chemical parameters of previously published data show that composition was mainly controlled by the Mor and Pab ranges in north-eastern part of the study area. The average value of the present study for pH is 7.23, Na^+ 331 mg/l, Cl^- 522 mg/l, SO_4^{2-} 307mg/l, 50% of sample shows high salinity hazard, the ionic ratio of HCO_3^-/Cl^- is 0.43 and Na/Cl is 0.97 depict the impact of seawater intrusion in groundwater. The estimated irrigation water quality

parameter shows the average value of RSC is -7.6 (suitable), Na% 50.1, SAR 5.8 (suitable), MAR 50.6, PS 18 and PI 133.3 (good). The increase in the pH value of groundwater decreased the concentration of trace element of study area. The estimated average values are very close to permissible limit and maximum value in most of the samples exceeds the irrigation water quality standard and deteriorates the soil and crops of the area. The integrated geophysical and hydrochemical parameter maps can be utilized to categorize the low-high risk zone for agriculture activities and domestic use of water. The pumping of groundwater should be stopped from tube wells near to the coast such as UF, UG, UN, US, UD, UL, UR, UG, UT, UP, PS, KA, KZ, KT, KA and KQ. The study area is strategically very important regarding China Pakistan Economic Corridor. Urbanization and industrialization are increasing rapidly and directly stress groundwater production for agricultural activity eventually the impacts are estimated from the present study. The sustainable development of Winder is highly dependent on groundwater effective management, mitigation of seawater intrusion and government policies to exploit groundwater.

TABLE OF CONTENTS

LIST OF TABLES

LIST OF FIGURES

LIST OF ABBREVIATIONS

AB	Current Electrode
Ca^{2+}	Calcium ion
Cd	Cadmium
Cl^{-}	Chloride
Co	Cobalt
Cr	Chromium
Cu	Copper
DZ	Dar Zarrouk
EC	Electrical Conductivity
Eh	Oxidation/Reduction Potential
ERS	Electrical Resistivity Survey
Fe	Iron
GPS	Geographical Position System
HCO_3^{-}	Bicarbonates
HFE-D	Hydrodynamic Facies Evolution, Diagram
IP	Induced Potential
K^{+}	Potassium
KR	Kelley's ratio
LDP	Lime Deposition Potential
Mg^{2+}	Magnesium
MAR	Magnesium Absorption Ratio
Mn	Manganese
MN	Potential Electrode

Na^+	Sodium
Ni	Nickle
Pb	Lead
pH	Potential of Hydrogen
PI	Permeability Index
PS	Potential Salinity
R	Resistance
L	Longitudinal resistivity
RSC	Residue Sodium Carbonate
Tr	Transverse Resistance
Sc	Longitudinal Conductance
SAR	Sodium Absorption Ratio
T	Transverse Resistivity
TDS	Total Dissolve Solid
SO_4^{2-}	Sulfate
TDS	Total Dissolved Solid
VES	Vertical Electrical Sounding
WHO	World Health Organization
Zn	Zinc

LIST OF SYMBOLS

I	Current
K	Geometric factor
V	Voltage
Ω	Resistance
ΔV	Potential difference
ρ	Apparent resistivity
Ωm	Ohm-meter
mg/l	Milligrams per liter
µg/l	Micrograms per liter
µS/m	Micro siemens per meter
λ	Anisotropy
ppm	Parts per million
m	Meter
meq/l	Milliequivalents per litre

CHAPTER 1

INTRODUCTION

1.1 Background

Sustainable groundwater resources with respect to quality and quantity play a vital role in irrigation, industrial development and human consumption (Sabale et al., 2023; Tran et al., 2021; Adimalla et al., 2020). It has become an essential resource in coastal regions, where groundwater is severely contaminated by pollution and seawater intrusion (Biswas et al., 2023; Solangi et al., 2023; Lu et al., 2020). The world's largest freshwater resources are preserved in groundwater (Abba et al., 2023). Approximately 50% of the population worldwide relies on groundwater aquifers for domestic use and 43% of water is utilized for irrigation purposes (Kumar & Mathur, 2022). Moreover, 2.5 billion people worldwide depend entirely on groundwater to fulfil their daily necessities (Belhassan, 2021).

The hydrological cycle of the earth acts like a giant pump of water that constantly circulates the freshwater i.e., from oceans to the land and back to the ocean (Bogardi & Fekete, 2021). The total global water comprises 2.5% freshwater, 96.5% ocean and other saline water is 0.9%. The 2.5% freshwater is further classified into 68.7% glacier/ice caps, 1.2% surface water and 30.1% present in groundwater (Pointet, 2022). In developing countries like India, Bangladesh, China, Nepal, Africa and Pakistan most of the people relied on groundwater where the estimated annual

withdrawal is about 320 billion meter^3 out of which Pakistan has 60 bm^3, India 230 bm^3 and Bangladesh 30 bm^3 (Schwartz et al., 2020; Qureshi, 2015). Over the last decades, groundwater degradation has been associated with overexploitation, the use of pesticides in agriculture activities, the discharge of wastewater without treatment and industrial development (Chen et al., 2020; Habib et al., 2020; Hossain & Patra, 2020).

The arid regions where drought recurs and surface water resources commonly unreliable around the world are more vulnerable in terms of groundwater scarcity. The over-stressed on groundwater resulting depletion and quality deterioration (Roshni et al., 2022). The long-term utilization of polluted groundwater for irrigation and drinking purpose adversely affect the natural ecosystems and it also leads to impact the human health such as cancer & cardiovascular diseases (Kaur et al., 2021; Saha & Rahman, 2020; Bai et al., 2019; Tran & Nguyen, 2018; Bartzas et al., 2015). Seawater intrusion in coastal aquifer systems, toxic chemicals and nitrate contamination in groundwater become a global issue (Jayarajan & Kuriachan, 2021; Martínez et al., 2021; Knoll et al., 2019; Wu et al., 2019). The higher concentration of salinity and nitrate contamination in groundwater impacts human health and agricultural systems (Zolekar et al., 2021; Lu et al., 2020; Bartzas et al., 2015). Nitrate is very life threatening in groundwater resource pollution which leads to cancer, neural tube defect and thyroid diseases (Ward et al., 2018). Longer exposure through ingestion of high concentrations of nitrate in groundwater was a major cause of carcinogenic risk among children and infants in India (Adimalla et al., 2021; Adimalla, 2019). Similarly, severe negative impacts observed worldwide due to nitrate contamination (Li et al., 2021; Ijumulana et al., 2020). The increase in salinity also became a subject of imminent concern all around the world (Rahaman et al., 2020).

Overall, sea-level rise because of global climate change and anthropogenic activities (e.g., overexploitation of groundwater, construction of dams along rivers) are the main factors contributing to increasing seawater intrusion, both at surface resources and aquifers in coastal areas (Zeynolabedin et al., 2021; Telahigue et al., 2020; Huerta et al., 2019). The ecosystem has a negative effect due to the increase in the ionic composition of freshwater. A schematic analogue study area diagram represents the water cycle and seawater intrusion in coastal aquifers due to over-pumping and sea-level rise (Figure 1.1). Due to intrusion, the increase in ionic compositions of aquifers

harms the ecosystem (Zhu et al., 2020) and also causes serious health problems (Rakib et al., 2020). The morphology of the study area is similar to Figure 1.1 where in north-east of the study area Mor and Pab ranges run parallel and move toward the south-west. The western side is covered by farming activity on plain areas and sand dunes along the coastal belt of Balochistan.

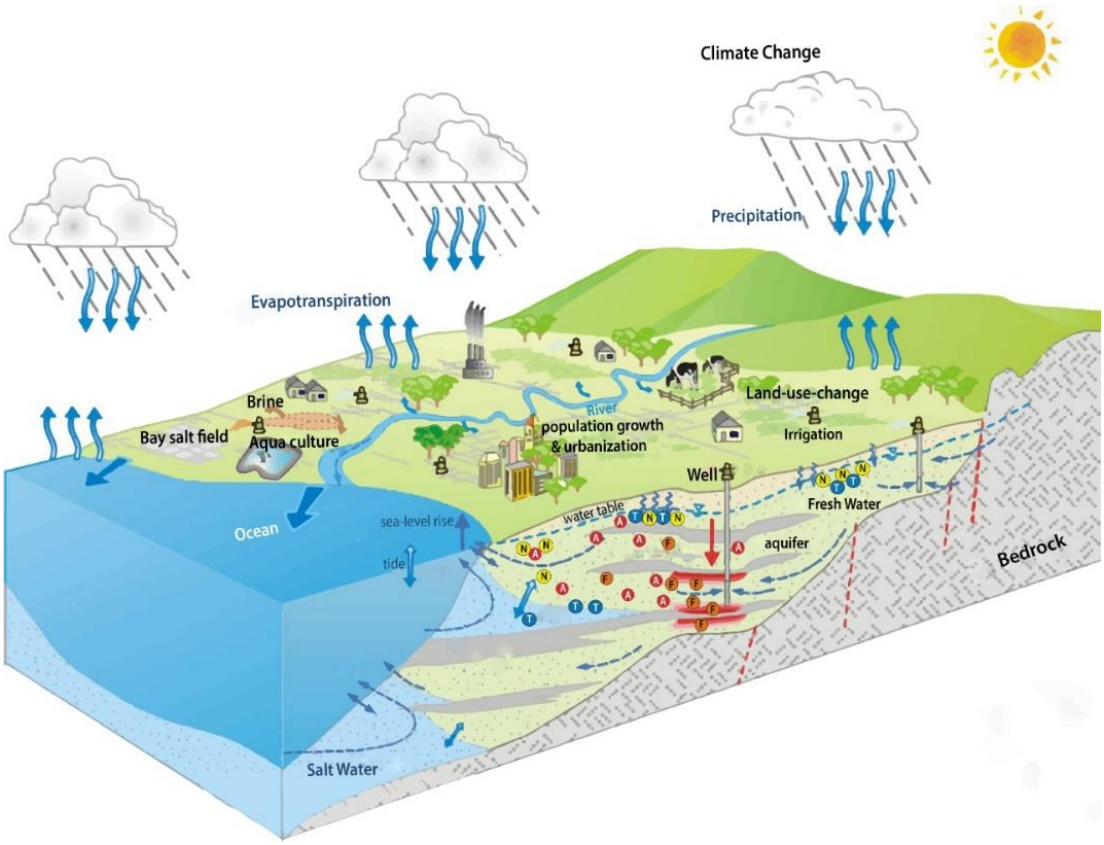

Figure 1.1 Schematic model of water cycle where anthropogenic activities are resulting in surface and groundwater contamination, a decline in water table and seawater intrusion (modified after Han & Currell, 2022).

The consumption of highly concentrated salt and hard (Ca & Mg) water in the long term increases the risk of chronic kidney diseases, coronary heart disease and hypertension (Rahaman et al., 2020; Shammi et al., 2019). Besides human health, these parameters' high concentration in water also deteriorates the soil fertility for irrigation and reduces crop production (Korres et al., 2019). The increasing pressure on

groundwater resource utilization continuously deteriorating the quality and it became very critical to protect the habitats, ecosystem and food security that mainly depend on groundwater. The groundwater quality deterioration by distinct pollutants could ruthlessly effect the ecosystem and human health. This issue is persistent that eventually gets worse because of rising pressure on groundwater reserves due to intensive agriculture, industrialization, population growth and other anthropogenic activities all around the globe. Therefore, the quality of groundwater & human health risk estimation is very crucial to protect individuals that are mostly dependent on groundwater resources (Kaur et al., 2020; Yin et al., 2020; Rezaei et al., 2019). These all consequences are the result of a lack of sustainable groundwater management. Therefore, the hydro-geochemical (Mukherjee & Singh, 2022) and hydro-geophysical (Anoop et al., 2021) understanding are very important to formulate strategies for the sustainability of groundwater.

Agriculture is the foundation of any country's economy, as it provides food and raw materials for industrial purposes. The crop yields do not solely rely on soil fertility, the irrigation water quality also plays a key role (Wang et al., 2022; Hassan et al., 2009). The overexploitation of groundwater and rapidly decreasing water table are causing deterioration of dried wells, springs and wetlands (Essefi & Hajji, 2023; Uchenna et al., 2023; Hora, 2022). Therefore, professionally, the study of aquifers is not only limited to environmentalists, geophysicists, hydrologists and geologists, but this problem demands the attention of economists, socialists, lawmakers, judges, communication skill experts, government municipal bodies and others as well.

Several case studies published in the literature for sustainable development of groundwater aquifers (Lino et al., 2023; Sadeqi, 2023; Ma et al., 2020) e.g., those in Jordan, focusing on the water quality trends and hydrographs imply a relationship between deterioration and reason of lowering water levels. Point and non-point source contaminations from industrial, domestic and agriculture, etc. and those stemming from groundwater over use also pose major problems. The researchers identify the vulnerable situation of groundwater quality and quantity due to droughts, overexploitation and intensive agriculture in Jordon (Gazal, 2021). The depletion of groundwater in India has become a prominent threat to food and water security because of the overexploitation of groundwater mainly for irrigation purposes. The decreasing quality,

shortage in supply of water and contaminants due to salinity in coastal areas impact the crops and soil. Moreover, it effects the country's economic growth (Dangar et al., 2021). In India, ~50% of the urban population and about 85% of the rural population rely on groundwater for domestic, drinking, irrigation and other purposes (Roy et al., 2023; Kumari & Rai, 2020). In the leading states, including Maharashtra, the groundwater resources quantity and quality have had a negative impact due to over-exploitation, where agricultural productivity has deteriorated. In the coming few decades' water scarcity is feared to effect crop sowing. The water table is also declining in Kabul, Afghanistan i.e. 1.7 m/year, and approximately 33% tube wells are abandoned (Noori & Singh, 2021). Bangladesh is also facing gradual decline and scarcity of groundwater due to hydrological, climate, and socio-economic changes. The water table is declining approximately 0.8-1.5 meter/year in Bangladesh (Fahim et al., 2023).

The overexploitation of groundwater is unsustainable production which exceed the recharge balance of aquifer. Pakistan is also facing over-exploitation of groundwater due to poor groundwater management (Ali et al., 2022; Rahman et al., 2022). Comprehensive research for the future sustainability of groundwater quality is needed to resolve the issue. Pakistan is one of the most overcrowded countries around the globe, the population trend is continuously increasing and is expected to reach 220 million by the year 2025 (Janjua et al., 2021). The great Indus basin covers an area of 566000 km^2 and 80% population of this region. Over the last decades, Pakistan is in the list of water-stressed countries (Akbar et al., 2021). According to the United Nation estimation the per capita water accessibility of Pakistan already attained 1090 m^3 (Afridi, 2022; Janjua et al., 2021). Irrigation is one of the main components of economic growth. Approximately 75% of Pakistan's population is dependent on agriculture. The agriculture activity also accounts for 60% of earnings from foreign exchange and accommodates 44% of labor employment. It contributes 20% to the GDP of Pakistan (Mahboob et al., 2021; Munir et al., 2021). The rapid increase in population needed more food production by using water resources in the agriculture sector (Baig et al., 2023; Syed et al., 2021). Due to the deficiency of surface water resources, the farmers are overexploiting unregulated groundwater in Pakistan for agriculture which also threatens the 20% GDP of the country (Habib, 2021).

The province of Balochistan is one of the most vulnerable regions in the decline of groundwater due to overexploitation where rate of discharge is greater than rate of recharge. It is also observed that due to the arid region, 97.4% of agriculture and domestic use of water depend on groundwater extraction from the tube-well. The total number of tube-wells drilled in Balochistan was 5000 in 1985, due to limited water resources, the groundwater was the only source in Balochistan to exploit and overcome the demand for domestic and agricultural activities. This resulted from a rapid increase in the number of tube wells all over the province and it became approximately 40,000 in 2015 (Ashraf, 2016). The increasing trend and the current scenario of Balochistan shows that the predicted number of tube wells in 2025 will be 45 thousand (Figure 1.2). The regional survey to evaluate the water resources in Balochistan was conducted by Halcrow (2007), and summarized the recharge and discharge of the balance of groundwater and surface water. The Polari River sub-basin shows a negative balance for groundwater in Table 1.1. The decline in the groundwater table is very common in the Province of Balochistan. The farmers are exploiting the deeper aquifer using a submersible pump from 250 meters depth (Steenbergen et al., 2015). Similarly, the major cities in Balochistan such as Quetta, Mastung, Pishin and Mangochar also experienced a rapid decline in the water table i.e. 0.23-3 m/year (Ashraf & Sheikh, 2017).

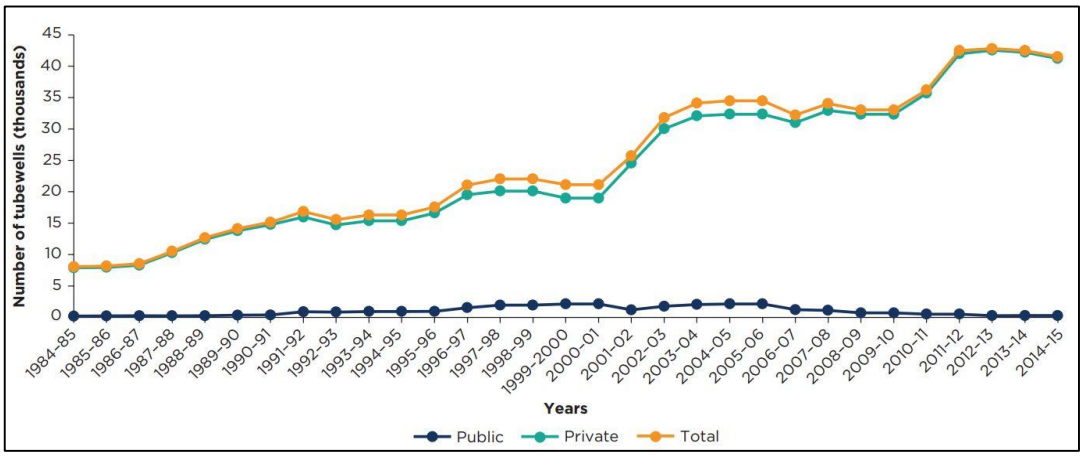

Figure 1.2 The statistics of number of tube wells drilled by private and public sectors in Balochistan from 1985 to 2015 (Ashraf, 2016).

Table 1.1 The Balochistan sub-basin annual water balance of surface and groundwater in billion cubic meters (Halcrow, 2007).

Province	water source	Recharge	Total flow	Balance	Usages			
					Agriculture	Nature	People	Livestocke
Balochistan	Groundwater (% of total)	2.210(17)	2.659(54)	-0.459	2.474(70)	n/a(n/a)	0.091 (71)	0.094(68)
	Surface water	10.793	2.221	8.572	1.059	1.079	0.038	0.045
Sub - Basines								
Dashit River Basin	Groundwater (% of total)	0.100(13)	0.94(59)	0.006	0.069(90)	n/a	0.013(81)	0.012(67)
	Surface water	0.66	0.83	0.577	0.008	0.066	0.003	0.006
Gaj River Basin	Groundwater (% of total)	0.007(23)	0.072(74)	-0.002	0.070(100)	(n/a)	0.001(100)	0.001(33)
	Surface water	0.233	0.025	0.208	0.000	0.023	0.000	0.002
Gawader-Ormera	Groundwater (% of total)	0.040(7)	0.025(28)	0.015	0.017(68)	(n/a)	0.004(80)	0.003(75)
	Surface water	0.546	0.064	0.482	0.008	0.055	0.001	0.001
Hamun-e-Lora	Groundwater (% of total)	0.040(17)	0.141(83)	-0.101	0.139(95)	(n/a)	0.001(100)	0.001(50)
	Surface water	0.189	0.028	0.161	0.008	0.019	0.000	0.001
Hamun-e-Mashkel	Groundwater (% of total)	0.300(13)	0.027(8)	6.273	0.012(11)	(n/a)	0.008(80)	0.007(70)
	Surface water	2.078	0.312	1.766	0.99	0.208	0.002	0.003
Hingol River Basin	Groundwater (% of total)	0.200(18)	0.168(55)	0.032	0.156(83)	(n/a)	6.005(50)	6.007(70)
	Surface water	0.942	0.136	0.806	6.033	0.094	0.006	0.003
Hub River Basin	Groundwater (% of total)	0.08(17)	0.088(52)	-0.008	0.086(68)	(n/a)	0.001(50)	0.001(50)
	Surface water	0.38	6.08	0.300	0.014	0.038	0.001	0.001
Kachi Plain	Groundwater (% of total)	0.180(9)	0.169(21)	-0.011	0.140(25)	(n/a)	0.017(61)	0.012(67)
	Surface water	1.902	0.634	1.268	0.428	0.008	0.011	0.006
Kadamai River Basin	Groundwater (% of total)	0.030(28)	0.115(92)	-0.085	0.110(100)	(n/a)	0.000(n/a)	0.005(7)
	Surface water	0.077	0.01	0.067	0.000	0.190	0.000	0.002
Kaha Basin	Groundwater (% of total)	0.1290(27)	0.319(76)	-0.129	0.315(87)	(n/a)	0.000(n/a)	0.004(67)
	Surface water	0.515	0.103	0.412	0.049	0.052	0.000	0.002
Kand River Basin	Groundwater (% of total)	0.010(36)	0.019(90)	-0.009	0.018(100)	(n/a)	0.000(n/a)	0.0000(n/a)
	Surface water	0.018	0.002	0.016	0.000	0.002	0.000	
Kunder River Basin	Groundwater (% of total)	0.050(33)	0.048(64)	0.002	0.048(75)	(n/a)	0.000(n/a)	0.0000(n/a)
	Surface water	6.103	0.027	0.076	0.016	0.010	0.000	
Mula River Basin	Groundwater (% of total)	6.120(26)	0.129(75)	-0.009	0.126(94)	(n/a)	0.002(100)	0.001(50)
	Surface water	0.338	6.043	0.691	0.008	0.034	0.000	0.001
Nari River Basin	Groundwater (% of total)	0.270(25)	6.180(59)	0.090	0.171(8)	(n/a)	0.006(80)	0.004(67)
	Surface water	0.817	6.126	0.691	0.014	0.082	0.001	0.002
Pishin River Basin	Groundwater (% of total)	0.170(36)	0.566(77)	-0.396	0.513(82)	(n/a)	0.024(71)	0.029(67)
	Surface water	6.302	0.169	0.133	0.115	0.030	0.010	0.002
Porali River Basin	Groundwater (% of total)	1.40(11)	0.146(38)	-0.006	0.142(52)	(n/a)	0.002(50)	0.003(75)
	Surface water	1.106	0.237	0.869	0.123	0.111	0.002	0.001
Rakhshan River Basin	Groundwater (% of total)	0.050(14)	0.081(70)	-0.031	0.075(100)	(n/a)	0.003(67)	0.003(75)
	Surface water	0.320	0.034	0.286	0.000	0.032	0.001	0.001
Zhob River Basin	Groundwater (% of total)	0.160(37)	0.270(71)	-0.116	0.267(77)	(n/a)	0.002(100)	0.001(50)
	Surface water	0.267	0.110	0.157	0.082	0.027	0.000	0.001

The joint effort of the Japanese Government, with the Department of Agriculture District Lasbela, Balochistan, agriculture farms were established in (1993-1994) in Winder, District Lasbela, Balochistan. These farms are underlain by Cretaceous age ophiolitic rocks covered by windblown sediments. The main problem is the accessibility of irrigation water due to the arid climate. Winder River and tube wells serve as the main source of irrigation water for agriculture & human consumption (Bashir et al., 2007). The Winder Basin lies along the coast of Makran and it is a part of Lasbela Plain which has a triangular shape formed by the deposition of alluvial sediments of the Porali River and its tributaries (Spate & Learmonth, 2017). The main river of the study area is the Winder River. An estuarine delta is formed by the Winder River at the Miani-Hor & it drains, the eastern plain. Due to the heavy rainfall, washouts and alluvial silts overlie the whole basin and are appropriate for cultivation. The climate of Lasbela Plain is semi-arid to arid because of inadequate and unforeseeable rain (Sayal, 2015). Lasbela Plain lies in the transitional zone of the rainfall system of Pakistan and gets two rainfall from these systems i.e. the summer monsoon and by western depression in winter (Jan et al., 2022). Due to the extreme temperature and low rainfall, the semi-arid to arid climate is prevalent in southern Balochistan (Bashir et al., 2004).

Water is a vital resource not only for humans but also for agricultural and industrial purposes. The increasing agriculture activity in Winder, Balochistan has caused a shortage of water and led people to pump groundwater for agriculture and their uses, but the over-exploitation effected the water level and quality. Formerly, fresh water was at the depth of 15 meters below the surface, but now the situation is entirely changed. The shallow aquifers are abandoned whereas near coastal areas freshwater aquifers are highly effected by salinity. The limitation of water resources in Balochistan together with growing demand supports this study for suitable groundwater management.

An environmental geophysical and geochemical approach was adopted to assess the groundwater quality deteriorated by overexploitation in Winder, Balochistan. In this approach integrated analysis has been carried out using the geophysical characterization of the aquifer and hydro-geochemical analysis of groundwater. An environmental geophysical technique such as an electrical resistivity survey is systematic and cost-

effective for the sustainable exploration of groundwater resources. This method was extensively employed for the identification of geo-electrical and hydrogeological properties of subsurface layers in Winder, Balochistan. The electrical resistivity data were acquired by the vertical electrical sounding (VES) method. The Schlumberger electrode arrangement was engaged for 27 sites to map the aquifer. This configuration is comprised of four electrodes i.e., two current & two potential electrodes. Where the current electrodes were employed to inject the current into ground whereas the potential electrode were utilized to determine the potential change between two points (Zohdy et al., 1974). The four electrodes were set along a straight line, with current electrodes on the outer side while the potential electrodes were in between the current electrodes. The distance of the current electrode was gradually increased to get profound information about the subsurface (Okpoli, 2013). The resistance was measured at the field and the apparent resistivity (ρ) was computed by multiplying the geometric factor (k) with resistance (R). The apparent resistivity (ρ) is then plotted on Y-axis, against the current electrode spacing (AB/2), on X-axis to yield the resistivity, depth, thickness and number of model layers (Raji & Abdulkadir, 2020).

The previous work and public consultation were conducted to gather information related to the hydrogeology of the area. The hydro chemical examination was processed within a week after collection of sampling from study area. The physiochemical examination of chemical parameters and physical parameters for electrical conductivity (EC), total dissolved solids (TDS), and pH, were determined by utilizing portable meters on site. A total of 94 groundwater samples were collected based on the hydrogeological setting of the study area; further physiochemical parameters were estimated using the given methods of the American Public Health Association (Rice et al., 2017). The assessment of major cations namely Potassium (K^+), Magnesium (Mg^{2+}) Calcium (Ca^{2+}) and Sodium (Na^+) and major anions such as Chloride (Cl^-), Nitrate (NO_3^-), Sulphates (SO_4^{2-}), & Bicarbonates (HCO_3^-) was conducted in the laboratory. For quality assurance, an acceptable range of ionic balance error of ±5% was obtained for the physiochemical assessment of collected groundwater samples of Winder Balochistan. The geophysical results were integrated with the hydrogeological information and hydro chemical results of current and previous data to evaluate the impact on water quality due to overexploitation.

1.2 Problem Statement

The World is facing a great water shortage due to climate change. In this scenario, a country like Pakistan may face acute problems due to climate change as well as existing water management problems. Water management is a significant issue regarding consumption and distribution among their political-administrative units. The province of Balochistan observed the worst water scarcity due to drought.

The current aim of this research is to assess groundwater quality from the perspective of geologic environment in Winder Town, District Lasbela, Balochistan. The rapid increase in the number of tube-well dug may have a negative impact such as decreasing water levels in wells, decreasing water production, change in groundwater quality and ecological impacts on wetlands. Besides degradation and decreasing well yields, the quality of freshwater aquifers for shallow depth might be damaged by the intrusion of salinity near the coastal aquifers of Winder. The overexploitation was assessed during the data collection in study area. The current extraction of water from 250 tube wells is approximately 36.1 million cubic meter, previously it was 11.7 million cubic meter extraction from 80 wells. A drastic change in water table 2.2 meter/year estimated for the study area. Therefore, overexploitation of groundwater in Winder (Balochistan) requires comprehensive research work to mitigate the future impact by achieving following objectives for sustainable groundwater development.

1.3 Research Objectives

1. To conduct survey of the study area and gather tube-well information to examine the current problem related to groundwater quality and over-pumping.

2. To develop the geo-electric and hydrogeological characteristics of subsurface aquifers in Winder, District Lasbela, Balochistan.

3. To identify hydro-chemical facies and spatial mapping for evaluating the groundwater quality deteriorated by overexploitation.

4. Comparative analysis of calculated hydrochemical parameters to assess the temporal variation with the previous research work.

5. To construct risk maps to demarcate whether the condition of groundwater is suitable or not for agriculture/ low to high risk zone.

1.4 Research Significance

A survey of Winder Town was conducted, which highlighted the deterioration of groundwater quality due to overexploitation. The over-pumping and drop in water level were observed during the field survey. The shallow freshwater aquifer near the coast is polluted by seawater. Currently, there is no well present near the coast, all are abandoned. Therefore, the assessment of groundwater in winder area is very important, which includes all aspects (e.g., social, economic, or environmental) that are necessary for the understanding of groundwater quality and quantity. The significance of this research is to aware the local, concerned authorities and government officials about the threat of seawater intrusion on agriculture, demarcation of the saline zone and groundwater depletion due to over-pumping.

1.5 Thesis Structure

Chapter 1 of the thesis highlights the background of the research, groundwater overexploitation impact, research aim and objective, problem statement and research

significance. Chapter 2 comprises digitized location maps, physiography and drainage map, climate, hydrogeology, rainfall and soil detail of the study area. Chapter 3 includes comprehensive detail on the general geology of the region, previous research work related to hydro-geochemistry and geophysical investigation of groundwater, electrical resistivity technique literature and other information to support the methodology and results of research. Chapter 4 covers the phase-wise methodology of research work particularly for the hydro-geochemical and geophysical process to overcome the objective of the research. Chapter 5 comprises the results and discussion on geophysical groundwater characterization and modelled cross-section, hydro-geochemical analysis of groundwater samples and integrated analysis of hydro-geochemical and geophysical results. Finally, Chapter 6 incorporates a conclusion and recommendation for future research and development.

CHAPTER 2

STUDY AREA

2.1 Geographical Setting of Research Area

The study area “Winder Town” is located in Somiani Tehsil and Lasbela District in Balochistan, province of Pakistan having coordinates of 25° 23' 11.0832" N and 66° 39' 49.6620" (Figure 2.1).

2.2 Physiography and Drainage Pattern

Winder Basin is located in Lasbela Plain close to the Makran Coastal belt of District Lasbela Balochistan. The region is bounded in the east and northeast through the Pab and Mor ranges and the Haro, Harag Koh and Liddah Koh in the west and the north-west, whereas the Arabian Sea is situated to the south (Ahsanullah, 1971). The Winder valley is a north-south trending valley among the Pab and Mor ranges. It is

created in the smooth and simply abraded Cretaceous age rocks i.e., Goru and Sembar formations. The western belt i.e., the Mor Range, consists of intricately folded, rigid and impervious Jurassic age rocks of the Ferozabad Group, meanwhile, the eastern belt i.e., the Pab Range, consists of cliff-forming Cretaceous Rocks (Parh Limestone). Because of the extreme deformation, erosion and uplift, these mountains have rough topography. The approximate relief in the east is 660-1232 meters and western fold belts 300-1216 meters respectively (Naseem et al., 2002a). The study area comprises a variety of environments such as the ocean coast, sand hills, swamps, semi-arid settings, undeveloped areas, dry stream beds, sandy fields and mountain ranges. The Lasbela District can be isolated into three wide categories: Sloping Regions (Mountain Highland), Alluvial Plain (Piedmont Plain) and Coastal Regions (Valley Floor) (Ahsan & Mallick, 1999). The basin is entirely concealed by fresh silt (alluvial) deposits and the washout from torrential rain. In such cases, sediments deposited along the river are highly suitable for crop cultivation. The basin is covered by a significant vegetation cover. The rest of the area is covered by rangeland (Ahmed et al., 2013). Aridity mixed with intense south-west winds developed broad coastal sand dune belts, whose sea-ward margins are created by extended very fine beaches (Ahsanullah, 1971). Out of the total land part of Lasbela District, about 6% is under crop cultivation while 71.4 % of the total land is deemed as cultivable waste (Ahmed et al., 2013).

The triangular-shaped plain of Lasbela is formed by the alluvium sediment deposits of the Porali River and its tributaries (Chardonnet, 1956). The plain covered an area approximately 64 km^2 wide at its base and in north it is approximately 88 km^2 alongside the braided Porali River. The eastern part of the plain is drained by the Winder River. The river flows from north to south with various flow tributaries and streams draining through the Pab and Mor ranges (Figure 2.2). The drainage structure is sub-parallel to dendritic, which flows in the direction of southwest and finally forms, an estuarine delta at Miani-Hor in the west of Arabian sea. The small streams are fragmentary and seasonal meanwhile, the large one has restrained persistent flow such as Winder River (Bashir et al., 2007). The topography changes gently from higher altitude toward the north-east and decreases to the south-west with an altitude of approx. 8 meters above sea level. The valley is the lowest point on the Lasbela Plain (Burke et al., 2005). In dry weather, the flow of the river carries urban sewage that is ultimately drained into the Arabian Sea (Bashir et al., 2007).

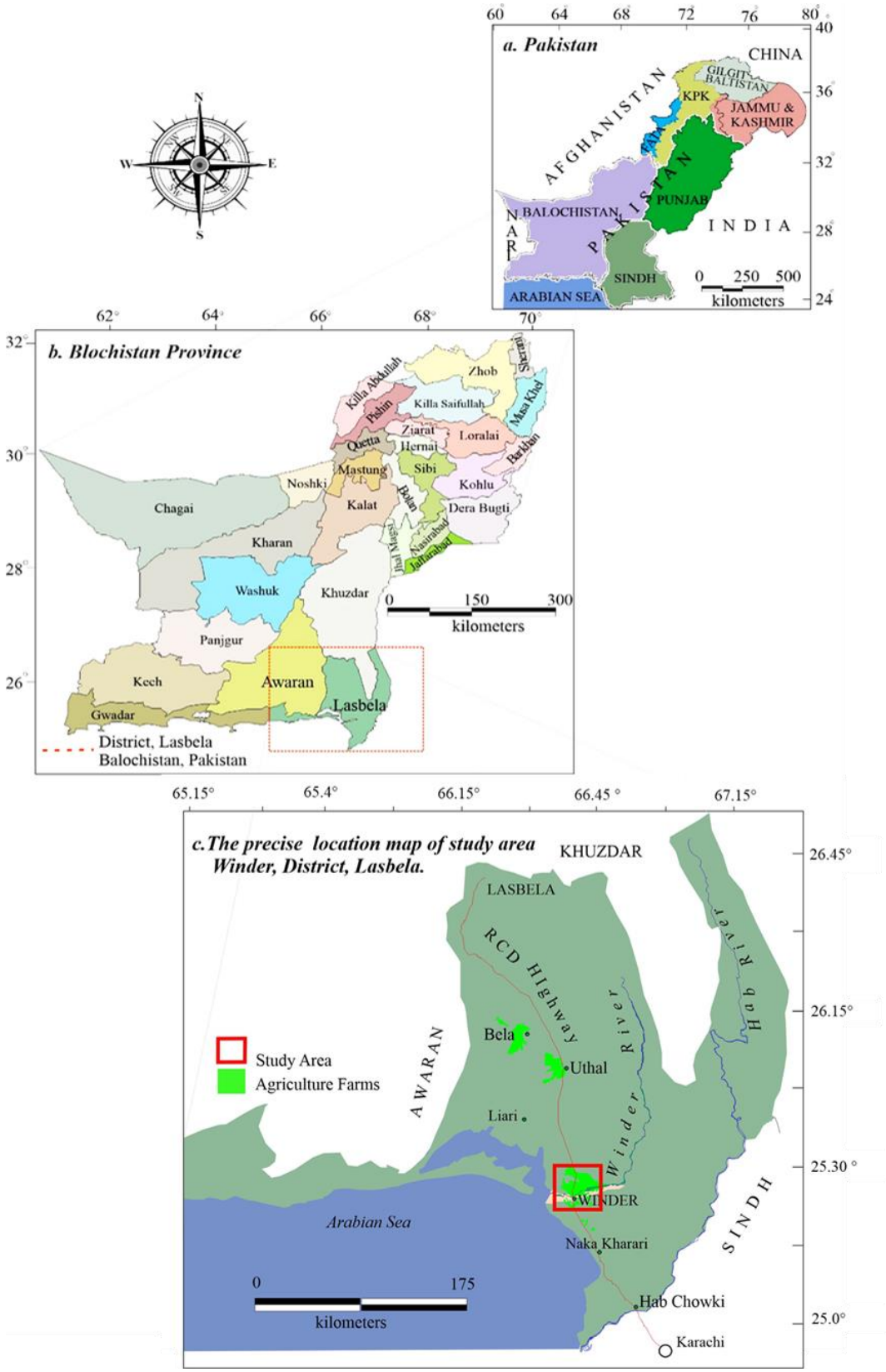

Figure 2.1 The precise location map of the study area Winder, Lasbela District, Balochistan, Pakistan (a) Pakistan and its provinces (b) Balochistan Province and district boundaries (c) Winder Town study area in District Lasbela (Arc GIS).

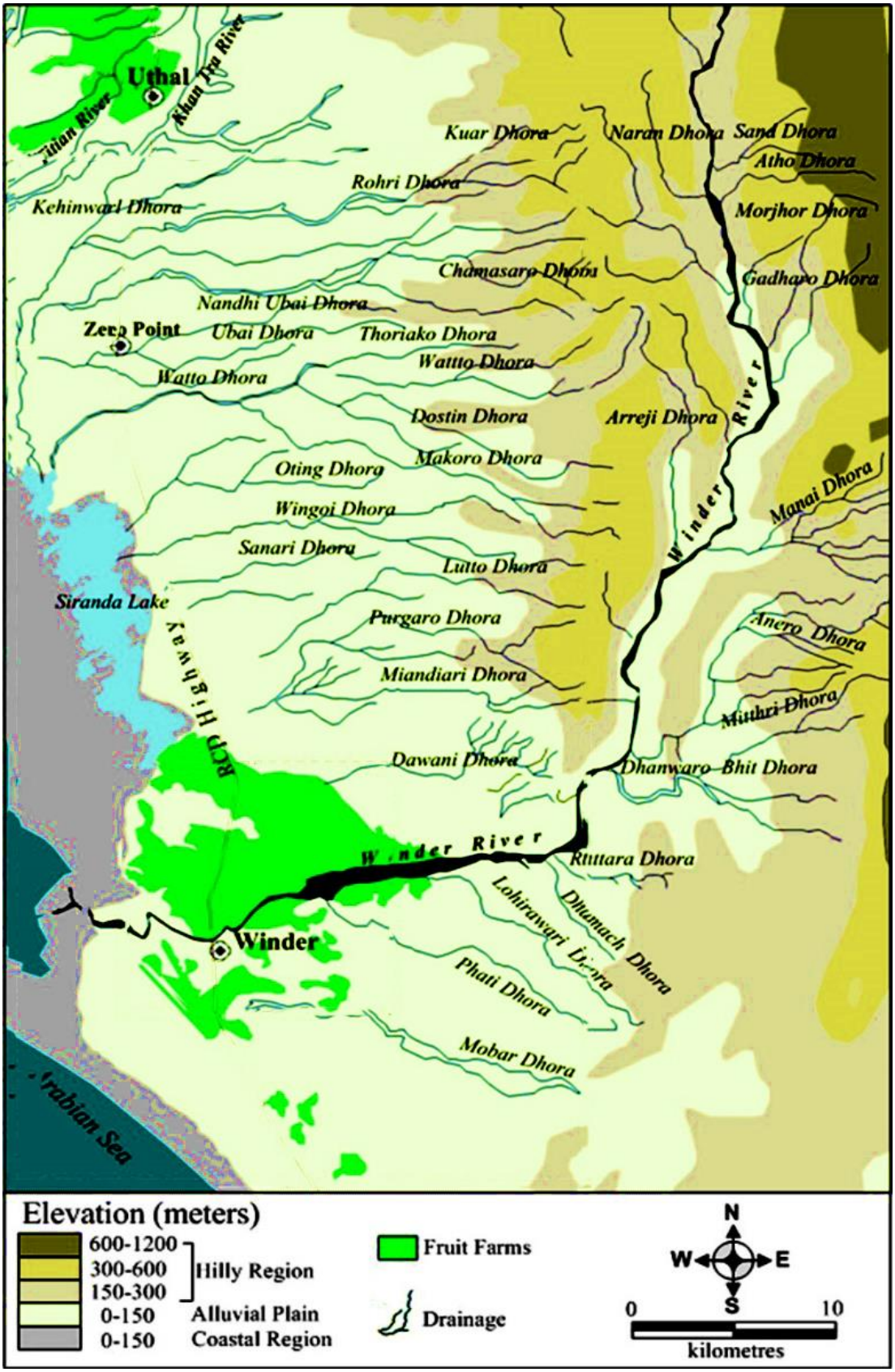

Figure 2.2 Relief map of study area showing the drainage pattern of Winder River in the northeast between Mor and Pab ranges and flowing toward the south and, finally entering into Arabian sea, in the west of study area.

2.3 Climate of Study Area

Climatic conditions of the Winder area are extremely dry, which is normally considered arid and remain dry and hot in summers but winters are fine and moderate. Dry weather, which is usually hot starts in April and continues till October. In between June and July, it seems to be the hottest of summer. The mid-November till the end of January temperature decreases and after February to the end of March temperature increases. The climatic condition of the study area allows it to have uncertain rainfalls during mid-summers which is very usual. Snowfall, hailstorms and rainfall occur from the beginning of December till starting of March. Annual rainfall in the region is around 243 mm with humidity around 34.99% (Naseem et al., 2005b).

The regional climate conditions of the area are high in temperature with very low precipitation. The average temperature in the region of Lasbela is 30^{o}C in summer and 15^{o}C in winter in District Lasbela. The graph represents the last 10 years of temperature data of this region (Figure 2.3). During mid-summers which start from May to the end of July, the temperature of the area is usually high which is the hottest month, whereas the temperature in winter is measured at around 4^{o}C minimum.

The Lasbela Plain is situated in the transitional zone of the rainfall regime of Pakistan (Khan, 1993). Therefore, this region gets rain from each system i.e. monsoon in the summer season and the western depression in the winter season (Figure 2.4). Due to inconsistent rain systems the tube wells are the primary source for irrigation. Lasbela Plain has semi-arid climatic conditions with unpredictable and insufficient rainfall patterns (Ahmed et al., 2013; Khan, 1993).

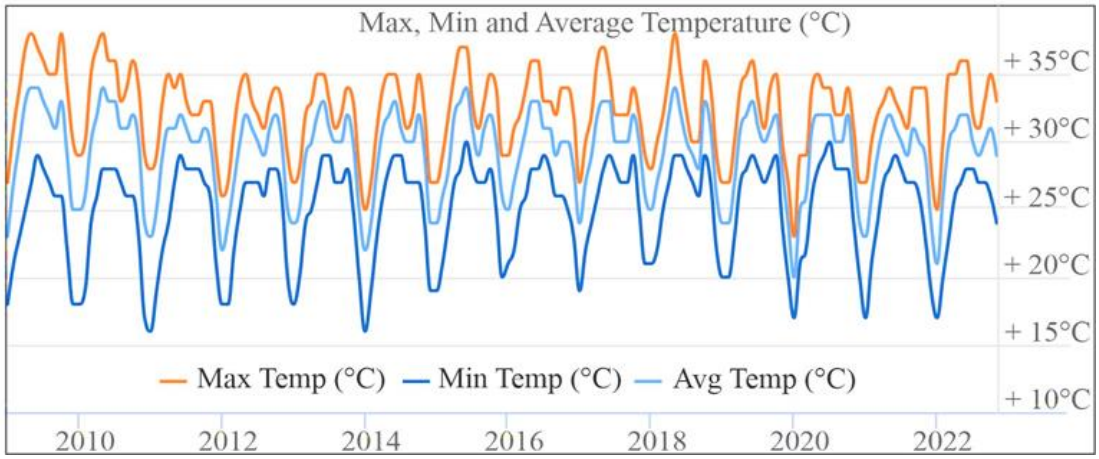

Figure 2.3 Maximum, minimum and average temperature data from 2010 to 2021, District Lasbela, Balochistan (Weather, 2022).

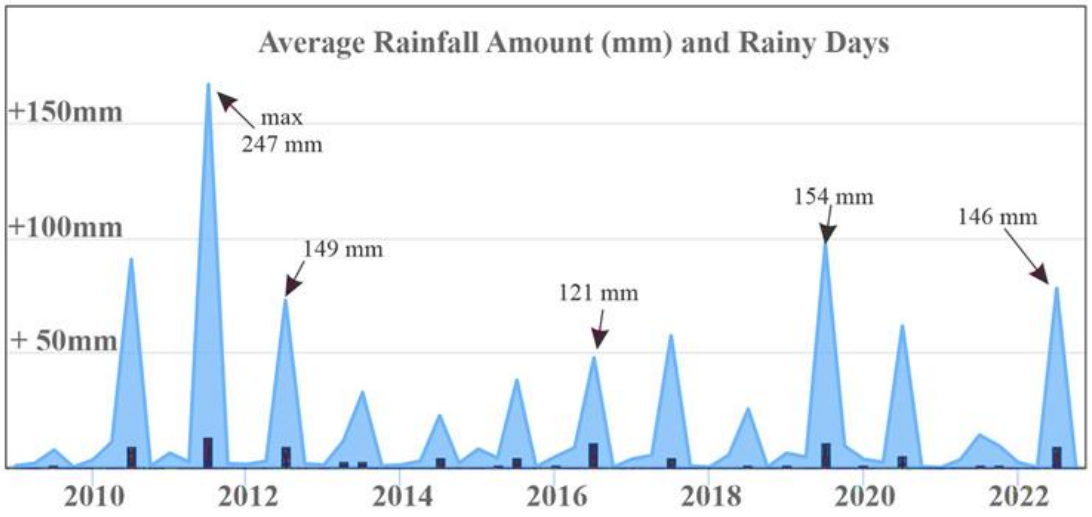

Figure 2.4 Rainfall data for the last 10 year 2010-2021 District Lasbela, Balochista.

2.4 Land Cover and Land Use

The land coverage of Pakistan is 881,913 km^2, out of which 803,940 km^2 is agriculturally used. A major percentage of crops are found in the Punjab Province, which is 70%. Sindh has 20% followed by Khyber Pakhtunkhwa having 10% and Balochistan have 1% (GoP, 2011). The area of cultivation has increased by 33%, but still Pakistan is far away from harvesting the large yield that can be produced (Pakistan, 2012). Lasbela plain is a cultivated land in Balochistan (Ahmed & Mahmood, 2007). The necessity of providing food to locals can be accomplished by managing the yield of crops only by adopting new ways of production with different technologies, accompanied by long-term planning in the whole region. Well-managed resources can enhance the economy of the local community, as well as surrounding areas can have a positive impact. Water management programs should be well managed for the Balochistan region to supply sufficient water to the local areas (Halcrow, 2007). Livestock production management can also enhance economic conditions. The land-mobilization movement is carried out, by the utmost primitive resources found in that environment i.e. manpower and energy supply. Especially in agricultural regions, the land is a pivotal resource for human dynamism and environmental amendments are intensely embedded in the way it is worn (Li et al., 2001). The location of this region, its physiography and vegetation cover predominantly defines Winder Basin as a very fruitful place for agriculture (Ahmed et al., 2013).

2.5 Soil Type

Due to the interactivity between the hydrosphere, lithosphere, biosphere and atmosphere, the soil derives from its source material (Makhfuza, 2022; Mikhailova et al., 2021). In the locality of an agricultural field, the surrounding rocks not only provide primary lithology such as soil but also supply major and trace elements to the soil. Some

of the trace elements provide vital minerals to human beings and they are primarily needed for the healthy growth of plants (Mehri, 2020; Naseem et al., 2012). The study area soils are composed of an aggregate of silt, sand and loam (Figure 2.5). They are obtained genetically from sedimentary rocks, ophiolites and windblown sediments. The soils have a poor top organic-rich horizon as the soil profile is not well flourished. R-horizon is found in the eminence of the rocky area. In the locality of the ophiolites, the soils evolved are medium-to-coarse grained, thinner and have a light brown colour. The southern & western portions of the area are composed of saline soils (Naseem et al., 2012).

Figure 2.5 Soil classification in study area A. Windblown sediment B. River channel deposits (Naseem et al., 2012).

2.6 Hydrogeology

Hydro-geologically, Winder lies in the Winder River Basin. The aquifer of Winder, therefore effectively recharged through seepage from its distinct river in rainfall periods. Winder River lies at the south-eastern frontier of Balochistan and for

some distance the boundary between Sindh and the Balochistan provinces. It is positioned approximately 77 km to the west of Karachi. It falls into the Arabian Sea close to Sonmiani Beach. During the past years, a range of pumping wells has been inaugurated to fulfil the necessities of irrigation water supply (to increase vegetables, fruits, dairy and poultry production) and drinking-water supplies for the town (Bank, 2008). The water table in Balochistan province is highly impacted due to the drought cycle and excessive pumping of groundwater (Akhtar et al., 2021). The aquifer water table in the research area was at a shallow depth and rapidly declined in the last 2 decades, which will give rise to water shortages in the future (BUITEMS & UNDP, 2015). Further, extreme salinity issues related to seawater intrusion arise in coastal regions of Balochistan, especially in Winder.

2.6.1 Surface Water

Winder is the primary river of the study area. It appears from north-east of Mor and Pab ranges, passing from the constricted valley of Winder, to the south-western plains and finally drains into an Arabian Sea. The streams are sub-parallel in the plain areas and have low density and are also identified as dendritic in high-relief regions. Small streams are transient while comparatively large streams have limited water flow over the year. For irrigation purposes, several large tube wells are located in the research area. The water-bearing aquifers are deep > 50 meters and are confined at the contiguity of the sub-recent unconsolidated deposits with the overlying sand dunes. The groundwater aquifer is primarily contain medium to coarse sand, gravel, pebbles and cobbles (Bashir et al., 2007). During flash floods, there are transient tributaries that drain into the main Winder River. There are several storage structures observed in this research to accommodate and regulate the flow to recharge the groundwater. This can be clarified by the fact that there are intermittent flash floods during monsoon season.

2.6.2 Groundwater

The physical & chemical consideration of the groundwater play a vital role for irrigation purposes (Hakim et al., 2009; Hassan et al., 2009). The relevance of groundwater for irrigation is liable to the effects of the mineral constituents concentration of the water on both the soil and the fruit plant (Raihan & Alam, 2008). In the study area, some water sources are contributing to groundwater recharge. Rainfall is the first viable source. As Winder Town experiences insufficient rainfall, the contribution to shallow groundwater reservoirs from rain is very small. However, rainfall in the hinterlands and different regions surrounding Winder may remarkably contribute to the groundwater flow-system. The two sources of freshwater are the Winder River and the Mobar, Dhora stream. Water from Sirandar Lake is channelled to different residential zones for domestic and irrigation purposes (Naseem et al., 2012).

2.6.3 Agricultural Potential

The single, distinct and largest sector of Pakistan's economy is agriculture. It provides (20%) of the GDP and also engages 44% of the labor force (GoP, 2012). It also accounts for about (70%) of the foreign exchange incomes, through the export of raw materials and semi-manufactured and processed agricultural goods, especially cotton cloth, cotton yarn, cotton in raw form and rice. Agricultural activity is proficient all over Pakistan, about (68%) of the rural population mainly relies directly or indirectly on the agriculture sector (Pakistan, 2012).

The main key to development, even at present, lies in the proper sustainable exploitation of agricultural resources. The planning of agriculture should be carried out only after proper evaluation (Alizai, 1998). Food security is a basic problem apparently in developing countries such as Pakistan, where the increasing population is a major

concern (Ali, 2005). Despite having a considerable land area of farmable activities, it has been victimized by intense urbanization and also by the factors such as waterlogging and salinity. In this way, it is a great loss of agricultural land and can be compensate by developing and cultivating new regions. To provide long-lasting food security and safety to the rapidly increasing population and to intensify agricultural yield. It is also important to use the advanced latest agricultural techniques, increase cropping intensity, change major agricultural structures and policies etc. Since the five decades, the agriculture sector of Pakistan has gained a significant status where an average growth rate of 4% per annum (GoP, 2012). The diversification in this field is largely the outcome of an enhancement in the irrigation system, use of machinery in farming, application of artificial fertilizers and better-quality seed varieties (Khan & Dhanani, 1998). However, in this case, the viability of domestic food security & safety depends on traditional processes and this is one of the important concerns in the agricultural sector countries. The traditional and outdated types of agriculture practices such as fruit gardening, cultivation of crops and rangelands have been witnessed within the study area (Ahmed et al., 2013).

Winder is situated in a semi-arid zone having unpredictable rain. Therefore, farming crops and fruits completely rely on irrigation. The role of irrigation nowadays is essential to increase crop production (Jhorar et al., 2009). Irrigated sectors are small-scale but very fertile for crop cultivation (Mahar et al., 2013). Commercially in the Winder area, the most commonly grown staple food crop cultivated is wheat. In the study area, fruit cultivation is also an important and primary activity. It is one of the high-yielding farming crop as it gives suitable returns. Relatively in smaller localities, a large number of trees are cultivated and their fruits are harvested.

Livestock plays an important role in the economy of Balochistan, as it is a sub-sector of agriculture. Through this sector, more than 20% of provincial income is produced (DAWN, 2007). In the rural area of Lasbela plain, livestock is the primary dominant economic activity. It covers a vast part of the land for agriculture. For the best usage and protection of natural resources, geospatial information on the present state and grazing intensity is needed (Kurtz et al., 2010). Lasbela has a vast potential to initiate its extensive coastal area and rangelands to enhance overall agricultural productivity.

CHAPTER 3

LITERATURE REVIEW

3.1 Previous Work

The published literature of the study area mostly covered the stratigraphy, structure, Bela Ophiolite and geochemistry of water. Initially, geology of Lasbela was described by a British geologist (Vredenburg, 1909). The research work on the geology of the area mostly covered by Ghulam Sarwar and cited by Sarwar (1992); Sarwar and DeJong (1984); Sarwar (1982); Sarwar (1981); Sarwar and DeJong (1979). The stratigraphy of the area studied and published by Shah (2009), Smewing et al. (2002), Fowler et al. (2004), Hedley et al. (2001), Bannert et al. (1995), Fatmi et al. (1986), Rizvi et al. (1992) & Khan et al. (2018). The agriculture, groundwater and geochemistry related work for Balochistan and district Lasbela covered by Akhtar et al. (2021), Bashir et al. (2007), Naseem et al. (2010) and Hamza et al. (2014). Following are the summary of the published papers on the groundwater of Balochistan and the study area.

3.1.1 Water Resources of Balochistan, Pakistan – A Review

Balochistan, the biggest province of Pakistan, is facing drought conditions, water scarcity and quality issues due to which the community's livelihood & health are adversely effected (Sultan et al., 2022). Generally, when discussing about water, its significance as a resource for human survival and global economic development is of major concern. The agriculture sector contributes more than 20% of the total gross domestic product to the country and provides employment opportunities to 44% of the total labor force. Therefore, groundwater is the only option for different activities in the 90% area of the province while the 10% area suffers waterlogging and an immense amount of bad-quality groundwater. As per natural resources of water, 30% of the world's freshwater exists as groundwater and alarmingly this percentage of freshwater provided as groundwater is endangered due to the increasing population. With the prolonged droughts and a growing number of tube wells for irrigation, the primary constituents for survival depend on water resource which is groundwater. Particularly, there are several diseases connected with polluted drinking water in Balochistan which are diarrhoea, typhoid, hepatitis along infant fatalities. Furthermore, the underground water resources are contaminated greatly with heavy metals and pesticides. The extra and inappropriate chemical uses for agriculture worsen the threat (Akhtar et al., 2021). Apart from these aspects, groundwater brought an agricultural boom in South Asia previously in the two decades. Therefore 55% to 60% of the residents are dependent on groundwater irrigation.

According to Balochistan conservation strategy within next 50 years, more than 90% of all usable water resources including share of the province from Indus water would be overstressed. As a result, it has become crucial to formulate a policy in terms of pumping the groundwater, and it is not controlled by any rule for agriculture providing a free hand to pump excessively. A 2007 report stated that there is no such authority that controls the pumping of groundwater in Balochistan, though the purpose of water committees in the district is only for sorting out complaints registered for the spacing of the tube wells. Combining all the elements, it is now mandatory for the government to establish a control unit that can tackle the threat and as a result maintain

the continuity of the crops which grow in the region and greatly contributes to the economy of the country. Resolving the water issues in Balochistan entirely depends upon the groundwater rights which would restrict the unnecessary pumping of groundwater. The Law-making body should report this alarming situation in such a way that it provides the province as well as the country itself with a massive GDP in terms of the agricultural zone which seems to decline due to the mentioned issues (Akhtar et al., 2021).

3.1.2 Sustainable Groundwater Management in Balochistan

Pakistan is considered to be one of the world's most groundwater-dependent countries, with fertile alluvial floodplains but poor and very erratic rainfall. The study was based on observations of the tube wells in Balochistan from late 1990s and early 2000s. Groundwater development is frequently linked to irrigation system development, which has greatly aided increased food production, poverty reduction and sanitary mismanagement. Poor laws and the implementation of proper jurisprudence are among the reasons contributing to the depletion of groundwater resources in Pakistan. Instability in politics and a lack of political awareness tend to exacerbate the problem. Because groundwater is a common-pool resource, its management is complicated. It is difficult to establish and implement efficient groundwater allocation and licensing strategies. Balochistan is the largest of Pakistan's four provinces in terms of area (347,190 km^2). With an average annual rainfall of 200-250 mm, the region is classified as a desert. It is well-known for growing a variety of high-value crops, such as fruits and vegetables. Pakistan's groundwater policies in the 1970s and 1980s attempted to provide an alternate source of irrigation to enhance farm production and thereby reduce poverty, as well as provide water for home use. Many rural regions have been electrified and communication networks have improved, resulting in a significant increase in tube wells and dug well irrigation. Karez and springs were primary sources of irrigation for most of Balochistan's highland districts until the 1970s. Tube wells began to be erected in portions of the province after rural electrification. Farmers were

able to convert more land to increase the crops. The Government of Pakistan also increased the number of tube wells and groundwater extraction between 1980 and 1990 to accommodate the demand. Groundwater resources were overexploited because of the development of high-water-using crops like horticulture. Drought (1998-2004) and aquifer overdraft have caused a substantial number of tube wells to fail since 2000. There is a real danger of losing effectiveness and efficiency if agencies are not brought together to plan and manage water resources effectively. The government has started drought repair programs. Many farmers have lost their supply of irrigation and, as a result, their livelihoods (Mushtaq et al., 2013).

The World Health Organization (WHO) has recommended a groundwater management blueprint that aims to improve institutional governance and efficacy, as well as supply- and demand-side components of groundwater management. Improved governance, effective governance, institutional efficiency, demand-and-demand-side groundwater management, community social adoption and effective coordination and cooperation are the five essential parts of the design. It also requires better quantification of groundwater yield and monitoring on a regular basis. The groundwater management should include a rational pricing system for efficient water use. One of the most critical elements toward sustainable groundwater management is community adoption. It entails giving regional groundwater resources a sense of ownership and forming basin-wide groundwater users' organizations (WHO, 2021).

To prohibit unlawful water extraction for agricultural and other reasons, social norms and rules must be executed. The outline for long-term groundwater management would necessitate extensive community participation in the planning process, particularly in terms of advising suitable uses and values of local groundwater systems. It would be necessary to have some decentralization as well as good vertical integration of different levels of government (provincial and local). This design for sustainable groundwater management in Balochistan includes essential features such as social acceptance and transforming groundwater cultures, which can internalize externalities (factors that have received insufficient attention in past plans). However, achieving sustainable groundwater resource management would be extremely difficult without strong political commitment and excellent coordination. Pakistan's groundwater policies are not well-designed to address the challenges of groundwater sustainability.

They are inadequately implemented and based on a lack of geophysical expertise. With the region's groundwater systems rapidly deteriorating, a transition from groundwater development to groundwater management policies is urgently required (Mushtaq et al., 2013).

3.1.3 Agricultural Potential in Winder Basin

Winder area holds potential for cultivation but this source could not be escapade appropriately. The main objective of the research was to discover the accessible activities for land reclamation which are carried out by the exploitation of resources found in the location and to find out the prospects for the future development of the area. This study presents the agricultural system prevailing in the Winder Basin and investigates the type of land cultivation activities in the area. It also helps to assess the ground utilization and hypothesize the future trends in the cultivation system in Winder Basin. Crop cultivation and fruit farming are important features of farming activities in the Winder Basin. The land of the area is being used for animal feed it is remarkably important. Rainwater and wells are used for land cultivation. Field observations deduced that the farming area will be raised in the future by replacing the land (Ahmed et al., 2013).

3.1.4 Geochemical Stream Sediment Survey in Winder Valley

The Winder stream and its tributaries were evaluated using a geochemical survey. The Winder stream collects silt deposits primarily from Pab and Mor ranges the southern extensions in the Lasbela District (Balochistan). Rocks ranging in age from the Jurassic to the Cretaceous are exposed in these two mountain ranges. The Ferozabad Group consists of Lower–Middle Jurassic carbonates and siliciclastic that make up

majority of the Mor Range. Mississippi Valley Type (MVT) and the Stratiform Sediment-Hosted (SSH) deposits host syngeneic and epigenetic Pb–Zn–Ba mineralization in these strata. Active stream sediments from the Winder and its tributaries were used to establish quantitative estimations of mobile and immobile components. Atomic absorption spectroscopy was used to look for Zn, Ag, Cu, Pb, Ni, V, Co, Mn, Fe and Ba in the samples. These elements' abundance is explored with the local region geological factors such as climate, bedrock, mobility, weathering and the pH of the dispersing fluids. In the research area, many Zn anomalies have been identified. The new regions for Zn mineralization have been identified at Kharrari (360 ppm), Sand (340 ppm) and Draber (210 ppm). The current analysis also suggests that the Mor Range rocks may contain Ag, Cu and V. Scatter diagram have been used to identify relationships between diverse elements, which indicate genetic correlations. Whereas the correlation between Cu–Zn (0.55, n=18) was positive and Cu–Pb (0.63) is linked to possible mineralization of sulphide (Naseem et al., 2002a).

3.1.5 Biogeochemical Prospecting of Sulphide Minerals in Winder Valley

The research aimed to ascertain the consequence and appropriateness of vegetation as a sampling medium in the exploration of mineral deposits in Winder valley. The concentration of Copper, Lead and Zinc was analyzed in three plant species such as Acacia Arabica, Tamarix Aphylla and Salvadora Oleoides. Variation in species was observed at the sampling station due to distance from bedrock, climate, mobility and exclusion mechanism of flora. The best result was observed in Acacia Arabica due to deep roots. In plant species, Cu and Zn were in high concentration as compared to Pb due to less mobility (Naseem & Sheikh, 2002).

3.1.6 Hydro-Geochemistry of Winder River & Adjoining Tributaries

A methodical approach is presented in this paper to assess the geochemistry of groundwater to determine the relationship between environmental conditions and bedrock which has an impact on the distribution of the elements in groundwater. Quantitative evaluation of groundwater and streams drained through Bela-Ophiolite and sedimentary rocks of Mor and Pab ranges has been made. The association of anions and cations has also been appraised to determine their mutual relationship. This study also determined the essential hydro-geochemical parameters for the evaluation of groundwater quality according to WHO standards for domestic uses. The results of this study conclude that groundwater geochemistry of Winder valley also depends on the climate, pH, degree of weathering of rocks exposed in the area, drainage pattern and movement of ions. The presence of Na^{+}, Mg^{2+} and Cl^{-} linked with the rocks exposed in study area. The major ions in collected water sample of study area are in the permissible limit as per WHO (Bashir et al., 2007).

3.1.7 Geochemistry of Cd in Groundwater of Winder, Balochistan and Suspected Health Problems

The research was conducted to analyze the groundwater of the Winder area and its surroundings for the presence of Cd and relate it to the health impacts on the local community. Winder is situated in the south of Balochistan, in the vicinity of exposed Pab and Mor ranges and Bela Ophiolite. The goal of this research was to characterize the abundance of Cd in the groundwater of Winder and to monitor its health impacts. A total of 48 samples of soil and groundwater were collected: 10 from mountain aquifers, 8 from the near river and the remaining from alluvial aquifers. Cadmium is a soft metal, with a low melting point, which is usually present as different hydrothermal cluster compounds. Cd can leach out by dissolution and form aqueous complexes in

groundwater. A high concentration of Cd (mean 10 µg/l) had been observed in the samples, mainly near the Winder River, with decreasing values moving away from the river. Sulphides from sedimentary rocks are responsible for high concentrations, while the Arabian sea is responsible for lower concentrations. pH influences the presence of Cd in groundwater; however, samples near the mountain aquifers showed an insignificant link with pH (Naseem et al., 2014).

3.1.8 Impact of Cadmium Polluted Groundwater on Human Health

Ongoing infections and geologic climate have a strong link. Geochemical condition has been viewed as a huge causative variable of major medical problems. Various examinations had been directed to interpret the connection between land climate, consumable/drinking water and infections as they were considered to have set off experiencing sicknesses among individuals. Persistent sicknesses and geologic climate have an interlinked relationship. Although infections brought about by microbes are liable for most medical issues, inorganic components particularly arsenic, cadmium (Cd) and mercury can be causal sources. The Cd a poisonous minor component, is found in many rocks, just as in coal and oil, in exceptionally low fixations, frequently in blend with zinc. Geologic stores of Cd can fill in as their sources to groundwater and surface water, particularly when in touch with delicate, acidic waters. Persistent iron deficiency can be brought about by delayed openness to drinking water defiled with Cd. The ebb and flow concentrate on have been led in those spaces where the substance of Cd in the groundwater was high. For this reason, a questionnaire-based survey was directed to correspond to Cd-borne infections among the occupants of the area. Field study is a typical technique for the fundamental examination of infirmities dependent on actual side effects. The assortment of 48 groundwater tests at a normal distance of 1 to 2 km between the examining destinations has empowered an adequate topographical portrayal of appropriation of minerals and components. Stream and groundwater tests were gathered in polyethylene bottles washed with inspecting water preceding water assortment. The examples were

separated through a 0.45 m layer and gathered in pre-sanitized polyethylene inspecting bottles (1.5 litre). Bottles were filled and fixed to prevent oxidation. Country regions are portrayed basically by a farming economy and a relaxed lifestyle. A moderate, unskilled, male overwhelmed society with took advantage of females, guys partake in their lives in a variety of ways, because of which unrefined birth rates are high, prompting joblessness, low earnings, neediness and hardship with a few indications, including un-healthiness and undernourishment. Winder Town is one of the urban communities of Balochistan and because of their low quality of life, occupants being uninformed about water palatable norms are neglectful of illnesses brought about by weighty metals like Cd, Pb, F, As, etc and henceforth continue to endure. Conducted questionnaire surveys gave significance among circumstances and logical results nature of Cd bearing sicknesses among which kidney, joint and night visual deficiency are more noticeable. Because of these peculiarities, the harmful danger of Cd in drinking water was high according to determined wellbeing peril records. The utilization of this water by the residents might cause medical issues and disorders among the occupants of the area (Burke et al., 2016).

3.1.9 Assessment of Geochemistry of Soils for Agriculture at Winder

The soil geochemistry assessed in accordance with its potentiality for agriculture principles and the accumulation of major and microelements in the soil. Seventy-two soil samples were obtained to measure their pH, electrical conductivity, organic matter and texture. Trace elements geochemistry of the Winder area soil shows relevancy with Bela Ophiolite and sedimentary rocks in the Mor and Pab ranges of Cretaceous and Tertiary ages respectively. This study is beneficial for cultivators to improve irrigation strategies in the area.

Ophiolitic rocks are the sources for the accumulation of trace elements such as Chromium, Copper, Cobalt and Cadmium, Iron and Zinc in the soil. Alkalinity, calcareous sandy soil and organic matter lower the concentration of these trace elements

than the average value in the study area. The XRD mineralogy indicates the presence of quartz and calcite in high concentration with iron oxides and clay minerals in variable quantity. The appropriate management of the nutrients is suggested by the analysis of trace element geochemistry. This will improve the constitution and efficiency of the crops and reduce the environmental damage to humans (Naseem et al., 2010).

3.2 Geology of Pakistan

Pakistan covers an area of 796000 sq. kilometres and comprises complex geological structures. Basically, Pakistan lies on Indian, Eurasian and Arabian plates. Indian and Eurasian plate collision in Tertiary (Copley et al., 2010) developed three highest orogenic belt such as Karakoram, Hindukush and Himalayas in north of Pakistan. Indian Plate rapid movement toward the Eurasian plate for collision summarized in Figure 3.1 resulted due to plume push and double subduction activity. The current movement is 10 cm/year and it was faster in Cretaceous ∼18 cm/year (Yoshida & Santosh, 2018). The Indian plate separated from Gondwana in southern hemisphere and cover 9000 km toward the northern hemisphere from 200 Ma to Present day (Figure 3.2). The Indian plate collided with the Eurasian plate ∼50 Ma.

The collisional belt obducted numerous geological feature exposure of granite, flood basalt Ophiolite and volcanic arcs in north (Figure 3.3). In south of Pakistan Arabian oceanic plate can be identified as subduction zone beneath the Makran block subpart of Eurasian plate. The plate boundaries interaction in tectonic of Pakistan developed classical example of structure and stratigraphic feature for geological field. Geologically region provides rich economic resource such as oil and gas reserves, minerals and water resources. Most of the Pakistan area covered by sedimentary rock and it is divided in to two main basins named as Indus and Balochistan basin. The basin further classified into two sub basin (Figure 3.4). The Indus basin preserve the history from Precambrian to Cenozoic sediments whereas Balochistan basin comprised a succession of Mesozoic to Recent.

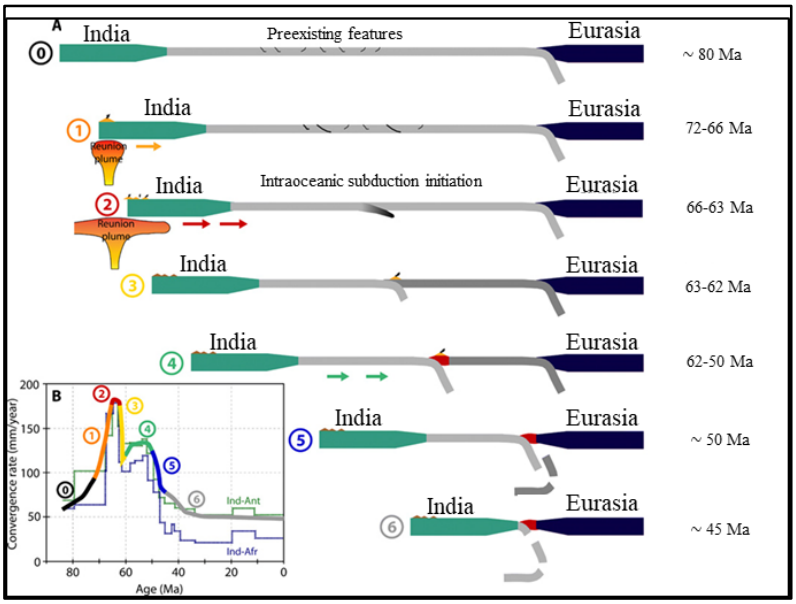

Figure 3.1 Indian and Eurasian plate convergence history since 80 Ma. A. represents the phases of convergence evolution of Neo Tethys sea, major events such as subduction, double subduction and collision. B. represent the hypothesized subduction rate vs age with reference to phases of convergence (Cande & Stegman, 2011).

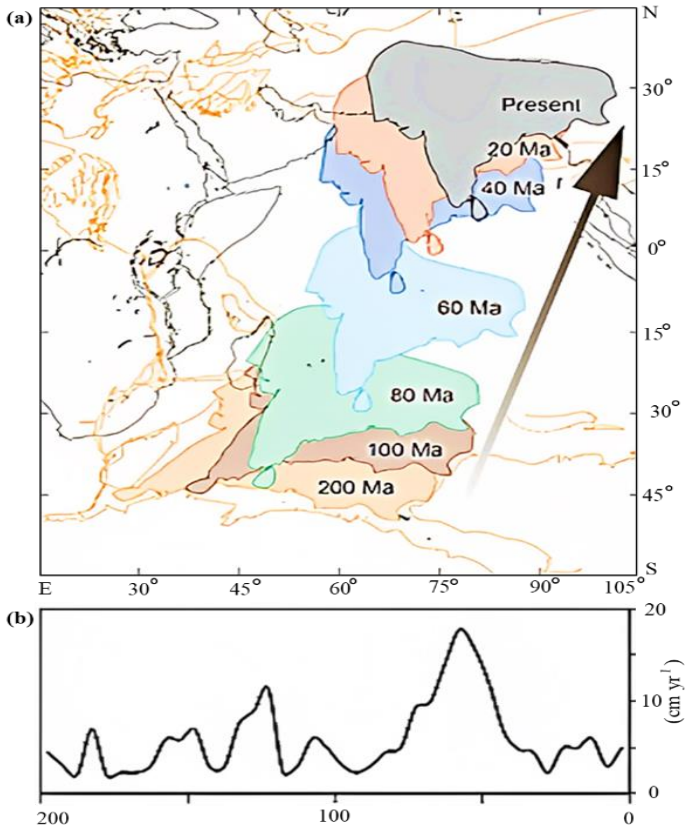

Figure 3.2 Indian Plate movement northward from 200 Ma to present respectively plotted on Gplates 2.0 software (Müller et al., 2018; Yoshida & Santosh, 2018; Seton et al., 2012).

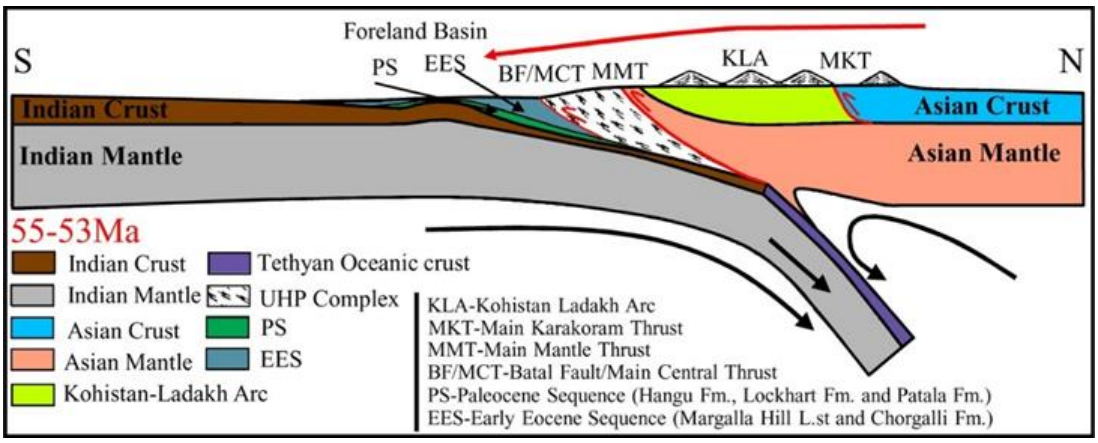

Figure 3.3 Indian and Eurasian collision obducted complex features of continental and oceanic crust (Ding et al., 2016).

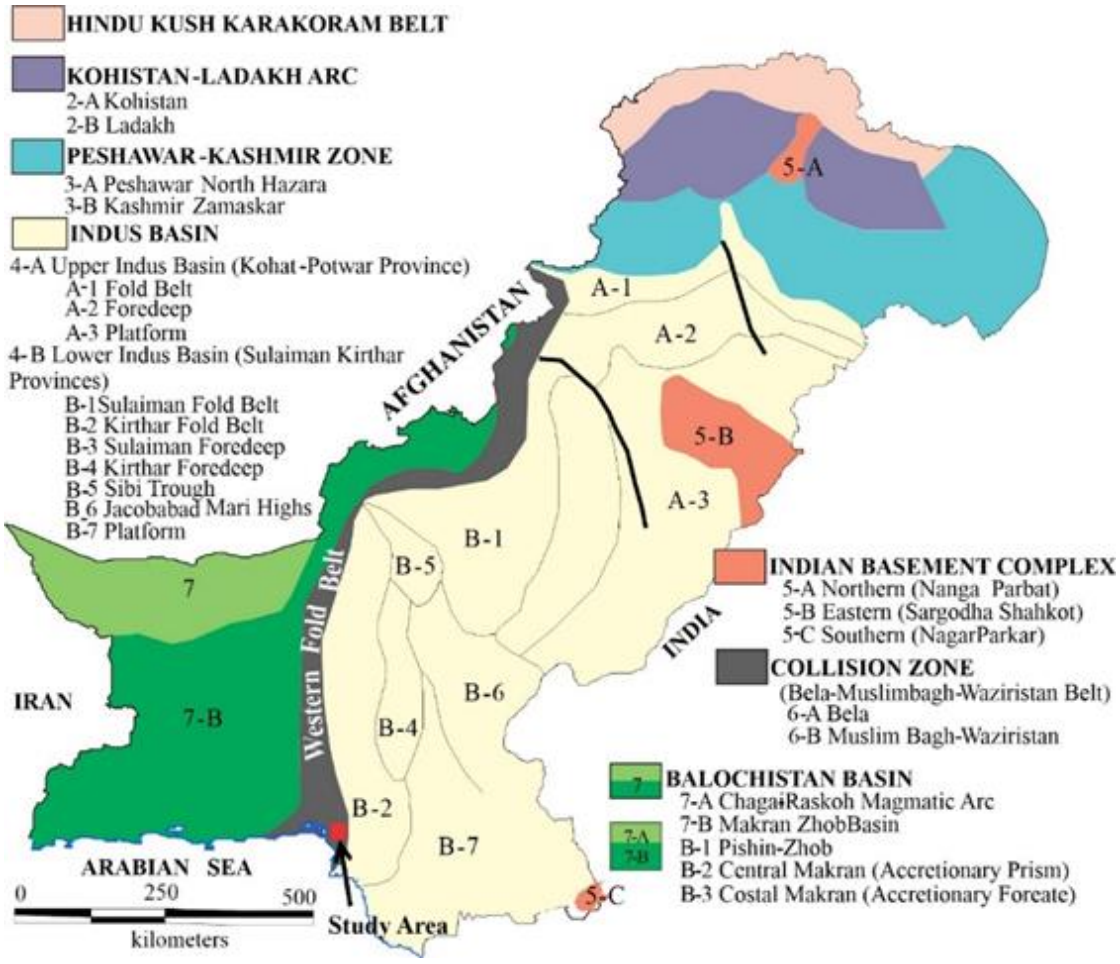

Figure 3.4 Map shows the division of the sedimentary basin of Pakistan, fold belt, Arc and basement complex (modified after Qureshi et al., 1993).

The vigorous nature of Indian Plate movement resulted volcanism, high sedimentation and sea level fluctuation effecting the Cretaceous rock (Spicer et al., 2003). The research area is situated in south-west of Pakistan and represents the southern edge of western fold belt. It also represents fascinating geological features and is surrounded by Pab & Mor range in the eastern part. The triple junction zone and Makran subduction in south-west, Khuzdar-Knot in the north and Ornach-Nal fault in the western side of study area (Figure 3.5).

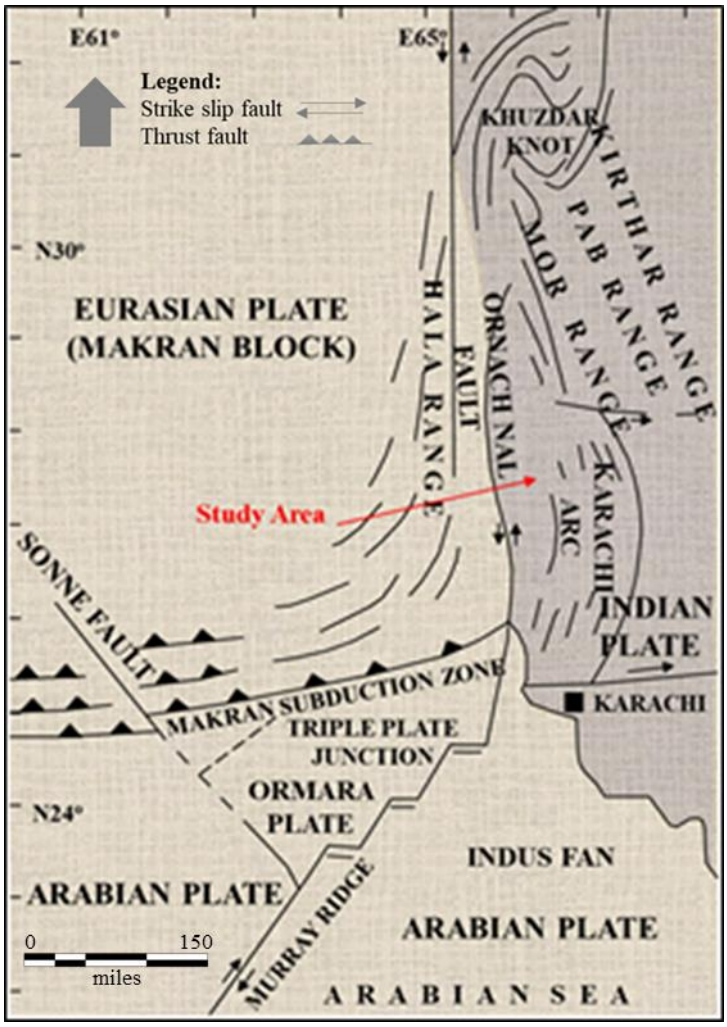

Figure 3.5 Study region surrounded by Pab & Mor Ranges in the east, Subduction zone in the south and Ornach Nal fault in the west (modified after Sarwar, 2004).

The outcrop exposure is mainly covered by Jurassic to Tertiary rocks consisting of sedimentary and igneous rocks (Figure 3.6). To understand the detail geology and regional tectonic of area the stratigraphic record, tectonic event and Ophiolite formation and composition were reviewed from published literature.

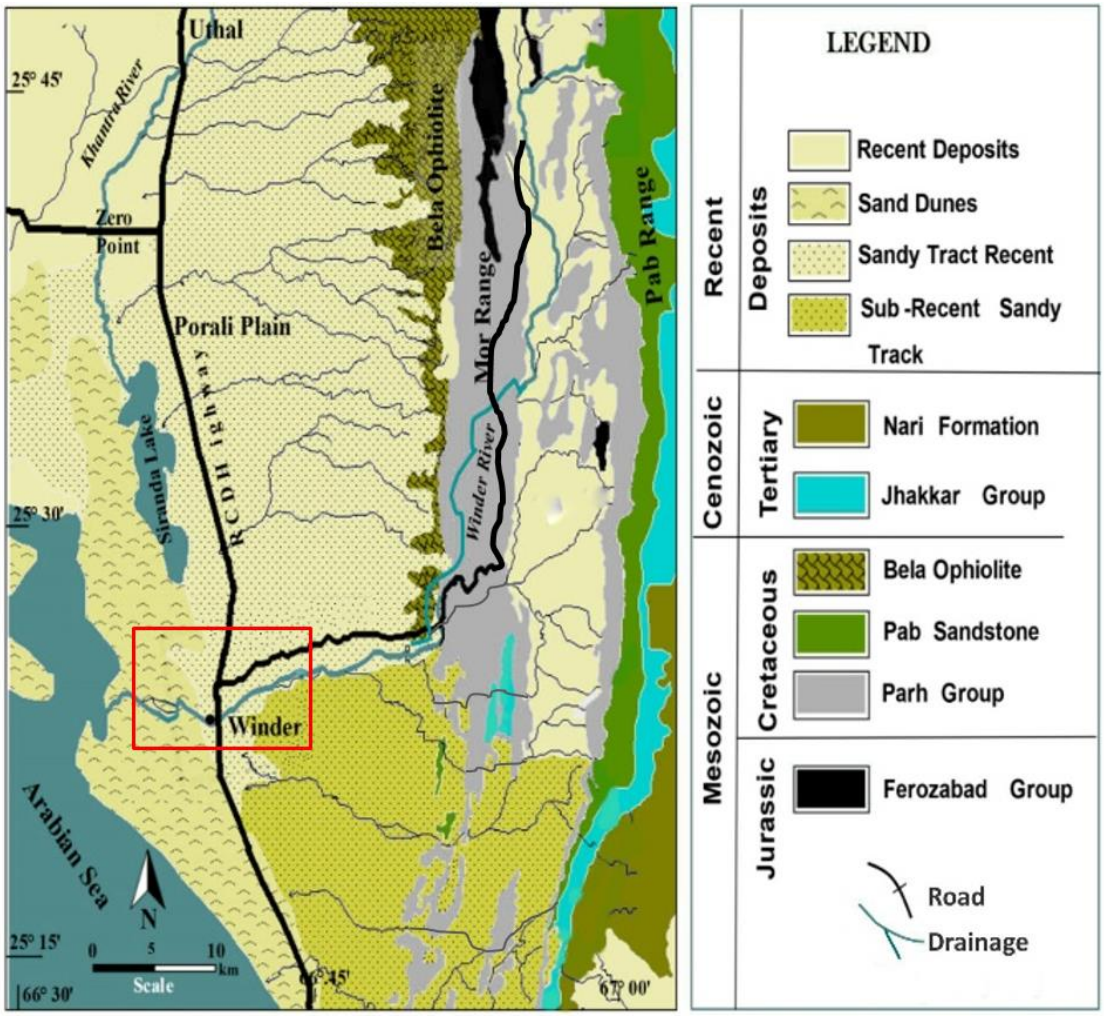

Figure 3.6 Outcrop exposed in the vicinity of study area covered by Jurassic to Recent sedimentary and igneous rock (modified after HSC, 1960).

3.3 Regional Tectonics

Tectonic cycles in past shaped a continent and later fragmented into pieces and drifted over a viscous asthenosphere. There are two main super continent of different ages Rodinia 1100 Ma, Pannotia shaped and remaining 550 Ma age before the dispersal. Finally, Pangea was formed surrounded by the Panthalasa Ocean. During Jurassic the Pangea split into Laurasia and Gondwana continents (Condie, 1997). Further sub-continent were also formed such as Africa, India, Australia and Antarctica (Kumar et al., 2007). The Indian Plate drift was initiated approximately 130 Ma earlier before separation from Antarctica and Australia. Northwest drift of Indian plate relative to Antarctica and Australia at the rate of (3-5 cm/year) and further extended east of the Madagascar 90 Ma ago. Indian plate separated from the Madagascar in late Cretaceous. The breakup increases the movement rate by 150 to 170 mm/year during 80 to 50 Ma (Mahoney, 1988). On the other hand Indian plate lower part turned out and thinned because of the plume activity (Kumar et al., 2007). In last Indian Plate movement direction became anticlockwise and collided with the Eurasian Plate 55-50 Ma (Figure 3.7).

The evolution of oceanic crust Bela Ophiolite gives two contrasting ages. The lower unit of Bela Ophiolite (accretionary prism) build in Albian at approximately (90 Ma) and the top unit is set up all through Senonian ~80Ma) (Gnos et al., 1997). These Ophiolite had drifted the north alongside the Indian-Seychelles block throughout Late Senonian 70 Ma. The movement resulted the development of east-west dipping subduction regions between Asia & India (Peters, 2000). The region from westward dipping subduction process was preserved in the form of metamorphic body in Bela & Muslim Bagh ophiolites (Khan et al., 2007a; Khan et al., 1999; Mahmood et al., 1995) display that the intra-oceanic subduction originated among 70 & 65 Ma. The obduction originated through 65 Ma onto passive margin of Indian Plate. The last thrusting comes to an end in early Eocene 55 Ma. Along the Ornach-Nal fault, a western margin of the Indian Plate more specifically Bela-Khuzdar region collided to the Eurasian Plate specifically Makran in the Late Eocene to the Early Oligocene. This event made a

complex indirect collision tectonic setting of the region in a record (Yoshida et al., 1997).

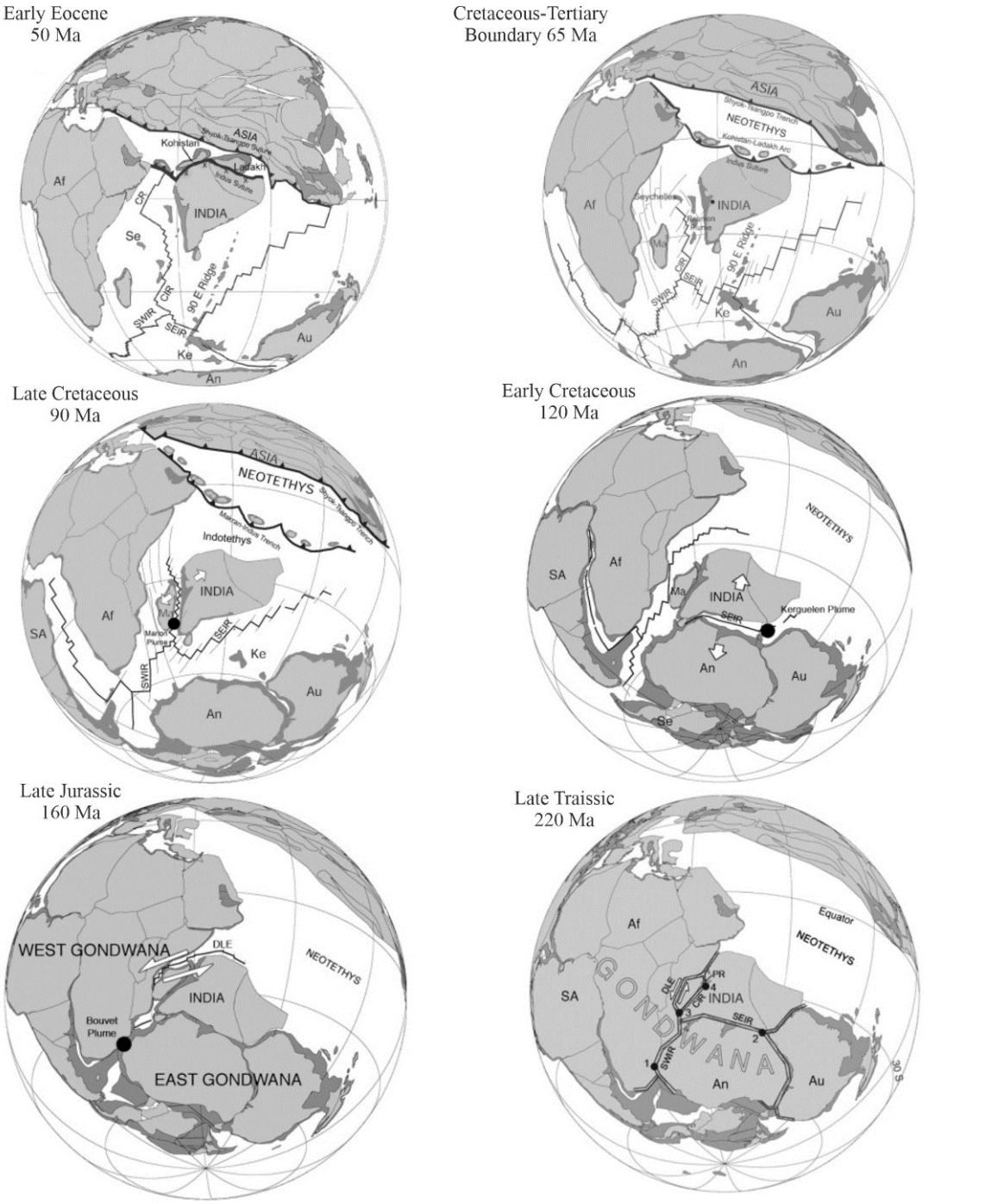

LEGEND: 1. Bouvet plume (~180 Ma) 2. Kerguelen plume (~118 Ma) 3. Marion plume (~88 Ma) and 4. Reunion plume (~65 Ma). Af, Africa; An, Antarctica; Au, Australia; CIR, Central Indian Ridge; DLE, Davie and Lebombo–Explora transforms; PR, Palitana Ridge; Sa, South America; SEIR, South East Indian Ridge, and SWIR, Southwest Indian Ridge.

Figure 3.7 Paleogeographic reconstruction shows the position of the Indian plate approximately from 220-50 Ma. (a) 50 Ma initial collision of Indian plate with Asia and Neotethys sea closure (b) Indian plate movement relative to Gondwana during Cretaceous-Tertiary (modified after Chatterjee et al., 2013).

3.4 Major Regional Structural Features

The major structural features are the Chaman Fault (Lawrence et al., 1981), fold belts, transform fault and Khuzdar Knot (Niamatullah, 1998) (Figure 3.8).

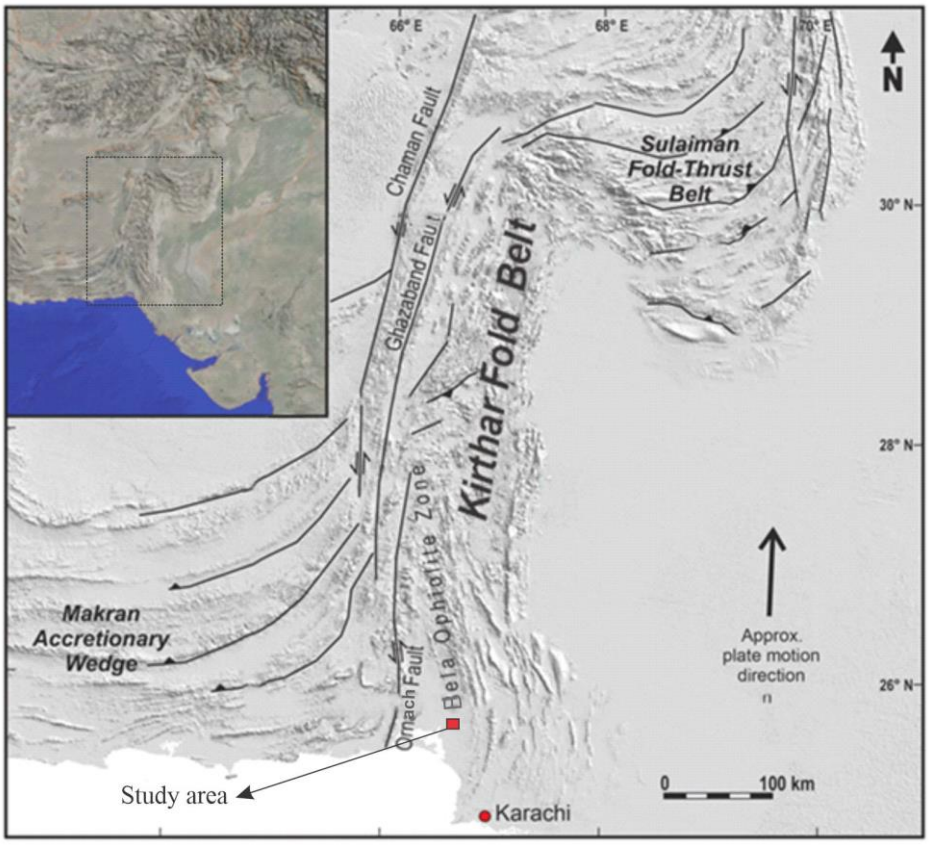

Figure 3.8 Structural and relief map of western Pakistan represent the major structural features extension (Bela Ophiolite and southern edge of Kirther fold belt in the vicinity of study area (Hinsch et al., 2019).

The Arabic plate subduction comprises an 800 km long Makran accretionary wedge, a Triple Junction where three plate boundaries meet and mud volcanoes at the foot of the Makran continental margin (Delisle, 2004; Wiedicke et al., 2001; White &

Louden, 1982). Chaman transform zone in the western margin of Pakistan can be identified as the boundary between the Indian and Eurasian plates (Farah et al., 1984). This transform zone extends north-south across Balochistan. The Chaman transform zone contains sub-parallel transform fault such as Chaman, Ornach Nal, Hoshab and Ghazaband (Shah et al., 2021). The Ornach Nal fault is present in the west of the study area near the Nal in the north and extended toward the south in Makran region (Niamatullah, 1997). It separates the Makran flysch in the west and Bela Ophiolite in east. The Ornach (south) and Nal (north) are the names of a village on the east of fault (HSC, 1960). The fault developed in 20-25 Ma and become active in the Late Oligocene to Early Miocene (Lawrence et al., 1981).

Khuzdar-Knot is a complex structure formed in Khuzdar toward north (Figure 3.8). It was identified as a swirling feature in the middle of Kirther fold belt (Sarwar & DeJong, 1979). Sedimentary rocks (Mesozoic age) cover approximately 5000 km^2 area.

Makran accretionary wedge is 800 km east-west trending features from Iran to the coastal area of Pakistan (Priestley et al., 2022). This feature formed as a result of Arabian Plate subduction beneath the Eurasian Plate during the Palaeocene at a rate of ~10mm/year (Byrne et al., 1992). The thick Cretaceous to Tertiary succession covered the accretionary prism comprising ~7 km thick sequence supplied by river's erosional material from the mountains (Kaveh et al., 2022). The surface exposure was identified as a thrust wedge and asymmetrical tight folds (Khan et al., 1991).

Karachi arc is located the southeast of Winder. Tectonically this region lies within the Karachi-Khuzdar block (Bannert et al., 1995). Karachi arc is a thin-skinned thrust and folds belt presently it is moving the east on the decollement surface, facilitated by Sembar & Goru shale of Cretaceous age (Sarwar & DeJong, 1979). Karachi arc consist of Tertiary sequence which are gently dipping (plunging folds) with northwest & south-west axes. The east-west fault distinct the limit of the southern fringe of Karachi-arc (Thakur & Wesnousky, 2002). A triple Plate Junction comprises Eurasian Plate (continental) west of the Chaman Fault, Indian Plate (Continental) east of Chaman Fault and Arabian plate (Oceanic) south of Makran subduction zone is a prominent geological feature in south-west of study area (Qasim et al., 2021).

3.5 Stratigraphy

The stratigraphic sequence of the study area was reviewed to understand the mineral composition and provide a base to correlate and assess the influence of rock on the surface and groundwater of region. Unlike the Indus Basin (Kohat-Potwar zone) the Balochistan Basin does not have the stratigraphic succession from Precambrian to Recent. The Balochistan comprises the stratigraphic record from Mesozoic to Recent age sediments. The Mor Range (Jurassic), Winder Valley and Pab Range (Cretaceous) represent the stratigraphy of study area (Figure 3.9).

Province	Age	Formation	Description
Pab Range	Cretaceous	Pab sandstone	fine-coarse grained medium thick beddded quartz rich sandstone with minor shale.
		Parh limestone	white, bluish, white, medium light grey, creamy thin bedded, limestone rich in fossils
Winder Valley		Bela Ophiolites	harzburgite, lherzolite, dunite peridotite, serpentine, olivine gabbro & pillow basalt
		Goru formation	pink, light grey creamy thin bed with pink light grey shale & sst.
		Sembar formation	dark greenish grey, olive green belemnitic shales with siltstone and nodular limestone
Mor Range	Jurassic	Anjira formation	argillaceous limestone, calcareous shales
		Loralai formation	platform facies micrite limestone with shale beds
		Spingwar formation	sandstone with calcareous beds increasing up section & interbeds of glauconitic sandstone

Figure 3.9 The Jurassic-Cretaceous stratigraphy of the Mor Range, Winder Valley and Pab Range (modified after Shah, 2009).

3.5.1 Ferozabad Group

Fatmi et al. (1986) modify the classification of the Jurassic sequence in Khuzdar region and referred as Ferozabad Group. Moreover, the Jurassic rock is classified into groups and formations (Kazmi & Abbasi, 2008).

3.5.1.1 Kharrari Formation

Primarily the Spingwar Formation (Fatmi et al., 1986) was the name of the Kharrari formation (Fatmi et al., 1999). Jurassic is the age of formation which also extend into Triassic (Shah, 2009). The formation consists of limestone and dolomite and a thick sequence of sandstone, siltstone and shale deposits. The limestone was identified as grey colour; calcite vein is present. The sandstone is green to brownish colour, clays show black to greenish grey colour having fissile and flaky nature. The thickness of the formation at the type section is 464m. The clastic sequence formation also comprises sulphide mineral veins (Ahsan & Mallick, 1999). Deltaic conditions were identified from the petrified wood in lower part (Ahsan, 1995).

3.5.1.2 Malikhore Formation

The type locality of formation is located near Khuzdar city approximately 27 km toward the west. This formation is mainly dark grey to black colour, thin to medium compacted deposits and comprises crystalline limestone (Shah, 2002; Ahsan & Mallick,

1999; Kadri, 1995). The transition contact is marked with the overlying Anjira Formation (Shah, 2009; Fatmi, 1977).

3.5.1.3 Anjira Formation

The uppermost formation of the Ferozabad Group is known as Anjira Formation (Anwar, 1991). The lithology depicts a thin calcareous mudstone bed, shale and limestone shallowing upward environment of deposition. The lower contact is conformable in most locations whereas the upper contact is disconformable and overlain by Sembar Formation (Ahsan, 1995).

3.5.2 Sembar Formation

In the Cretaceous sequence, the oldest formation in the study area is the Sembar Formation (Kazmi & Jan, 1997). Clastic rocks are significantly comprised in this formation, where the paramount part accommodates black shale eventually by sandstone & siltstone with nodular limestone. The Sembar Formation comprises glauconitic shale and siltstone (Kadri, 1995). In the study area, exposure of Sembar Formation characterizes by argillite and weathered into pencil shape sediments. In Sembar Pass the type locality of the formation is present, at approximate thickness of deposits 133 m, whereas 262 m for the Mughal Kot (Kazmi & Jan, 1997). In this formation observed common fossil was belemnite. The Sembar sequence comprises foraminifera. Sembar Formation age is Neocoian but is more likely to extend into the Late Jurassic. The Chichali Formation of Kohat-Potwar Province is correlated with the Sembar Formation (Shah, 2009).

3.5.3 Goru Formation

The type locality of formation is Goru village showing 536m thickness. In study area the Goru Formation is uncovered along the foothill of Mor Range. It consists of thin bedded argillaceous rocks grey to black colour (Williams, 1959). Limestone is present at topmost part and base of formation. The lower part is interbedded with thin shale deposits (Kazmi & Jan, 1997). Upper section contains thin bedded and light colour with subordinate shale succession. Sand is rare in upper part of this formation (Kadri, 1995). An unconformity is present between Goru and Parh limestone (Ahsan, 1995).

3.5.4 Parh Limestone

The Parh Limestone is present in the rocks of the Parh Range. The multi coloured limestone is resistant and consists of medium to thin beds. Foraminifera indicates the Late Cretaceous age (Shah, 2002; Allemann, 1979). The limestone thickness is 268 m in the Parh Range type locality (Khan, 1998; Kazmi & Jan, 1997). The Limestone is overlain by the Cretaceous agglomerate of Porali, the east of Lasbela (DeJong & Subhani, 1979). The complete section is not exposed in study area.

3.5.5 Fort Munro Formation

The upper part of the formation is sandy and the lower section is argillaceous limestone (Akhter & Masood, 1991). It is thick bedded and grey to black color. The

reef building fossil was also reported and associated with shallow marine environment (Naseem et al., 2005c).

3.5.6 Pab Sandstone

The Pab Sandstone description was presented by Vredenburg (1909) from Pab Range. The type locality is in the north-east of the study area. The formation contains medium to coarse grain sandstone and interbedded shale. The colour of the sandstone is white, off-white, cream, grey and brown (Shah, 1977).

3.5.7 Korara Shale

Korara Shale is present on the southern side of the Pab Range. The Jakkher Lak identified as the type locality. The Khadro Formation in the lower Indus Basin is equivalent to Korara Shale (HSC, 1960). The formation comprised olive grey to dark grey shale deposits with a minor trace of clay and fine grain sandstone. In Pab Range thickness of shale is 460m. Phosphatic nodules are common in south-east of study area. The intrusive dykes of dioritic, gabbroic and sills of Porali are emplaces in some localities.

3.5.8 Kirthar Formation

Kirther Range Eocene strata are named as Kirther Formation (Noetling, 1903). The formation can be found to the north of Quetta and Thatta in the south (Iqbal & Shah, 1980; Shah, 1977). Kirthar Formation primarily consists of thick limestone with minor bedding of marl (Shah, 2002). It also has caverned features and the upper portion is cliff-forming. Towards the northeast of the study area especially in Shah Noorani large caves are present in this formation.

3.5.9 Nari Formation

Nari Formation is recognized by the stratigraphic committee of Pakistan (Shah, 2002). The formation mainly comprises sandstone, shale and siltstone. In subordinate thick reefal limestone is also present. The depositional environment of sandstone was placed in shallow marine, fluvial to fluvio-marine conditions. It can be revealed by the grain size evaluation and thin-section studies. The formation further divided into five units from older to recent in the Karachi vicinity as Orangi, Ghora Lakhi, Halkani, Pir Mangho and Tobo members.

3.6 Mineralization in Study Area

The host rocks of the study area contain sulfide deposits which consist of metallic minerals (Zinc, Lead, Copper, Barite etc). These deposits are linked with the Sedex, Kipushi, MVT, and Manto types (Megaw et al., 1996; Smith, 1996). The

Ferozabad Group also contains different types of sulphide mineralization deposits and is associated with MVT, Sedex and vein-type mineralization (Ahsan & Mallick, 1999). The Angira Formation in Mor Range comprises Sedex-type (Malikhore and Kharrari).

3.7 Ophiolites Sequence

An Ophiolite is a Greek word; Ophio means snake and Lite means lithos (stone). The name ophiolite was introduced in 1821, by Alexandre Brongniart for a variety of uncommon rock suites. These rocks were composed of serpentine (snake stone in Latin) and other mafic and ultramafic rocks. Similar rocks were also observed by European geologist in the Alps which were very uncommon on land. The ophiolite rock sequence represents the ancient oceanic crust preserved in orogenic belts and provides 3D records to examine the product of magmatic, geochemical, metasomatic & tectonic processes operating at the seafloor spreading centre and subduction zone (Dilek, 2006).

The concept of plate tectonic clears the formation of ophiolites and exposure on land. Worldwide large-scale ophiolites are present, during a process of obduction, structurally this feature appears as a coherent and prominent allochthonous thrust complex of remnant oceanic crust. The continental margin sedimentary rock, pelagic sediment and volcanic sequence are also associated with ophiolites emplaced on the continental margins (Coleman, 1977). Within an oceanic basin, the ophiolites sequence is created by seafloor spreading. Along the margin of major tectonic plates they are mostly confined, formed either in an ordinary mid-oceanic ridge (Martínez et al., 2021) or the back-arc basin (BAB). Ophiolites may arise as a nappe (intact thrust sheet), melange (tectonic mixture of fragments), or dismembered ophiolites (preserved in a highly dismembered state).

Ophiolites are of variable thicknesses and are mostly composed of six distinct segments. There is no identical thickness of ophiolites throughout the globe. Only a few have comprised complete sequence, the classic examples are Bela Ophiolite in Pakistan

and Semail ophiolites in Oman (Cox & Cox, 2000). In the majority cases, sub units are missing in ophiolites (Condie, 1989). The parts of ophiolites in the form of graphical illustration have been demonstrated by many ophiolite geologists (Condie, 1989). The descriptions of each segment of Ophiolite are given below and the ideal Ophiolite sequence is presented in Figure 3.10.

3.7.1 Ideal Ophiolites Sequence

The ideal ophiolites sequence consists of Ultramafic tectonite, Gabbro rocks, Sheeted Dykes, Extrusive Basalt and Pelagic sediment at top (Moores, 1982). The lower most sequence of ophiolites is composed of Peridotites from the residual mantle. It consists of fertile mantle rocks composition, enriched in lherzolite. The composition changes upward gradually into Harzburgite-depleted mantle rocks. The unit is separated by Mohorovicic discontinuity from overlain Gabbro unit. The rock crystallized due to the partial melting of underlying peridotite rocks which produce the main magmatic chamber under the spreading centre. Gabbro shows cumulus texture in the lower part. Pyroxene mineral layering is present in gabbro due to differential segregation.

The dykes marked the transition zone between extrusive and intrusive rocks. Rising magma at mid-ocean ridge (MOR) spread apart and connects the intrusive and extrusive upper volcanic. The extensional regime formed the vertical subparallel dykes at MOR. Dykes act as a conduit for magma to erupt at the seafloor and form a pillow. Plagiogranite is also found at the base of sheeted dykes in association with mafic gabbro. The upper most igneous part of Ophiolite is basalt. Pillow structure forms due to the crystallization of magma in cold sweater circulation. The chemical composition of pillow lava mainly contains Fe, Ti and K. Fine crystalline material is the product of rapid cooling due to marine water at the upper part of Basalt. Copper silicate ($CuSiO_3$) and Chrysocolla mineral are frequently found in contact with a chilled margin.

The top section of Ophiolite characterizes by deep abyssal plain oceanic sedimentary rocks underlain by pillow basalt. The thickness of sediment covers depends on the sedimentation. It consists of hematite-rich argillites, radiolarian cherts, limestone and greywacke sandstone. The variation in colour pelagic sediments is due to fluctuation in depositional environment pH, Eh etc. The emplacement of Ophiolite on continental margin is the product of obduction after the formation of sequence (Moores, 1982; Gass, 1980). According to the emplacement styles the ophiolites can be classified into two major types named Cordilleran type and Tethyan type ophiolites sequence. The Cordilleran type ophiolites are usually found on the hanging wall of subduction zone emplace on the active plate margin whereas Tethyan-type ophiolites emplaced on the passive margin (Dilek & Furnes, 2014; Dilek, 2003; Dilek & Newcomb, 2003).

3.8 Global Ophiolite Belts and Nomenclature

The ophiolites sequence nomenclature is used to differentiate the type on the basis of orogeny, genetic, emplacement and composition. Major orogenic events related to ophiolites are the late Proterozoic Pan African orogenic belt, Early Palaeozoic Appalachian-Caledonian belt, Mesozoic Alpine Himalayan belt and Circum-Pacific orogenic belt (Ishiwatari, 1994; Yakubchuk et al., 1994). The Tethyan (0phiolites) are part of the great Palaeozoic Ocean/ Paleo Tethys Sea formed due to the breakup of the Pangea. In Triassic, a new ocean was formed named as Neo-Tethys sea (Bortolotti & Principi, 2005). The ocean zone of large Mesozoic oceanic crust referred as Neo-Tethys. Proto-Tethyan ophiolites was developed throughout the rifting in the eastern tropical part of the Pangea. The Paleo-Tethyan ophiolites sequence is broadly exposed in Myanmar and China, whereas Eastern Europe, Arabia and Pakistan-Iran preserved the Neo-Tethyan ophiolites. There are two distinct settings for the development of ophiolites sequence. Supra subduction Zone (SSZ) and Mid Ocean Ridge (Martínez et al., 2021). During the rifting in the oceanic interior, the melting of the mantle occurs. The hot lava eruption forms a new ridge known as Mid Oceanic Ridge (Martínez et al.,

2021). MOR ophiolites are further classified based on growth rate low (1-3 cm/year) and fast (10-17 cm/year). The SSZ ophiolites are formed due to the closure of basin when the collision of two oceanic plate begin and finally one plate subduct under the other and may develop an arc. The SSZ ophiolite is formed by older asthenosphere melting and represents the composition of MOR basalt and island arc tholeiite to boninite rocks (Dilek, 2006). The geochemical composition of Neo Tethyan SSZ contains island arc tholeiite (Patriat & Achache, 1984) and MORB (Dilek et al., 2007). Mostly SSZ ophiolites are part of fore arc basin whereas back arc basin is not important for the subduction related ophiolites. However, in the subduction back arc ophiolites composition is very close to MORB (Shervais et al., 2004; Shervais, 2001). Himalayan to Mediterranean region the ophiolites are initiated at convergent plate margin and also interrupted by hotspot magma (Khan et al., 2007a). This has been verified by the presence of rock island arc basalt (IAB), oceanic island basalt (OIB) & the mid-ocean ridge basalt (MORB) in Bela Ophiolite (Sheth, 2008).

The ophiolites of world can be divided into two classes based on morphology, thickness and composition of magma (Nicolas, 2012). In first class harzburgite ophiolites developed by the depleted mantle rocks (Timotewos & Reddythota, 2000). They are melted below a MOR to construct the overlying oceanic exterior in the ophiolite sequence. In second class Iherzolite (Bortolotti & Principi, 2005) represents the lower segment of mantle typically more fertile. This type is not common and its occurrence is very rare. On the basis of tectonic and geochemical properties (Figure 3.11), the Bela Ophiolite identified as first-class HOT type (Bashir, 2008).

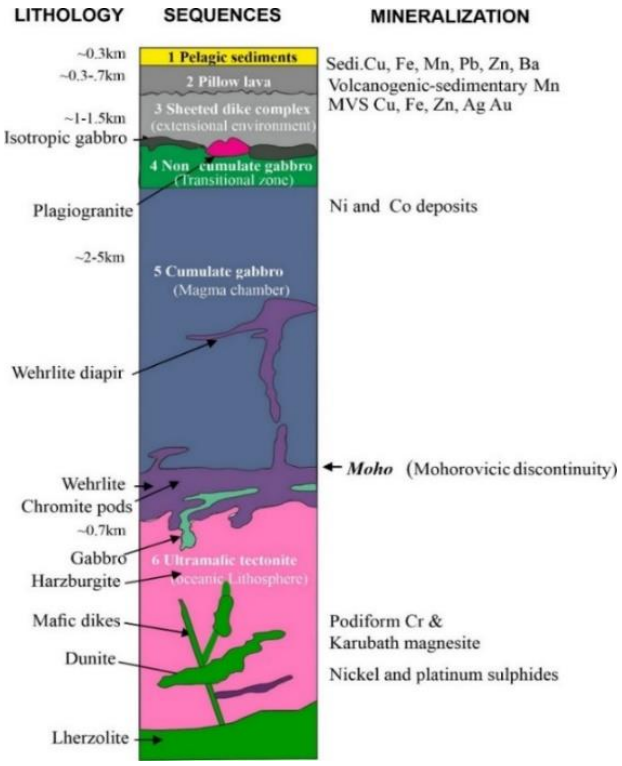

Figure 3.10 Ideal ophiolites cross-section representing lithology, mineralization and thickness of each unit (modified after Mahmood et al., 1995; Coleman, 1977).

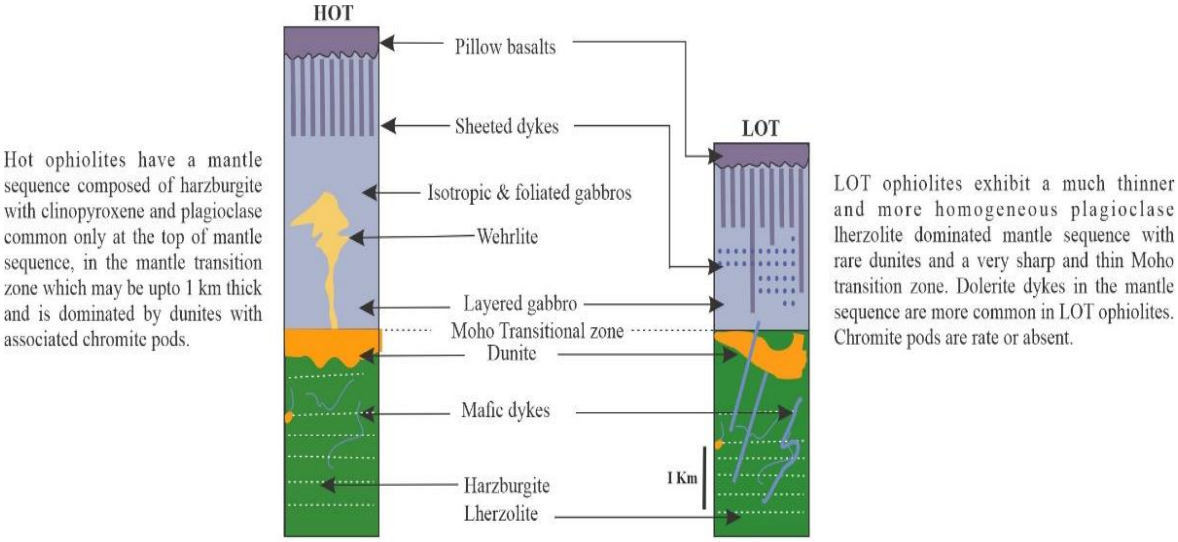

Figure 3.11: Difference between HOT and LOT Ophiolites.

Ophiolites are abundant in varieties of non-metallic & metallic minerals (Mitchell & Garson, 1981). However due to the difference in formation and origin, the mineral composition is not uniform in the ophiolites of the world. The pelagic deposits

are a rich sources of Nickel, Chromium, Titanium, Cobalt, Manganese, Vanadium and Copper etc. In study area, composition of ophiolites has a major influence on a sedimentary sequence.

The sites of ophiolites are rich in economic minerals (Kearey et al., 2009). The lower part of the sequence of ultramafic igneous rock comprises platinum, nickel, chromite and magnesite (Bashir et al., 2009). In Pillow lava section the large amounts of sulphides (Fe, Cu, Ag, Zn and Au) are confined. The Fe and Mn is present in the upper contact of pillow basalt and pelagic sediment. The topmost section of pelagic deposits mainly comprises Cu, Fe, Pb and Mn etc.

3.9 Ophiolites in Pakistan

Ophiolites of Pakistan are associated with an Alpine Himalayan Orogenic Belt. It extends from the Maghrebides in northwest Africa and covers through European Alps, the Dinarides-Albanides-Hellenides in the Balkan Peninsula, the Anatolide-Taurides in eastern Mediterranean, Oman and Makran in west of Indian Ocean, Tibetan Himalayan in the east and finally to Indo-china Peninsula in southeast. The approximate area is a 10000 km^2 long high elevated mountain exposed at surface characterized by young orogenic crust and widespread active seismic activity (Dilek, 2006). The belt was developed during the evolution of Tethys Ocean as discussed earlier through continued complex processes of opening & closing of Plate and Neo Tethyan sea (Dilek & Furnes, 2019; Dilek & Yang, 2018; Stampfli & Hochard, 2009; Stampfli & Borel, 2002).

The ophiolites of Pakistan formed on Neotethys ocean floor during Late Cretaceous. The composition is harzburgite type. In Pakistan, the Ophiolite sequences are situated along a belt in the western and northern margins of the Indian Plate (Khan et al., 2018; Khan et al., 2007b**).** The ophiolites of Masirab, Semail, Muslim Bagh,

Bela, Waziristan and Ras Koh are underlain by well-established and preserve accretionary wedge embracing pelagic deposits of lower-middle Cretaceous The pelagic sediment further grade up into the emplacement associated calcareous turbidites (Gnos et al., 1997).

The ophiolites of Pakistan can be correlate with the SSZ origin based on the formational processes, geochemical composition and nature of metamorphic rock (Sheth, 2008; Mahmood et al., 1995). The emplacement of ophiolites on passive margin of Indian Plate (continental) occurred during the time of late Cretaceous (Allemann, 1979). Tectonically, ophiolites in the western belt of Pakistan trend north-south at the southern edge of the Eurasian Plate. It also depict the contact between the Afghan block (Eurasian Plate) and Indian continental plate (Gnos et al., 1997). The major feature is Ornach-Nal & Chaman strike slip fault on western side of the Indian Plate (Ahmed, 1993).

Ophiolites are less deformed in the western part and hold a complete sequence and are rarely found in large sizes. They are dominated in an array from north to south. The Helmond Block of Afghanistan is also the part of Ras Koh Ophiolite dipping under the Chagai arc that occurs fully with sediments cover and represent subduction features in Ras Koh mountain (Gnos et al., 1998). The subduction of the Indian Plate beneath the Eurasian, ophiolites are placed in northern Pakistan that are evident along the thrust/suture region (Qasim et al., 1993). The suture zone appends the Main Karakoram Thrust (MKT), Main Mantle Thrust (MMT), and Main Boundary Thrust (MBT). Ophiolites in the northern belt of Pakistan exhibit parallel structures to the regional features (formation and structures) (Khan et al., 2007a). Unlike Bela, the ophiolites are tectonically disturbed due to the stresses of the main mantle thrust (Kazmi & Abbasi, 2008).

The Bela Ophiolite (BO) outcrop is a most comprehensive and prime feature of oceanic lithosphere in the geology of Pakistan (Khan et al., 2018). It is the southern part of an approximately 450 km belt striking north-south exposed in Gadani in the south and Sange Siah in the north of study area (Kazmi & Abbasi, 2008). In north-east of study area, it consists of 3-5 km thick sequence comprising Pillow Basalt, sedimentary rock (Argillite, Chert and Limestone) and Gabbro sills. Debris of serpentine in large

blocks up to kilometers, carbonate-serpentine breccia, pelagic limestone and less commonly gabbro, basalt, peridotite and metamorphic equivalents present throughout the sequence (Sarwar, 1992). The age of ophiolite on the basis of pelagic micro-fauna is Albian (Gnos et al., 1998).

In southern Tethys between Indian Plate and Africa during Cretaceous, the tectonostratigraphic substructure of the Bela Ophiolite occurred whereas the regional tectonic evolution suggests that the Ophiolite likely develops along the fracture zone. During Paleocene to early Eocene the fracture zone was shifted to transform movement gradually into convergence which resulted in Ophiolite emplacement (Sarwar, 1992).

On the basis of emplacement style and age difference, Bela Ophiolite further subdivided into two units i.e. upper unit and a lower unit. The tectonic accretionary wedge of older material consists of lower unit. Ophiolite's true sequence starts from Sonaro (north) which represents the upper unit of Bela Ophiolite. Dolerite dykes and sills intrude the upper unit. The lower part of a top unit is a metamorphic sole and is overlain by a basaltic flow and intrusive rocks (gabbro and granite) (Khan et al., 1999). The northern Bela Ophiolite composition is mainly based on ultramafic rocks. It contains serpentinized and other rock units at top gabbro, basalt, diabase, plagiogranite and doleritic sheeted dykes (Bashir et al., 2004). The southern part mainly contains pillow basalt in large size and irregular form mostly exposed in the southern tail of Bela Ophiolite. The composition of pillow basalt tholeiitic, low-K collection lavas also detect component signatures of E-kind MORB (Khan et al., 1999). Sarwar (1992) on the basis of REE and other factors depict that Bela Ophiolite created in MORB region and has the feature of IAT. According to Arif et al., (1997) & Gnos et al., (1998), based on the geochemistry, Bela Ophiolite developed in the SSZ site. The ophiolites is complex and clear stages of origin (Gnos et al., 1998; Arif et al., 1997). The primarily established totally on geo-chemical research confirmed that the BO devise in SSZ site. The BO is complex and has clear phases of its origin (Khan et al., 2007a). BO formed as a result of Neo-Tethyan obduction of oceanic crust at the rifted Indian Plate (MORB) western margin, back arc basins in a massive oceanic fracture zone and obduction of island-arc (Sheth, 2008).

3.10 Electrical Resistivity Method in Environmental Geophysics

Environmental Geophysics can be well defined as the usage of geophysical methods to image and know subsurface rock properties and related processes (Hatch & Street, 2021; Styles, 2012). The term Environmental Geophysics deals with the estimation of physical properties in the shallow subsurface (Soupios & Kokinou, 2016; Annan, 1997; Sharma, 1997) The application of environmental geophysics involves laboratory studies, theoretical modelling and fieldwork (Styles, 2012). The depiction of the near surface geological features is achieved by applying a diverse geophysical method under variety of conditions (Christensen, 2000). These techniques are divided into active & passive groups. The active methods cover ground penetrating radar, seismic refraction/reflection and electric/electromagnetic which use artificially created fields on the earth's surface to measure and understand the response of the earth. Whereas, passive method (Soupios & Kokinou, 2016) are gravity, magnetics and self-potential, measuring the subsurface and interpreting signals, which are generated by the natural fields of the earth. The shallow subsurface Geophysical method is cost-effective and fast way to examine the subsurface hydrogeology (Parker et al., 2022; Kearey et al., 2002).

An intense increase has been observed in using the geophysical methods for groundwater exploration and quality mapping for the last two decades due to advanced development in electronic technology and modelling (Metwaly et al., 2010; Olayinka, 1992). The ultimate objective of the above revealed geophysical techniques is to gather all the information regarding the near-surface interior. It also contributes to the construction and safety of human infrastructures, the health and heritage of living beings, the protection of life and the preservation of natural resources in condensed populated regions. More specifically, environmental geophysics is involved in the investigation, detection and monitoring of construction works (Adamo et al., 2021; Kokinou & Sarris, 2011; Wightman et al., 2003; Hinze, 1990; Daniels, 1988) such as dams, highways & bridges, underground pipelines and tanks and any related technical near surface problem. Dangerous pollutants to public health and the surroundings (Ntarlagiannis et al., 2016; Power et al., 2014; Georgaki et al., 2008; Wilson et al.,

2006) such as fertilizers in soils, heavy metals and the groundwater. Mapping of archaeological sites (Sarris et al., 2013).

Environmental Geophysics largely applies non-destructive methods to explore the shallow subsurface in limited and extensive areas, in certain conditions (Yiran et al., 2022). The presence of contrast in subsurface physical properties, during acquisition the sampling parameter with respect to time and space are selected to account all existing information which provide true subsurface conditions, the method provides the solution based result in all conditions and also the appropriate data processing play a vital role in geophysical projects misleading erroneous processing step will pride wrong interpretation of subsurface image structure and physical properties.

Electrical Resistivity is an active technique used to achieve objective of the research. It is one of the effective techniques to map the subsurface resistivity and potentials of aquifers. The electrical resistivity survey is convenient, due to lucrative and efficient method for analysing the occurrence of groundwater in the aquifer (Parker et al., 2022). Geophysicists extensively use this method to determine clay aquitards, saltwater intrusion, the thickness of bedrock, the types of soil and the spreading of groundwater contamination (Bayowa et al., 2022). In this method, continuous electric current is penetrated through the rocks (Ahmed et al., 2020). The electrical resistivity technique is a part of geophysical methods which utilized as a preliminary step for groundwater exploration (Ahmed et al., 2020; Dor et al., 2011). It has been employed to compute the thickness of layered media and used to map the geological environment of aquifer. It has been successfully used for groundwater mapping due to efficiency, simplicity and non-destructive approach as compared to conventional techniques (Heaney, 2017; Dor et al., 2011). The accuracy of this method is great and is sufficient for electrical interference. The electrical resistivity technique applying vertical electrical sounding is extensively gaining application in groundwater, environmental and geotechnical engineering geophysical investigation (Ouzerbane et al., 2022; Yonis, 2022; Afolayan et al., 2004; Auken & Christiansen, 2004).

3.11 Resistivity Theory

The Electrical Resistivity technique is mostly utilized to calculate & map the resistivity of subsurface rock properties (Fajana, 2020; Loke et al., 2020). It is also known as a survey that is employed to present the image of subsurface electrical properties by penetrating an electrical current along the numerous diverse paths and determining the associated voltage (Abidin et al., 2011). The electrical resistivity technique depends on the response between the earth and electrical current flow. It is very sensitive to differences present within the electrical resistivity of the subsurface and measured in Ohm meter (Ωm). Resistivity measurements are achieved by inducing an electric current into the earth, using two current electrodes (A and B) and measuring the output voltage at potential electrodes (M and N). The apparent resistivity (ρa) can be intended from the current (I) and voltage (V) by using equation 3.1.

$$\rho a = K * V/I \quad \text{……..……..} \qquad \text{eq. (3.1)}$$

Where k represented the geometric factor that depends on the arrangement of four electrodes.

The depth of imaging depends on the electrical resistivity method according to the spacing between electrodes. Greater depth is attained by increasing the electrode spacing during the data acquisition. The total length of the electrode layout also plays a significant role in resulting in larger subsurface depth imaging (Lech et al., 2020).

3.12 Basic concept (Resistance, Voltage & Current)

In an electric circuit, Resistance is well-defined as the measure of opposition to the flow of current. It is measured in ohms' units and it is denoted by omega (Ω). Ohms is defined by the German physicist named Georg Simon Ohm (1784-1854), who examined the connection among voltage, resistance and current. The change in an electrical potential between two points, which (in a stationary electric field) is described as the work required per unit of charge to move a test charge among the 2 points, is known as voltage. Volts is the SI unit for voltage and is denoted by (Newell & Tiesinga, 2019).

The rate of flow of electric current past a region is distinct as an electric current. It exists wherever there is a net flow of electric charge through an area. In the international System of Units (SI), the unit of electric current is known as Ampere. It is defined as the flow of electric charge through an outward at a rate of one coulomb per second. The device that is used to measure the electric current is known as Ammeter. Ohm's law provides the relationship between Resistance, Voltage and Current. Ohm's Law states that the current (I) passing through a conductor is directly proportional to the voltage (V) across it, therefore equation 3.2.

$$V \alpha I$$

Simply,

$$V = IR \qquad \text{……..……..……} \qquad \text{eq. (3.2)}$$

Where R is Resistance a constant, which is defined as the resistance available by the material of the conductor to flow of current through it (Heaney, 2017).

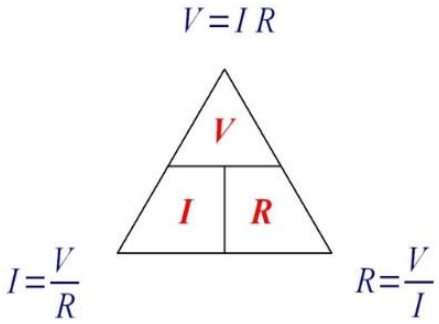

Figure 3.12 Relationship between current, voltage and resistance (Heaney, 2017)

The association between Voltage (V), and Current (I) in a circuit of constant Resistance, (R) produce a straight line i.e. relationship with the slope equivalent to the value of the resistance as shown in Figure 3.12.

The resistance of an object is directly proportional relation to the resistivity of the material it is designed from, proportional to the object's length. It is inversely proportional to the object cross-sectional area. The resistance of a wire with its cross sectional area (A) & length (L), the material of resistivity (ρ), is shown in Figure 3.13 and given by the following equation 3.3 (Heaney, 2017).

$$R = \frac{\rho L}{A} \qquad \ldots\ldots\ldots\ldots\ldots\ldots\ldots\ldots\ldots\ldots\ldots\ldots\ldots\ldots \qquad \text{eq. (3.3)}$$

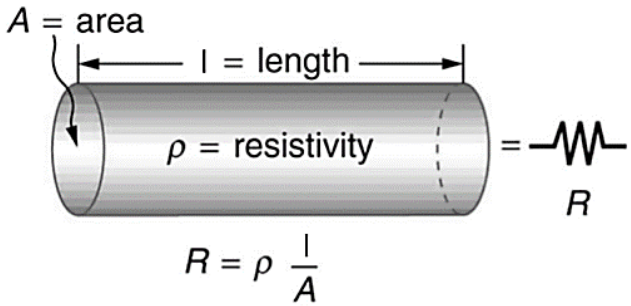

Figure 3.13: Relation between the length of a wire and its cross-sectional area, where R is the resistance of the wire (Heaney, 2017).

3.13 Resistivity Measurement

The electrical resistivity (ρ) can be intended by the electrical resistance of a uniform specimen of the material and the cross-sectional area of the specimen (Tumanski, 2006) as presented in **(**Figure 3.14).

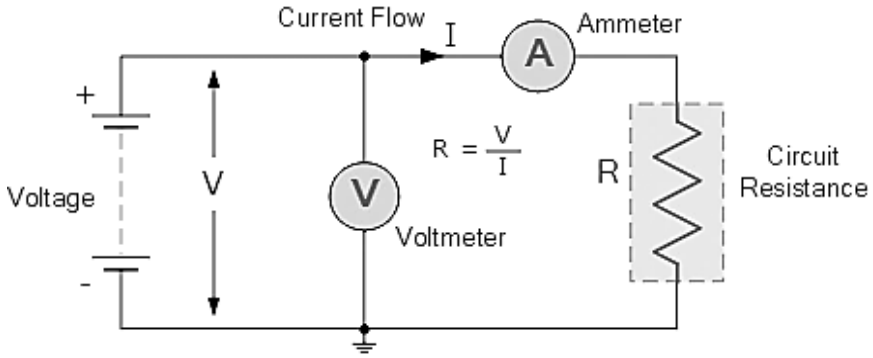

Figure 3.14 Schematic illustration shows the resistance of a conductor.

Where are: V- Voltage, A-Ammeter, R-Resistance, I-Current and Ohm-meter (Ωm) is the SI unit of electrical resistivity (Reissland, 1989).

3.14 Resistivity

Resistivity generally depends on conducting salt presence, moisture contents, compaction and temperature (Tung & Lim, 2017). Conducting salts might be present naturally in the soil or they can be added externally for decreasing the resistivity. Nitrate, chlorides and sulphates of sodium, magnesium or calcium, potassium usually utilized as soil additives (Virkutyte et al., 2002). These additive salts dissolved in the moisture present in the soil in order to decrease the resistivity and the provision should be made for water addition in to the soil surrounding. Moisture is an important condition for increasing soil conductivity. The moisture present in soil can differ with the season and it is suitable for this reason to pinpoint the electrodes at a depth where moisture is

present throughout the year. Because of this, the soil resistivity does not fluctuate abruptly during the annual weather variation. temperature variation also effects soil resistivity. It has a major effect on soil resistivity at or near 0º C where resistivity sharply increases. The compaction parameter also controls the resistivity, generally resistivity increase with the compaction of rock (Seladji et al., 2010).

3.14.1 Refraction of Electrical Current

In resistivity, current electrodes utilized to add electrical current in the ground resulting potential is calculated by the potential electrodes located in the ground. The inner electrodes which are also the potential electrodes are associated with the voltmeter whereas the outer electrodes known as the current electrodes are connected with an ammeter to pass current into the ground. The current will move radially symmetric with two electrodes placed at a distance in the uniform body of earth having no restrictions. If the boundaries are existing or lithology changes, the current will flow from a resistive medium to a more conductive medium. The charachterstic of current is that it flows to a more conductive medium than the resistive medium. Because to this, the flow of current refracts from its track if the resistivity changes across the medium (Keller & Frischknecht, 1966).

3.14.2 Current Flow in Geological Material

The flow of an electric current i.e. the movement of charges in subsurface rocks and minerals takes place in three means that are electronic, electrolyte and dielectric condition.

i. Electronic (ohmic) condition

In an Electronic (ohmic) condition, the current flow in materials covering free electrons such as metals. It is very significant for the exploration of mineral prospects (Parkhomenko, 2012).

ii. Electrolyte condition

In an electrolyte condition, the current is supported by ions at a relatively slow rate, because most of the rocks are poor conductors and would have very large resistivity despite the point that they are generally porous and the pores are occupied with fluids, predominantly water (Keller & Frischknecht, 1966). Due to an electrolyte condition, DC current flow in rocks which depends on pore fluid and pore geometry. The impact of mineral grains of the matrix is very little, except if it is a metal ore. The large differences in resistivity are shown by geological materials, $1.6x10^{-8}$ for native silver to $1x10^{6}$ for pure sulphur.

iii. Dielectric condition

This kind of conduction occurs in poor conductors or insulators, which have very limited free carriers or none at all. The atomic electrons are expatriate slightly as regards their nuclei, under the influence of varying external electric fields. This slight relative separation of positive and negative charges is identified as dielectric polarization of the material and a current is produced known as the displacement current (Parkhomenko, 2012).

3.14.3 Resistivity Scale for Different Types of Rocks

Out of all the geophysical properties of rocks, electrical resistivity is by distant the utmost variable. Values reaching as much as 10 orders of magnitude may be met and even distinct rock types can vary by numerous orders of magnitude (Palacky, 1987). A representative chart is shown in Figure 3.15 which illustrates the overall resistivity of important rock groups when compared to each other. The scale is logarithmic and indicates a wide range in conductivity/resistivity among rocks. From the given chart it can conclude that massive sulphides and graphite bearing rocks are highly conductive, carbonate sequence and loose/unconsolidated sediment are very resistive in dry conditions, igneous and metamorphic rock fractured or weathered are more conductive than the tectonically undisturbed igneous and metamorphic rocks, sedimentary rocks comprised clay minerals are generally conductive and presence of saltwater in pore spaces of rock increase the conductivity whereas freshwater identified as less conductive (Parkhomenko, 2012).

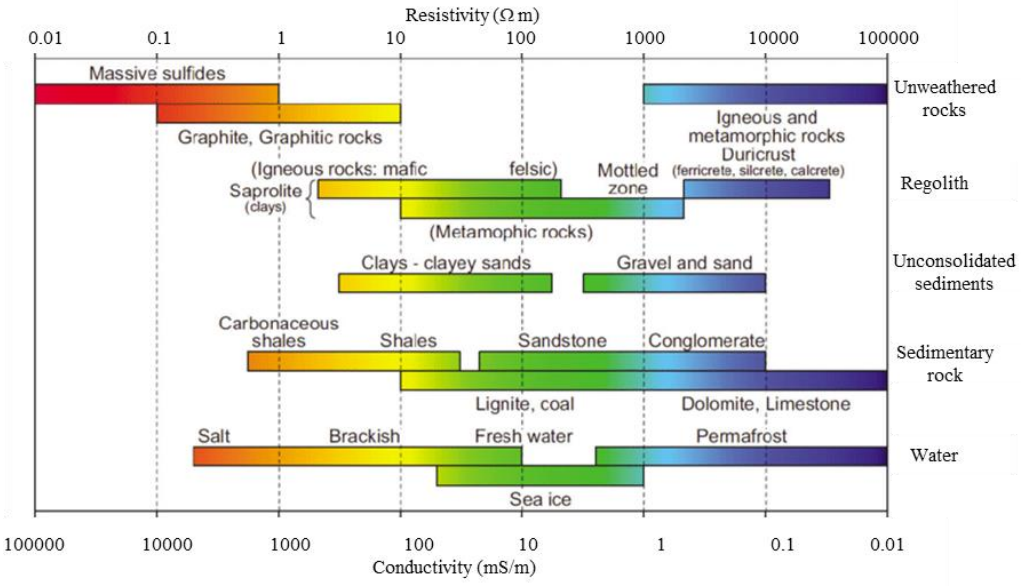

Figure 3.15: Resistivity scale for igneous, sedimentary and metamorphic rocks (Palacky, 1987).

3.15 Applications of Electrical Resistivity Method

The most popular applications of the resistivity method to map the subsurface geological structure, depth of bedrock, groundwater depth, soil properties, groundwater pollution and seawater intrusion (Almeida et al., 2021; Anoop et al., 2021; Hasan et al., 2020b; Hasan et al., 2020a; Hilbich et al., 2009; Georgaki et al., 2008; Samouelian et al., 2005). The electrical resistivity technique is a better geophysical method for groundwater exploration. Water content and its dissemination changes the electrical properties of subsurface rocks. Generally, the resistivity is inversely proportional to water saturation and porosity of rock. The salinity of water also performs an essential part, resistivity value decreases with an increase in salinity. The presence of clay in the rock also reduces the resistivity (Reynolds, 2011; Telford et al., 1990; Zohdy et al., 1974). Electrical resistivity technique is generally used for groundwater exploration studies (Tsourlos, 1995). Provide information about the vertical dissemination and aerial extent of fresh, saline and brackish water bodies can be found by vertical electrical Sounding method (Auken & Christiansen, 2004). It is helpful in identifying potential groundwater-bearing zones in the relevant areas and provide aid in drilling programs planning. Utilized for the identification of groundwater potential zones produced a drop-in failure rate of boreholes. The depth of the freshwater boundary can be identified by electrical resistivity method and the thick clay layer bounding the aquifer can be easily detected on a sounding curve.

3.16 Electrode Configuration

In electrical resistivity survey reliability, high resolution and good imaging are dependent on the selections of electrode configuration or array (Aizebeokhai, 2010). Numerous research has been conducted about the effectiveness of several arrays. In resistivity data acquisition, there are numerous types of arrays to be employed. The

most important utilized array to investigate the problems for subsurface layers are Schlumberger, Wenner, Dipole-dipole, Pole-dipole and Pole-pole array (Oldenburg et al., 2022). The array design has a considerable impact on the sensitivity, resolution and depth of investigation for effective results. The Table 3.1 shows the attributes of each array design in terms of the sensitivity of the array to horizontal & vertical heterogeneities, horizontal data coverage, depth of investigation and signal intensity each layout has its particular gains and constraints (Samouelian et al., 2005).

In profiling and sounding, there is a scope provided for electrode arrangement to be made in many ways within the field and such measures are called configurations. The various electrode configurations commonly differ in terms of the amount of electrode used, common interval electrodes and arrangement of electrodes for the targeted purpose of investigation on the field.

Table 3.1 Characteristics of array configuration (Samouelian et al., 2005).

	Wenner	Schlumberger	Dipole-dipole	Pole-pole	Pole-diploe
Sensitivity of the array horizontal structures	++++	++	+	++	++
Sensitivity of the array vertical structures	+	++	++++	++	+
Depth of investigation	+	++	+++	++++	+++
Horizontal data coverage	+	++	+++	++++	+++
Signal strength	++++	+++	+	++++	++
The labels are classified (+) to (++++) equivalent at poor sensitivity to high sensitivity for the different configuration					

3.16.1 Wenner Array

The Wenner electrode arrangement is the simplest array. In this array, four electrodes, C_1, P_1, P_2, & C_2 are positioned in line and set apart equidistant from each other. The outer electrodes C_1 & C_2, are current electrodes and the two inner electrodes,

P_1 and P_2, are potential electrodes (Figure 3.16). In the Wenner array, the resistivity of subsurface formation is quantified by increasing the distance between electrodes while maintaining the position of the centre point of deployed array. The apparent resistivity formula for the Wenner array is given below in equation 3.4 (Hassan et al., 2017).

$$\rho a = 2K\frac{\Delta V}{I} \quad \ldots\ldots\ldots\ldots\ldots\ldots\ldots\ldots\ldots \text{ eq. (3.4)}$$

The Wenner array is usually used in profiling for lateral imaging or exploration of the ground, such as soil testing and horizontal layers' characterization (Loke et al., 2020). The disadvantage of Wenner array is usually found in carrying a VES survey in which all four electrodes move out for each measurement at a certain depth This results in laborious work to increase electrode spacing in acquiring a large line to cover greater depth (Shariah & Shariah, 2019).

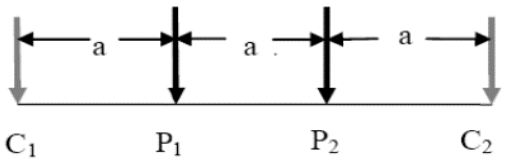

Figure 3.16 Wenner electrode configuration P (Potential electrode), C (Current electrode) and a (Electrode spacing) (Aizebeokhai et al., 2011).

The Wenner electrode array is employed for profiling or mapping the soil analysis, by using a standardized test in ASTM G57, specifically written for electrical soil testing. The standard specifies profiling layout in Wenner array consider cost-effective and high resolution results.

3.16.2 Dipole-Dipole Array

A dipole-dipole array consists of two current electrodes and 2 potential electrodes (Figure 3.17). This configuration provides an approach to plot the raw data to obtain an idea of the earth's cross-section (Salman et al., 2020). When frequency-domain induced-polarization surveys are performed, the dipole-dipole array is employed to attenuate the inductive coupling between the transmitting and receiving dipoles (Bodmer & Ward, 1968).

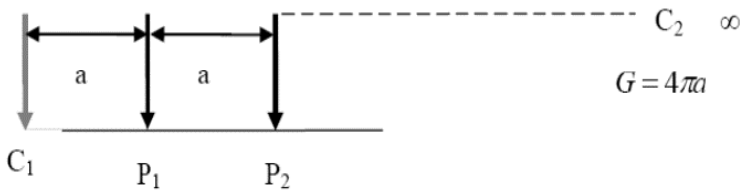

Figure 3.17 Dipole-Dipole electrode configuration P (Potential electrode) , C(Current electrode) and a (Electrode spacing) (Aizebeokhai et al., 2011).

The primary significance of the dipole-dipole array arrangement is its great resolution and multi-channel capacity; it gives an in depth image instead of delivering a big picture or image like Wenner array. The main disadvantage of this array is that if the dipole is set apart too far, the signals will drop and as a result the capacity to see deeper into the earth diminishes (Bodmer & Ward, 1968). The dipole-dipole array was formerly applied for mineral exploration along with the induced polarization (IP) technique. The dipole-dipole survey made it simple to plot the collected data in form of 2D manual contour plots. However this practice generates an impeccable image of the ground but it gave an approximate image that can interpret the geology (Hassan et al., 2017).

3.16.3 Pole-Dipole Array

The four collinear electrodes establish a pole-dipole array. There are 2 current electrodes & 2 potential electrodes (Figure 3.18). In this arrangement, one current electrode is positioned at infinity which is nearly 5 to 10 times the depth of survey, while the other one is set in the surroundings of the 2 potential electrodes (Smith, 1986).

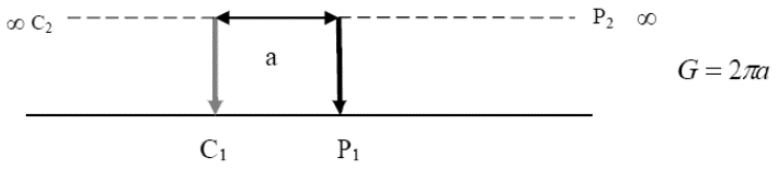

Figure 3.18: Pole-Dipole electrode configuration P (Potential electrode) , C(Current electrode) and a (Electrode spacing) (Aizebeokhai et al., 2011).

A pole represents a single transferring electrode and a dipole covers a pair of oppositely charged electrodes that are placed so close together that the electric field appears to be a single electrode in its place of fields from two distinct electric poles (Elawadi et al., 2001). The geometric factor formula for the Pole-Dipole array is given below in equation 3.5 (Lowry & Shive, 1990).

$$\rho a = 2\pi n(n+1)a\frac{\Delta V}{I} \qquad \ldots\ldots\ldots\ldots\ldots\ldots\ldots \qquad \text{eq. (3.5)}$$

3.16.4 Schlumberger Array

The Schlumberger configuration comprises four collinear electrodes positioned on the ground. The external two electrodes are the current electrodes and the inner two electrodes are the potential electrodes (Figure 3.19). The potential electrodes are mounted at the centre of the electrode configuration with a small separation. Usually, less than one fifth of the spacing between the current electrodes. The current electrodes are moved to a greater distance during the survey whereas the potential electrodes stay in the same position until the examined voltage becomes very low to measure. Typically, increasing the current electrode spacing appears roughly six times. (Keller & Frischknecht, 1966). The main advantages of the Schlumberger array are that only current electrodes need to move while potential electrodes remain fixed. The soundings usually have deeper probing depth of investigation, better resolution & effective time consuming during acquisition layout placement as compared to Wenner array.

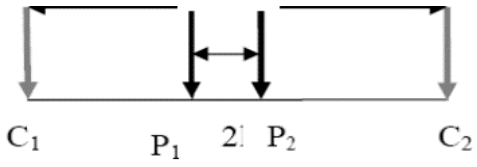

Figure 3.19 Schlumberger electrode configuration P (Potential electrode), C(Current electrode) and a (Electrode spacing) (Aizebeokhai et al., 2011).

3.17 Vertical Electrical Sounding

In Pakistan Schlumberger array for vertical electrical sounding has been utilized by the researcher to provide a detail understanding of aquifer and related environmental issues (Niaz et al., 2021; Hasan et al., 2020c; Hasan et al., 2020b; Hasan et al., 2020a;

Ahmed et al., 2020; Awan, 2019; Akhter & Hasan, 2016). In the study area vertical electrical sounding has been conducted using Schlumberger electrode configuration for subsurface groundwater mapping. Vertical electrical sounding is one of the useful and cost-effective resistivity survey techniques. In this method, Current is moved through the subsurface from a single current electrode to the other and the potential as the current moves is an observer. From this information, resistivity values of various layers are attained and layer thickness can be identified. The procedure involved in Vertical Electrical Sounding (Auken & Christiansen, 2004) is completely based on the idea that the subsurface is comprised of horizontal stratigraphy. It is composed of horizontal, homogenous, separate and isotropic layers.

The measurements are completed by slowly increasing the current electrode distances while at some stations, the potential electrodes stay constant. The depth increases at which the current infiltrate beneath the surface of the ground, with the increasing distances between the current electrodes, therefore aggregating the depth of investigation. In this manner, the vertical resistivity spreading is estimated below the centre of the array. These are generally plotted as depth against resistivity, so the resistivity values at different depths are investigated. The vertical electrical sounding (Auken & Christiansen, 2004) technique has been applied for inspecting subsurface layer properties and groundwater aquifer's potential. By this means, the subsurface classification is decided to determine based on the resistivity variation with depth. The range of particular resistivity values indicates the presence of distinct rock mass characteristics (Saleh & Samsudin, 2013).

3.17.1 Types of VES Curve

The type of curves obtained by sounding on top of the stratified horizontal medium is a function of layers' thicknesses and resistivity in addition to the configuration of electrodes. The curve is represented by plotting the apparent resistivity together with electrode spacing and this is assumed by matching the field curve with the master curve (Bhattacharya, 2012; Koefoed & Principles, 1979; Zohdy, 1965).

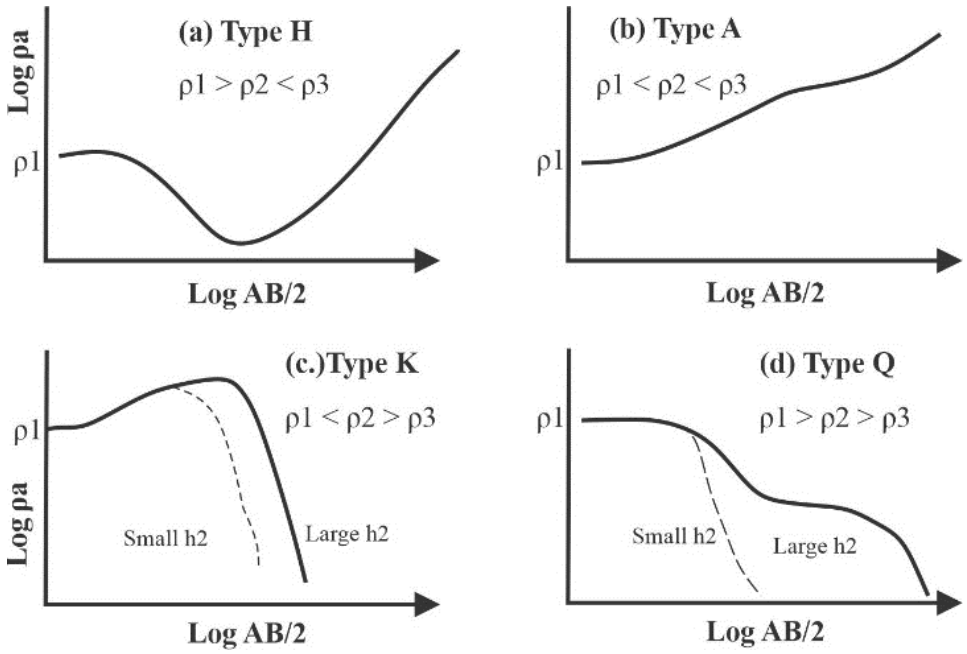

Figure 3.20 Types of VES curves (modified from Telford et al., 1976).

The 3-layer earth model can be categorized into H, K, A and Q-type curves as shown in Figure 3.20 (Bhattacharya, 2012; Telford et al., 1990; Telford et al., 1976), based on shape. The type of curve for the three-layer model is identified as H type ($\rho1 > \rho2 < \rho3$), K type ($\rho1 < \rho2 > \rho3$), A-type ($\rho1 < \rho2 < \rho3$) and Q type ($\rho1 > \rho2 > \rho3$). The types H and K have a specific minimum and maximum, demonstrating irregular high or low resistivity beds at intermediate depth (Telford et al., 1976). Types A and Q demonstrates uniform resistivity change, the increasing 1st layer and the decreasing 2nd layer with depth. The collected field data curve was interpreted and matched with the master curve to identify the type of curve and trend of resistivity in subsurface.

CHAPTER 4

DATASET & METHODOLOGY

4.1 Overview

The dataset and methodology in order to accomplish the research are presented objective-wise in this chapter. The datasets collected in this study are divided into four categories i.e., Questionnaire Survey, Geological map and drilling data, Geophysical Electrical Resistivity data & Groundwater samples of study area, discussed as follow.

4.2 Questionnaire Survey

Phase 1 of this research had started with the preliminary research data collection during a comprehensive literature review from national and international published data to understand the geology and previous work related to groundwater issues. The geological maps, satellite images of the last 35 years from Google Earth and drainage maps were digitized for presentation in the Literature Review chapter. The

questionnaire was designed to collect information related to groundwater for domestic use and agricultural activity (Appendix A). The questionnaire survey covered information related to the water table, groundwater pumping, groundwater quality, local diseases, groundwater policies and management. Total 20 questions were prepared and approximately 150 locals (farmers, agriculture government officers and politicians) from Winder Town participated in a survey to examine the current issue of groundwater, over-pumping and groundwater quality deterioration. The questionnaire survey was evaluated to address the current situation of groundwater.

4.3 Geophysical Electrical Resistivity Data Collection and Analysis

The phase-2 comprised the acquisition of field data using a geophysical electrical resistivity survey to accomplish objective 2 (Appendix B). Initially, the reconnaissance examination of the study area was accompanied to design the geophysical acquisition following the preferred research objectives. Initially survey was designed in grid pattern to cover detail information of subsurface. But points were moved due to the inaccessibility and permission issue. 27 VES stations were covered to collect the subsurface resistivity information (Figure 4.1). The latitude and longitude of each VES station were read out using GPS (Table 4.1). Initially the survey was planned in grid form with spacing of 5 km to cover the region. During the data collection points were moved as per the field condition. The western part of the study area was not easily accessible due to security issues. The equipment utilized for obtaining the resistivity information was PASI-Earth (16 GLN) resistivity meter (Figure 4.2). The main component of the instrument comprised four metallic electrodes and four sets of electric link reels. During acquisition, two sets of cables were utilized for current and two for measuring the potential difference.

4.3.1 Field Data Acquisition

The geophysical survey started with gaining VES points data where the four electrodes were positioned uniformly on straight line. The current electrodes (AB) were placed on the outer side and the potential electrodes (MN) were placed inside in between A & B electrodes (Figure 4.3). The instrument PASI earth resistivity meter was coupled with electrodes and powered given by direct current (DC) using electric cables. Spacing of current electrodes (AB) was increased further outwards to acquire data from pronounced probing targeted depth whereas the potential electrodes remained fixed. Moreover, the potential electrodes were shifted outwards where the ratio of distance between current electrodes (AB) and of potential electrodes (MN) became significant to avoid error where the potential difference became insufficient to quantify. January to April is best time to collect the geophysical data due to pleasant weather in study area. The summer is very hot and dry in study area. Therefore, in the end of March 2021 the data was acquired. The equipment can be run in dry/hot season but due to labor work and equipment handling it is very difficult for the surveyor, especially when covering a large area.

The current electrode maximum spacing had been kept at 300 meters at surface (AB) to achieve a 150 meters' penetration depth. Designed arrangement of current electrode (AB) separation for the VES station to collect the Resistance (R), value from PASSI resistivity equipment was 2, 4, 6, 8, 10, 10, 15, 20, 25, 25, 30, 35, 40, 45, 50, 50, 60, 70, 80, 90, 100, 100 and 150 meters and potential electrode spacing 0.50, 2, 5, 10, 20 and at 50 meters. The values/readings from the meter were also repeated to compute the average of resistance value to avoid error at spacing of potential electrode (MN) i.e. 10, 25 and 50 meters. The practice of this exercise was carried out because the potential difference is extremely low and very tough to measure at a large layout of electrodes. Thus, the potential electrode (MN) was moved, whereas holding the current electrode position static (Sikandar et al., 2010).

Table 4.1 27 Vertical Electrical Sounding Station dataset Latitude and Longitude.

S. No	VES Station	Latitude	Longitude
1	R-1	25°24'43.92"N	66°38'46.04"E
2	R-2	25°26'2.03"N	66°38'37.00"E
3	R-3	25°23'16.71"N	66°42'49.57"E
4	R-4	25°24'17.58"N	66°40'0.14"E
5	R-5	25°26'6.02"N	66°41'6.35"E
6	R-6	25°25'48.86"N	66°43'40.51"E
7	R-7	25°26'28.54"N	66°46'31.55"E
8	R-8	25°27'51.72"N	66°43'43.72"E
9	R-9	25°22'43.01"N	66°40'14.83"E
10	R-10	25°22'19.84"N	66°43'12.26"E
11	R-11	25°21'16.99"N	66°46'3.72"E
12	R-12	25°22'4.50"N	66°41'27.93"E
13	R-13	25°20'47.17"N	66°41'57.94"E
14	R-14	25°20'23.80"N	66°43'29.09"E
15	R-15	25°19'31.87"N	66°39'51.47"E
16	R-16	25°22'48.50"N	66°45'31.28"E
17	R-17	25°24'47.84"N	66°45'1.90"E
18	R-18	25°24'15.24"N	66°42'2.97"E
19	R-19	25°26'5.44"N	66°39'50.47"E
20	R-20	25°27'37.10"N	66°40'24.41"E
21	R-21	25°26'42.03"N	66°42'17.41"E
22	R-22	25°25'14.85"N	66°41'55.23"E
23	R-23	25°25'4.87"N	66°40'52.12"E
24	R-24	25°22'33.63"N	66°38'17.06"E
25	R-25	25°21'1.23"N	66°39'2.72"E
26	R-26	25°27'9.51"N	66°38'59.89"E
27	R-27	25°25'22.15"N	66°35'52.62"E

The data collection delivers the series of resistance values for the potential electrode (MN/2) and current electrode (AB/2) spacing. The instrument does not calculate the true resistivity. It processes the $\Delta V/I$ and readouts the resistance of subsurface layers. The estimated resistance reading from equipment was utlized to calculate the apparent resistivity. It is done by multiplying the resistance (from equipment) values with the respective Geometric factor (k) as given in the equation 4.1 & 4.2 (Keller & Frischknecht, 1966).

$$K = \left[\frac{\left[\frac{AB}{2}\right]^2 - \left[\frac{MN}{2}\right]^2}{\left[\frac{MN}{2}\right]^2}\right]\pi \quad \ldots\ldots\ldots\ldots\ldots\ldots\ldots \quad \text{eq. (4.1)}$$

$$\rho a = K \times R \quad \ldots\ldots\ldots\ldots\ldots\ldots\ldots\ldots\ldots \quad \text{eq. (4.2)}$$

Where are:

AB = spacing/distance among two current electrodes (meters),

MN = spacing/distance among two potential electrodes (meters),

π = is constant and the value is 3.142,

ρa = apparent resistivity value computing using ohm's law (Ωm)

R = (ΔV/I) resistance (Ω) readout from an instrument

K= geometric factor represent the changes in the layout/ design of current (I) and the potential electrodes (V) (Koefoed & Principles, 1979).

The resistance values acquired in the field using resistivity meter had been multiplied by the Geometrical Factor (K) to estimate the apparent resistivity of subsurface layers.

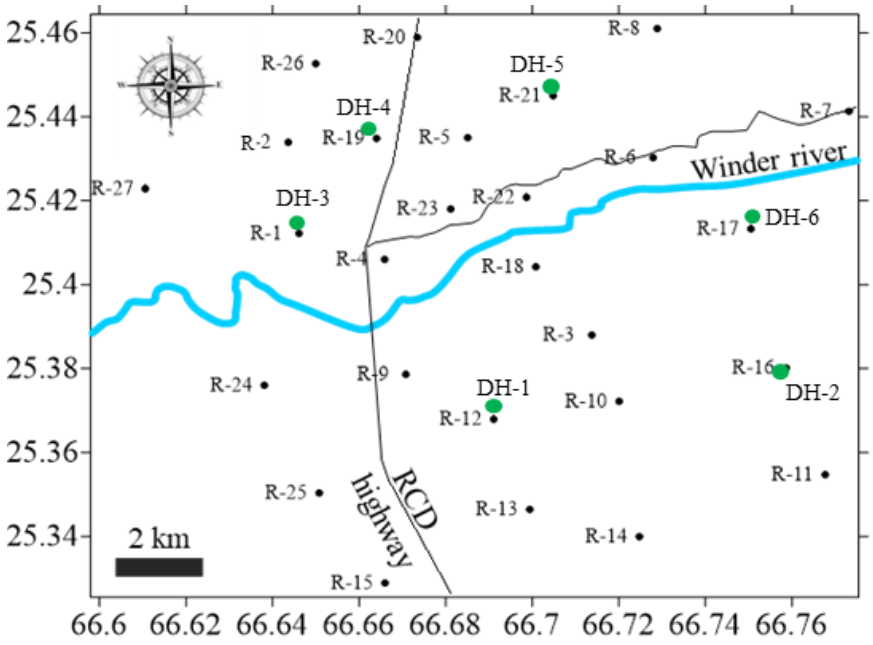

Figure 4.1: Base map of electrical resistivity survey (R) carried out for 27 stations and 6 Drill hole (DH) in Winder, Balochistan.

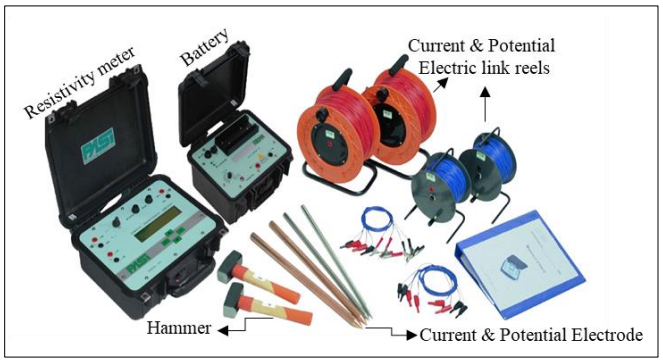

Figure 4.2 The instrument used for data acquisition PASI-Earth (16-GLN) resistivity equipment.

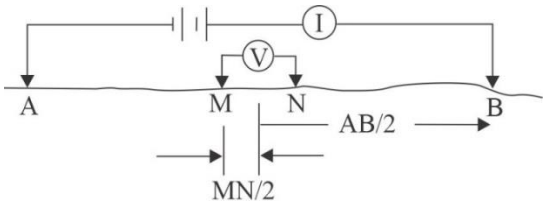

Figure 4.3 Vertical Electrical Sounding using schlumberger electrode configuration.

Beside. field acquired data was also plotted manually on a log-log graph paper, where apparent resistivity scaled on y-axis versus current electrode arrangement on x-axis during acquisition to minimize the error. In the case of anomalous value reading for specific AB/2 and MN/2 were repeated to confirm the unexpected difference. The final field curve obtained from each station was overlaid with master curves (H, A, Q and K). Moreover, the standard practice to match the curve was practiced in a way that the field plotted curve can be overlay/matched with the master curves (H, A, Q and K). The master curves types are published in the literature for two to three layers as auxiliary graphs (Koefoed, 1979; Bhattacharya & Patra, 1968; Zohdy, 1965).

4.3.2 Field Data Modelling and Interpretation using IPI2Win

Finally, the obtained field data from the geophysical survey (Appendix-C) was processed using the computer inversion program IPI2Win developed by Moscow State

University, Russia (Bobachev, 2002). Basically, this software exclusively designed for analysing geo-electrical data. Data input collected from the field was AB/2 current electrode spacing, MN potential electrode spacing and Geometric factor "k" from field data or auto-calculated by software using (equation 1) for a given electrode configuration. Indirect data can be imported which comprised calculated apparent resistivity value using (Equation 2) and AB current electrode spacing (Figure 4.4).

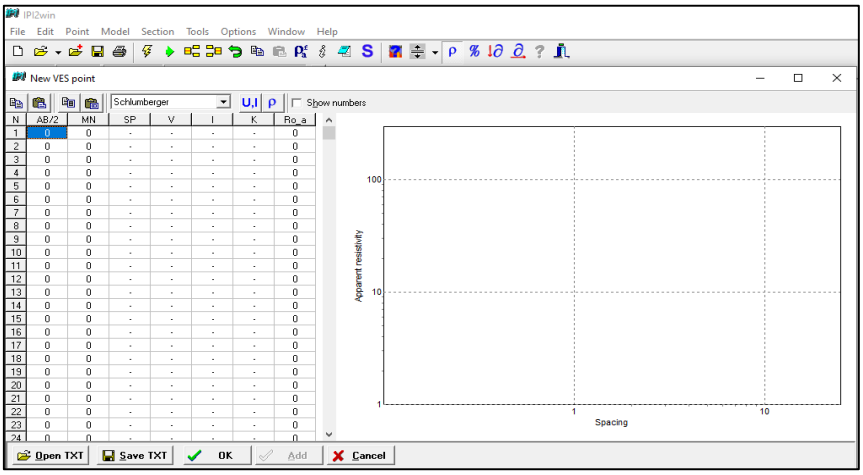

Figure 4.4 IPI2Win software main window to import field data and log-log graph apparent resistivity vs. current electrode spacing.

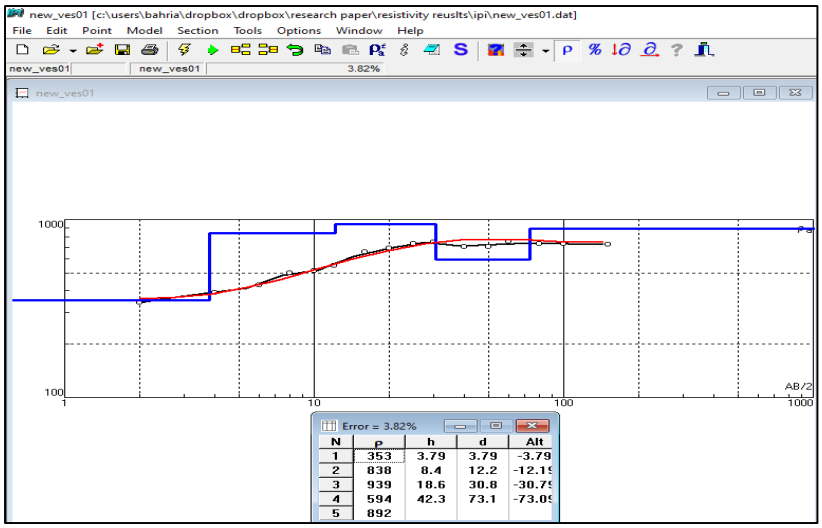

Figure 4.5 Apparent resistivity vs electrode spacing log-log graph represents the master curve (red) field curve (black), model layer (blue) and layers (resistivity, thickness and depth).

The plotted resistivity data on IPI2Win processed for the geo-electric curve. This was done by master and field curve matching technique to identify A, H, K and Q curve. The processed curve provides the modelled layer for a different geo-electric layers for horizontal stratification. Finally, the resistivity for a different medium, layer thickness and depth were identified in (Figure 4.5). The results were utilized to interpret the lithology based on two geo-electric parameters i.e., apparent resistivity and thickness. In homogeneous layer, the resistivity values are same in subsurface as it does not depend on location and electrode configuration whereas resistivity shows variation in heterogeneity (Gaffney et al., 2002). The resultant curve was quantitatively elucidated maximum 6 % RMS error using IPI2Win software for 27 VES points to decrease the percentage of root mean square error (RMS%), it also characterize the function of matching, between field curves and the theoretical curves, i.e. low RMS% eventually means better matching (Zohdy, 1989). The above steps were iterated for 27 VES stations spatially distributes across the study area using IPI2Win software.

To validate the interpretation of lithology test boreholes were drilled and analyzed to understand the subsurface stratigraphic distribution. Total of six boreholes were drilled using a straight rotary drilling rig to generate lithology logs near to VES station (R-1, R-5, R-12, R-16, R-19, R-21) as shown in Figure 4.6. The sample of drill cutting was preserved in a plastic bag at an interval of 1.5 meters to investigate the vertical grain size distribution. The sample was further analyzed in the lab to construct the lithology.

The standard type of VES curve (A, H, K & Q) defines the subsurface layer characteristics. The shape of curve is the function of resistivity of formation, layer thickness and the number of geo-electric layers (Figure 3.15). The x-axis represents AB/2 and the y-axis apparent resistivity. Resistivity variations for different type of rocks saturated and unsaturated such as gravel, sand, clay and compact layers were utilized to predict the lithology (Figure 3.15).

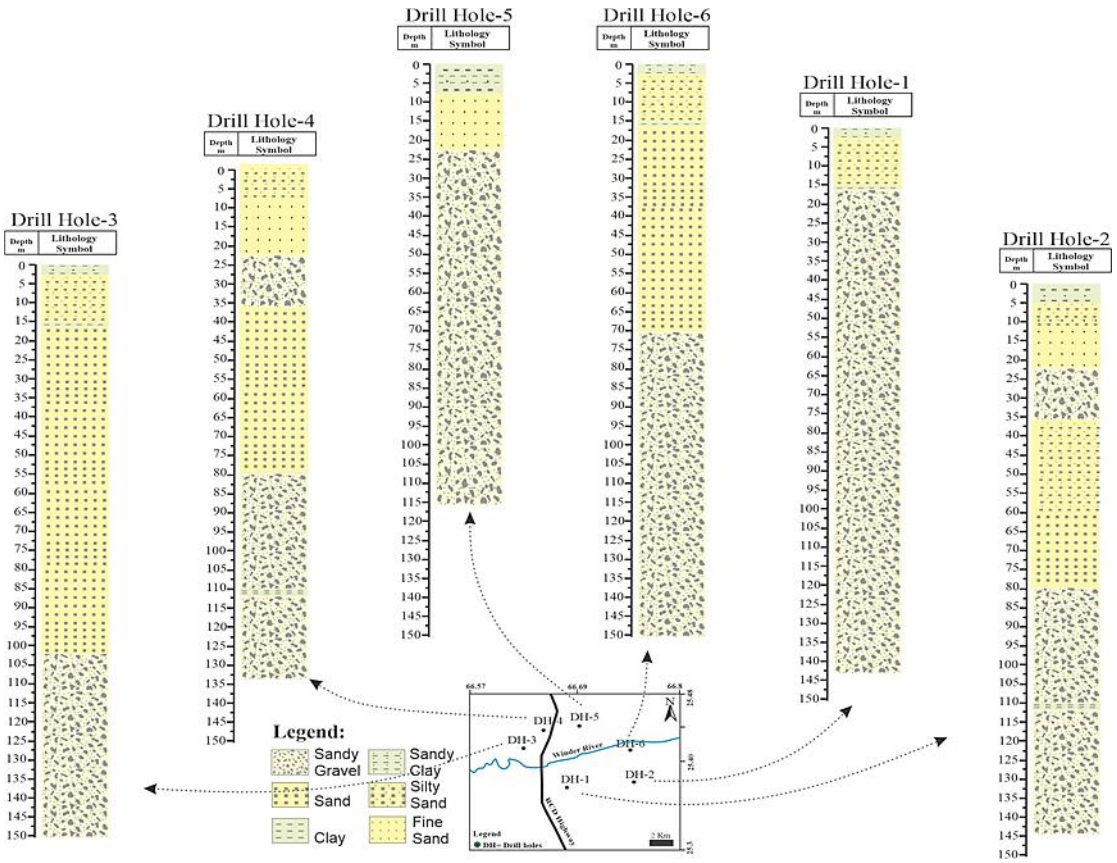

Figure 4.6 The lithology logs collected and acquired from six drilled borehole cutting samples

4.4 2D Inversion Model or Pseudo-sections

To represent the measured apparent resistivity in visualized 2D form and as a preliminary guide for additional quantitative interpretation, pseudo sections were used (Loke et al., 2020). The pseudo section contouring method was used to plot the data VES data for 2-D imaging. The inverted pseudo section was generated by plotting the apparent resistivity calculated values which are appropriate to present the data. It provides an estimated picture of the true resistivity distribution in subsurface. Three pseudo sections were created along the profiles i.e. A-A′ (R-15, R-25, R-24, R-1, R-2 and R-26), B-B′ (R-14, R-10, R-3, R-18, R-22 and R-21), C-C′ (R-11, R-16, R-17, R-6 and R-8), D-D′ (R-16, R-10, R-12, R-9) and E-E′ (R-25, R-7, R-6, R-22, R-23 and R-1) (Figure 4.7).

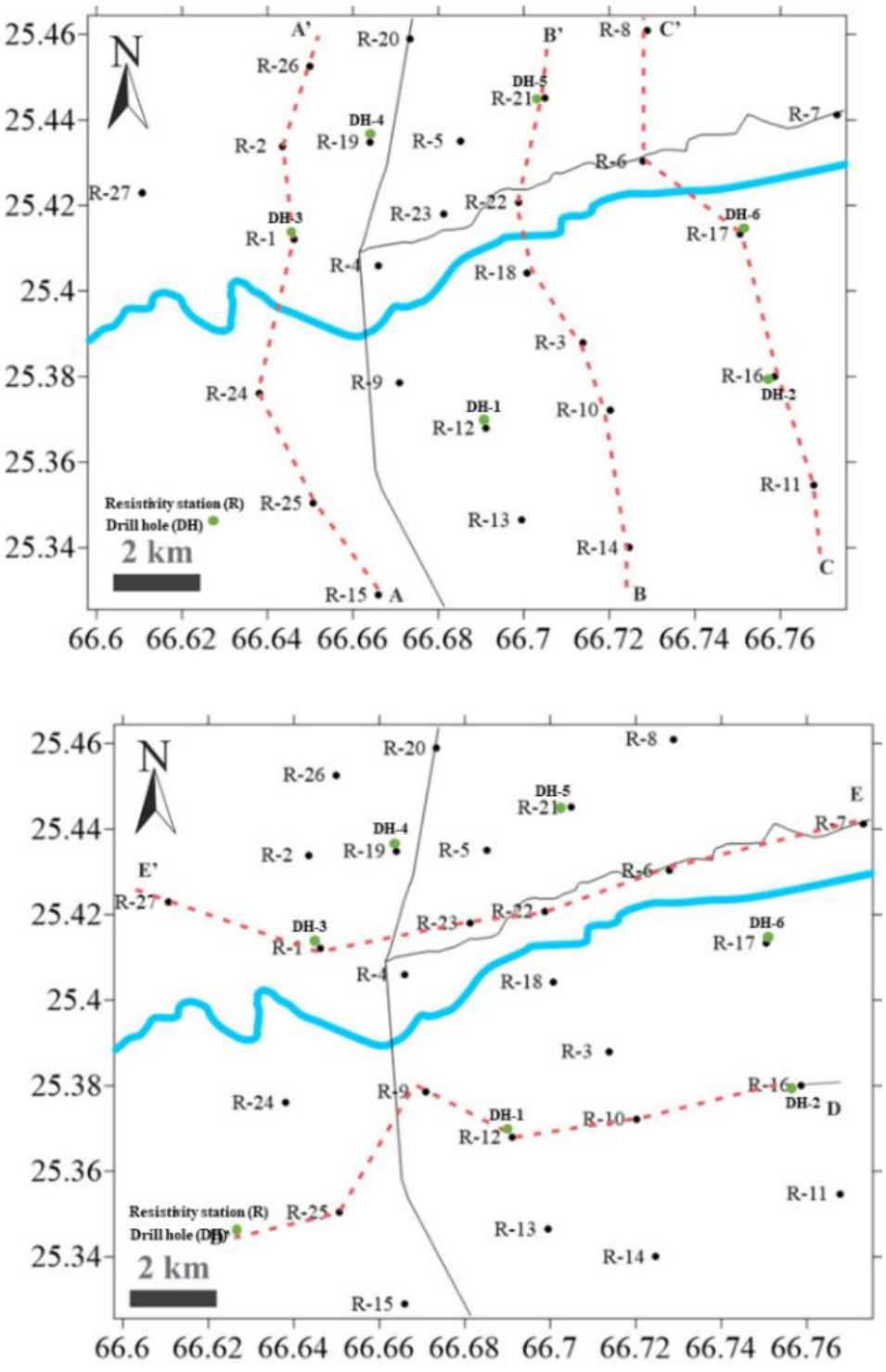

Figure 4.7 Geoelectric lithology cross-section traverses north-south and east-west.

4.5 Geo-electric Cross section

A geological cross-section is an illustration that displays geological relationships, in a vertical plane extending deep into the Earth. The subsurface information is generally derived from written logs of wells, samples and cores or geophysical techniques, electric logging and seismic surveys. Interpretation of rock distribution both in-depth & on the topographic surface help in the building of a geological cross-section. 2D section of stratified layers generated from electrical (resistivity) depth probing or drilling, where layers are defined by their apparent resistivity. The sections are created from the interpreted field data in combination with the geology and the lithology logs of a nearby drill borehole. The geo-electric sections describe the electrical resistivity of the sediments, depth to the bottom of sediments, the thickness of the deposits, their horizontal spreads and the sounding points. The values of resistivity that were of close depth & range for each sounding points were used to build the geo-electric layers. To evaluate the thickness and continuity of lithology five geo-electric traverses were constructed (Figure 4.7). The north-south and east-west Traverses were created using VES stations along the profile i.e. A-A′ (R-15, R-25, R-24, R-1, R-2 and R-26), B-B′ (R-14, R-10, R-3, R-18, R-22 and R-21), C-C′ (R-11, R-16, R-17, R-6 and R-8), D-D′ (R-16, R-10, R-12, R-9) and E-E′ (R-25, R-7, R-6, R-22, R-23 and R-1).

4.6 Dar-Zarrouk parameters

Dar-Zarrouk parameters are generally very important in the understanding and interpretations of geological models (Egbai & Iserhien-Emekeme, 2015). The geo-electric layer parameters are related to two fundamental combinations such as the thickness and resistivity of each geo-electric layer in the model (Braga et al., 2006; Singh et al., 2004). For the sequence of horizontal, homogeneous/same and isotropic layers of resistivity ρ. The Dar-Zarrouk parameters was evaluated, built on layer

thickness (h), resistivity (ρ), Longitudinal Conductance (S), transverse resistance (T) and coefficient of electrical anisotropy (λ) (Singh et al., 2021).

$$S_c = \sum_{i=1}^{n} \frac{hi}{\rho i} \quad \ldots\ldots\ldots\ldots\ldots\ldots\ldots\ldots \quad \text{eq. (4.3)}$$

Longitudinal unit conductance is basically a conductance parallel to the face for a unit cross-section presented in equation 4.3. This was used to calculate longitudinal unit conductance for n layers, where h is thickness and ρ is resistivity and n is the total number of a layer in the model, the measured unit of S_c is Ω^{-1}

$$T_r = \sum_{i=1}^{n} hi\rho i \quad \ldots\ldots\ldots\ldots\ldots\ldots\ldots \quad \text{eq. (4.4)}$$

Transverse resistance is basically a resistance (normal to the face) for a unit cross-section. The equation 4.4 is used to calculate Transverse unit resistance for n layers,, where (h) represent the thickness and (ρ) is resistivity and n is total number of a layer in the model, a measured unit of T_r is Ωm^2

If the total thickness of the layers in the geo-electric section considered is H, then the average longitudinal resistivity ρ_L is given by equation 4.5.

$$\rho_L = \frac{H}{Sc} \quad \ldots\ldots\ldots\ldots\ldots\ldots\ldots\ldots \quad \text{eq. (4.5)}$$

and the average transverse resistance ρ_t is given by equation 4.6

$$\rho_t = \frac{Tr}{H} \quad \ldots\ldots\ldots\ldots\ldots\ldots\ldots\ldots \quad \text{eq. (4.6)}$$

ρ_t is always greater than ρ_l. Therefore, the entire section will thus be anisotropic regarding electrical resistivity (Christensen, 2000; Watson & Barker, 1999). The coefficient of electrical anisotropy is defined in equation 4.7.

$$\lambda = \frac{\sqrt{S_c \times T_r}}{H} = \sqrt{\frac{\rho_t}{\rho_L}} \quad \ldots\ldots\ldots\ldots\ldots\ldots\ldots \quad \text{eq. (4.7)}$$

Where ρ_t & ρ_L are defined as average transverse resistivity & average longitudinal resistivity. In the case of a homogeneous isotropic medium $\lambda = 1$ and the range varies from 1-2 in an anisotropic homogeneous medium where $\rho_t > \rho_L$ (Christensen, 2000).

Flow chart as shown in Figure 4.8 represents a the summarized methodology in three main steps data, namely acquisition/survey planning, field activities and finally, processing and interpretation that aid to accomplish objective number 2 using a cost-effective Environmental Geophysical approach already discussed in the above sections.

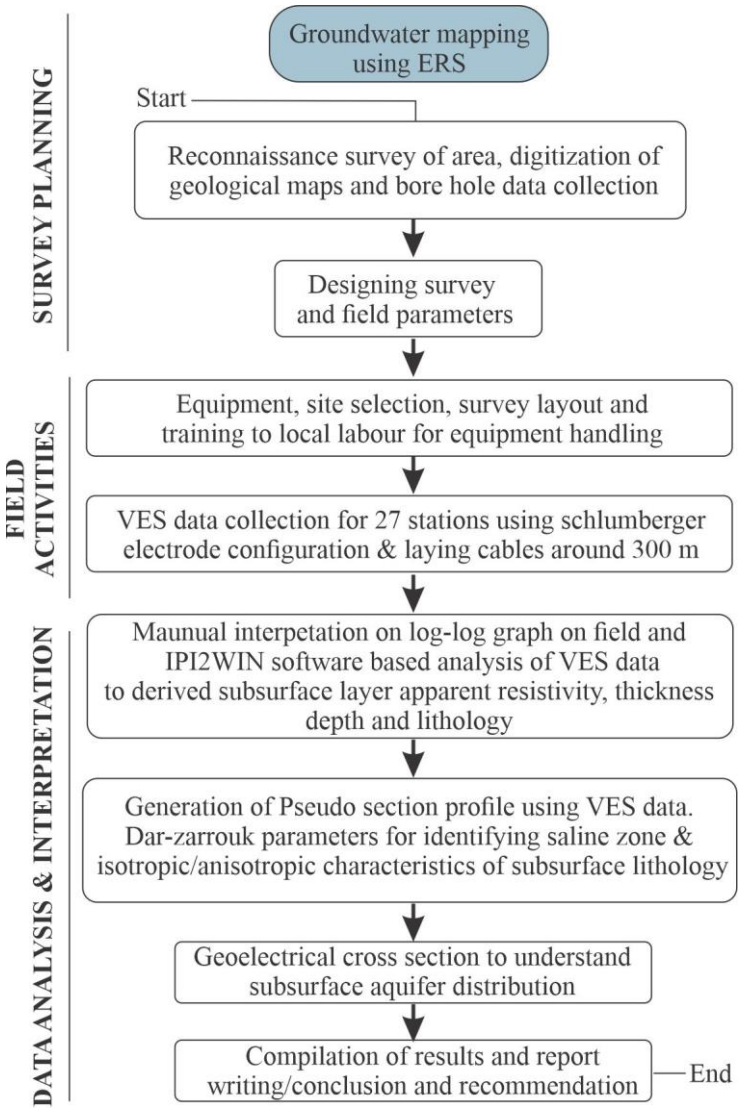

Figure 4.8 Methodology flow chart of geophysical electrical resistivity data acquisition planning, processing and interpretation.

4.7 Groundwater Sampling and Hydro-geochemical Analysis Technique

The Phase-3 of this research was conducted to accomplish objectives 3 & 4 (Appendix D). Groundwater samples of tube wells were collected for hydro-geochemical study of water to assess the quality. A clean and safe groundwater is an essential and strategic resource for societal and human sustainable development, mainly in arid and semi-arid regions (Gao et al., 2020). Therefore, the characterization of hydro-geochemistry and evaluation of groundwater quality precisely for domestic & irrigation purpose is very essential (Mukherjee & Singh, 2022). The factors which impact the quality of groundwater are soil, climate, groundwater circulation through rocks (geological formation) and intrusion of seawater in coastal areas. The quality and standard of groundwater for the domestic and agricultural purposes can be determined by hydro-geochemistry. The water movement through pore spaces are very slow during infiltration from the surface into an aquifer. The longer residence time of water in rock pore dissolve ions in water which remain for a long time due to very slow natural processing unlike the surface water bodies (Anoop et al., 2021).

The groundwater sampling in Winder, District Lasbela Balochistan was conducted to investigate the hydro chemistry and quality of groundwater. A total of 94 samples were collected from tube wells during May and June 2021. The total depth of tube wells ranges from 106.7-137 meters (Appendix E). The location map of 94 groundwater samples collected from study area (Figure 4.9). The source of pumping was a submersible pump operated by solar energy and a government electric supply. A standard procedure American Public Health Administration was adopted for sample collection (Rice et al., 2017). Pre-washed 1 litre polythene bottles were prepared and preserved from heat and sunlight during traveling from Karachi to Winder. Each bottle was rinsed with dilute nitric acid / distilled water in the laboratory and carefully labelled for ease of identification in the laboratory as per protocols assigned by American Public Health Administration. The geographical location of tube well was determined by Garmin Etrex 10 GPS device. The samples were collected at an interval of 1-2 km in study area. Before collecting the sample, the tube well was purged for 2-3 minutes to stabilize the physiochemical parameter and drain the stagnant water. The sample bottle

rinsing and washing practices were carried out 3-5 times from each respective location. At every station, 3 bottles were filled from tube well using 0.45 µm, and filter paper were used for various physiochemical analyses. Then, about 100 ml Nitric Acid (HNO_3) was mixed on the field in one bottle to confirm the metals are dissolved and to prevent microbial activities.

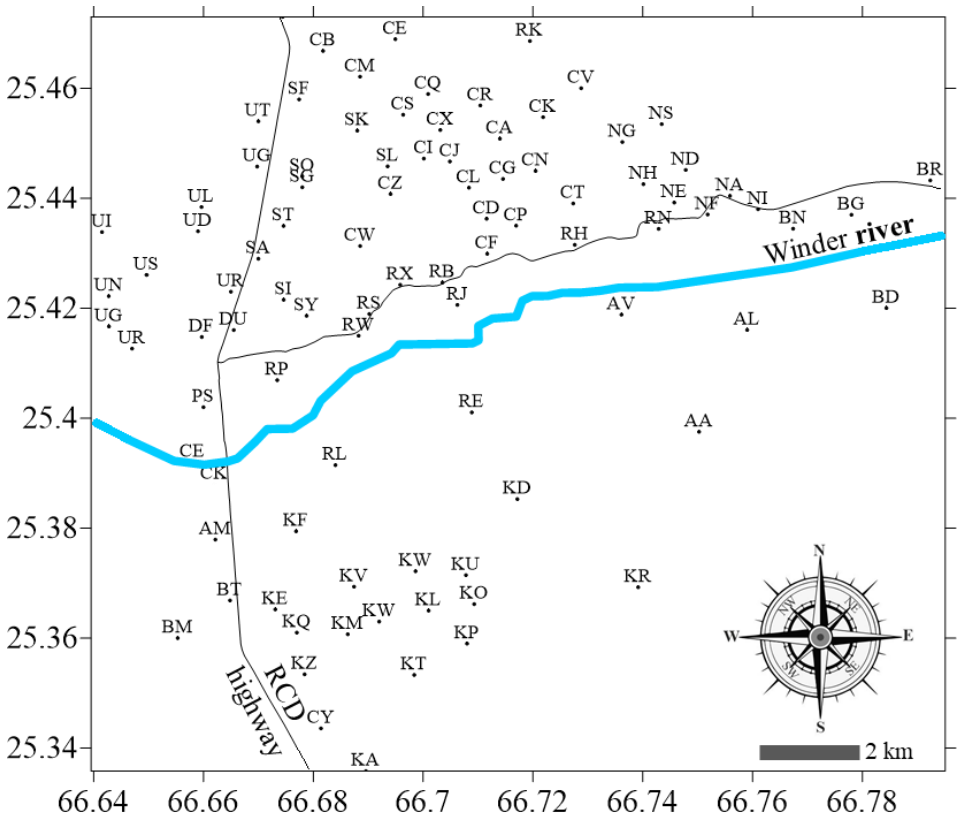

Figure 4.9 Base map of 94 groundwater samples collected from Winder Balochistan

The in-situ measurements were conducted for an unstable water quality parameter, namely Total Dissolved Solids (TDS), pH and Temperature by using the portable meter. The reading was repeated to assure accuracy in the field. The samples were transported from the field to laboratory carefully maintained at a temperature of 4°C in the sealed ice box and remaining parameters were measured for analysis. As instructed by (APHA 2017) the laboratory analysis protocol was adopted to ensure the

quality control processes for physiochemical analysis. The Nitrate (NO_3^-) and Sulphate (SO_4^{2-}) were assessed by utilizing a UV–visible spectrophotometer. Chloride (Cl^-) results were measured by applying the ($AgNO_3$) titration technique. The magnesium (Mg^{2+}) was quantified by using the equation.

$$\text{Magnesium Hardness (MgH)} = \text{Total Hardness (TH)} - \text{Calcium Hardness}$$

$$(\text{CaH})Mg^{2+}\ (\text{mg/l}) = \text{MgH} \times \text{Equivalent weight of } Mg^{2+} \times \text{Normality of EDTA}$$

The calcium (Ca^{2+}) and total hardness ($CaCO_3$) were computed by utilization EDTA titration method. K^+ and Na^+ were determined by using a flame photometer. The determination of (HCO_3-) was carried out by using methyl orange indicator and standard solution of (H_2SO_4). Finally, the ion selected electrode method was used to determine the fluoride (Danoff, 2000). The summarized chemical analysis of the groundwater sample is illustrated in Table 4.2. A similar methodology as per the standard of APHA (Rice et al., 2017) was adopted for hydro-geochemical analysis (Mukherjee & Singh, 2022; Kadam et al., 2021; Modi et al., 2021; Adimalla & Taloor, 2020; Mohammad & Rind, 2020; Noble et al., 2020).

Table 4.2 Instrumental, titrimetric and calculation methods used for chemical analysis of groundwater samples

Parameters	Unit	Analytical method	Reagents
pH	/	pH	pH Meter, Hanna Instrument, Model 8519, Italy
EC	µS/cm	EC	Potassium chloride
TDS	mg/l	TDS meter	Potassium chloride
Ca^{2+}	mg/l	Titrimetric	EDTA, sodium hydroxide and murexide
Mg^{2+}	mg/l	Calculation	MgH = TH - CaH Mg^{2+} = MgH × Eq.Wt of Mg^{2+} × Normality of EDTA
Na^+	mg/l	Flame photometric	Sodium chloride (NaCl) and KCl
K^+	mg/l	Flame photometric	NaCl and KCl
SO_4^{2-}	mg/l	UV visible spectrophotometer	HCl, ethyl alcohol, NaCl, barium chloride, sodium sulphate
NO_3^-	mg/l	UV visible spectrophotometer	HCl, ethyl alcohol, NaCl, barium chloride, sodium sulphate
Cl^-	mg/l	Titrimetric	Silver nitrate ($AgNO_3$) and potassium chromate (K_2CrO_4)
HCO_3^-	mg/l	Titrimetric	Hydrosulfuric acid (H_2SO_4) and methyl orange indicator

During the water sample collection from Winder, a questionnaire survey was also formulated and the response was documented from locals, tube well owners, farmers and drilling contractors. It includes the depth of the well, depth of the water table, the duration of discharge per day, the diameter of tube well, the source of power (solar/electrical), the quality of water and depth of the aquifer. It is very essential to understand the hydro-geochemical process of an aquifer in the study area (Nadiri et al., 2013). The detail of physiochemical parameters for laboratory experiments and calculations are given below.

4.7.1 pH

The pH of a solution is defined as a concentration of hydrogen ions (H^+). It is one of the important parameters to determine the corrosive nature of water. The higher pH value was identified as corrosive nature (Zhang et al., 2021). The range of the pH scale is 0-14 which represents the alkalinity and acidity of a substance and scale 7 is marked the neutrality at 25^{o}C (Akram et al., 2007). The pH value <7 show acidic and pH value >7 is basic for the irrigation water. The pH value is the main factors to address the usage of water for irrigation. The pH value of natural water relies upon the presence of carbon dioxide, carbonate and bicarbonate equilibrium (Zhang et al., 2020). On-site, the pH value was measured for each sample site. The calibration of meter was based on a buffers solution of pH 4 and 6.68 before measurement. The electrode of the pH meter was continuously washed with distilled water for accurate measurement and then with sample water. The pH meter was dipped into the unstirred solution and stabilize reading was noted to avoid the loss of carbon dioxide (Hamam et al., 2020).

4.7.2 Electrical Conductivity

EC (Electric conductivity) is the capability of an aqueous solution to transmit the current (Kozheshkurt et al., 2021). This property depends on various physical & chemical parameters such as pH value, alkalinity, total dissolved solids (TDS), total hardness, total solids, calcium, chemical oxygen demand, chloride, temperature and iron concentration of water (Shrestha & Basnet, 2018). The conductivity of rivers and stream is effected primarily by the exposed geology of the region through which water flows (Rao et al., 1997). Groundwater inflows also have the similar effects depending on the subsurface bedrock geology they flow through (Moore & Walsh, 2021). The discharges to streams can change the conductivity depending on their make-up (Flynn et al., 2021). The estimation of electrical conductivity offers a quick and appropriate means to compute the concentration of electrolytes in water comprising mostly mineral salts. The device used for this examination was the EC meter, HACH-44600, USA. The samples were stirred before getting any measurements and then permitted to stabilize till the removal of air bubbles in a beaker. The meter was standardized with the support of potassium chloride (KCl) solution, 0.01 M at 25°C constant temperature. The distilled water was used to wash the conductivity cell and then with sample water for EC measurement. The value was noted on the EC meter for each sample.

4.7.3 Total Dissolved Solids

Total Dissolved Solids (TDS) can be found in streams in different forms i.e. dissolved, suspended and volatile (Patil & Prasad, 2020). Suspended solids contain charged ions, dissolved organic material, inorganic ions, etc. (Walker, 2020). Dissolved solids can pass through filter, whereas suspended solids cannot pass. Fertilizers from farming fields and grasslands can also add a variety of ions to stream water. In addition, numerous forms of aquatic life are impacted negatively if the TDS levels are high (Timotewos & Reddythota, 2000). The TDS was measured by the gravimetric method.

Initially suspended particles were filtered by a standard glass fiber. Almost 500 ml filtrate is collected in a flask. In a pre-weighted dish, it is then transferred and it is further heated in an oven to remove water from the filtrate. Then filtrate is again weighed. TDS is then calculated in ppm by using the given equation 4.8.

$$\text{Total Dissolved Solid in ppm} = (W*10^{6})/500 \quad \ldots\ldots\ldots \quad \text{eq. (4.8)}$$

Where "W" is the weight of a dissolved solids in 500 gm of water (Patil & Prasad, 2020).

4.7.4 Chloride

One of the main inorganic anions usually found in water and wastewater is the Chloride (Cl^-) ion. Chloride concentrations in drinkable water can cause a salty taste, which varies and depends on the chemical makeup of the water (Mahlet, 2022). Whereas, if the cation is sodium and water containing 250 mg Cl/l concentration may taste salty to the palate. However, when calcium and magnesium cations predominate, the usual salty taste may be absent in water with as much as 1000 mg/l. The Titration standards method was employed for this analysis. The collected representative samples were placed in clean, chemical-resistant plastic bottles. 100 ml was the maximum amount of sample that was needed. The samples could be stored without the need for any additional preservatives. By employing potassium chromate as an indicator and standard silver nitrate for titration, chloride can be measured in a natural or slightly alkaline solution. Prior to the formation of red silver chromate, silver chloride quantitatively precipitates. The chloride ion is used to measure the equivalents of bromide, iodide and cyanide. The presence of thiocyanate, thiosulfate, cyanide, sulphide, iron (if concentration present >10 mg/l) and orthophosphate (if concentration present >25 mg/l) are the main interfering substances. Samples that are turbid or highly coloured need to be pre-treated. The following reagents were used in this analysis i.e. Solution of standard Silver Nitrate $AgNO_3$ (0.0141 N) and Potassium chromate K_2CrO_4 solution as an indicator. A conical flask was used to collect a 20 ml sample. K_2CrO_4

few drops added as an indicator solution and the reaction was titrated up to a reddish endpoint using a conventional $AgNO_3$ (titrant) solution. The accuracy was verified using a standard of 100 ppm NaCl.

Cl^- concentration (mg/l) = AB x N x 35.45 x 1000/V (Bugica et al., 2020)

Where:
A and B represent the total volumes of silver nitrate solution required for lab sample and blank, N =Normality of $AgNO_3$ used & V = Volume of sample in ml.

4.7.5 Sulphate

Natural water usually contains sulphate ions. while many sulphide compounds can easily mix in water such as atmospheric sulphur dioxide that can easily dissolved in to become sulphate compounds of water (Manisalidis et al., 2020). Most sedimentary rocks contain sulphur-rich minerals which can contaminate the groundwater as well (Kushawaha & Aithani, 2021). In the process of weathering, sulphide minerals are oxidized, forming sulphate that is carried away by water (Timotewos & Reddythota, 2000). The method used to measure sulphate content was the "Titration Method" (Karunanidhi et al., 2021). Higher sulphate intake could result in many health diseases related to digestion, diarrhoea, catharsis, stomach irritation, dehydration, etc. (Karunanidhi et al., 2021). Sulphates can also be found in organic substances that contain sulphur and in the discharge of industrial waste. The amount of sulphate in one litre of natural water might range from a few milligrams to several hundred mg. The maximum desirable sulphate concentration has been determined by the WHO to be 250 mg/l. To lessen the chance of bacterial conversion of sulphate to sulphide in contaminated or polluted samples, the samples were preserved in uncontaminated plastic bottles and instantly keep in storage at 4^oC. At quantities greater than those in the list below, the following substances interfere: Chloride 40,000 mg/l as Cl, Calcium 20,000 mg/l as $CaCO_3$, Silica 500 mg/l as SiO_2, and Magnesium 10,000 mg/l as $MgCO_3$.

A well-known and most employed technique of Turbidimetric technique was employed for the examination of sulphate. The sample's sulphate ion interacts with crystals of barium chloride to produce an insoluble barium sulphate turbidity. The ratio of the Sulphate concentration to the amount of turbidity generated. The analysis was conducted using an Analytic Jena UV-VIS Spectrophotometer. In a thoroughly cleaned beaker, a 10 ml of deionized water was added, followed by 2ml buffer solution sulphate and one pinch crystals of barium chloride. After mixing the solution for a minute vigorously, actual water samples were used to measure the absorbance at a wavelength of 420 nm after five minutes of reaction time. The following equation 4.9 was used to calculate the concentration of sulphate:

$$\text{sample conc.} = (Abs.of\ sample)\ x\ conc.of\ \frac{standard}{Abs}.of\ standard \quad \text{.....eq. (4.9)}$$

4.7.6 Calcium

Calcium, in the form of the Ca^{2+} ion, is one of the important positive ions, or inorganic ions found in freshwater and saltwater (Bhagat et al., 2021). The source of calcium can originate from the detachment of salts, such as calcium sulphate or calcium chloride, in water. Most of the calcium in surface water derives from streams flowing over the limestone, $CaSO_4$ $2H_2O$, $CaCO_3$, gypsum and other calcium-containing rocks and minerals (Oster et al., 2021). $CaCO_3$ is somewhat insoluble in water. But it can dissolves more frequently the water comprising dissolved carbon dioxide (Tang et al., 2021). Calcium present in freshwater range from 0 to 100 mg/l and most commonly has the highest concentration of any freshwater cation. The upper limit of Ca^{2+} recommended in drinking water is 50 mg/l. High levels of calcium is not considered a health concern. If the calcium ion level dropped in freshwater below 5 mg/l, it can only support animal life and sparse plant, a condition known as oligotrophic (Timotewos &

Reddythota, 2000). Seawater most commonly contains Ca^{2+} levels of about 400 mg/L. Calcium like sulphate is also estimated by the titration method (He et al., 2020).

4.7.7 Magnesium

The EDTA titration method was used to measure Mg^{2+}. Magnesium concentration is an essential content to examine water quality (Princela et al., 2021). It has a positive relation with TDS and electric conductivity (Amiri et al., 2021). Magnesium is usually mixed with water from limestone, dolomitic limestone and ferromagnesian minerals, which are found as a contaminant (Mebarki et al., 2021). Magnesium plays a vital role in determining the hardness of water (Amiri et al., 2021). A higher quantity of magnesium in water can initiate problems such as irregular heartbeat, low blood pressure, slowed breathing, and coma among the locals who consume it (Mebarki et al., 2021).

4.7.8 Sodium

A high sodium ratio in the soil can harm soil permeability (Wantasen et al., 2021). Sodium is estimated with the help of the flame photometer method (Yaghi et al., 2020). The instrument is adjusted according to the given standard with the known concentration of sodium ions (1 to 100 mg/L) (Timotewos & Reddythota, 2000). Relatively high concentrations may be found in hard water and brine softened by the sodium exchange process (Li et al., 2021). Sodium can be easily determined by a flame photometer which has a high resolution (Chebet et al., 2020). Sodium high-level intake can cause severe heart and kidney problems or insomnia (Banerjee & Prasad, 2020).

4.7.9 Phosphorus

Phosphorus is an important nutrient for animals and plants (Li et al., 2021). Phosphorus is found in low amounts in most freshwaters, even a minor increase in phosphorus level can trigger a whole chain of undesirable natural processes in water including frequent plant growth, low dissolved oxygen, algae bloom and the loss of certain fish, aquatic animals and other invertebrates (Timotewos & Reddythota, 2020). There are various uncountable sources of phosphorus, both anthropogenic and natural. In nature, phosphorus normally exists as part of a phosphate molecule (PO_4) (Hasan & Tewari, 2020d). Plants usually require phosphorus in inorganic form (Zeitoun & Biswas, 2020). Animals can use either inorganic or organic phosphate (Dobenecker et al., 2021). Both organic and inorganic phosphorus can be suspended and attached to particles in the water or either be dissolved in the water (Hasan & Tewari, 2020d).

4.7.10 Nitrate

Anthropogenic activities like pesticide spray and fertilizers can increase the volume of nitrate in groundwater (Singh et al., 2022). Nitrate (NO_3^-), has the ability to penetrate the ground under dry conditions (Arulnangai et al., 2021). According to the World Health Organization (WHO), the ideal value for nitrate is 50 mg/l (Claeson, 2021). The value of nitrate was derived by titration method and also by using a spectrophotometer (Troudi et al., 2020). Fertilizers from cultivated land, drainage from livestock, as well as feed lots and some home and industrial wastes are significant sources of nitrate. Natural water that hasn't been contaminated typically only has trace quantities of nitrate. Infants are thought to be at risk from drinking water with an excessive amount of nitrate. The boric acid (2 ml/l samples) and polycarbonate bottles were used to collect the samples, which were subsequently chilled to 4^oC. Warming the samples to room temperature and neutralizing them with a 5.0N sodium hydroxide

standard solution were done before analysis. The UV Spectrophotometric method was used to measure the nitrate. 0.2 ml of (1 N HCl) was added to 10 ml deionized water in a 25 ml container. It first received special correction or blank correction, then 10 ml of standard. The sample's nitrate concentration was measured using an absorbance reading at 220 nm and the sample's organic interference was measured using a measurement at 275 nm. In order to get the adjusted result, subtract the reading of absorbance at 275 nm two times from the reading at 220 nm. The following equation 4.10 was used to calculate the concentration.

$$\text{Conc. of sample} = \text{Abs. of sample x Conc. of standard} / \text{Abs. of standard} \quad \ldots\ldots \text{eq. (4.10)}$$

If the Spectrophotometer is set for the concentration determination, it is possible to directly measure the concentration of Nitrate in mg/l from the calibration curve.

4.7.11 Irrigation Water Quality

The irrigation water quality was assessed using a standard diagram for suitability of water in irrigation using, the Trilinear diagram, Sodium (Na%), Potential salinity (PS), Residue sodium carbonate (RSC), Wilcox diagram, Sodium adsorption ratio (SAR), Magnesium absorption ratio (MAR), Kelley's ratio (KR), Permeability index (PI) and Kelley's Ratio (KR). Table 4.3 summarizes the maximum permissible limit and highest desirable limit of chemical parameter pH, EC, TDS, Ca^{2+}, Mg^{2+}, Na^{+}, K^{+}, HCO_3^{2-}, Cl^{-} and SO_4^{2-} present in domestic water as per World Health Organization standards. The measured parameters in laboratory were compared with the World Health Organization 2021 standard to evaluate the maximum permissible limit and higher desire limit in groundwater sample of study area (Table 4.3). Finally, the trace element was also analyzed for the sample WR, NA, KA, KU, AA, AL, AM, DU, UG, UP, RW, RE, CM, CZ, CL, CN, UL, and ST using an Atomic Absorption Spectrometer.

Table 4.3: Groundwater maximum permissible limits (MPL) prescribed by World Health Organization standard for domestic purposes (WHO, 2021).

Parameters	**Unites**	WHO (2021)	
		HDL	**MPL**
pH	----	7.0	8.5
EC	µS/cm	Nil	1500
TDS	mg/l	500	1500
Ca^{2+}	mg/l	75	200
Mg^{2+}	mg/l	30	150
Na^{+}	mg/l	Nil	200
K^{+}	mg/l	Nil	30
HCO_3^{2-}	mg/l	200	350
Cl^{-}	mg/l	250	400
SO_4^{2-}	mg/l	200	400
NO_3^{-}	mg/l	45	No relaxation
F^{-}	mg/l	1	1.5
HDL: Highest Desirable Limit. MPL: Maximum Permissible Limit.			

CHAPTER 5

RESULTS & DISCUSSION

5.1 Questionnaire Survey Analysis

A total of 150 respondents actively participated during the awareness seminar on sustainable groundwater management in Winder, Balochistan. The interaction with local tube well owners, irrigation department representatives, social workers and young farmers supported summarizing the present situation of groundwater. The survey form was also filled out by the participants during the consultation, in which 52% of the respondent age group was from (50-65 years) providing effective hydrogeological information of the study area, previous water table and decline in the last 10 years based on their observation and experience, while 17% individuals were of (35-50 years) this age group was also important to collect the information of last decades as an active farmer, 31% was young local farmers, social workers and students to discuss the smart farming ideas and mitigation to control the adverse impact of groundwater on agriculture and health of locals.

During the sampling of water, the interaction with local female farmer's responses was also incorporated, which was not possible in the seminar due to local culture and tradition. The awareness seminar was also recorded by Dunya news and published in a newspaper by editor Mustafa Habib (Appendix F). This represents and highlights the issue to the Government of Balochistan and concerned authorities for present groundwater overexploitation and its impact on quality. The questionnaire survey analysis shows that there are no hydrogeological studies had been conducted to explore the aquifer, water table and thickness in the study area before drilling a tube-well. The local driller is using a straight rotary drilling technique to drill a well. On completion of the tube well no drilling report, log and pumping test were submitted to the concerned departments. The study area relies mainly on groundwater for domestic and irrigation activities whereas the river flow is seasonal. Furthermore, during the discussion with farmers and local government officials, it was also observed that there is no monitoring of the tube well for static water table, abstraction and quality. There is no permission or procedure required by the provincial government, anyone can drill a tube-well on his farm for groundwater abstraction. The main driving reason to adopt the tube well in this region can be summarized as the area being in an arid region, limited surface water bodies, a lack of planning by the government and providing subsidiaries on electricity for tube wells, poverty alleviation and rapid rural development. Therefore, the tube well is the primary source of irrigation in the study area (Figure 5.1).

Field data collection (questionnaire survey) shows the total number of drilled wells in the study area are more than 250 and approximately 378 cubic meters per day of water is extracted from each well by using a submersible pump. The number of tube wells in 2010 was 80 and annual production was 11.7 million cubic meters. The drastic increase in the number of tube wells increases the annual production by approximately 36.1 million cubic meters for 2021 (Figure 5.2). The current depth of drilled tube wells ranges from 106.5 meters to 137 meters, a decade ago the maximum depth was 45-106 meters. Most of the wells that were drilled a decade ago are still producing but the water table declined rapidly and many shallow tube wells are abandoned (Figure 5.3). Due to the increase in the depth of the water table, the pumping depth also increased which is more than 92 meters. The cost of the development tube well was approximately Rs. 0.5 million before 2010 that has already increased to Rs. 2 million.

The major source of power is an electric and solar pump, where people are shifting their well toward solar tub wells (Figure 5.4). This is also leading to an increase in over-extraction of groundwater in the study area as there is a government subsidiary on solar-based tube wells. Previously a subsidy of Rs. 27 billion was on the electricity bill, as result in a dramatic rise was experienced and more than 30,000 tube wells were drilled all over Balochistan in the last two decades. However, this subsidy offered by provincial and federal governments finally became a financial burden. Therefore, both the federal and provincial governments decided to shift 30,000 electric-operated tube wells into solar with an estimated budget of Rs. 145 billion. The main objective of this project is to relieve the stress on the financial budget for electric subsidies and the adoption of renewable energy resources. This policy is very useful in terms of saving 900 MW of electricity all over Balochistan but at the cost of providing a disaster recipe in form of a blank cheque to the farmers of Balochistan. The subsidy and accessibility of solar on instalments provide an opportunity to increase agricultural activity by increasing the number of tube-well and abstraction due to no electric bills. In long-term sustainability, this may will directly impact the groundwater table.

The over-extraction of water not only causes a decline in water table ranges from 25-45 meters at the present situation in the study area (Figure 5.5). The water table is declining by approximately 2.2 meters per year in tube wells. The irrigation representative and farmers were also complaining about the quality of the water. In the last decade, farmers experienced a change in crops pattern. For instance, the Banana crop is almost finished due to higher TDS of groundwater; the banana farm is replaced by the Chikoo plantation during the last decade. The identified stations were also visited and analyzed using satellite images which also depict the change in crops pattern from Banana to Chikoo farm (Figure 5.6). Station 1, 2 and 3 in 2009 was covered by Banana crops and the increase in TDS of groundwater sample gradually replace the Banana crops with the Chikoo plantation. The development and rapid growth in the agriculture sector of the study area can be observed on google earth images from 1985-2021. There was very limited agricultural activity in 1985 mainly dependent on utilizing surface water resources Figure 5.7. The green revolution in the farming sector of Winder was started after 1990 as a result of collaboration with Japan government and the provincial agriculture department. The image from 2005 till recent show that both sides of the

Winder River is covered by a farmer and it is already analyzed that groundwater is the major source to develop the economy of the area (Figure 5.7).

During the visit of coastal area, it was observed that local communities were used to get fresh water from hand pumps which are now abandoned due to increase in salinity. There were no filtration or reverse osmosis plant to treat the water for locals living in study area. The local farmers residing in the study area are using groundwater for drinking purpose without any treatment however, except in the city some private filtration plant is using treated water. The local farmer and social workers are unaware of groundwater overexploitation, groundwater management, a threat to sustainability and seawater intrusion. However, at this stage, the economy of the study area is growing as a result of farmers which were migrated from other districts of Balochistan in the last two decades due to the availability of water and government subsidiaries on agriculture. As the economic development relies on excess groundwater pumping, it is feared that this will hardly sustain and may lead to the depletion of aquifers. The deterioration of water quality will be a threat to the agriculture sector in the future, moreover, it will severely impact the farmers because agriculture is the primary source of income in Winder Balochistan.

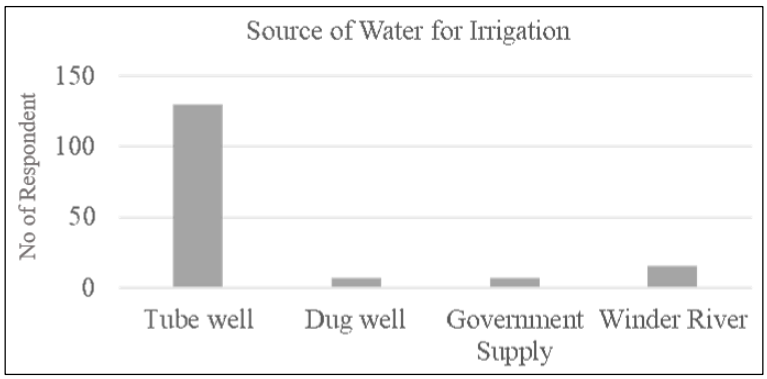

Figure 5.1 The number of respondent identifying different source of water for agriculture activity in Winder Balochistan.

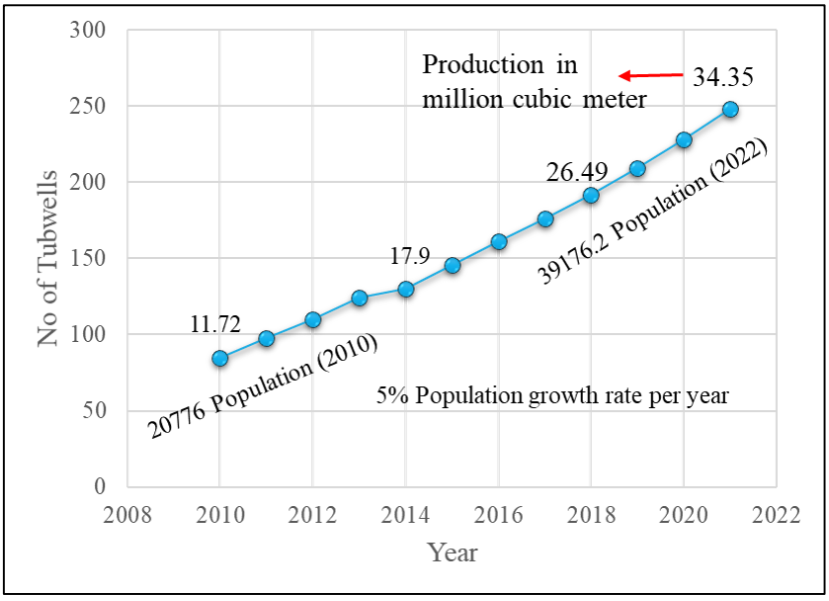

Figure 5.2 The number of tube well, abstraction of groundwater in million cubic meters and population from 2010 to 2021 in the study area.

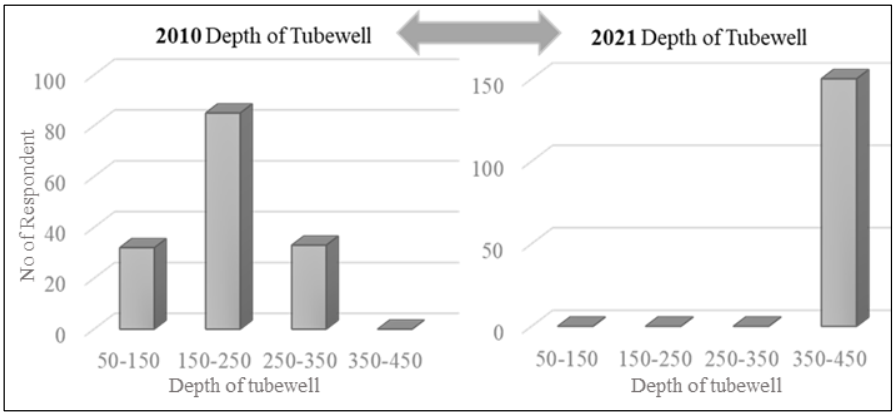

Figure 5.3 Depth of tube well in 2010 and 2021 for groundwater pumping.

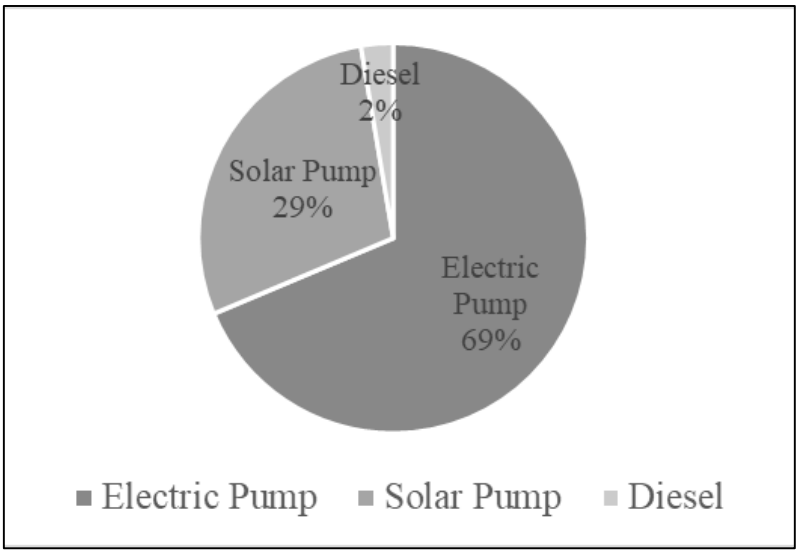

Figure 5.4 Source of pumping groundwater in Winder Balochistan.

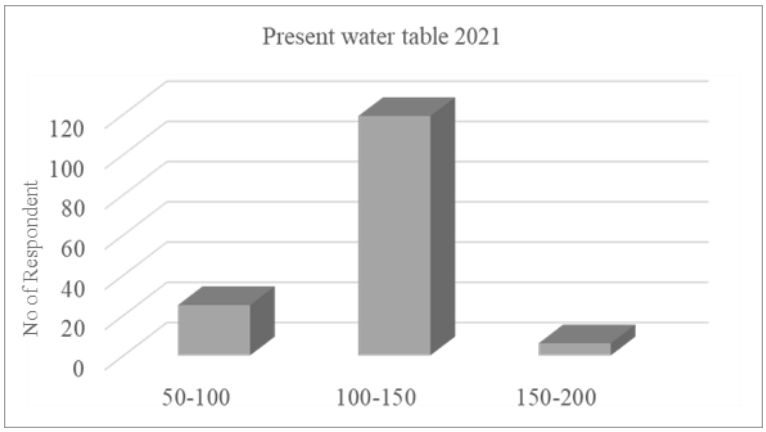

Figure 5.5 The present groundwater table in tub-wells of Winder Balochistan.

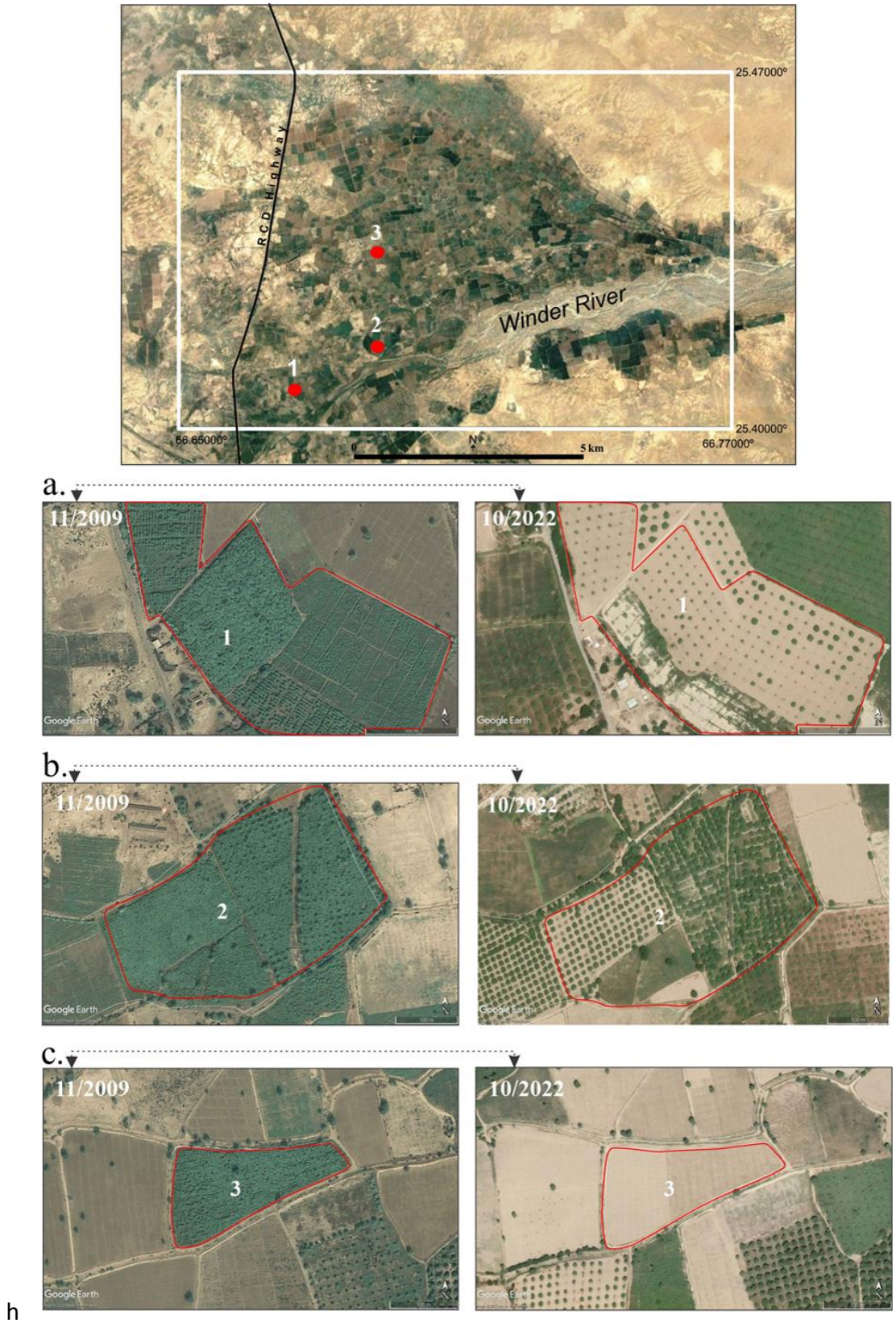

h

Figure 5.6 The temporal analysis of satellite image to observe the Banana crop replacement by Chikoo plantation from 2009 and 2022 for three different stations in the study area. (a.) represent the station 1 (2009-2022), (b.) shows the station 2 comparision for the year 2009-2022 and (c.) highlight the variation from 2009-2022.

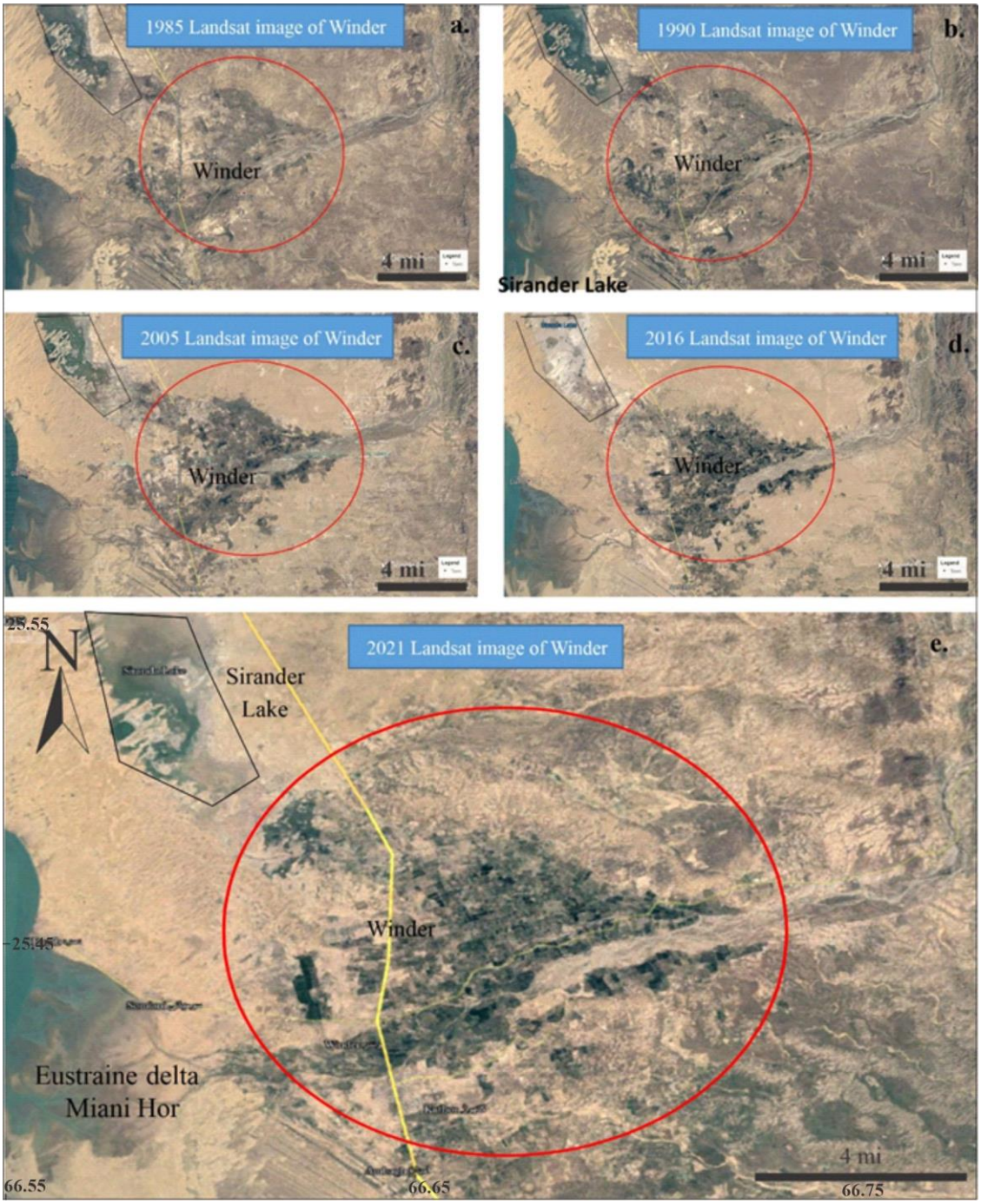

Figure 5.7 Google Earth images taken for the month of December (a) 1985 Landsat image of Winder, Balochistan (b) 1990 Landsat image of Winder, Balochistan (c) 2005 Landsat image of Winder, Balochistan (d) 2016 Landsat image of Winder, Balochistan (e) 2021 Google Earth Landsat image of Winder represent the geomorphological features comprises mountain in NE, NE-SW river flow, Siranda lake in NW and Agriculture activity around the Winder river.

5.2 Geo-electrical characterization of Groundwater

The data of 27 vertical electrical soundings (VES) stations were collected by using Schlumberger configuration in Winder, Balochistan. The results of 27 VES curves and modelled layers (thickness, resistivity and depth) were used, which revealed different lithological layers, through the study area at depth of 150 m. The interpreted lithology includes clay, sandy clay, silty sand & sandy gravel units. VES curve and geo-electric model show the occurrence of five geologic layers. These units are contained of sand, clay, sandy clay, silty sand and sandy gravel. The fifth layer maximum depth was unknown due to the survey limit. The results of 27 VES stations are the following:

5.2.1 R-1 Electrical Sounding using Schlumberger Layout

The probe was acquired at (Lat. 25° 24' 43.92" N, Long. 66° 38' 46.04" E) along, the left side of the RCD highway in the north of Winder Town towards Uthal which depicts that a total of five layers were delineated (Figure 5.8). The interpreted curve using IPI2Win presents the first layer with a resistivity of 11 Ωm up to a depth of 3.79 m and lithology inferred as sandy clay, the second unit with a resistivity of 27 Ωm at depth of 12.2 m (8.4 m thick) represents a very high resistive layer in the sand, third layer with a resistivity of 31.8 Ωm up to a depth of 30 m (18.6 m thick) is characterized as very high resistivity and depict the presence of sandy gravel, the fourth layer with the resistivity of 24.1 Ωm up to a depth of 87.4 m (56.6 m thick) shows the resistivity of sand deposits. The 5th layer resistivity is 20 Ωm and interpreted lithology is silty sand. The type of curve is AKQ i.e. ($\rho_1 < \rho2 < \rho3 > \rho4 > \rho5$). R-1 contained a thick sequence of unconsolidated deposits of sandy gravel and sand deposits.

5.2.2 R-2 Electrical Sounding using Schlumberger Layout

The R-2 station was acquired out at (Lat. 25°26'2.03"N, Long. 66°38'37.00"E) on the left side of the RCD highway. The interpreted curve using IPI2Win in Figure 5.9 represent the first layer with an apparent resistivity of 12.4 Ωm up to a depth of 3.28 m (3.28 m thick) characterizes the sandy clay. Similarly, the second unit with a resistivity of 28.2 Ωm up to a depth of 12.7 m (9.43 m thick) represents sand deposits, third layer with a resistivity of 26 Ωm up to a depth of 28.4 m (15.7 m thick), a fourth layer having the resistivity of 32.3 Ωm up to a depth of 99 m (70.6 m thick) sandy gravel. The fifth layer silty sand resistivity is 23.6 Ωm. However, the thickness and maximum depth were unknown due to the survey limit. The type of curve is KHK i.e. ($\rho1 < \rho2 > \rho3 < \rho4 > \rho5$), R-2 contained a thick deposit of unconsolidated sand and sand gravel deposits having good porosity and permeability.

5.2.3 R-3 Electrical Sounding using Schlumberger Layout

R-3 station was carried out at (Lat. 25°23'16.71"N, Long. 66°42'49.57"E) east of Winder Town. The interpreted curve using IPI2Win in Figure 5.10 represent the first layer with the apparent resistivity of 19.5 Ωm up to a depth, less than 2.64 m (2.64 m thick) represents the silty sand, the second layer with a resistivity of 13.3 Ωm up to a depth of 8.81 m (6.17 m thick) represents sandy clay deposits, third layer with a resistivity of 31.3 Ωm up to a depth of 26.1 m (17.3 m thick) sandy gravel, a fourth layer showing the resistivity of 34.8 Ωm up to a depth of 101 m (74.9 m thick) sandy gravel. The fifth layer resistivity 17.1 Ωm represents silty sand, the thickness and maximum depth was unknown due to the survey limit. Thus, the curve is HAK i.e. $\rho_1 > \rho2 < \rho3 < \rho4 > \rho5$.

5.2.4 R-4 Electrical Sounding using Schlumberger Layout

R-4 station was acquired at (Lat. 25°24'17.58"N, Long. 66°40'0.14"E) on the right side of RCD highway, north of Winder Town. The interpreted curve using IPI2Win in Figure 5.11 represent the top layer with an apparent resistivity of 22.1 Ωm up to a depth of 2.65 m and 2.56 m thick unit characterizes the sand, the second unit with a resistivity of 34.5 Ωm up to a depth of 3.87 m (1.31 m thick) represents sandy gravel deposits, third layer with a resistivity of 50.4 Ωm up to a depth of 13.4 m (9.49 m thick) characterizes very high resistivity and shows the presence of sandy gravel filled with a freshwater, fourth layer showing the resistivity of 33.3 Ωm up to a depth of 62.2 m (48.9 m thick) shows the low resistivity in sandy gravel deposits. The fifth layer resistivity is very low 17.4 Ωm in silty sand. The type of curve is AKQ i.e. ($\rho_1 < \rho2 < \rho3 > \rho4 > \rho5$). R-4 consists of a thick sequence of unconsolidated succession i.e. sandy clay, sandy gravel and silty sand deposits.

5.2.5 R-5 Electrical Sounding using Schlumberger Layout

R-5 station was acquired at (Lat. 25°26'6.02"N, Long. 66°41'6.35"E) the north of Winder Town on the right side of the RCD highway. The interpreted curve using IPI2Win in Figure 5.12 represents the top layer, the apparent resistivity of 8.84 Ωm up to a depth of 2.09 m (2.09 m thick) characterizes the clay, the second layer with a resistivity of 20.9 Ωm up to a depth of 6.61 m (4.52 m thick) represents sand deposits, the third layer with a resistivity of 28.7 Ωm up to a depth of 27.9 m (21.3 m thick) characterizes as sand filled with fresh water, a fourth layer depicting the resistivity of 33.3 Ωm up to a depth of 99.1 m (71.2 m thick) shows sandy gravel. The fifth layer resistivity is 38 Ωm in sandy gravel is AAK i.e. ($\rho_1 < \rho2 < \rho3 < \rho4 > \rho5$).

5.2.6 R-6 Electrical Sounding using Schlumberger Layout

R-6 station was acquired at (Lat. 25°25'48.86"N, Long. 66°43'40.51"E) in the northeast along the Winder River. The interpreted curve using IPI2Win in Figure 5.13, presents the top layer with an apparent resistivity of 9.38 Ωm up to a depth of 2.03 m (2.03 m thick) characterizes the clay, the second layer with a resistivity of 22.5 Ωm up to a depth of 7.01 m (4.98 m thick) represents sand deposits, the third layer with a resistivity of 33.9 Ωm up to a depth of 32.2 m (25.2 m thick) characterizes high resistivity and indicate the presence of sand gravel filled fresh water, a fourth layer with the resistivity of 28.7 Ωm up to a depth of 101 m (68.5 m thick) also shows the sand deposits. The fifth layer high resistivity was interpreted as sandy gravel 36 Ωm the thickness and maximum depth were unknown due to the survey limit. Thus the overall type of curve is AKQ i.e. ($\rho_1 < \rho2 < \rho3 > \rho4 > \rho5$). R-6 contains a thick deposits of unconsolidated sand, sandy clay and sandy gravel.

5.2.7 R-7 Electrical Sounding using Schlumberger Layout

R-7 was acquired at (Lat. 25°26'28.54"N, Long. 66°46'31.55"E) northeast of Winder River which represents five lithological layers. The interpreted curve using IPI2Win is represented in Figure 5.14, the top layer shows apparent resistivity of 8.84 Ωm up to a depth of 1.65 m interpreted as clay, the second layer with a resistivity of 37.2 Ωm up to a depth of 9.3 m (7.65 m thick) represents sandy gravel, third layer with a resistivity of 43.1 Ωm up to a depth of 51.1 m (41.8 m thick) characterizes very high resistivity and depicts the presence of sandy gravel lithology, a fourth layer with the resistivity of 51.6 Ωm up to a depth of 101 m (49.9 m thick) shows the resistivity of sandy gravel deposits. The fifth layer resistivity is also very high 40.6 Ωm shows the presence of sandy gravel, the thickness and maximum depth were unknown due to the

survey limit. The standard curve type is AAK i.e. ($\rho_1 < \rho2 < \rho3 < \rho4 > \rho5$). R-7, a thick sequence of unconsolidated sandy gravel, sand and thin deposits of clay

5.2.8 R-8 Electrical Sounding using Schlumberger Layout

R-8 was acquired at (Lat. 25°27'51.72"N, Long. 66°43'43.72" E) northwest of Winder River and demarcate that five lithological layers. The interpreted curve using IPI2Win is represented in Figure 5.15, the top layer apparent resistivity of 32.7 Ωm up to a depth of 1.94 m and characterizes the sand, the second layer with a resistivity of 24.1 Ωm up to a depth of 4.73 m (2.79 m thick) represents sand, the third layer with a resistivity of 20.4 Ωm up to a depth of 23.9 m (19.2 m thick) characterizes very low resistivity and shows the presence of silty sand lithology, a fourth layer showing the resistivity of 28.7 Ωm up to a depth of 99.3 m (75.5 m thick) shows the resistivity of sand deposits. The fifth layer resistivity is very high 47.3 Ωm showing the presence of sandy gravel, the thickness and maximum depth were unknown due to the survey limit. The type of curve is QHA i.e. ($\rho1 > \rho2 > \rho3 < \rho4 < \rho5$). R-8 encompasses a thick sequence of unconsolidated sandy clay, sandy gravel and sand with a thin deposits of silty sand having good porosity and permeability of the aquifer.

5.2.9 R-9 Electrical Sounding using Schlumberger Layout

R-9 was acquired at (Lat. 25°22'43.01"N, Long. 66°40'14.83"E) southwest of Winder River along RCD highway. The interpreted curve using IPI2Win (Figure 5.16) presented the top layer showing the apparent resistivity 15.9 Ωm up to a depth 1.69 m characterizes the sandy clay, the second layer resistivity is 27.25 Ωm up to a depth of 6.74 m (5.05 m thick) represents sand, the third layer with a resistivity of 34.88 Ωm up

to a depth of 30.7 m (23.43 m thick) characterizes high resistivity and shows the presence of sandy gravel lithology, a fourth layer showing the resistivity of 36.17 Ωm up to a depth of 99.28 m (69.11 m thick) shows the resistivity of sand gravel deposits. The fifth layer resistivity is low 19.94 Ωm and shows the presence of sand, the thickness and maximum depth were unknown due to the survey limit. The type of curve is AAK i.e. ($\rho_1 < \rho2 < \rho3 < \rho4 > \rho5$). R-9 encompasses a thick layer of unconsolidated sandy gravel and sand deposits.

5.2.10 R-10 Electrical Sounding using Schlumberger Layout

R-10 probe was acquired at (Lat. 25°22'19.84"N, Long. 66°43'12.26"E) southeast of Winder Town. The interpreted curve using IPI2Win represented in Figure 5.17, the top layer shows the apparent resistivity of 11.5 Ωm up to a depth of 2.59 m characterizes the sandy clay, the second unit resistivity is 20.5 Ωm up to a depth of 5.09 m (2.5 m thick) sand deposits, third layer with a resistivity of 24.8 Ωm up to a depth of 20.2 m (15.1 m thick) characterizes as sand, a fourth layer having the resistivity of 37 Ωm up to a depth of 54.3 m (34.1 m thick) depicts the resistivity of sandy gravel. The fifth layer resistivity is 25.7 Ωm comprising sand deposits, the thickness and maximum depth was unknown due to the survey limit. The type of curve is AAK i.e. ($\rho_1 < \rho2 < \rho3 < \rho4 > \rho5$). R-10 includes thick sediments of unconsolidated sandy gravel and sand deposits.

5.2.11 R-11 Electrical Sounding using Schlumberger Layout

R-11 probe was acquired at (Lat. 25° 21' 16.99"N, Long. 66°46'3.72" E) southeast of Winder toward Kathor. This station also shows the five layers. The

interpreted curve using IPI2Win is represented in Figure 5.18. According to this, the top layer apparent resistivity is 28.3 Ωm up to a depth of 2.09 m characterizes the sand, the second unit with a resistivity of 17.9 Ωm up to a depth of 14.2 m (12.1 m thick) silty sand deposits, third unit with a resistivity of 38.7 Ωm up to a depth of 47.3 m (33.1 m thick) characterizes very high resistivity and shows the presence of sandy gravel lithology of recent deposits, a fourth layer having the resistivity of 17.1 Ωm up to a depth of 105 m (57.7 m thick) shows the resistivity of silty sand. The fifth layer resistivity is 15.5 Ωm also comprises silty sand deposits, the thickness and maximum depth was unknown due to the survey limit. The type of curve is HKQ i.e. ($\rho_1 > \rho 2 < \rho 3 > \rho 4 > \rho 5$). R-11 encloses a thick succession of unconsolidated deposits.

5.2.12 R-12 Electrical Sounding using Schlumberger Layout

R-12 probe was acquired at (Lat. 25°22'4.50"N, Long. 66°41'27.93"E) located near Winder Town toward the east. As per interpreted curve using IPI2Win is represented in Figure 5.19, the top layer apparent resistivity is 2.06 Ωm up to a depth of 1.96 m (1.96 m thick) characterizes the clay, the second layer resistivity is 6.32 Ωm up to a depth of 8.39 m (6.43 m thick) clay deposits, third unit shows a resistivity of 15 Ωm up to a depth of 31.6 m (23.2 m thick) shows the presence of silty sand lithology of recent deposits, a fourth unit with the resistivity of 18.6 Ωm up to a depth of 102 m (70.3m thick) depicts the resistivity of sand. The fifth layer resistivity is 25.5 Ωm also comprises sand deposits, the thickness and maximum depth were unknown due to the survey limit. The type of curve is AAA i.e. ($\rho_1 < \rho 2 < \rho 3 < \rho 4 < \rho 5$). R-12 contains thick strata of unconsolidated sandy gravel & sand deposits containing a good porosity and permeability of the aquifer.

5.2.13 R-13 Electrical Sounding using Schlumberger Layout

R-13 probe was acquired at (Lat. 25°20'47.17"N, Long. 66°41'57.94"E) south of Winder Town. The interpreted curve using IPI2Win is represented in Figure 5.20, and shows the first layer apparent resistivity 9.76 Ωm up to a depth 2.93m characterizes the sandy clay, the second unit resistivity is 25.3 Ωm up to a depth of 9.09 m (6.16 m thick) sand deposits, third layer with a resistivity of 31.6 Ωm up to a depth of 30.8 m (21.7 m thick) characterizes very high resistivity and demarcate the presence of sandy gravel lithology of recent deposits, a fourth unit having the resistivity of 38.8 Ωm up to a depth of 87.3 m (56.5 m thick) shows the resistivity of sandy gravel. The fifth layer resistivity is 16.6 Ωm comprising silty sand deposits, the thickness and maximum depth was unknown due to the survey limit. The type of curve is AAK i.e. ($\rho_1 < \rho2 < \rho3 < \rho4 > \rho5$). R-13 encompasses a thick zone of unconsolidated clay, sandy clay and silty sand deposits.

5.2.14 R-14 Electrical Sounding using Schlumberger Layout

R-14 probe was acquired at (Lat. 25°20'23.80"N, Long. 66°43'29.09"E) southeast of Winder Town. The interpreted curve using IPI2Win is presented in Figure 5.21, the first layer apparent resistivity 17.6 Ωm up to a depth of 1.62 m characterizes the silty sand, the second unit resistivity is 29.7 Ωm up to a depth of 3.95 m (2.33 m thick) sand deposits, third layer with a resistivity of 35.4 Ωm up to a depth of 19.8 m (15.8 m thick) characterizes very high resistivity and depicts the presence of sandy gravel lithology of recent deposits, a fourth layer having the resistivity of 49.8 Ωm up to a depth of 32.6 m (52.4 m thick) also shows the resistivity of sandy gravel. The fifth layer resistivity is 18 Ωm comprising silty sand deposits, the thickness and maximum depth was unknown due to the survey limit. The type of curve is AAK i.e., $\rho1 < \rho2 <$

ρ3 < ρ4 > ρ5. R-14 consists of a thick layer of unconsolidated sandy gravel, sand and silty sand deposits.

5.2.15 R-15 Electrical Sounding using Schlumberger Layout

R-15 probe was acquired at (Lat. 25°19'31.87"N, Long. 66°39'51.47"E) southwest of Winder Town. The interpreted curve using IPI2Win is presented in Figure 5.22. According to this, the first layer apparent resistivity 32.9 Ωm up to a depth of 2.16 m characterizes the dune sand, the second unit resistivity is 19.2 Ωm up to a depth of 9.93 m (7.77 m thick) silty sand deposits, third unit with a resistivity of 25.9 Ωm up to a depth of 29.5 m (19.6 m thick) characterizes as sand lithology of recent deposits, a fourth unit showing the resistivity of 17.1 Ωm up to a depth of 81 m (51.5 m thick) shows the resistivity of silty sand. The fifth layer resistivity is 32.2 Ωm also comprises sandy gravel, the thickness and maximum depth were unknown due to the survey limit. The type of curve is HKH i.e. (ρ1 > ρ2 < ρ3 > ρ4 < ρ5). R-15 contains a thick layer of unconsolidated silty sand and sand deposits.

5.2.16 R-16 Electrical Sounding using Schlumberger Layout

R-16 probe was acquired at (Lat. 25°22'48.50"N, Long. 66°45'31.28"E) east of Winder Town. The interpreted curve using IPI2Win is presented in Figure 5.23 and shows the first layer apparent resistivity 15.4 Ωm up to a depth of 2.79 m characterizes the sandy clay, the second unit with a resistivity of 11.9 Ωm up to a depth of 8.94 m (6.16 m thick) sandy clay deposits, the third unit with a resistivity of 24.4 Ωm up to a depth of 22.5 m (13.6 m thick) characterizes as sand deposits, a fourth unit having the resistivity of 30.5 Ωm up to a depth of 57.8 m (35.3 m thick) shows the resistivity of

sandy gravel. The fifth layer resistivity is 18.4 Ωm comprising sand deposits, the thickness and maximum depth was unknown due to the survey limit. The type of curve is HAK i.e. ($\rho_1 > \rho2 < \rho3 < \rho4 > \rho5$). R-16 encompasses a thick layer of unconsolidated sandy gravel and silty sand deposits.

5.2.17 R-17 Electrical Sounding using Schlumberger Layout

R-17 probe was acquired at (Lat. 25°24'47.84"N, Long. 66°45'1.90"E) northeast of Winder. The interpreted curve using IPI2Win is presented in Figure 5.24 the first layer apparent resistivity 14.3 Ωm up to a depth of 1.96 m (1.96 m thick) characterizes the sandy clay, the second unit with a resistivity of 42 Ωm up to a depth of 13.4m (11.4 m thick) sandy gravel deposits, third layer with a resistivity of 31.5 Ωm up to a depth of 48.1 m (37.7 m thick) characterizes very high resistivity and depicts the presence of sandy gravel lithology of recent deposits, a fourth unit has the resistivity of 27.5 Ωm up to a depth of 114 m (66.6 m thick) indicate the resistivity of sand. The fifth layer resistivity is 35 Ωm also comprises sandy gravel, the thickness and maximum depth were unknown due to the survey limit. The type of curve is KQH i.e., $\rho_1 < \rho2 > \rho3 > \rho4 < \rho5$. R-17 consists of thick sediments of unconsolidated sandy gravel and sand deposits encompasses good porosity and permeability of the aquifer.

5.2.18 R-18 Electrical Sounding using Schlumberger Layout

R-18 probe was acquired at (Lat. 25°24'15.24"N, Long. 66°42'2.97"E) northeast of Winder Town along near the river. The interpreted curve using IPI2Win is presented in Figure 5.25 the top layer apparent resistivity 3.06 Ωm up to a depth of 1.46 m characterizes the clay, the second layer with a resistivity of 16.8 Ωm up to a depth of

3.21 m (1.75 m thick) silty sand deposits, the third unit with a resistivity of 30.6 Ωm up to a depth of 25.2 m (22 m thick) characterizes very high resistivity and shows the presence of sandy gravel lithology of recent deposits, a fourth unit having the resistivity of 41.2 Ωm up to a depth of 91.7 m (66.5 m thick) and indicate the resistivity of sandy gravel. The fifth layer resistivity is 51.4 Ωm also comprises sandy gravel, the thickness and maximum depth were unknown due to the survey limit. The type of curve is AAA i.e. ($\rho_1 < \rho2 < \rho3 < \rho4 < \rho5$). R-18 encompasses a thick zone of unconsolidated sand, sandy clay & sandy gravel deposits.

5.2.19 R-19 Electrical Sounding using Schlumberger Layout

R-19 probes were acquired at (Lat. 25°26'5.44"N, Long. 66°39'50.47"E) northwest of Winder Town along the RCD highway. The interpreted curve using IPI2Win is presented in Figure 5.26 the first layer apparent resistivity 4.23 Ωm up to a depth of 1.9 m characterizes the clay, the second unit with a resistivity of 24.4 Ωm up to a depth of 9.86 m (7.96 m thick) sand deposits, third layer with a resistivity of 30.8 Ωm up to a depth of 39.7 m (29.8 m thick) characterizes as sandy gravel of recent deposits, a fourth unit has the resistivity of 41.3 Ωm up to a depth of 98.2m (58.5 m thick) and shows the resistivity of sandy gravel. The fifth layer resistivity is 27.1 Ωm comprising sand deposits, the thickness and maximum depth was unknown due to the survey limit. The type of curve is AAK i.e. ($\rho_1 < \rho2 < \rho3 < \rho4 > \rho5$). R-19.

5.2.20 R-20 Electrical Sounding using Schlumberger Layout

R-20 probe was acquired at (Lat. 25°27'37.10"N, Long. 66°40'24.41"E) northwest of Winder. The interpreted curve using IPI2Win is presented in Figure 5.27

the first layer apparent resistivity 16.9 Ωm up to a depth of 2.33 m characterizes the silty sand, the second layer with a resistivity of 30.5 Ωm up to a depth of 5.96 m (3.63 m thick) sandy gravel deposits, third unit with the resistivity of 37.4 Ωm up to a depth of 25.7 m (19.7 m thick) characterizes very high resistivity and shows the presence of sandy gravel lithology of recent deposits, a fourth unit has the resistivity of 23.7 Ωm up to a depth of 74.9 m (40.7 m thick) and shows the resistivity of sand. The fifth layer resistivity is 37.8 Ωm comprising sandy gravel deposits, the thickness and maximum depth was unknown due to the survey limit. The type of curve is AKH i.e. ($\rho_1 < \rho2 < \rho3 > \rho4 < \rho5$). R-20 contains a thick sequence of unconsolidated deposits of sandy gravel and sand depicting the good porosity and permeability of an aquifer.

5.2.21 R-21 Electrical Sounding using Schlumberger Layout

R-21 probe was acquired at (Lat. 25°26'42.03"N, Long. 66°42'17.41"E) northeast of Winder. The interpreted curve using IPI2Win is presented in Figure 5.28. As per this, the first layer apparent resistivity 9.92 Ωm up to a depth of 3.95 m characterizes the sandy clay, the second unit with a resistivity of 16.1 Ωm up to a depth of 13.5 m (9.59 m thick) silty sand deposits, third layer resistivity is 22.5 Ωm up to a depth of 34.2 m (20.7 m thick) and shows the presence of sand lithology of recent deposits, a fourth layer has the resistivity of 32 Ωm up to a depth of 74.9 m (40.7 m thick) and shows the resistivity of sandy gravel. The fifth unit resistivity is 41.6 Ωm also comprises sandy gravel, the thickness and maximum depth were unknown due to the survey limit. The type of curve is AAA i.e. ($\rho_1 < \rho2 < \rho3 < \rho4 < \rho5$). R-21 encompasses thick sediments of unconsolidated sandy clay and sandy gravel deposits.

5.2.22 R-22 Electrical Sounding using Schlumberger Layout

R-22 probe was acquired at (Lat. 25°25'14.85"N, Long. 66°41'55.23"E) northeast of Winder. The interpreted curve using IPI2Win is presented in Figure 5.29 the top layer apparent resistivity is 26.4 Ωm up to a depth of 2.36 characterizes the sandy gravel, the second unit resistivity is 32 Ωm up to a depth of 5.75 m (3.39 m thick) sandy gravel deposits, the third layer with a resistivity of 42.6 Ωm up to a depth of 30.3 m (24.5 m thick) characterizes as sandy gravel lithology of recent deposits, a fourth unit has the resistivity of 24.9 Ωm up to a depth of 98.2 m (68 m thick) and shows the resistivity of sand. Similarly, the fifth layer resistivity is 21.4 Ωm also comprises sand deposits, the thickness and maximum depth was unknown due to the survey limit. The type of curve is AKQ i.e. ($\rho_1 < \rho2 < \rho3 > \rho4 > \rho5$). R-22 holds thick layers of unconsolidated sandy gravel and sand deposits.

5.2.23 R-23 Electrical Sounding using Schlumberger Layout

R-23 probe was acquired at (Lat. 25°25'4.87"N, Long. 66°40'52.12"E) north of Winder Town. The interpreted curve using IPI2Win is presented in Figure 5.30, and depicts the five layer including the top layer apparent resistivity is 7.94 Ωm up to a depth of 2.08 m characterizes the sandy clay, the second unit with a resistivity of 16.4 Ωm up to a depth of 7.6 m (5.52 m thick) silty sand deposits, the third layer with a resistivity of 22.1 Ωm up to a depth of 29.8 m (22.2 m thick) characterizes as sand deposits, a fourth unit has the resistivity of 30.5 Ωm up to a depth of 86.8 m (27 m thick) and shows the resistivity of sandy gravel. The fifth unit resistivity is 20.5 Ωm also comprises sand deposits, the thickness and maximum depth was unknown due to the survey limit. The type of curve is AAK i.e. ($\rho_1 < \rho2 < \rho3 < \rho4 > \rho5$). R-23 encompasses a thick sequence of unconsolidated sandy gravel and deposits sand.

5.2.24 R-24 Electrical Sounding using Schlumberger Layout

The interpreted curve using IPI2Win is presented in Figure 5.31 and delineated multiple layers. The apparent resistivity of top layer is 25.6 Ωm up to a depth of 1.84 m (1.84 m thick) characterizes the sand, the second layer resistivity is 20.2 Ωm up to a depth of 6.08 m (4.23 m thick) sand deposits, third layer with a resistivity of 17.1 Ωm up to a depth of 31.5 m (25.4 m thick) characterizes as low resistivity and indicate the presence of silty sand, a fourth layer has the resistivity of 13.5 Ωm up to a depth of 61.3 m (29.9 m thick) interpreted as silty sand. The fifth layer resistivity is 19.5 Ωm also comprises silty sand deposits, the thickness and maximum depth were unknown due to the survey limit. The type of curve is QQH i.e. ($\rho1 > \rho2 > \rho3 > \rho4 < \rho5$). R-24 consist of a thick zone of unconsolidated sandy gravel and sand deposits.

5.2.25 R-25 Electrical Sounding using Schlumberger Layout

R-25 probe was acquired at (Lat 25°21'1.23" N Long 66°39'2.72" E) southwest of Winder Town. The interpreted curve using IPI2Win is presented in Figure 5.32 the first layer apparent resistivity is 38.6 Ωm up to a depth of 2.17 m characterizes the sandy gravel, the second u winitth a resistivity of 22.1 Ωm up to a depth of 6.21 m (4.04 m thick) sand deposits, third layer with a resistivity of 17.3 Ωm up to a depth of 21.2 m (14.8 m thick) characterizes sand, a fourth unit has the resistivity of 46.1 Ωm up to a depth of 98 m (77 m thick) indicate the resistivity of sandy gravel. The fifth layer resistivity is 19.1 Ωm comprises silty sand deposits, the thickness and maximum depth was unknown due to the survey limit. The type of curve is QHK i.e., $\rho_1 > \rho2 > \rho3 < \rho4 > \rho5$. R-25 encompasses thick sediments of unconsolidated sandy gravel and sand deposits.

5.2.26 R-26 Electrical Sounding using Schlumberger Layout

R-26 probe was acquired at (Lat 25°27'9.51" N Long 66°38'59.89" E). The interpreted curve using IPI2Win is presented in Figure 5.33 the top layer apparent resistivity is 30.6 Ωm up to a depth of 1.95 m characterizes the dune sand, the second unit with a resistivity of 22.7 Ωm up to a depth of 4.76 m (2.81 m thick) sand deposits, third layer with a resistivity of 14.8 Ωm up to a depth of 15.8 m (11.1 m thick) characterizes as the sand of recent deposits, a fourth unit resistivity is 40.2 Ωm up to a depth of 50.4 m (34.5 m thick) shows the resistivity of sandy gravel. The fifth layer resistivity is 25.1 Ωm also includes sand deposits, the thickness and maximum depth was unknown due to the survey limit. The type of curve is QHK i.e. ($\rho_1 > \rho2 > \rho3 < \rho4 > \rho5$).

5.2.27 R-27 Electrical Sounding using Schlumberger Layout

R-27 probe was acquired at (Lat 25°25'22.15" N Long 66°35'52.62" E) near the coast, the village named Damb. The interpreted curve Figure 5.34 using IPI2Win presented the first layer apparent resistivity 32.4 Ωm up to a depth of 3.09 m characterizes the dry dune sand, the second unit resistivity is 17 Ωm up to a depth of 6.4 m (3.31 m thick) sand, third layer resistivity is 28.1 Ωm up to a depth of 26.8 m (20.4 m thick) & depict the presence of sandy gravel deposits, a fourth unit has the resistivity of 17.2 Ωm up to a depth of 88.9 m (62.2 m thick) demarcate the resistivity of sand deposits. The fifth layer resistivity is 14.1 Ωm comprises silty sand, the thickness and maximum depth was unknown due to the survey limit. The type of curve is HKQ i.e. ($\rho_1 > \rho2 < \rho3 > \rho4 > \rho5$).

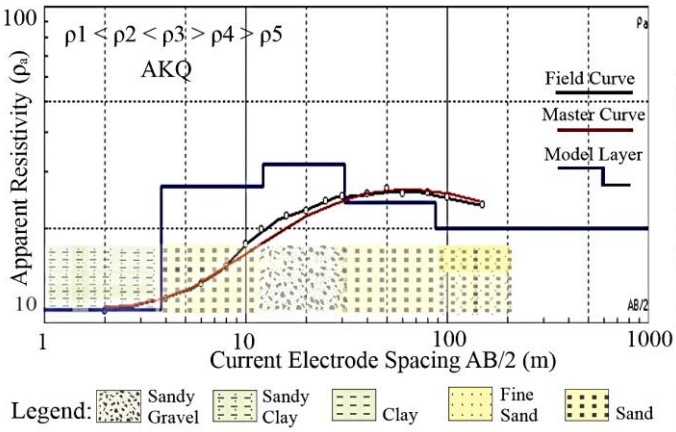

R-1 Station

Error=3.79%

N	ρ	h	d
1	11	3.79	3.79
2	27	8.4	12.2
3	31.8	18.6	30.8
4	24.1	56.6	87.4
5	20		

Figure 5.8 Graphical presentation of interpreted VES data for resistivity (ρ), thickness (h), layer depth (d) and type of lithology for station R-1 using IPI2Win.

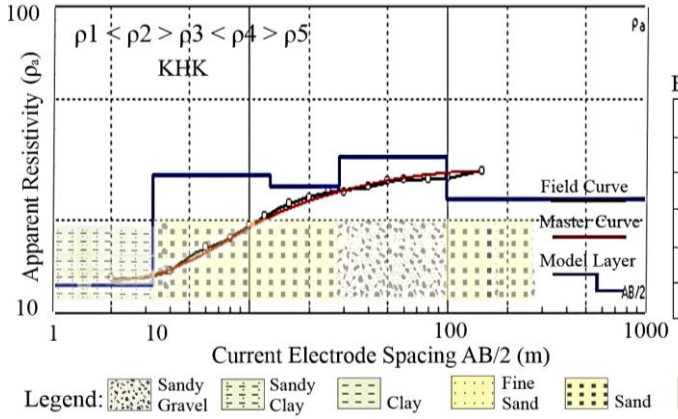

R-2 Station

Error=2.28%

N	ρ	h	d
1	12.4	3.28	3.28
2	28.2	9.43	12.7
3	26	15.7	28.4
4	32.3	70.6	99
5	23.6		

Figure 5.9 Graphical presentation of interpreted VES data for resistivity (ρ), thickness (h), layer depth (d) and type of lithology for station R-2 using IPI2Win.

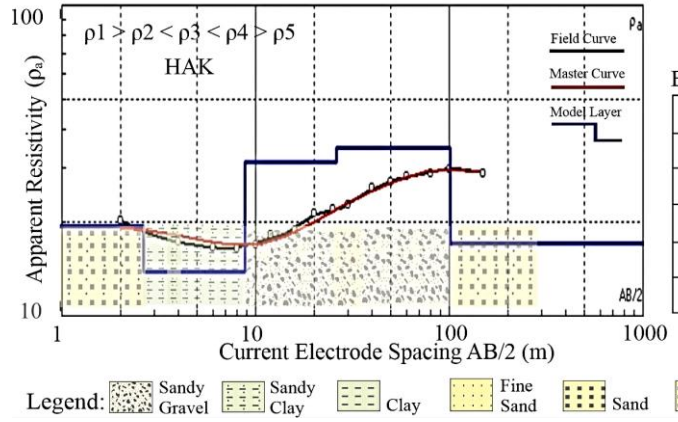

R-3 Station

Error=3.14%

N	ρ	h	d
1	19.5	2.64	2.64
2	13.9	6.17	8.81
3	31.3	17.3	26.1
4	34.8	74.9	101
5	17.1		

Figure 5.10 Graphical presentation of interpreted VES data for resistivity (ρ), thickness (h), layer depth (d) and type of lithology for station R-3 using IPI2Win.

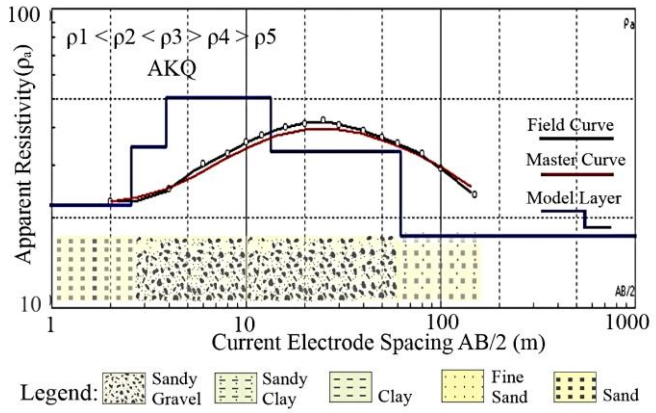

R-4 Station

Error=3.39%

N	ρ	h	d
1	22.1	2.56	2.56
2	34.5	1.31	3.87
3	50.4	9.49	13.4
4	33.3	48.9	62.2
5	17.4		

Figure 5.11 Graphical presentation of interpreted VES data for resistivity (ρ), thickness (h), layer depth (d) and type of lithology for station R-4 using IPI2Win.

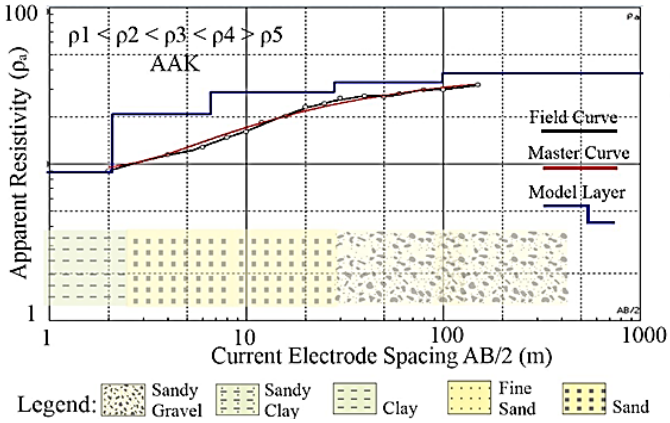

R-5 Station

Error=3.94%

N	ρ	h	d
1	8.84	2.09	2.09
2	20.9	2.25	6.61
3	28.7	21.3	27.9
4	33.3	71.2	99.1
5	38		

Figure 5.12 Graphical presentation of interpreted VES data for resistivity (ρ), thickness (h), layer depth (d) and type of lithology for station R-5 using IPI2Win.

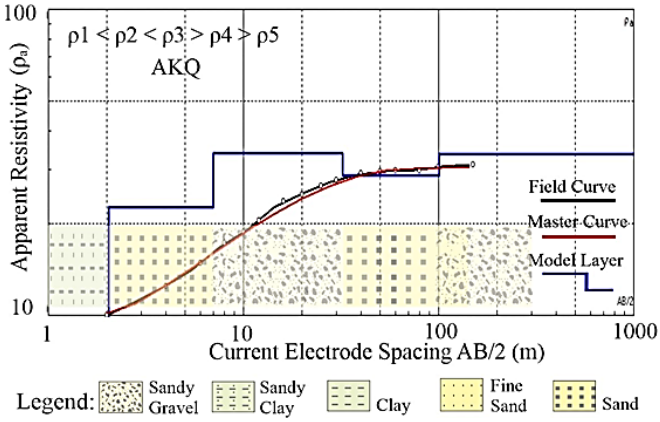

R-6 Station

Error=2.11%

N	ρ	h	d
1	9.38	2.03	2.03
2	22.5	4.98	7.01
3	33.9	25.2	32.2
4	28.7	68.5	101
5	33.6		

Figure 5.13 Graphical presentation of interpreted VES data for resistivity (ρ), thickness (h), layer depth (d) and type of lithology for station R-6 using IPI2Win.

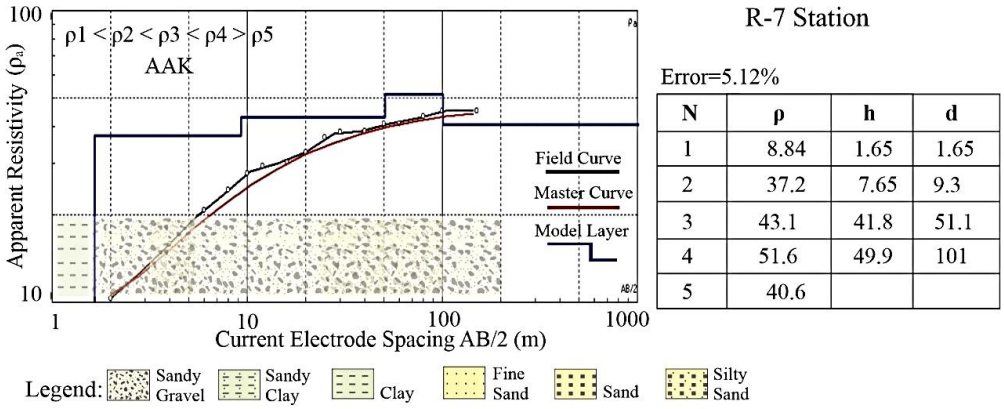

R-7 Station

Error=5.12%

N	ρ	h	d
1	8.84	1.65	1.65
2	37.2	7.65	9.3
3	43.1	41.8	51.1
4	51.6	49.9	101
5	40.6		

Figure 5.14 Graphical presentation of interpreted VES data for resistivity (ρ), thickness (h), layer depth (d) and type of lithology for station R-7 using IPI2Win.

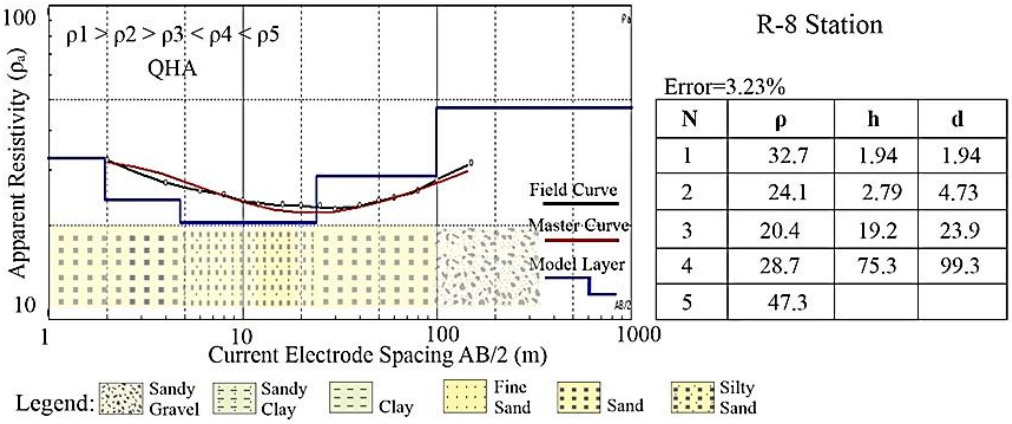

R-8 Station

Error=3.23%

N	ρ	h	d
1	32.7	1.94	1.94
2	24.1	2.79	4.73
3	20.4	19.2	23.9
4	28.7	75.3	99.3
5	47.3		

Figure 5.15 Graphical presentation of interpreted VES data for resistivity (ρ), thickness (h), layer depth (d) and type of lithology for station R-8 using IPI2Win.

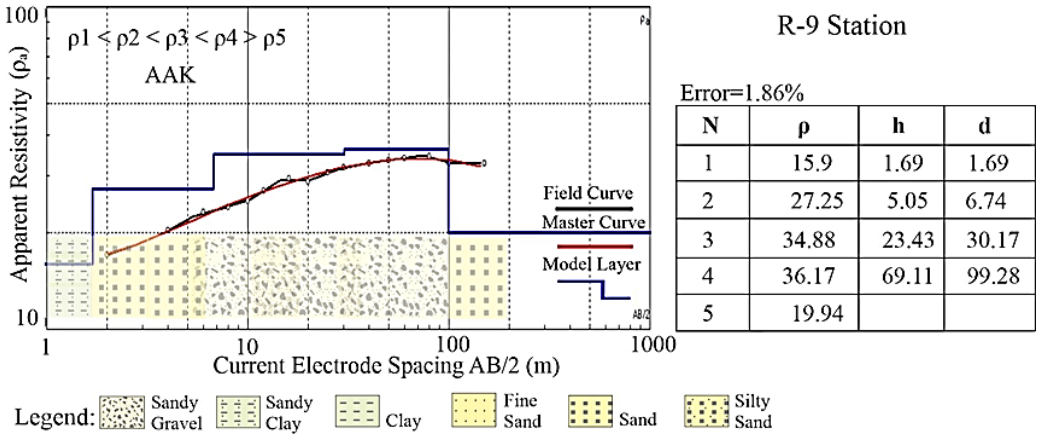

R-9 Station

Error=1.86%

N	ρ	h	d
1	15.9	1.69	1.69
2	27.25	5.05	6.74
3	34.88	23.43	30.17
4	36.17	69.11	99.28
5	19.94		

Figure 5.16 Graphical presentation of interpreted VES data for resistivity (ρ), thickness (h), layer depth (d) and type of lithology for station R-9 using IPI2Win.

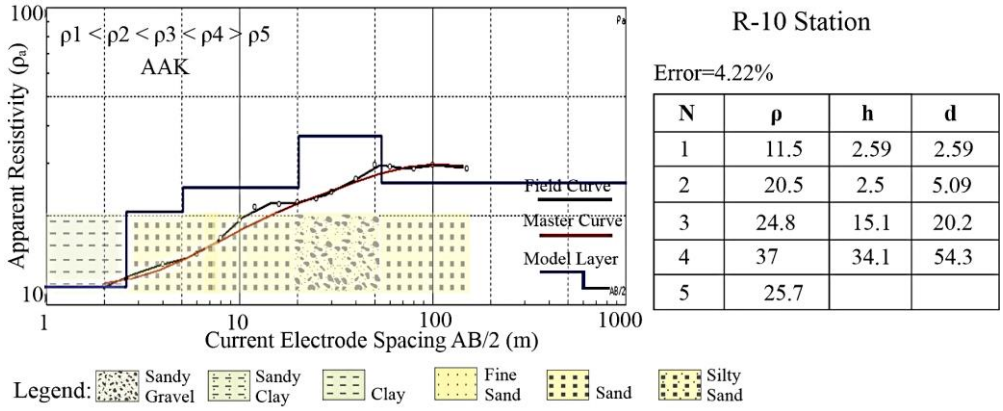

N	ρ	h	d
1	11.5	2.59	2.59
2	20.5	2.5	5.09
3	24.8	15.1	20.2
4	37	34.1	54.3
5	25.7		

Figure 5.17 Graphical presentation of interpreted VES data for resistivity (ρ), thickness (h), layer depth (d) and type of lithology for station R-10 using IPI2Win.

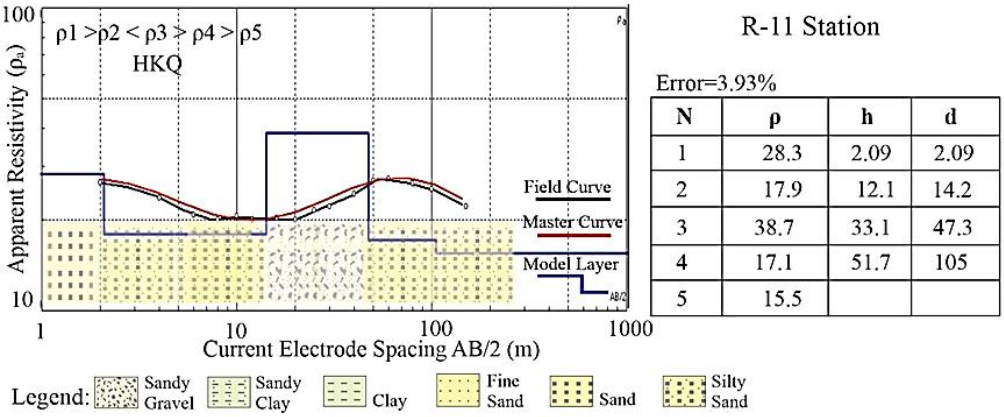

N	ρ	h	d
1	28.3	2.09	2.09
2	17.9	12.1	14.2
3	38.7	33.1	47.3
4	17.1	51.7	105
5	15.5		

Figure 5.18 Graphical presentation of interpreted VES data for resistivity (ρ), thickness (h), layer depth (d) and type of lithology for station R-11 using IPI2Win.

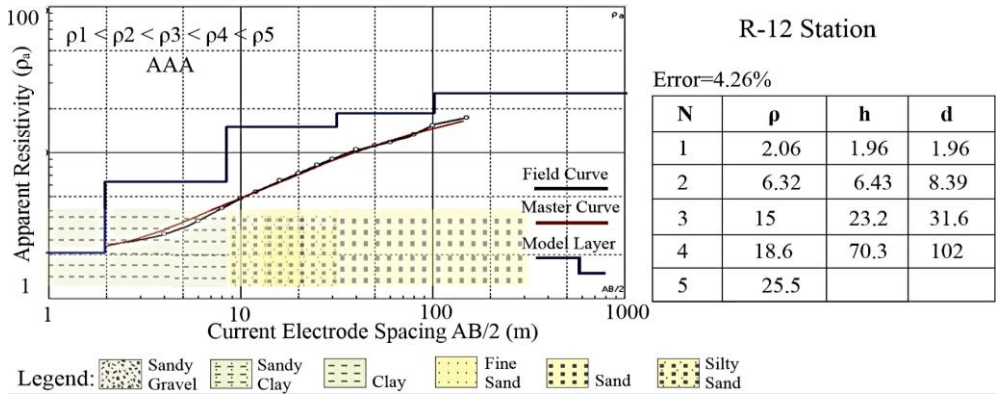

N	ρ	h	d
1	2.06	1.96	1.96
2	6.32	6.43	8.39
3	15	23.2	31.6
4	18.6	70.3	102
5	25.5		

Figure 5.19 Graphical presentation of interpreted VES data for resistivity (ρ), thickness (h), layer depth (d) and type of lithology for station R-12 using IPI2Win

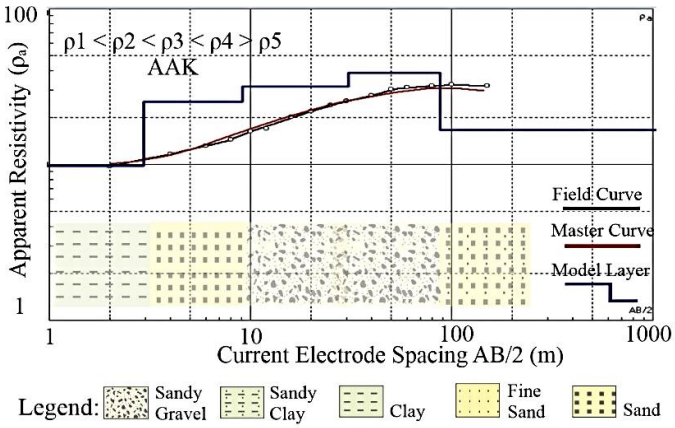

R-13 Station

Error=3.89%

N	ρ	h	d
1	9.76	2.93	2.93
2	25.3	6.16	9.09
3	31.6	21.7	30.8
4	38.8	56.5	87.3
5	16.6		

Figure 5.20 Graphical presentation of interpreted VES data for resistivity (ρ), thickness (h), layer depth (d) and type of lithology for station R-13 using IPI2Win.

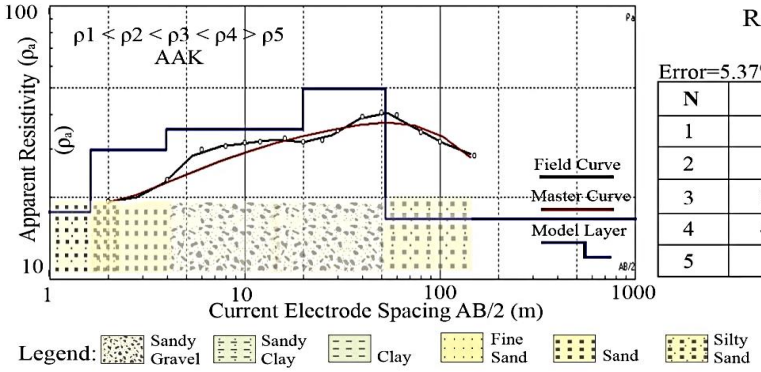

R-14 Station

Error=5.37%

N	ρ	h	d
1	17.6	1.62	1.62
2	29.7	2.33	3.95
3	35.4	15.8	19.8
4	49.8	32.6	52.4
5	16.6		

Figure 5.21 Graphical presentation of interpreted VES data for resistivity (ρ), thickness (h), layer depth (d) and type of lithology for station R-14 using IPI2Win.

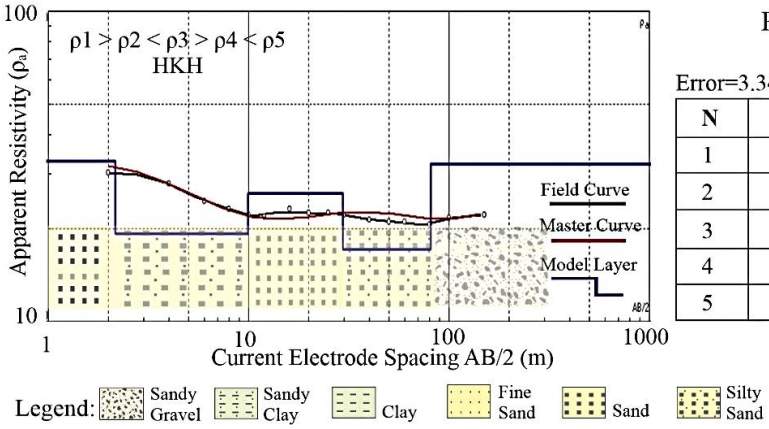

R-15 Station

Error=3.34%

N	ρ	h	d
1	32.9	2.16	2.16
2	19.2	7.77	9.93
3	25.9	19.6	29.5
4	17.1	51.5	81
5	32.2		

Figure 5.22 Graphical presentation of interpreted VES data for resistivity (ρ), thickness (h), layer depth (d) and type of lithology for station R-15 using IPI2Win.

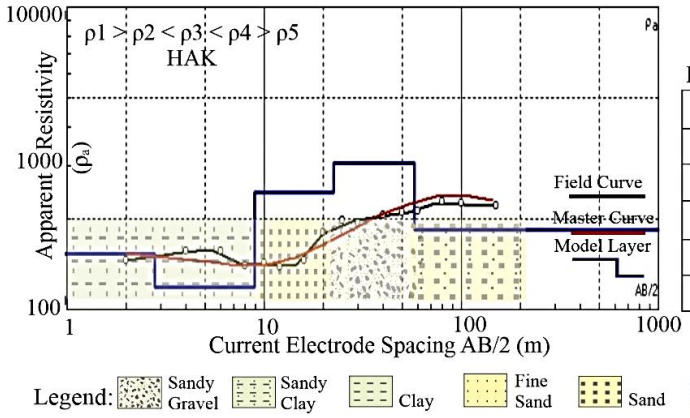

R-16 Station

Error=5.44%

N	ρ	h	d
1	15.4	2.79	2.79
2	11.9	6.16	8.94
3	24.4	13.6	22.5
4	30.5	35.3	57.8
5	18.4		

Figure 5.23 Graphical presentation of interpreted VES data for resistivity (ρ), thickness (h), layer depth (d) and type of lithology for station R-16 using IPI2Win.

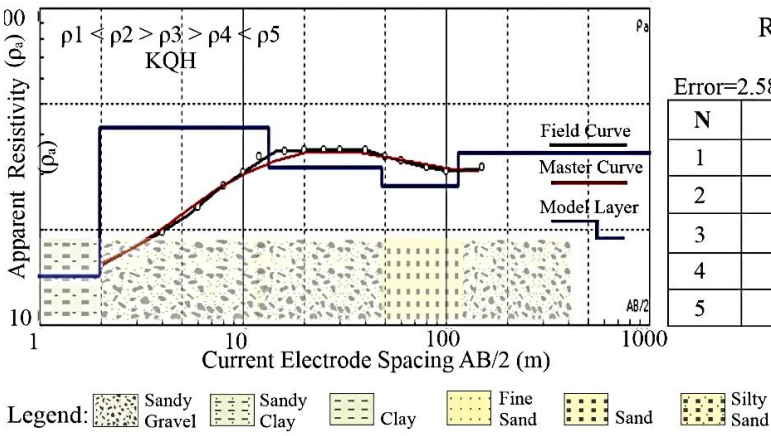

R-17 Station

Error=2.58%

N	ρ	h	d
1	14.3	1.96	1.96
2	42	11.4	13.4
3	31.5	34.7	48.1
4	27.5	66.4	114
5	35		

Figure 5.24 Graphical presentation of interpreted VES data for resistivity (ρ), thickness (h), layer depth (d) and type of lithology for station R-17 using IPI2Win.

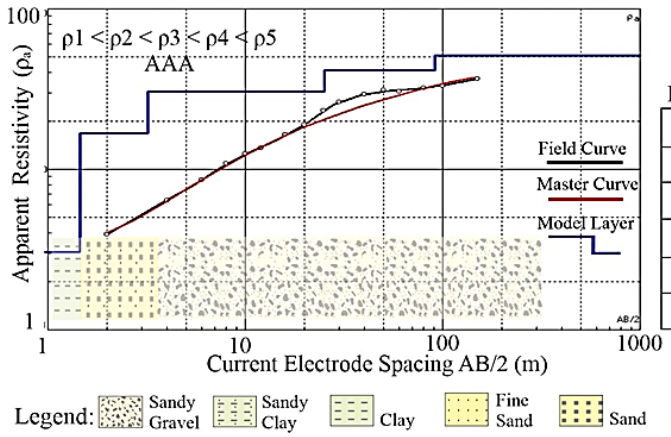

R-18 Station

Error=5.97%

N	ρ	h	d
1	3.06	1.46	1.46
2	16.8	1.75	3.21
3	30.6	22	25.2
4	41.2	66.5	91.7
5	51.4		

Figure 5.25 Graphical presentation of interpreted VES data for resistivity (ρ), thickness (h), layer depth (d) and type of lithology for station R-18 using IPI2Win.

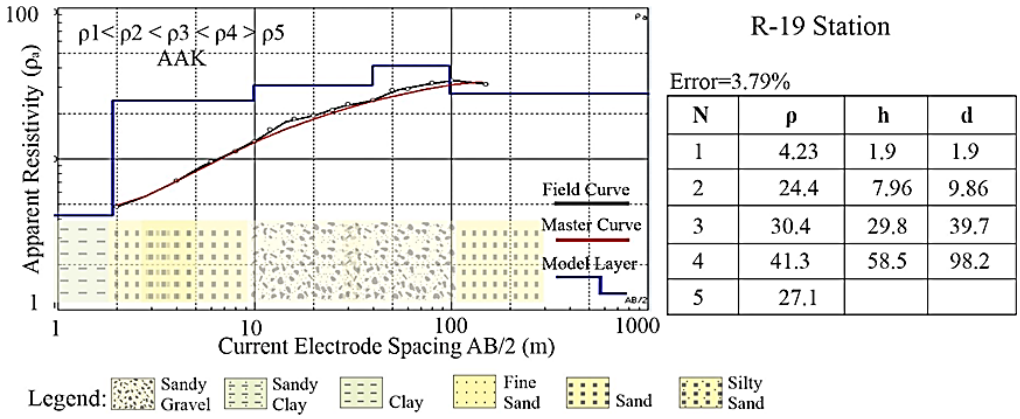

R-19 Station

Error=3.79%

N	ρ	h	d
1	4.23	1.9	1.9
2	24.4	7.96	9.86
3	30.4	29.8	39.7
4	41.3	58.5	98.2
5	27.1		

Figure 5.26 Graphical presentation of interpreted VES data for resistivity (ρ), thickness (h), layer depth (d) and type of lithology for station R-19 using IPI2Win.

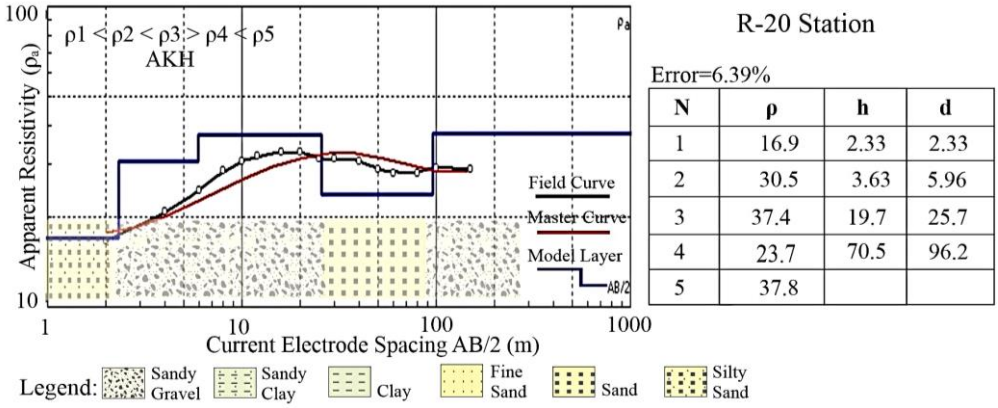

R-20 Station

Error=6.39%

N	ρ	h	d
1	16.9	2.33	2.33
2	30.5	3.63	5.96
3	37.4	19.7	25.7
4	23.7	70.5	96.2
5	37.8		

Figure 5.27 Graphical presentation of interpreted VES data for resistivity (ρ), thickness (h), layer depth (d) and type of lithology for station R-20 using IPI2Win.

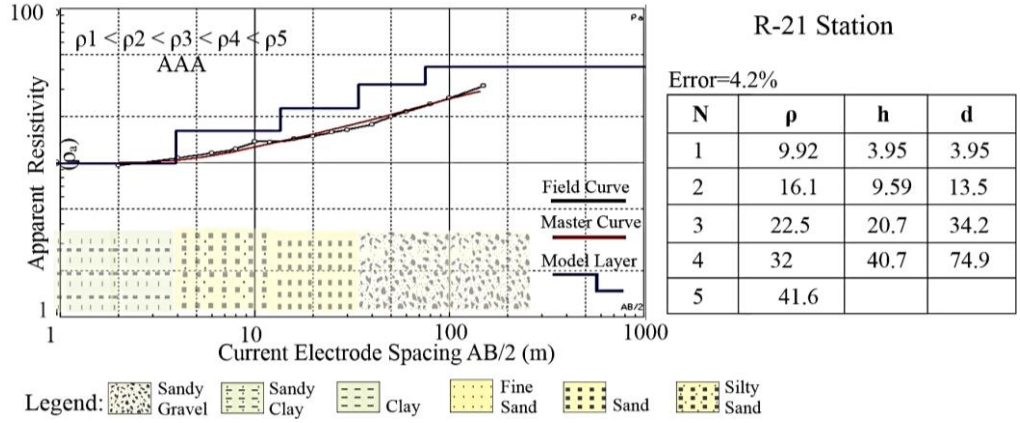

R-21 Station

Error=4.2%

N	ρ	h	d
1	9.92	3.95	3.95
2	16.1	9.59	13.5
3	22.5	20.7	34.2
4	32	40.7	74.9
5	41.6		

Figure 5.28 Graphical presentation of interpreted VES data for resistivity (ρ), thickness (h), layer depth (d) and type of lithology for station R-21 using IPI2Win.

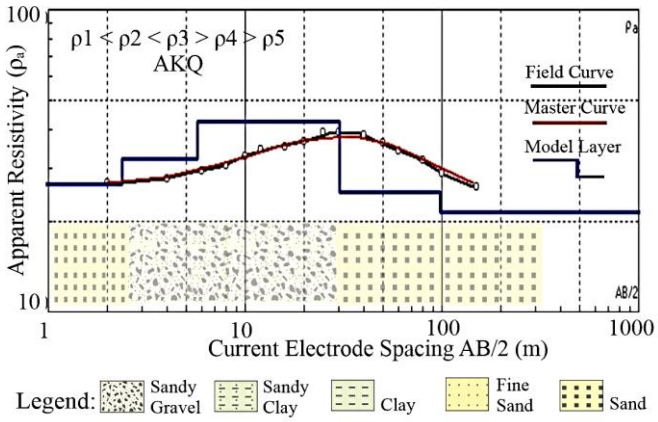

R-22 Station

Error=2.18%

N	ρ	h	d
1	26.4	2.36	2.36
2	32	3.39	5.75
3	42.6	24.5	30.3
4	24.9	68	98.3
5	21.4		

Figure 5.29 Graphical presentation of interpreted VES data for resistivity (ρ), thickness (h), layer depth (d) and type of lithology for station R-22 using IPI2Win.

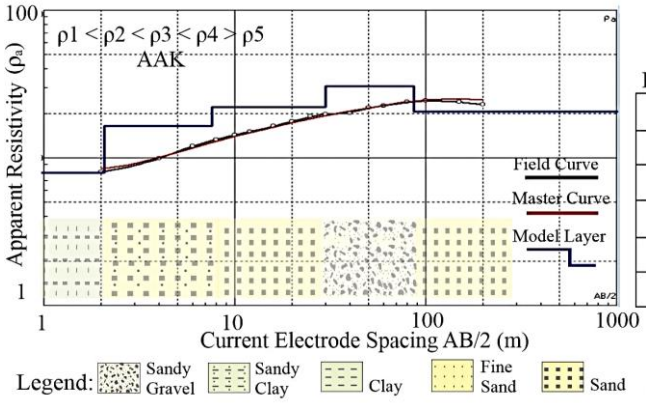

R-23 Station

Error=3.13%

N	ρ	h	d
1	7.94	2.08	2.08
2	16.4	5.52	7.6
3	22.1	22.2	29.8
4	30.5	57	86.8
5	20.5		

Figure 5.30 Graphical presentation of interpreted VES data for resistivity (ρ), thickness (h), layer depth (d) and type of lithology for station R-23 using IPI2Win.

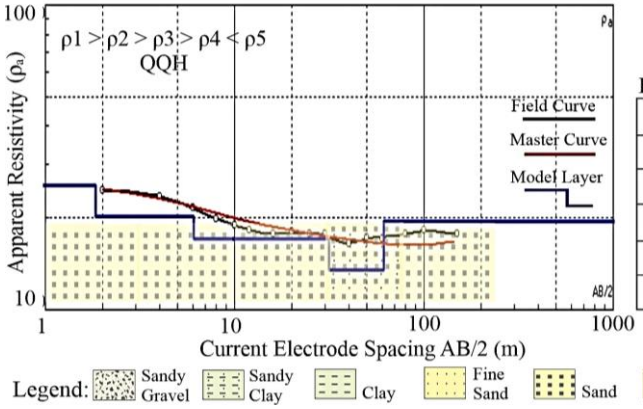

R-24 Station

Error=4.92%

N	ρ	h	d
1	25.6	1.84	1.84
2	20.2	4.23	6.08
3	17.1	25.4	31.5
4	13.5	29.9	61.3
5	19.5		

Figure 5.31 Graphical presentation of interpreted VES data for resistivity (ρ), thickness (h), layer depth (d) and type of lithology for station R-24 using IPI2Win.

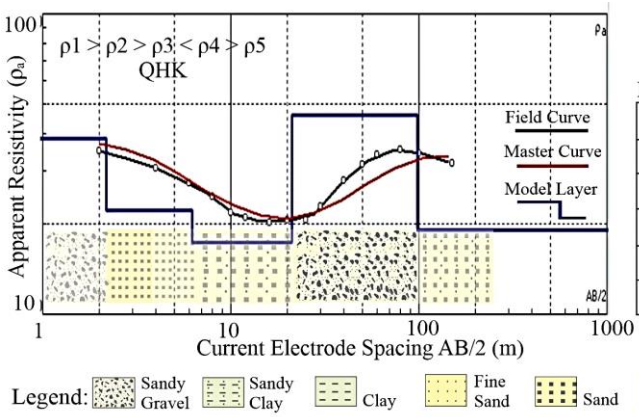

R-25 Station

Error=6.97%

N	ρ	h	d
1	38.6	2.17	2.17
2	22.1	4.04	6.21
3	17.3	14.8	21.2
4	46.1	77	98
5	19.1		

Figure 5.32 Graphical presentation of interpreted VES data for resistivity (ρ), thickness (h), layer depth (d) and type of lithology for station R-25 using IPI2Win.

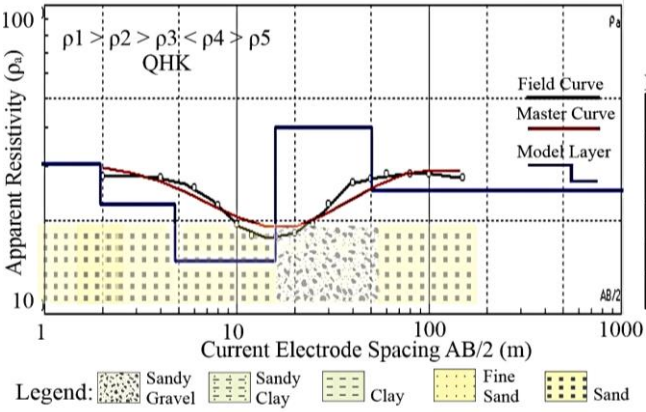

R-26 Station

Error=5.46%

N	ρ	h	d
1	30.6	1.95	1.95
2	22.7	2.81	4.76
3	14.8	11.1	15.8
4	40.2	34.5	50.4
5	25.1		

Figure 5.33 Graphical presentation of interpreted VES data for resistivity (ρ), thickness (h), layer depth (d) and type of lithology for station R-26 using IPI2Win.

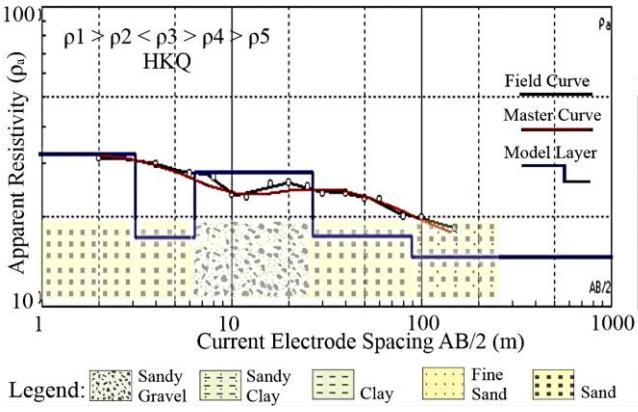

R-27 Station

Error=3.2%

N	ρ	h	d
1	32.4	3.09	3.09
2	17	3.31	6.4
3	28.1	20.4	26.8
4	17.2	62.1	88.9
5	14.2		

Figure 5.34 Graphical presentation of interpreted VES data for resistivity (ρ), thickness (h), layer depth (d) and type of lithology for station R-27 using IPI2Win.

The resistivity curves A, Q, H and K types were interpreted from modelled data. Basically, there are three different types of curves that can be interpreted based on layers' resistivity. In H type ($\rho1 > \rho2 < \rho3$), Q type ($\rho1 > \rho2 > \rho3$), A type ($\rho1 < \rho2 < \rho3$) and K type ($\rho1 < \rho2 > \rho3$). The interpreted data in Table 5.1, shows five layers, therefore curve-matching techniques for multiple layers were utilized to identify the combination for each point. A combination of the basic curve was obtained for more than three layers. The following combinations were observed for 27 VES stations. The AAK type ($\rho_1 < \rho2 < \rho3 < \rho4 > \rho5$) interpreted for R-5, R-7, R-9, R-10, R-13, R-14, R-19 and R-23. The AKQ type ($\rho_1 < \rho2 < \rho3 > \rho4 > \rho5$) for R-1, R-4, R-6 and R-22, AAA type ($\rho_1 < \rho2 < \rho3 < \rho4 < \rho5$) for R-12, R-18 and R-21, HKQ type ($\rho_1 > \rho2 < \rho3 > \rho4 > \rho5$) for R-11 and R-27, QHK type ($\rho_1 > \rho2 > \rho3 < \rho4 > \rho5$) for R-25 and R-26 HAK type ($\rho_1 > \rho2 < \rho3 < \rho4 > \rho5$) for R-3 and R-16, KHK type ($\rho_1 < \rho2 > \rho3 < \rho4 > \rho5$) for R-2, QHA type ($\rho1 > \rho2 > \rho3 < \rho4 < \rho5$) for R-8 , HKH type ($\rho_1 > \rho2 < \rho3 > \rho4 < \rho5$) for R-15, KQH type ($\rho_1 < \rho2 > \rho3 > \rho4 < \rho5$) for R-17, AKH type ($\rho_1 < \rho2 < \rho3 > \rho4 < \rho5$) for R-20, QQH type ($\rho_1 > \rho2 > \rho3 > \rho4 < \rho5$) for R-24.

5.3 Inversion Model of 2-D Resistivity or Pseudo-section

The pseudo-section offers an approximate picture of resistivity distribution in the subsurface for quantitative interpretation. It is an effective method to image the calculated apparent resistivity with respect to depth and location in the 2D section. These sections also help to remove the unusually high or low values to enhance the data quality assurance. In this study vertical electrical sounding data of 150-meter depth half of AB/2 utilized to construct the pseudo-section along the profile A-A′, B-B′, C-C′, D-D′ and E-E′ to evaluate the north-south and east-west apparent resistivity resulting due to change in lithology, saturated and unsaturated zone and groundwater quality. The constructed pseudo section is divided into three major zones namely high resistivity zone, low resistivity zone and medium resistivity zone.

Table 5.1 Summary of interpreted results from the acquired geoelectrical resistivity data of 27 VES station Winder.

VES	ρ_1	ρ_2	ρ_3	ρ_4	ρ_5	h_1	h_2	h_3	h_4	d_1	d_2	d_3	d_4
R-1	11	27	31.8	24.1	20	3.79	8.4	18.6	56.6	3.79	12.2	30	87.4
R-2	12.4	28.2	26	32.3	23.6	3.28	9.43	15.7	70.6	3.28	12.7	28.4	99
R-3	19.5	13.3	31.3	34.8	17.1	2.64	6.17	17.3	74.9	2.64	8.81	26.1	101
R-4	22.1	34.5	50.4	33.3	17.4	2.56	1.31	9.49	48.9	2.56	3.87	13.4	62.2
R-5	8.84	20.9	28.7	33.3	38	2.09	4.52	21.3	71.2	2.09	6.61	27.9	99.1
R-6	9.38	22.5	33.9	28.7	36	2.03	4.98	25.2	68.5	2.03	7.01	32.2	101
R-7	8.84	37.2	43.1	51.6	40.6	1.65	7.65	41.8	49.9	1.65	9.3	51.1	101
R-8	32.7	24.1	20.4	28.7	47.3	1.94	2.79	19.2	75.5	1.94	4.73	23.9	99.3
R-9	15.9	27.25	34.88	36.17	19.94	1.69	5.05	23.43	69.11	1.69	6.74	30.7	99.28
R-10	11.5	20.5	24.8	37	25.7	2.59	2.5	15.1	34.1	2.59	5.09	20.2	54.3
R-11	28.3	17.9	38.7	17.1	15.5	2.09	12.1	33.1	57.7	2.09	14.2	47.3	105
R-12	2.06	6.32	15	18.6	25.5	1.96	6.43	23.2	70.3	1.96	8.39	31.6	102
R-13	9.76	25.3	31.6	38.8	16.6	2.93	6.16	21.7	56.5	2.93	9.09	30.8	87.3
R-14	17.6	29.7	35.4	49.8	18	1.62	2.33	15.8	32.6	1.62	3.95	19.8	52.4
R-15	32.9	19.2	25.9	17.1	32.2	2.16	7.77	19.6	51.5	2.16	9.93	29.5	81
R-16	15.4	11.9	24.4	30.5	18.4	2.79	6.16	13.6	35.3	2.79	8.94	22.5	57.8
R-17	14.3	42	31.5	27.5	35	1.96	11.4	37.7	66.4	1.96	13.4	48.1	114
R-18	3.06	16.8	30.6	41.2	51.4	1.46	1.75	22	66.5	1.46	3.21	25.2	91.7
R-19	4.23	24.4	30.8	41.3	27.1	1.9	7.96	29.8	58.5	1.9	9.86	39.7	98.2
R-20	16.9	30.5	37.4	23.7	37.8	2.33	3.63	19.7	70.5	2.33	5.96	25.7	96.2
R-21	9.92	16.1	22.5	32	41.6	3.95	9.59	20.7	40.7	3.95	13.5	34.2	74.9
R-22	26.4	32	42.6	24.9	21.4	2.36	3.39	24.5	68	2.36	5.75	30.3	98.3
R-23	7.94	16.4	22.1	30.5	20.5	2.08	5.52	22.2	27	2.08	7.6	29.8	86.8
R-24	25.6	20.2	17.1	13.5	19.5	1.84	4.23	25.4	29.9	1.84	6.08	31.5	61.3
R-25	38.6	22.1	17.3	46.1	19.1	2.17	4.04	14.8	77	2.17	6.21	21.2	98
R-26	30.6	22.7	14.8	40.2	25.1	1.95	2.81	11.1	34.5	1.95	4.76	15.8	50.4
R-27	32.4	17	28.1	17.2	14.1	3.09	3.31	20.4	62.2	3.09	6.4	26.8	88.9

VES: Vertical Electrical Sounding, d: depth (meter), h: thickness (meter), ρ: apparent resistivity (ohm meter Ωm)

5.3.1 Pseudo-section A-A′

The Pseudo-section A-A′ covered a 14 km profile trending from a north-south parallel direction to the coastal belt of the study area (Figure 5.35). The distance of the cross-section from the coast is approximately 6 km. The topmost layer represents the high resistivity toward the north from R-24 to R-15 and is interpreted as dry sand deposits, whereas R-1 and R-2 depict low resistivity and are identified as sandy clay.

The approximate water depth along this profile is 10 meters and the lower resistivity of sand is interpreted as brackish water intruded by sea. The R-25, R-1, R-2 and R-26 contain freshwater aquifer at a 20-meter depth where high resistivity can be observed in Profile A-A′.

5.3.2 Pseudo-section B-B′

The pseudo-section represents three zones along B-B′ profile approximately 14 km trending north-south (Figure 5.36). This profile covers the agricultures farms where the topmost depicts a low resistivity zone comprising sandy clay and silty sand deposits, while a middle moderate resistivity zone is interpreted as sand. The high resistivity zone observed below the 30-meter depth at R-14, R-3, R-18 and R-22 contains high potential of a fresh unconfined aquifer.

5.3.3 Pseudo-section C-C′

The Pseudo-section C-C′ covers approximately 14 km profile trending north-south (Figure 5.37). The topmost layer depicts a low resistivity zone and characterizes as clay and sandy clay. The high resistivity can be observed at R-17 and R-16 stations located near the Winder River. The high resistivity is interpreted as sandy gravel filled with fresh water. The water table depth is shallow at R-16 to R-17 ranging from 25-30 meters whereas deeper for other stations.

5.3.4 Pseudo-section D-D′

The Pseudo-section was constructed along the profile D-D′ trending east-west perpendicular to the coastal belt (Figure 5.38). R-12, R-10 and R-9 lie within the agriculture form and topmost layer characterized as clay and sandy clay. The moderate to low resistivity zone can be observed in shallow and deeper parts interpreted as silty sand except for R-9 and R-12 where sand is underlain by sandy gravel deposits. The profile contains a thick sequence of sand and silty sand for the aquifer.

5.3.5 Pseudo-section E-E′

The pseudo-section E-E′ is generated perpendicular to the sea and covers the 17 km profile of 6 VES stations. The stations R-7, R-6, R-22, R-23, R-1 and R-23 run parallel to the Winder River and the R-27 station is located near the Miani Hor (Figure 5.39). The topmost layer from R-7 to R-1 depicts a low resistivity zone and is interpreted as clay and sandy clay. The R-27 topmost shows high resistivity due to the occurrence of dry sand and unconsolidated deposits. The high potential zone of the freshwater aquifer is present at depth ranges of 25-30 meters for R-7 to R-22. The R-27 and R-1 station near the coastal zone depict moderate to low resistivity, resulting because of intrusion by seawater into the aquifer.

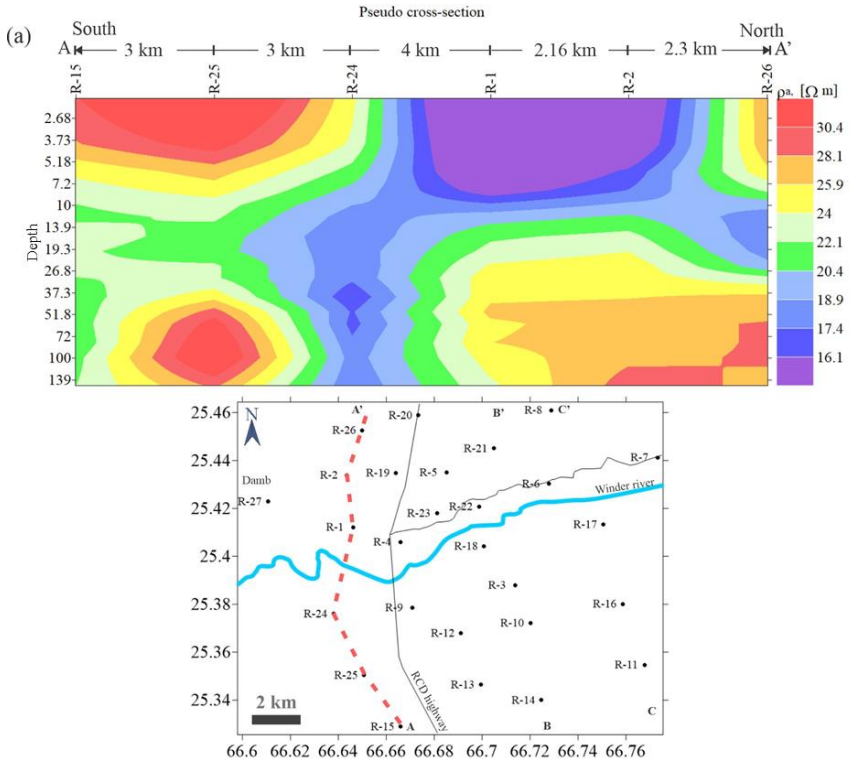

Figure 5.35 Pseudo-section A-A′ trending north-south generated from VES station R-15, R-25, R-24, R-1, R-2 and R-26. The resistivity variation, red for high and purple for low resistivity zone in Ωm. Y-axis for subsurface depth AB/2 in meter.

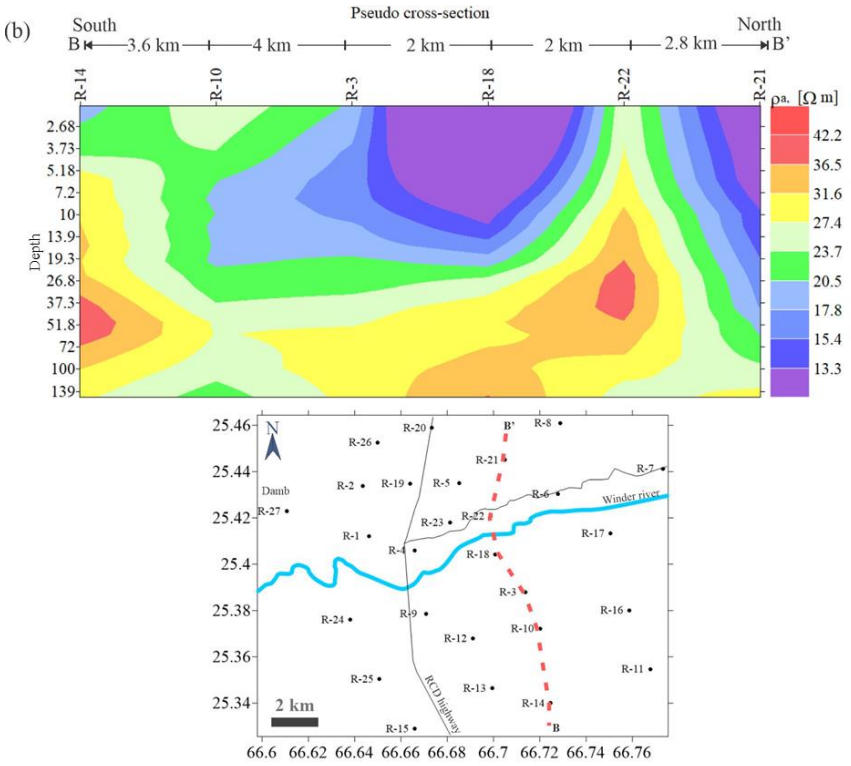

Figure 5.36 Pseudo-section B-B′ trending North-South generated from VES station R-14, R-10, R-3, R-18, R-22 and R-21. The resistivity variation of red for high and purple for low resistivity zone in Ωm.. Y-axis for subsurface depth AB/2 in meter.

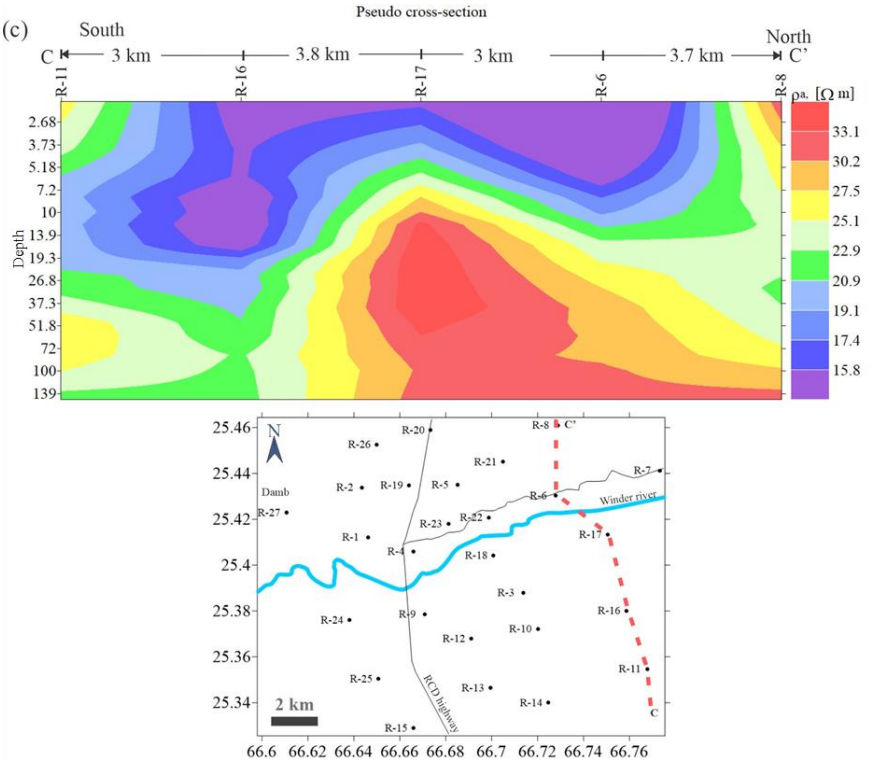

Figure 5.37 Pseudo-section C-C′ trending north-south generated from VES station R-11, R-16, R-17, R-6 and R-8. The resistivity variation of red for high and purple for low resistivity zone in Ωm.. Y-axis for subsurface depth AB/2 in meter.

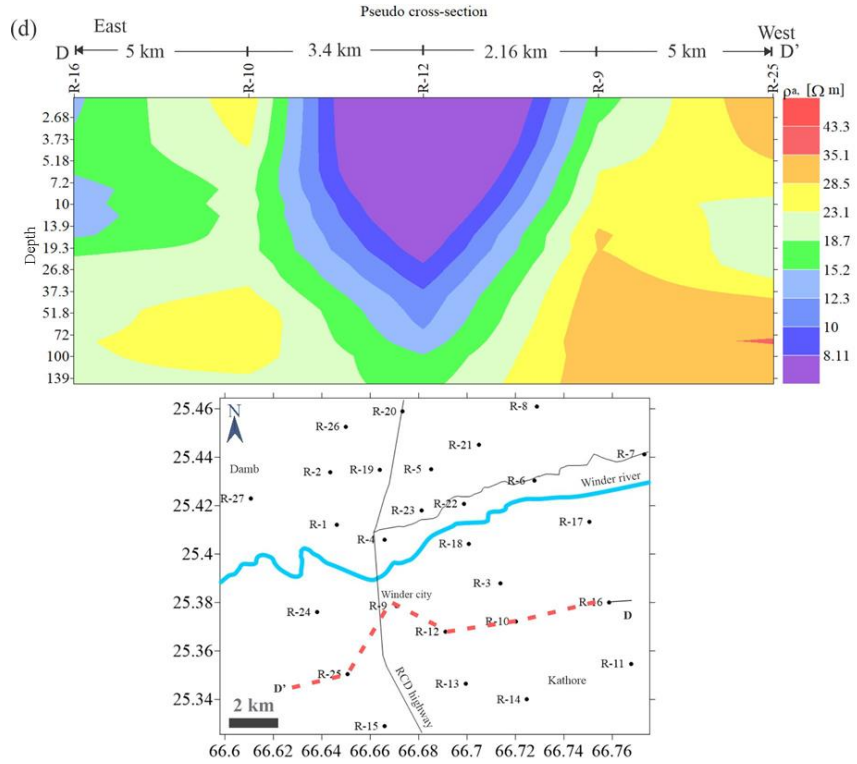

Figure 5.38 Pseudo-section D-D′ trending East-West generated from VES station R-16, R-10, R-12, R-9 and R-25. The resistivity variation of red for high and purple for low resistivity zone in Ωm. Y-axis for subsurface depth AB/2 in meter.

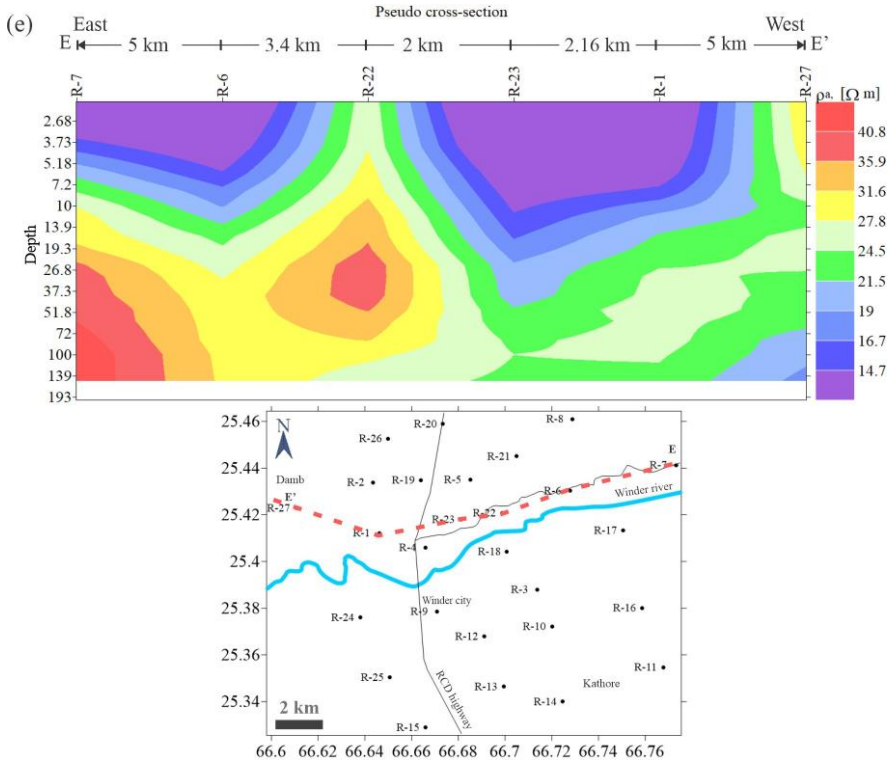

Figure 5.39 Pseudo-section E-E′ trending East-West generated from VES station R-7, R-6, R-22, R-23, R-1 and R-27. The resistivity variation of red for high and purple for low resistivity zone in Ωm. Y-axis for subsurface depth AB/2 in meter.

In conclusion, the Pseudo-section represented the north-south and east-west variation in resistivity. This variation not only provides information on lithology but also covers great knowledge in the high potential zone of fresh water as discussed above. The impact of seawater can be observed more specifically in R-27 and R-1 where high variation can be observed as compared to the point located away from the sea. It is also identified that the station near to river contains a high potential of fresh water and the water table depth is approximately 25-30 meters whereas moving away from the river water table depth is below 30 meters with low resistivity due to high TDS of water.

5.4 Geo-electric Lithology Cross-section

The Geo-electric cross-section is a graphical representation of lithology correlation interpreted for each section. To evaluate the geology of the area this will help to determine the thickness, lithological variation, pinch out and aquifer type with respect to lithology across the study region using VES points. The correlation of the VES point represents the geological cross section integrated with the subsurface geology and is also useful to predict the information where the drilled borehole was not available. The section also depicts the vertical and lateral changes in resistivity and lithology integrated with local hydrogeological information. Furthermore, north-south and east-west transverses were generated to visualize the subsurface thickness variation, dryness, moisture and lithology in the study area. The modelled subsurface geological cross section comprises recent unconsolidated sediments deposited within the Polari river basin. The detail of geo-electric cross sections is following.

5.4.1 Geo-electric Lithology Cross-section A-A′

The traverse north-south represent the correlation of the total five interpreted layer in Figure 5.40. However, the layer 5 total depth was unknown due to the survey limit. Layer-1 represents high variation in resistivity due to the lithological variation where R-15, R-25, R-24 and R-26 are interpreted as dry sand. R-1 & R-2 contains sandy clay with moisture of irrigation in agriculture farm. The range of layer-1 resistivity is 11-38.6 Ωm and thickness range from 1.84-3.79 meters. The layer-2 consists of unsaturated sand deposits resistivity range from 19.1-27 Ωm and thickness varies from 2.8-8.4 meters. A thick package in Layer 3 represent the sandy gravel and sand, value of resistivity ranging from 14.8-31.8 Ωm. and thickness varies from 11.1-25.4 meter. Likewise, the layer 4 also contained a thick sequence of silty sand, sand & sandy gravel and is referred to as an unconfined aquifer because there is no continuous confined layer of clay present at the top in cross sections A-A′. The resistivity ranges from 13.5-46.1

and the thickness varies from 29.9-77 meters. Lastly, the fifth zone also contains sandy gravel and sand deposit resistivity range from 19.1-32.2 Ωm.

5.4.2 Geo-electric Lithology Cross-section B-B′

The ranges of resistivity and thickness trend of each layer were evaluated for B-B′ geo-electric cross-section trending north-south (Figure 5.41). The traverse passes through the agriculture farms in the study area. In layer-1 R-10, R-3, R-18 and R-21 consist of clay and sandy clay deposits of a flood plain and R14 and R-22 contain sand and sandy gravel of recent deposits. The resistivity for layer-1 ranges between 3.06-26.4 Ωm and thickness varies from 1.46-3.95 meters. Layer -2 also shows variation ranges from 13.3-32 Ωm and thickness varies from 1.75-9.59 meters. Layer 3 encompasses a thick sequence of sandy gravel and sand except R-18 where sandy clay is present. The range of resistivity for this zone is 22.5-42.6 Ωm and thickness varies from 15.1-24.5 meters. Layer 4 consists of thick saturated sandy gravel deposits except R-22 where sand is preserved. The resistivity range for this zone is 24.9-49.8 Ωm. and its thickness varies from 32.6-74.9 meters. Layer 5 correlation also depicts the presence of sand and sandy gravel deposit interpreted from resistivity ranges from 17.1-51.5 Ωm.

5.4.3 Geo-electric Lithology Cross-section C-C’

The traverse north-south passed through seven VES points (R-11, R-16, R-17, R-6 and R-8) as shown in Figure 5.42. The ranges of resistivity and thickness trend of each layer were evaluated. The correlation results show that layer-1 near the surface comprised resistivity ranging from 9.38-32.7 Ωm and represented by topsoil. The variation in resistivity resulted due to clay, sand and silty sand. The thickness ranged between 1.94-2.79 m. In layer-2 the correlation shows the sand clay, silty sand, sand

and sandy gravel deposits, which also varied in resistivity values due to dry alluvium thicker than the surface layer, resistivity values in this zone ranged between 11.9-42 Ωm, while thickness between 2.79-12.1 m. The third zone represents the unconfined aquifer and resistivity ranged between 20 and 38.7 Ωm and overall thickness ranged between 13.6 and 37.7 m. The zone consisted of thick sandy gravel, sand and, sandy clay deposits. Layer 4 comprises sandy gravel, sand & silty sand, resistivity ranges of 17.1-30.5 Ωm and thickness of 35.5-75.5 m. The layer-5 resistivity range was 15.5-47.3 Ωm.

5.4.4 Geo-electric Lithology Cross-section D-D′

The correlation result in Figure 5.43 shows that layer-1 near the surface comprised resistivity ranging between 2.06-38.6 Ωm. It was represented by topsoil. The variation in resistivity was a result due to the combination of dry sand and clay with moisture, while the thickness ranged between (1.69-2.79 m). The higher resistivity zones showed the presence of sand in the topsoil, while those with relatively low resistivity values indicated the presence of clay or intercalation of clay with sand. In layer-2, the correlation shows the sand and sandy gravel deposits, which also varied with the resistivity values due to dry alluvium being thicker than that in the surface layer. Resistivity values in this zone ranged between 6.32 and 27.25 Ωm , while thickness is between 2.5 and 6.43 m. The layer-3 represents the unconfined aquifer and resistivity ranged between 15 and 34.88 Ωm, Overall thickness ranged between 13.3 and 23.43 m. The zone consisted of thick sand and sandy gravel succession. The depth of this layer was higher on the eastern side and shallow in the northwest and southwest of the study area. Layer-4 comprised sandy gravel, silty sand and sandy clay deposits with a resistivity range of 18-46.1 Ωm and a thickness between 34.1 and 77 m. The layer-5 resistivity ranges between 18.4 and 25.7 Ωm.

5.4.5 Geo-electric Lithology Cross-section E-E′

The correlation result in Figure 5.44 shows that layer-1 near the surface comprised resistivity ranging between 7.94-32.2 Ωm. It was represented by topsoil. The variation in resistivity was a result due to the combination of dry sand and clay with moisture, while the thickness ranged between (1.65-3.79 m). The higher resistivity zones showed the presence of sand in the topsoil, while those with relatively low resistivity values indicated the presence of clay or intercalation of clay with sand. In layer-2, the correlation shows the sand and sandy gravel deposits, which also varied with the resistivity values due to dry alluvium being thicker than that in the surface layer. Resistivity values in this zone ranged between 16.4 and 37.2 Ωm , while thickness is between 1.31 and 8.4 m. The layer-3 represents the unconfined aquifer and resistivity ranged between 22.1 and 50.4 Ωm, Overall thickness ranged between 9.49 and 41.8 m. The zone consisted of thick sand and sandy gravel succession. The depth of this layer was higher on the eastern side and shallow in the northwest and southwest of the study area. Layer-4 comprised sandy gravel, silty sand and sandy clay deposits with a resistivity range of 17.2-51.6 Ωm and a thickness between 27 and 68.5 m. The layer-5 resistivity ranges between 14.1 and 40.6 Ωm.

In the nutshell, the Pseudo section and litho-electric cross section shows the widespread thick packages of sandy gravel and sand aquifer overlain by the permeable bed. The aquifer in the study area is interpreted as an unconfined aquifer (Miller, 2000) due to the missing overlain impermeable clay layer. The unconfined aquifer directly recharges from the surface water and precipitation (Cobourn et al., 2017).

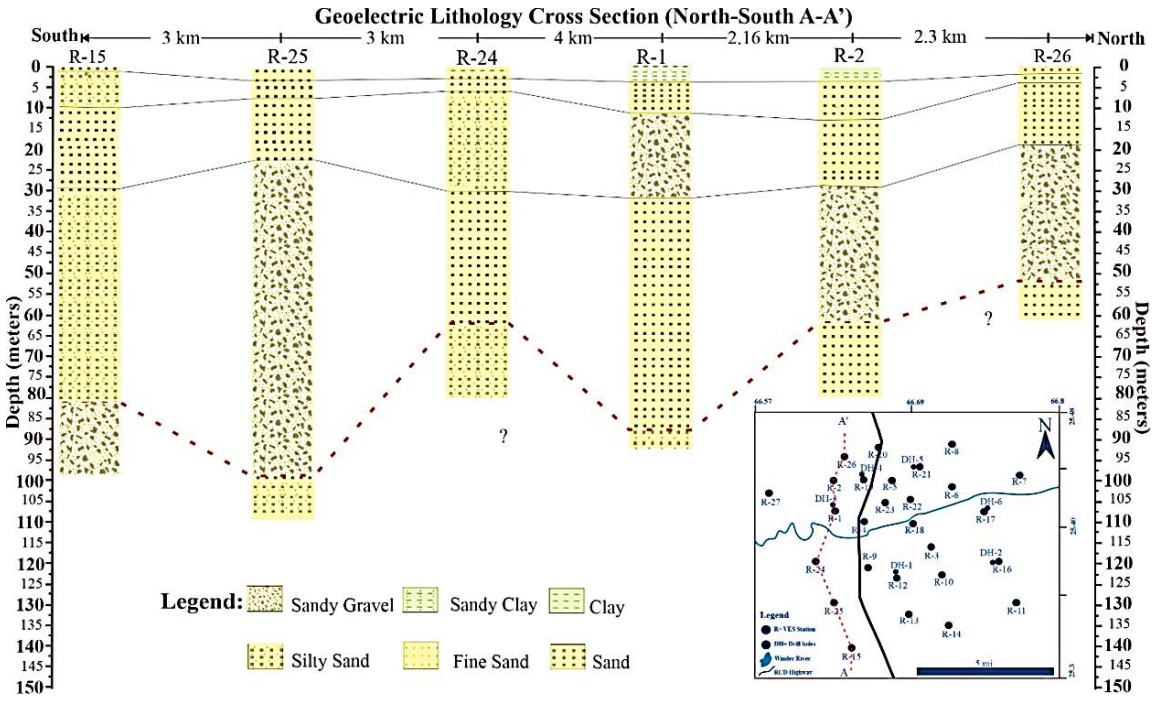

Figure 5.40 North-South Geo-electric lithology cross-section A-A′, VES station R-15, R-25, R-24, R-1, R-2 and R-26.

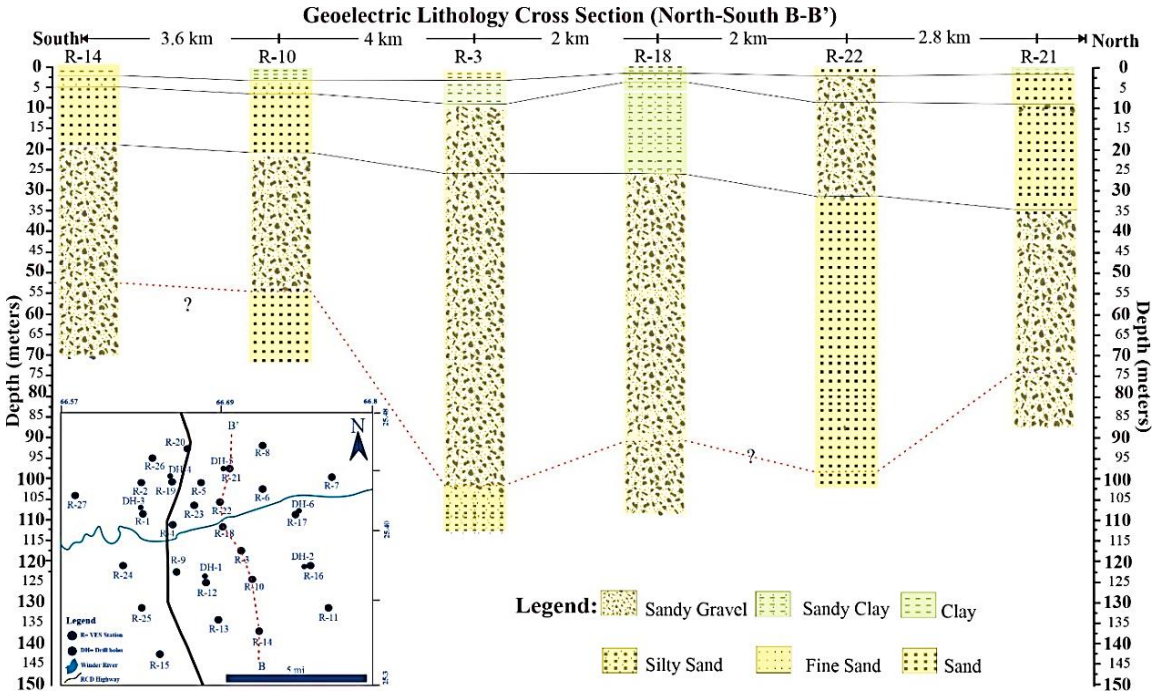

Figure 5.41 North-South Geo-electric lithology cross-section B-B′, VES station R-14, R-10, R-3, R-18, R-22 and R-21.

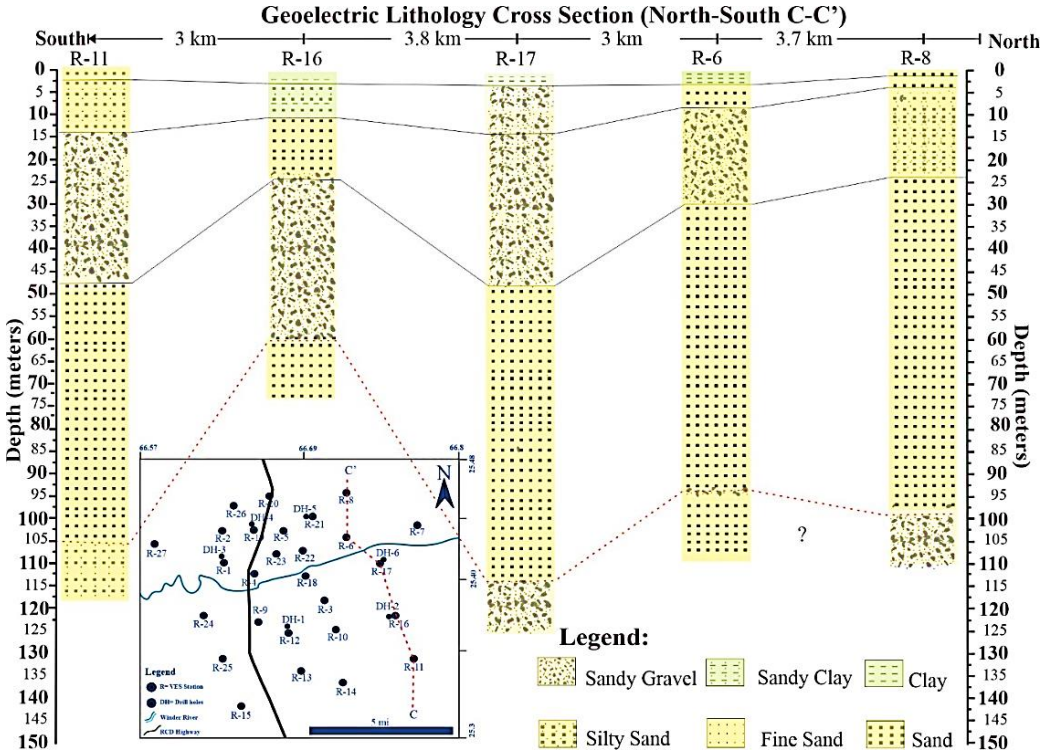

Figure 5.42 North-South Geo-electric lithology cross-section C-C′, VES station R-11, R-16, R-17, R-6 and R-8.

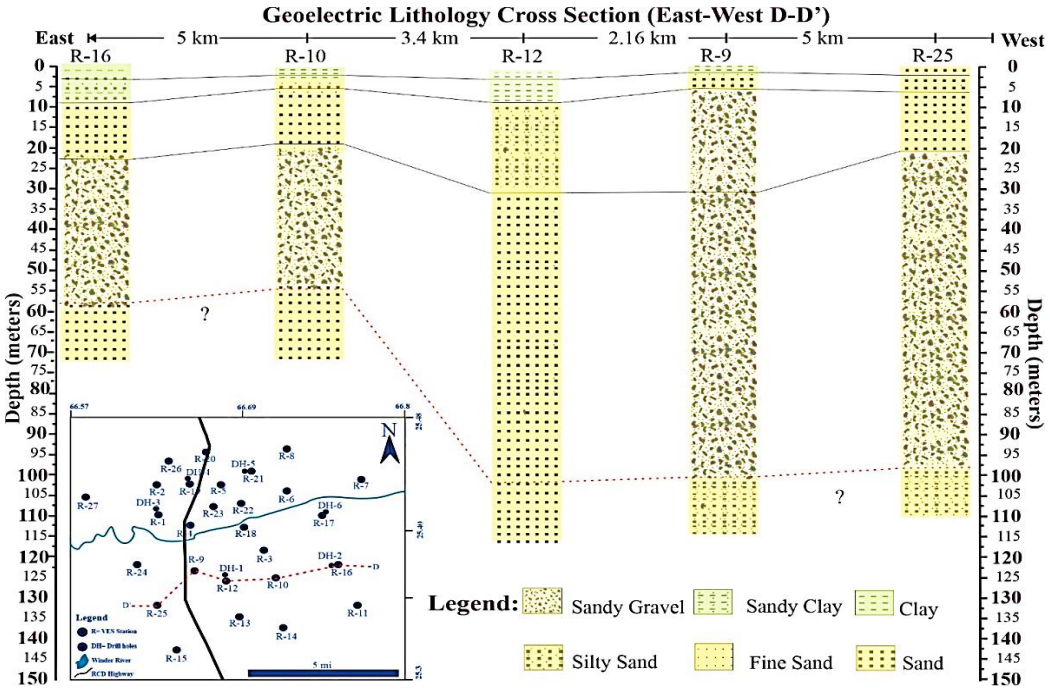

Figure 5.43 East-West Geo-electric lithology cross section D-D′, VES station R-16, R-10, R-12, R-9 and R-25.

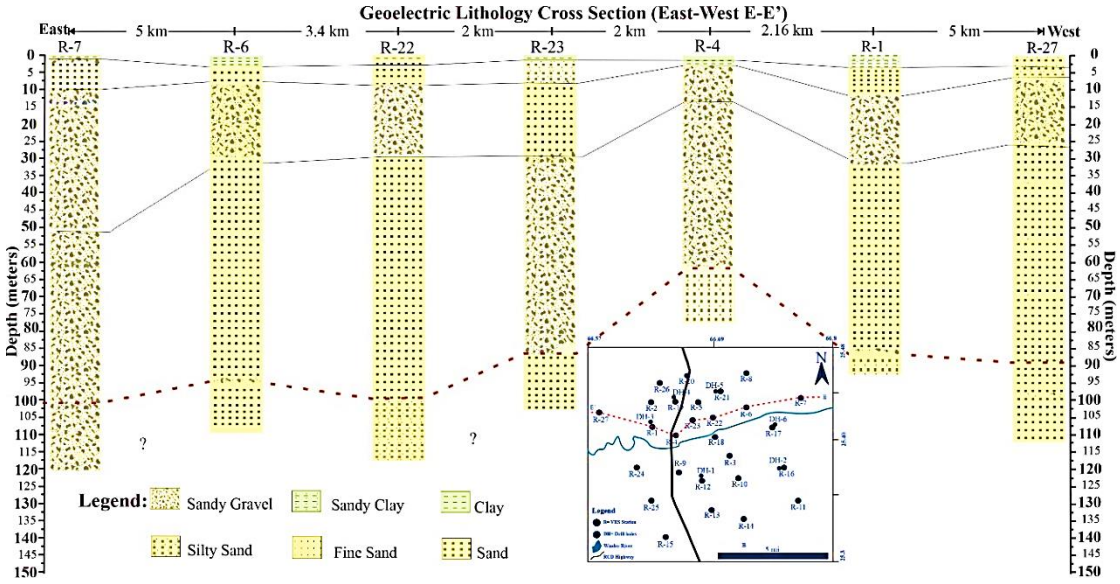

Figure 5.44 East-West Geo-electric lithology cross section E-E′, VES station R-7, R-6, R-22, R-23, R-4, R-1 and R-27.

5.5 Iso Resistivity and Thickness Maps

The apparent resistivity distribution for layer-1 shows that the resistivity is higher toward the west and south-west due to dry and unsaturated sand dunes deposits. The lower resistivity pattern on the left side of the RCD highway and adjacent to Winder River depicts the moisture of agricultural activities and the presence of sandy clay and clay (Figure 5.45). The layer-2 resistivity variation indicates the higher resistivity zone toward the north-east presence of sandy gravel whereas the south-west and north-west of the study area represent the presence of sand (Figure 5.46). The layer 3,4 and 5 show higher resistivity in the central and eastern parts of the study area whereas the western side shows low resistivity zones. The layer 4 and 5 are saturated and low resistivity depicts the brackish water condition toward the western side, the higher resistivity closure along the Winder River is delineated as a high potential freshwater zone (Figure 5.45-549).

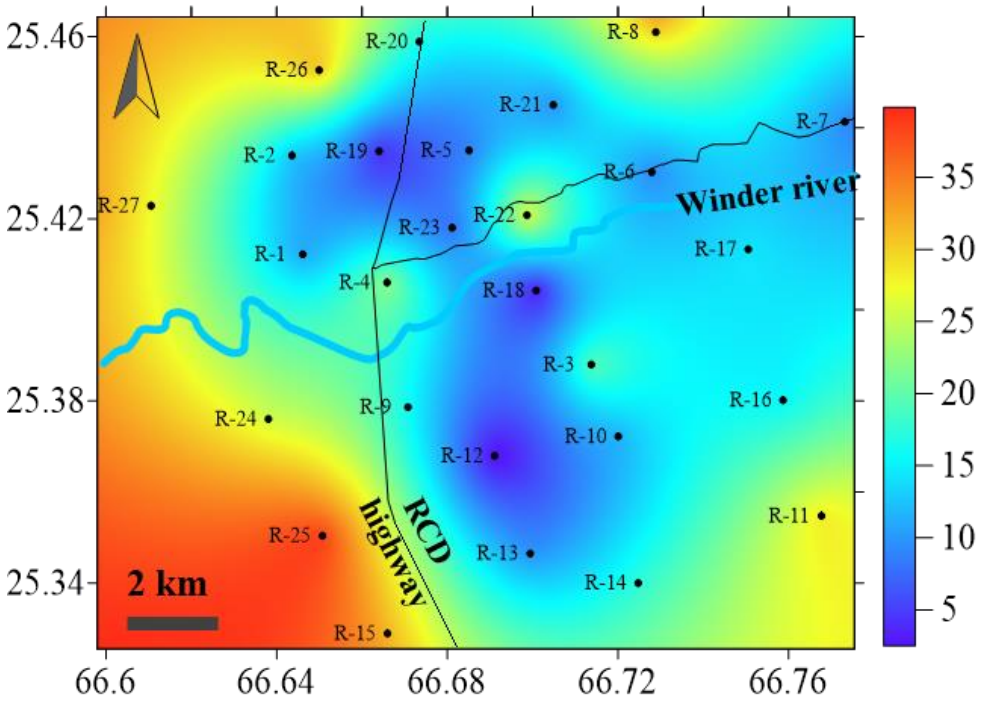

Figure 5.45 Spatial distribution map of resistivity (Ωm) for layer-1.

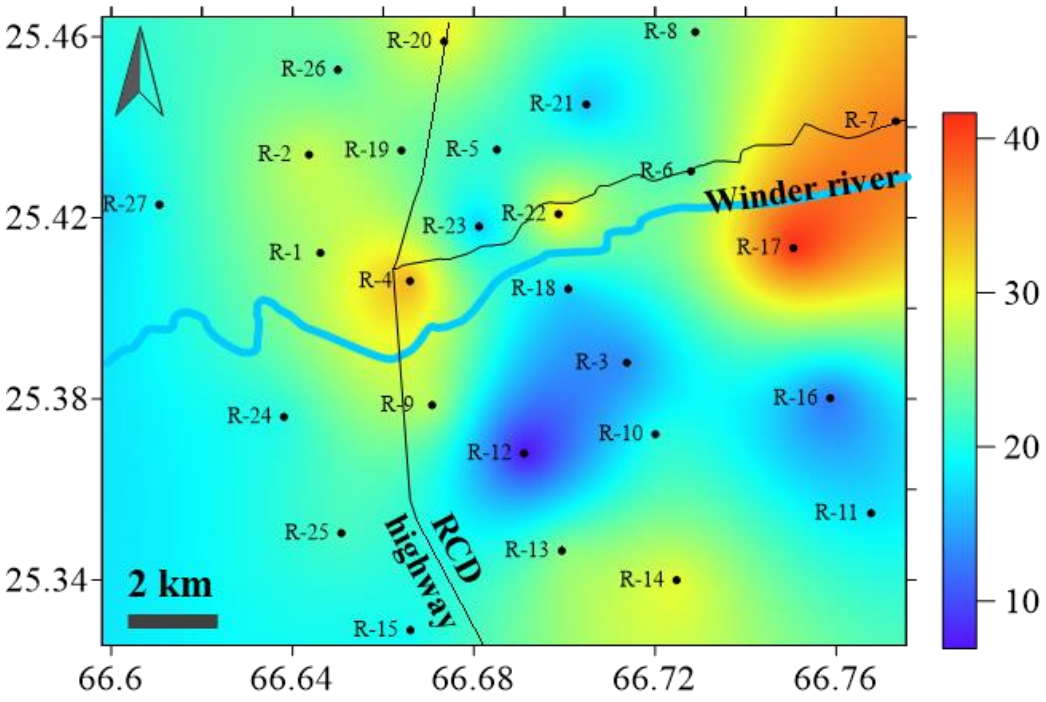

Figure 5.46 Spatial distribution map of resistivity (Ωm) for layer-2.

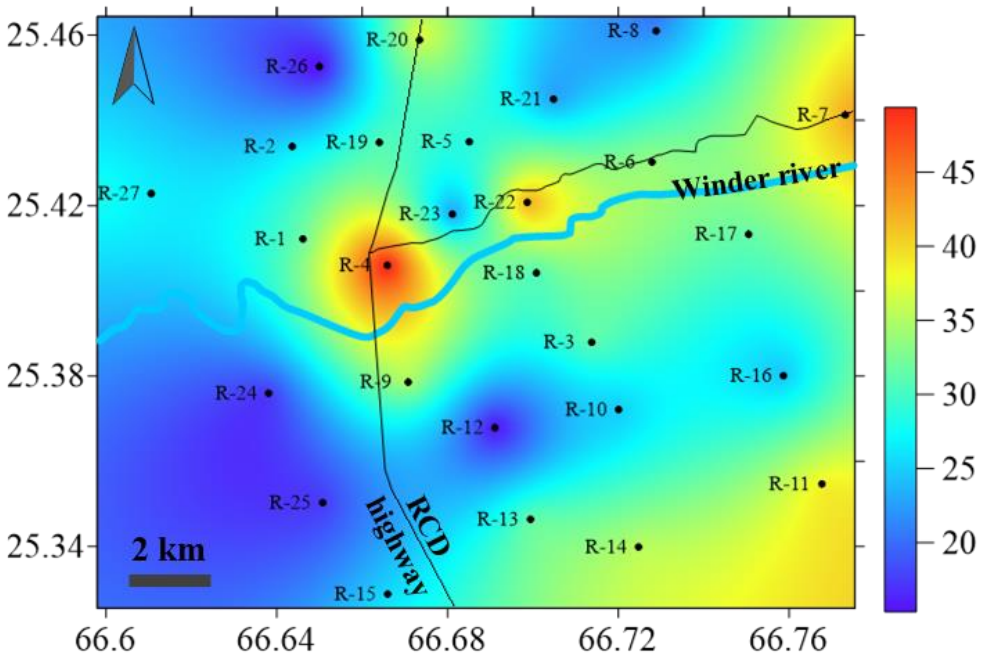

Figure 5.47 Spatial distribution map of resistivity (Ωm)) for layer-3.

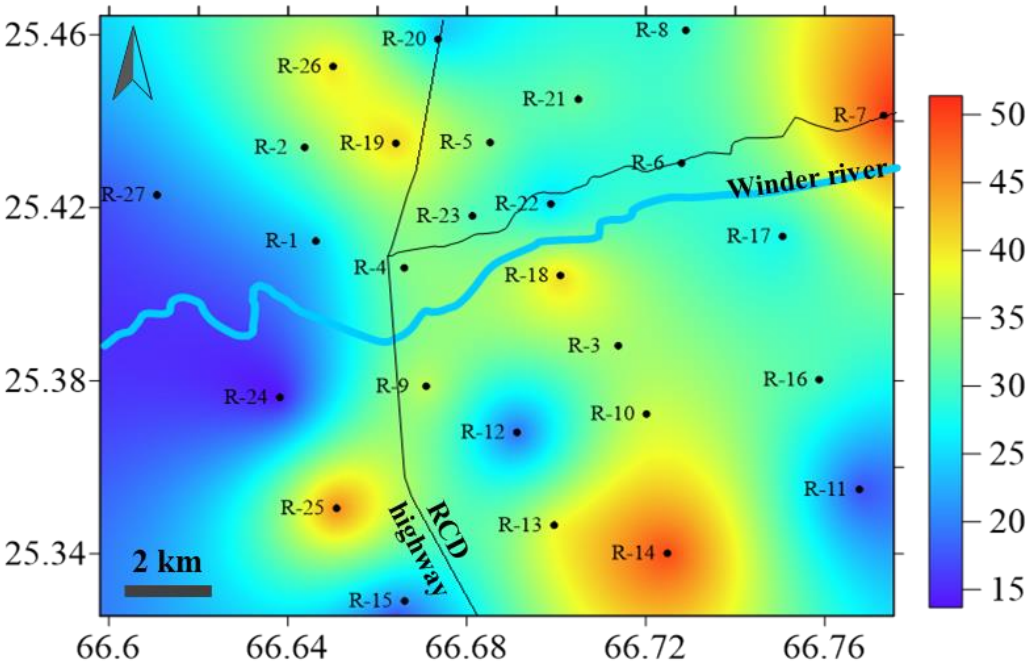

Figure 5.48 Spatial distribution map of resistivity (Ωm) for layer-4.

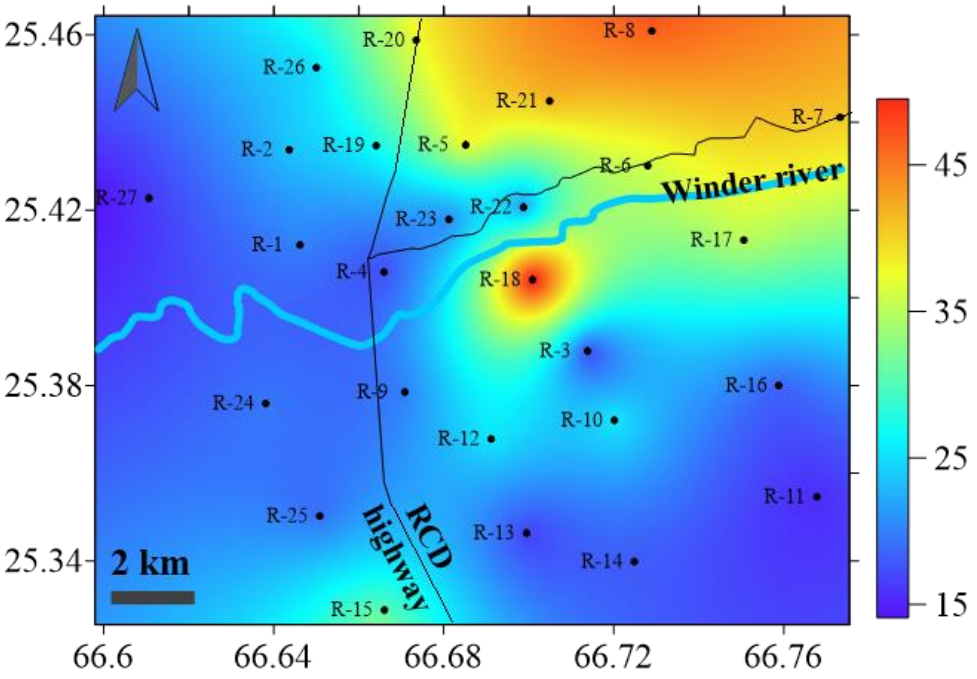

Figure 5.49 Spatial distribution map of resistivity (Ωm) for layer-5.

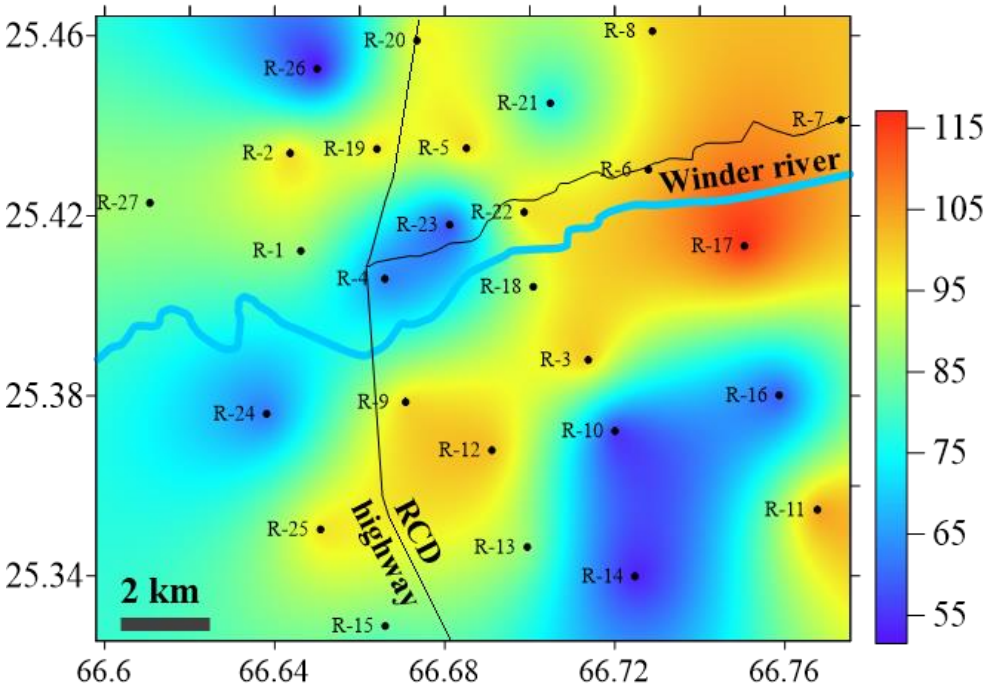

Figure 5.50 Thickness map (meters) of recent deposits in Lasbela plain, Winder Balochistan.

The thickness map of the study area provides the distribution of Quaternary sediment deposited over the triangular-shaped Lasbela Plain. The source of sediment is from the north-east of the study area where the maximum thickness of sediment was observed for modelled layers and the main sediment was contributed from the Mor and Pab ranges. The interpreted subsurface geology and drilled log suggested that the depositional environment of deposited sediment is from high-energy rivers and distributaries of the Polari Basin. The sand and sandy gravel deposited by the river and coastal belt are covered by aeolian sand deposits. The minimum thickness contour closures at R-26 & R-24 were observed in the west close to the coastal area, R-10 and R-16 south-east Kathore and R-23 & R-4 central part of the study area. The maximum 117-meter thickness of layers toward the north-east (Figure 5.50). The thick sequence of sandy gravel and sand deposits contains an unconfined aquifer in the study area. The sediment is unconsolidated which provides high porosity and permeability for the aquifer in comparison with the bedrock or compacted sandstone (Worthington, 2022).

5.6 Dar-Zarrouk Parameters (D-Z)

D-Z Parameters are utilized for aquifer characterization in determining the potential of groundwater and quality variation in the targeted study areas (Hasan et al., 2020c; Bassey et al., 2019). The D-Z parameters estimation has been very helpful in identifying the higher TDS zones and detecting variants in heterogeneity. Usually an average, electrical characteristic of a single stratigraphic succession can easily be defined by estimation of D-Z parameters (Maillet, 1947). Therefore, the D-Z parameters have been utilized to map for this region. The two terminologies namely, Transverse resistance (Tr) & longitudinal conductance (S) from D-Z parameters characterize the resistance (normal to the face) and also (parallel to the face) for a unit cross-sectional area. Additionally, both parameters are also utilize in distinguishing the anisotropic & isotropic characteristics of subsurface units (Yeboah-Forson & Whitman, 2014; Singh et al., 2004).

5.6.1 Transverse Resistance (Tr)

The Transverse resistance was computed using the 27 VES station (Figure 5.51). The Tr value has a direct association with the aquifer transmissivity & T maps normally used for demarcating high groundwater potential areas (Toto et al., 2008; Braga et al., 2006). In addition, Tr also helps to delineate and interpret saline zone (Singh et al., 2021; Hasan et al., 2020b; Singh et al., 2004). The higher value of Tr present in the north-east and along the Winder River of the study area where thickness is maximum indicates the good groundwater potential and high transmissivity. The transverse resistance map of the study area showed contours ranging from 1690 Ωm^2 to 3700 Ωm^2 over the study area. The lower values Tr < 2000 Ωm^2 were observed in the south-east and toward the western part of the study area due to high conductance, effected by seawater intrusion (Singh et al., 2021; Hasan et al., 2020a; Coker, 2012; Srinivasa 2004). The higher value of T also represents the presence of sandy gravel and sand whereas lower values indicate silt, sand and clay.

5.6.2 Longitudinal Conductance (Sc)

In the same way, the Sc values were utilized to prepare the map (Figure 5.52). Longitudinal conductance (Sc) defined as the current transmission is in the direction of the bedding plane, through the column of 1 meter and determined using the sum of "n" layers thickness/resistivity ratio (Oliver & Raj, 2012; Parasnis, 2012; Slater, 2007). The unit conductance used to demarcate clay and sand water aquifer region (George, 2021; Oliver & Raj, 2012), protective capacity of overburden sequence on basis of thickness and type of rock overlain the aquifer (Nugraha et al., 2022; Chukwuma et al., 2015; Henriet, 1976). The estimated value of Sc for 27 VES stations up to 150-meter depth shows high variation ranges from 1.27-7.29 mho for the study area. The low to

moderate values are observed over the study area except higher in the south near Winder Town and toward the west near the Arabian coast.

The Sc value is divided into fresh and brackish water. The lower values of Longitudinal Conductance "Sc" < 2 mhos indicate the fresh zone, 2-4 interpreted as brackish water and higher values >4 identified as saline water (Singh et al., 2021). The overburdened material in the area from the geo-electric log is interpreted as a thick continuous unconsolidated recent deposit of sand and sandy gravel. For good protective capacity, at least 10-meter-thick shale is required to protect the aquifer from surface contamination. Therefore, it can be said that the study area lies under weak protective zone. In this case the surface anthropogenic activities can easily contaminate the groundwater and also sea water intrusion is rapidly replacing replace the aquifer due to its depleting. The presence of weak protective zone on other hand can be useful for artificial groundwater recharge.

5.6.3 Longitudinal Resistivity (L)

A contour map was generated by using the calculated longitudinal resistivity for the study area (Figure 5.53). The lower values for longitudinal resistivity are interpreted as saline toward the coastal belt of the study area and higher values were identified as good quality water in the northeast and southeast. The value is in the range of 13.96-43.36 Ωm. The value of Longitudinal Resistivity "L" < 20 is saline and > 20 is considered of good quality.

5.6.4 Transverse Resistivity

A contour map was generated by using the calculated transverse resistivity for the study area (Figure 5.54). The lower values for transverse resistivity were interpreted as saline toward the coastal belt of the study area and higher values are identified as good quality water in the north-east and south-east. The value of transverse resistivity is in the range of 15.8-46.2 Ωm.

5.6.5 Anisotropy (λ)

Anisotropy is calculated from the ratio of transverse resistivity and longitudinal resistivity parameters for a block layer which acts as one unit and is considered anisotropic (Zohdy, 1965; Maillet, 1947). The presence of anisotropy in a rock is caused by the grain orientation, layering, fracturing, metamorphism and disseminated ore grain (Watson & Barker, 1999; Habberjam, 1972). The coefficient of anisotropy is usually > 1 and the value exceeds 2 in a rare case for complex geological conditions. The range of anisotropy from 1 and up to 1.5 is interpreted as a potential groundwater zone (Singh et al., 2021; Abrar et al., 2019; Yusuf & Abiye, 2019; Olasehinde & Bayewu, 2011). The anisotropy surface represents the homogenous nature of the sand and sandy gravel aquifer distribution in the subsurface. The coefficient of anisotropy values ranged from 1.007 to 1.09 λ. The homogeneous condition shows high permeability in sand and sandy gravel depict the high vulnerability of sea water into the coastal aquifer of Winder (Figure 5.55).

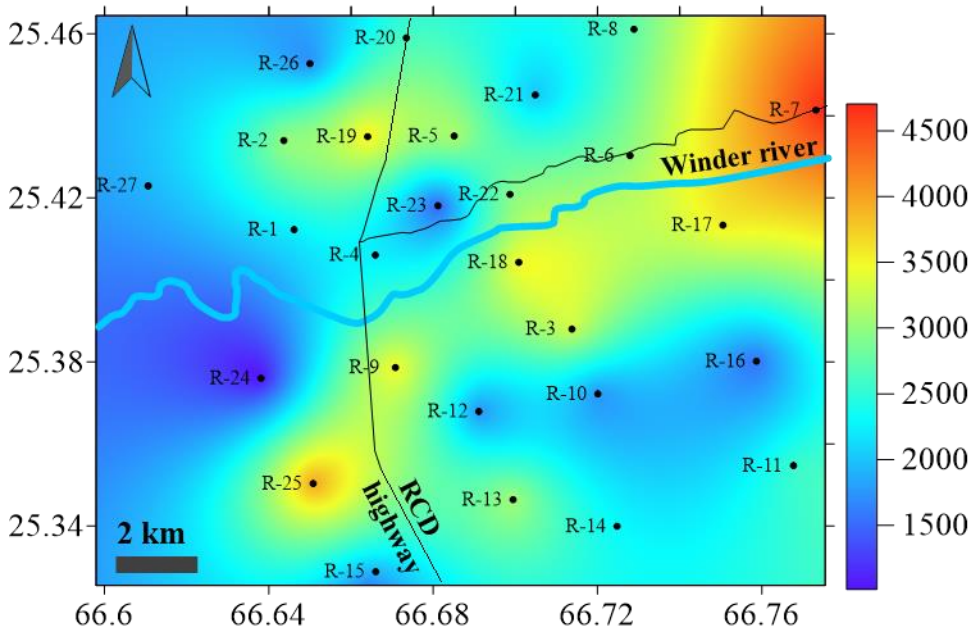

Figure 5.51 Transverse resistance computed using the 27 VES station of the study area and unit is Ωm^2.

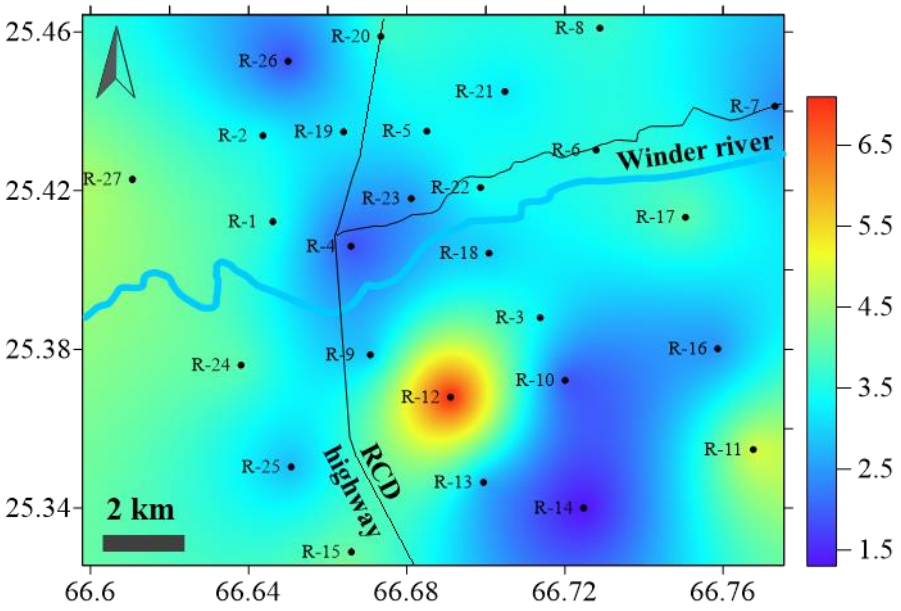

Figure 5.52 Longitudinal unit Conductance map of the study area and unit is mho.

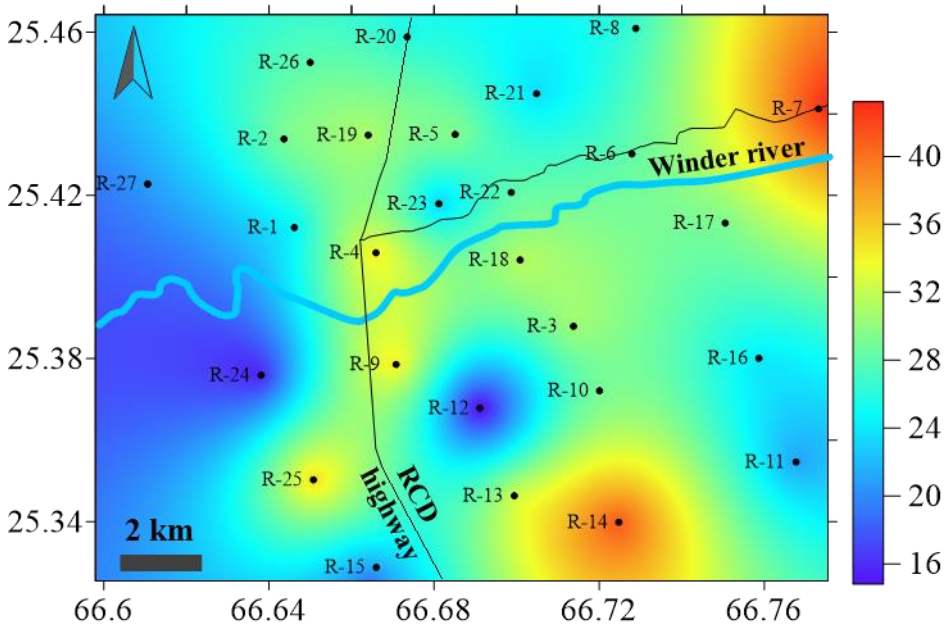

Figure 5.53. Longitudinal Resistivity map of study area and unit is Ωm.

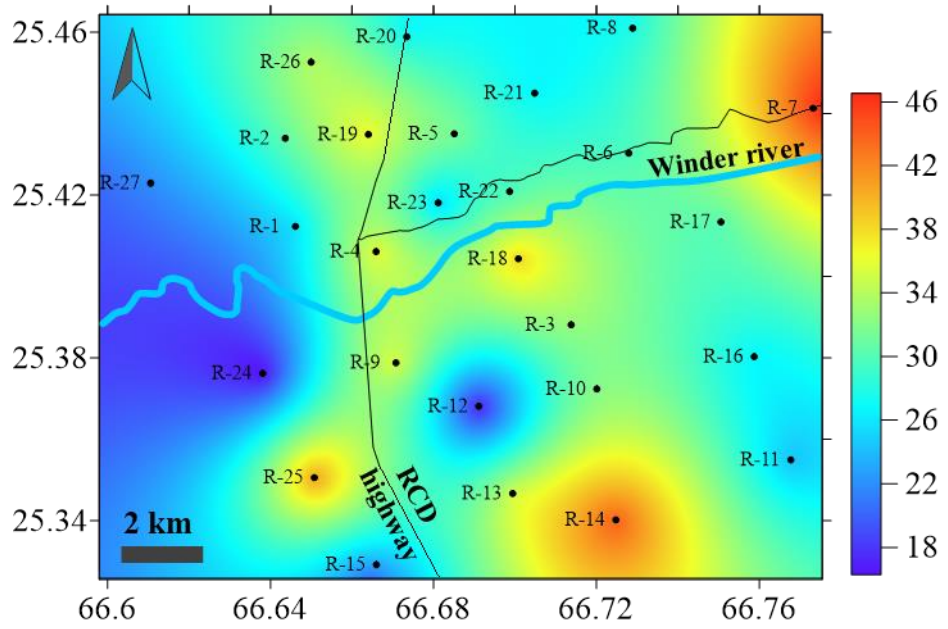

Figure 5.54 Transverse Resistivity contour map of study area and unit is Ωm.

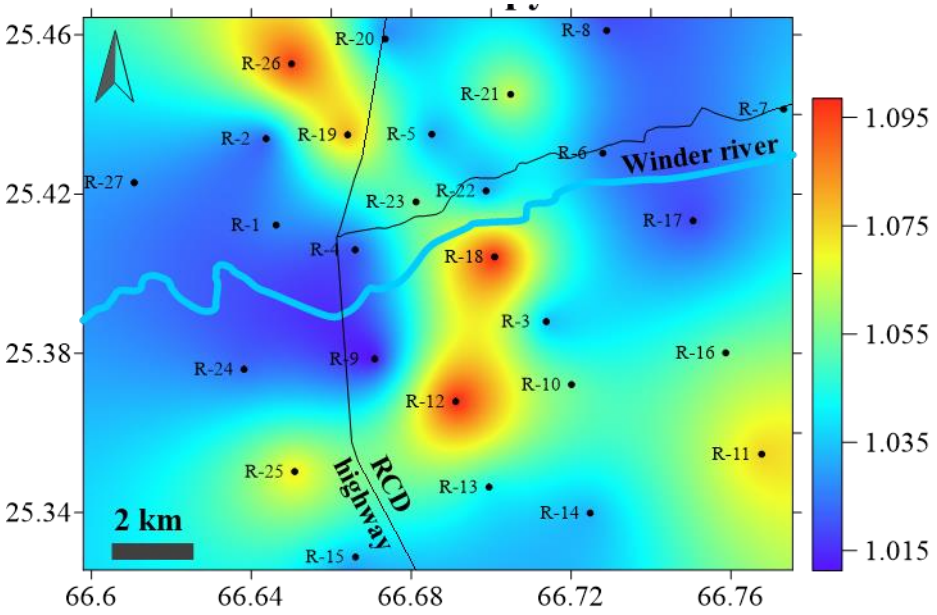

Figure 5.55 Anisotropic contour map of the study area.

5.7 Hydro-Chemical Analysis of Groundwater Samples

The physiochemical analysis of groundwater plays a vital role in the classification and assessment of water quality for drinking and irrigation purposes (Maghraby & Bamousa, 2021; Khalid, 2019). The groundwater is present in rock pore spaces therefore rock composition also contributes to groundwater geochemistry (Chen et al., 2021a; Kaleem et al., 2019; Redwan et al., 2016). The study area ophiolites have a major impact on water and soil quality. The ophiolites dissolution provides a discrete accumulation of ions in soil (Eliopoulos et al., 2020). The ion exchange process between soil and groundwater plays an important role in composition (Kumar et al., 2020; Naseem et al., 2010). The Stiff and Piper diagram quickly demonstrates the complexities present in groundwater and classifies the parameters by utilizing graphical plotting (Gabr et al., 2021; Arulnangai, 2020; Wang et al., 2020; Rajendra et al., 2009). Moreover, the geostatistical examinations are essential for a better understanding of

rock-water association (Cangemi et al., 2021; Osiakwan et al., 2021). A stiff diagram is useful to deduce ionic composition and stability in various pairs of ions plotted in (meq/l). A Piper diagram helps to demarcate the chemical composition and assess the type of water and its potential source (Xi et al., 2021). Similarly, results are interpreted using various plots and geostatistical techniques for effective discussion. Trace element analysis is the key factor for assessing quality of water (Hossain & Patra, 2020; Snousy et al., 2020; Hamza et al., 2013). In conclusion the hydro geochemical parameter estimation and their spatial distribution in groundwater helps to understand the relative abundance and mutual relationship. The variety of standard diagrams and plots are investigated to deduce the contribution of effective groundwater quality for irrigation and seawater intrusion. The summary of the chemical parameter analyzed in laboratory is presented in Table 5.2.

Table 5.2 Summary of Chemical parameter analysis of study area.

	Ca^{2+}	Mg^{2+}	Na^{+}	K^{+}	HCO_3^{-}	Cl^{-}	SO_4^{2-}	NO_3	IBE	pH	EC	TDS
Min	75.3	30.0	120.0	2.0	138.0	232.0	119.7	41.0	-5.3	6.5	1.5	493.0
Max	280.0	152.0	896.0	24.0	775.0	1270.0	555.0	110.0	15.2	8.5	4.6	5200.0
Mean	133.3	83.8	331.5	6.1	361.9	522.2	306.9	66.0	0.1	7.3	2.7	1872.2
SD	35.4	23.4	130.5	4.0	97.9	178.8	92.2	10.0	3.3	0.4	0.9	922.0

5.8 Ionic Composition

The most important step in water analysis is a calculation of the Ionic Balance Error of positive or negative ions of groundwater (Osiakwan et al., 2021). According to the principle of electro-neutrality water fulfil the balance of +/- ions. It can be evaluated by using the equation 5.1 mentioned as follows (Hem, 1985; Freeze & Cherry, 1979).

$$\text{Ion Balance Error \%} = \left[\frac{\sum_{cations} - \sum_{anions}}{\sum_{cations} + \sum_{anions}}\right] \times 100 \quad \ldots\ldots\ldots\ldots \quad \text{eq. (5.1)}$$

The Ionic Balance Error should be less than 5% (Hounslow, 2018). However for groundwater analysis, a value less than 10 % is also acceptable (Katz & Collins, 1998). The current study sample analysis is under the acceptable limit maximum of 3.5% observed which shows the quality assurance of results and analytical work conducted during analysis.

5.8.1 pH and Alkalinity

The pH of water influences the water suitability for irrigation. The range of pH is from 6.5-8.4 considered normal for the agriculture activity (Bouaroudj et al., 2019). The sample of the study area lies in the range of 6.5-8.5. The mean value is 7.24 representing the suitability of water for irrigation. The result shows a similar range of pH in comparison with the ranges of other sites in Pakistan (Ali et al., 2021; Lanjwani et al., 2021; Rasool et al., 2017). A higher value greater than 8 was observed in samples US, UI, UN, UG, UR, UD, UT, ST, SA, AM, BM, BT and KA near to the coastal belt. The higher value of these stations is plotted on the right side of the graph in (Figure 5.56). In standard irrigation pH<7 is acidic and pH>7 is indicated as basic. The alkalinity is observed due to HCO_3 ions in groundwater & bicarbonate ions show a direct relationship with pH. The sample shows 138-755 mg/l HCO_3 ions in the study area. The HCO_3 mean value is 361 mg/l, is higher than the permissible upper limit for the crops which is 244mg/l (Flynn, 2009). A pH greater than 8.2 indicates the presence of high CO_3 ions in a sample. The assessment of pH range is very useful in order to evaluate the micronutrient availability such as Mn, Fe, Cu, Zn, etc. The availability of micronutrients provides healthy growth in Plants (Langridge, 2022; Siddiqui et al., 2022; Wei et al., 2006). Generally, lower pH increases the absorption of these element in water. The slightly higher pH range in study area as compare to the previous data (Naseem et al., 2013) is not favourable for the occurrence of trace elements (Figure 5.56). The presence of bicarbonate ions is high and they are not dangerous, but the combination with Mg^{2+} or Ca^{2+} precipitate in carbonate is risky for irrigation. It might

decrease the concentration of Zn & other metals required for the growth of plants (Ayer & Westcot, 1985).

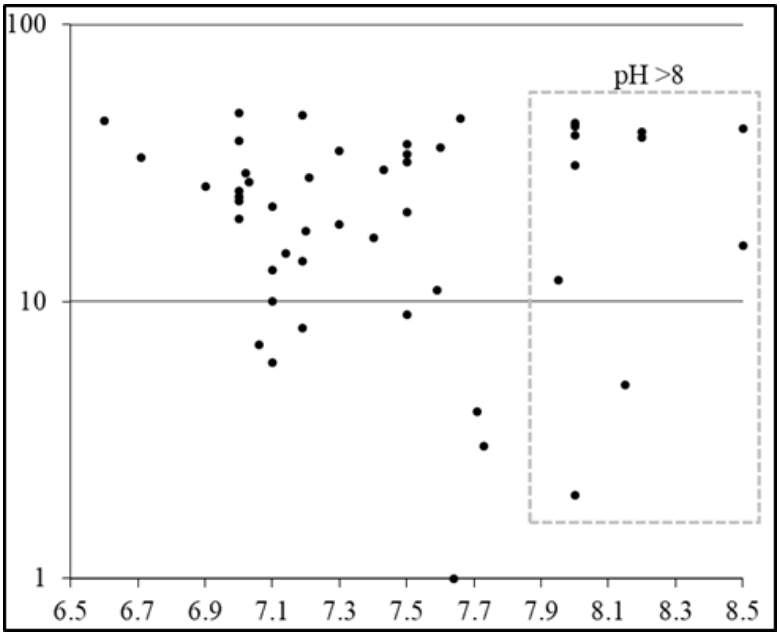

Figure 5.56 pH value ranges from 6.5-8.5 in a sample of the study area.

5.8.2 Total Dissolved Solids (TDS) & Electrical Conductivity (EC)

Water is hazardous for human consumption and crop activities because salinity is the most important parameter in quality of water (Egbueri et al., 2021; Troudi et al., 2020). In the study area, most of the samples show high salinity as per the WHO standards for drinking water and irrigation, the maximum recommended value of TDS is 1000 ppm (WHO, 2021; Pakistan, 2007). The estimated range of TDS from the groundwater analysis is 1076-3000 mg/l and an average value is 1872 mg/l. The range depicts in 94 samples among which only 10% samples represent medium salinity hazard, 40% for high and 50% are very high. Above average EC value of 2.7 of water decreases the capacity of the plant to gain water and other essential ions in solution

whereas the permissible limit of EC is 1.5 dsm^{-1} (Pakistan, 2007). The distribution of TDS in study area shows higher TDS values towards the north-west & south-east of study area (Figure 5.57).

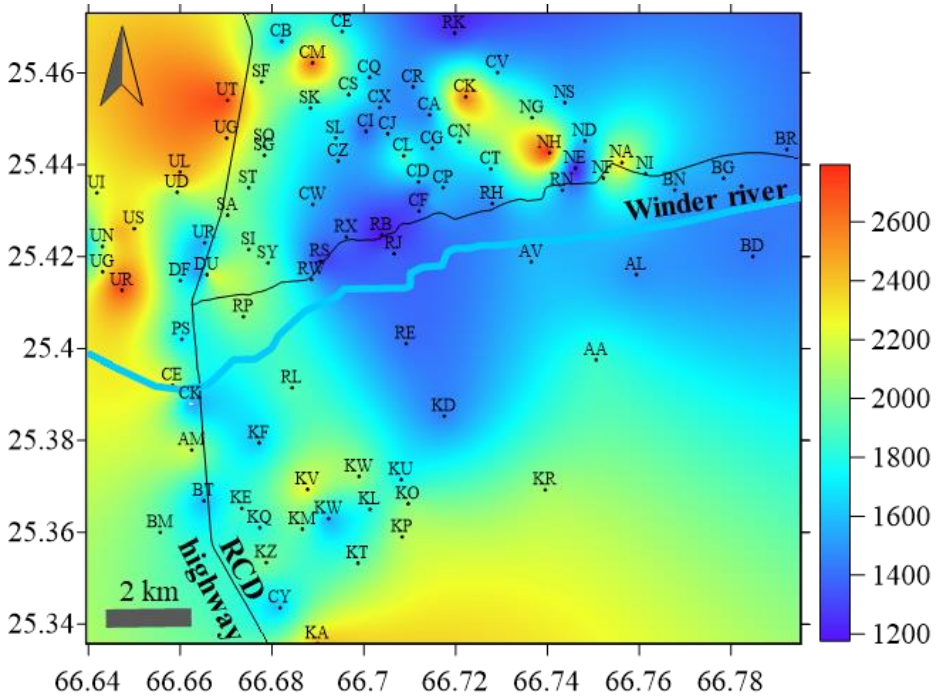

Figure 5.57 Spatial distribution of (TDS) for groundwater sample of study area. The contour interval is 200 ppm.

5.8.3 Chloride (Cl^-)

The presence of chloride was evaluated to observe the high concentration which can impact irrigation and it can cause toxicity in crops. The safe value of chloride is <70 for irrigation but some plants are sensitive and may impact in 70-140 range. More than 350 mg/l becomes a hazard and impacts severely (Mallick et al., 2021; Mokoena et al., 2020; Bauder et al., 2011). The investigated samples show the richness of Cl^- anions values varies from 232 to 1270 mg/l, and an average concentration of 522 mg/l. Spatial distribution map depicts the variation and presence of higher concentrations in

the study area (Figure 5.58). The Cl^- ions reveal a linear association with Na^+ (Figure 5.59). The higher values of Na and Cl represent the cluster of US, UI, UN, UG, UR, UD, UT, ST, SA, AM, BM, BT and KA.

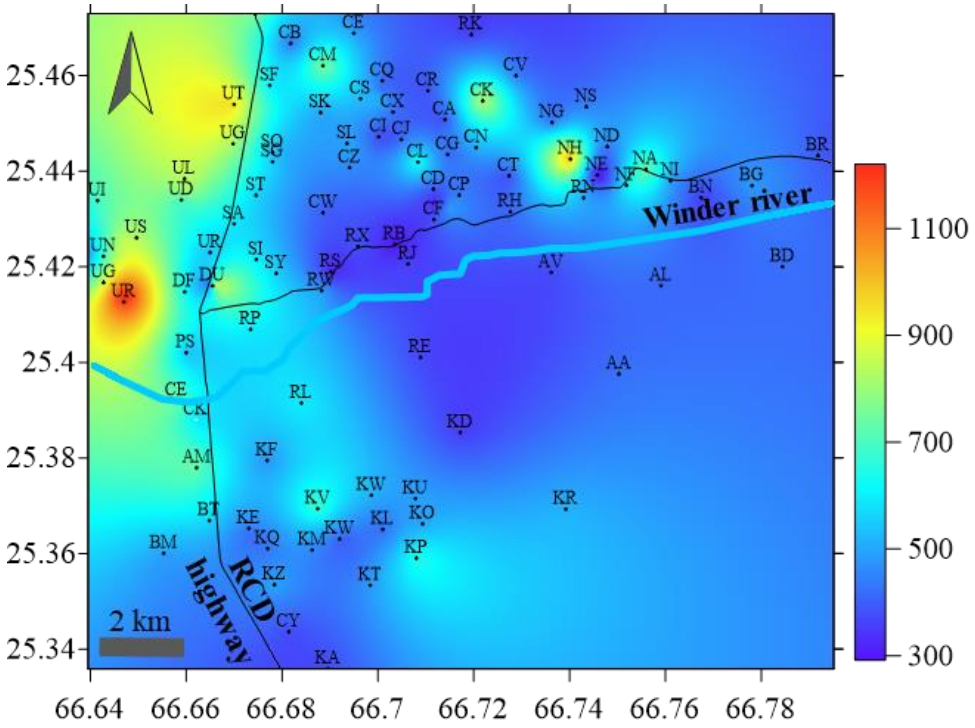

Figure 5.58 Distribution map of Chloride concentration measure from groundwater samples of study area.

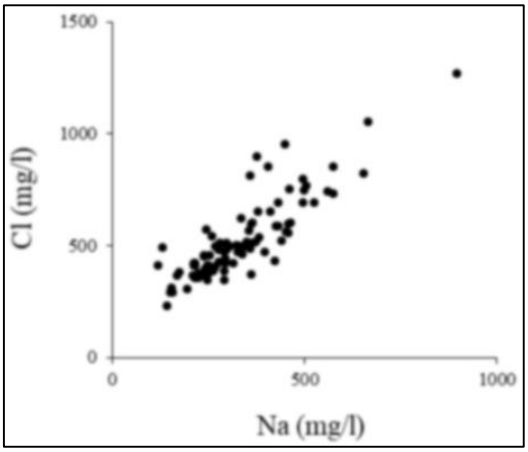

Figure 5.59 Sample of the study area represents a linear relationship between Chloride Cl^- and Sodium Na^+.

The Na Vs Cl graph of groundwater sample shows a linear relationship and a slope of 0.81 (Figure 5.59). The global slope value for the seawater mixing line is 0.858 (Lekshmi & Kani, 2017). The ionic ratio of Na/Cl for seawater is usually less than 0.86 (Shunmugam, 2022; Asare et al., 2021; Ouhamdouch et al., 2021). The range of Na/Cl in the study area is 0.40-1.50. It clearly depicts the sample less than 0.86 are impacted by intrusion and the remaining reveal the presence of Na is originated from the rocks bearing Na or can be exchanged with Ca.

The Cl^- ions show a moderate relationship with another (HCO_3) anion. It is reflected in plots (Figure 5.60). The average ratio of HCO_3/Cl^- is significant to differentiate, both rock weathering and seawater intrusion. The range of HCO_3/Cl^- 0.06-1.22, the lower values are observed in a station on the left side of RCD highway (US, UI, UN, UG, UR, UD, UT, ST, SA, AM, BM, BT and KA) and higher toward the right side. It is essential to note that the average ratio of HCO_3/Cl^- in the study area is 0.43 has been decreased in comparison with the previous result 0.71 (Naseem et al., 2012). Although this ratio is very high than average seawater intrusion ratio which is 0.0069 (Lee & Song, 2007) but decreasing trend clearly suggests the impact of intrusion from the sea. The higher value of HCO_3/Cl^- can be interpreted as the result of carbonate rock weathering (Naseem et al., 2010) which is exposed in the eastern side of study area.

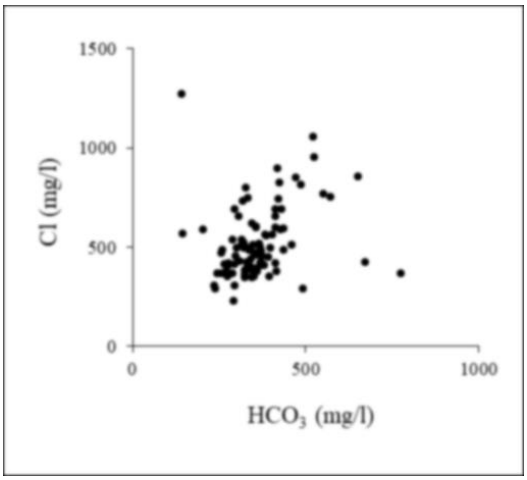

Figure 5.60 Groundwater sample shows Cl^- ions medium relationship with another (HCO_3) anion.

The Gibbs diagram was employed to recognise the source of a dissolved constituent in the groundwater of study area (Ekwule et al., 2022; Bari et al., 2021). It represents the chemical composition of water in three distinct zones. This analysis shows that the groundwater sample composition of study area is controlled by the weathering of rock, evaporation and seawater intrusion (Figure 5.61). There are two plots to establish the relationship of TDS with $Cl^-/Cl+HCO_3$ and $Na^+/(Na^+ + Ca^{2+})$ using the standard Gibbs diagram (Gibbs, 1970). The present study shows that most of the samples in the TDS and $Na^+/ (Na^+ + Ca^{2+})$ relationship were plotted near the seawater and evaporation. The lower value TDS & $Na^+/ (Na^+ + Ca^{2+})$ depict the contribution of the host rock. The abundance of chlorides ion present in groundwater is mainly due to brine conditions evolved from seawater intrusion. The relationship of TDS with $Cl^-/Cl+HCO_3$ also portrays the contribution of seawater intrusion. Groundwater comes up with less Cl^- ion and higher HCO_3 depicting the no input of pollutants in natural water (Chebet et al., 2020). The present condition suggests that seawater is also contributing in groundwater recharge due to overexploitation.

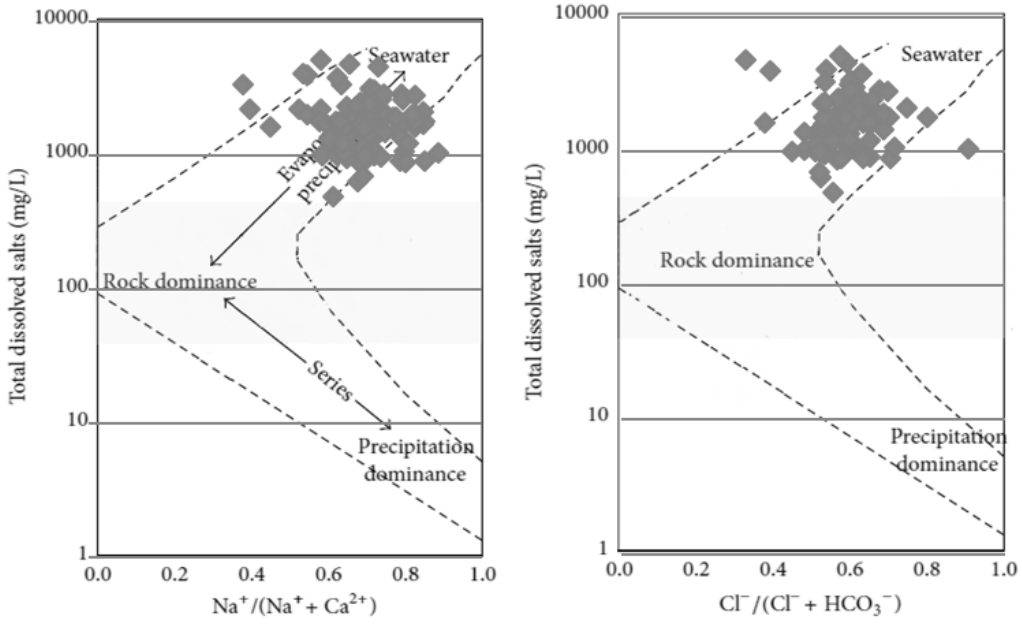

Figure 5.61 The relationship of TDS with $Cl^-/Cl+HCO_3$ and $Na^+/(Na^+ + Ca^{2+})$ plotted on Gibbs diagram for 94 groundwater samples of Winder.

5.8.4 Sulphate (SO_4^{2-})

The study area sedimentary sequence comprised Gypsum $Ca.SO_4\ 2H_2O$ and Anhydrite $CaSO_4$ rocks. The presence of Sulphate (SO_4^{2-}) in groundwater is due to the chemical disintegration of these rocks. During oxidation, the minerals pyrite, galena, chalcopyrite and sphalerite etc. also impact the geochemistry of groundwater. The higher concentration (SO_4^{2-}) ions are in the eastern part of the study area and near the Winder River.

The variation in a range of ions shows the water interaction in a different time, climate, exposed outcrop and soil. The range of (SO_4^{2-}) is 120-555 and the mean concentration is 307 mg/l. The concentration of sulphate is within permissible limits whereas if the concentration is greater than 1000 mg/l it is harmful for crops. The previous researcher range of (SO_4^{2-}) was 97-845 and the mean concentration 360 mg/l (Naseem et al., 2010). The SO_4^{2-} ions show a positive association with Mg and it is not remarkable for Ca^{2+} (Figure 5.62).

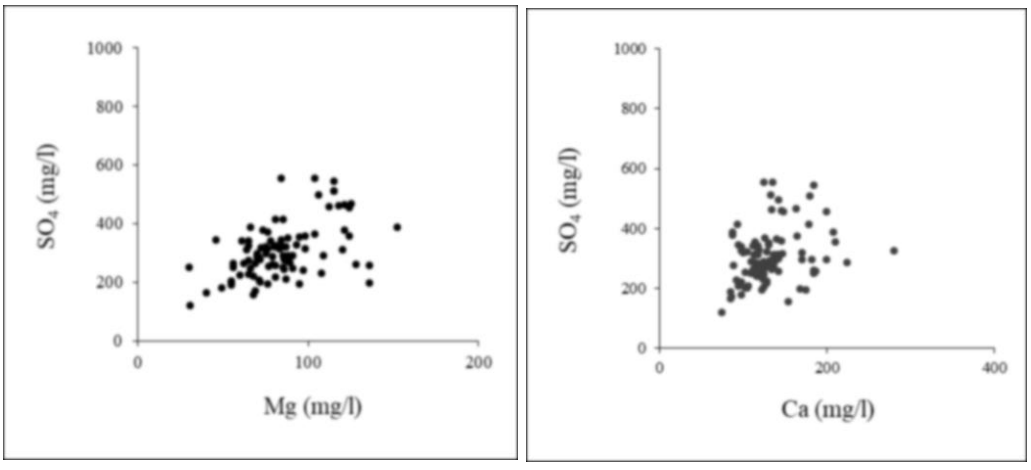

Figure 5.62 Magnesium (Mg^{2+}) and Sulphate (SO_4^{2-}) , Calcium (Ca^{2+}) and Sulphate (SO_4^{2-}) association.

The positive relationship between Mg^{2+} and SO_4^{2-} ions is also due to the presence of sulphide mineral in Ferozabad group and MVS deposits of ophiolites (Ahsan & Mallick, 1999). This is also supported by the ratio of Ca/SO_4 which is a 1.107 average value exceeding the intrusion value of 0.10. The value 1.0 may result from the dissolution process of minerals. To distinguish sedimentary and igneous rock from sulphate dissolution the molar ratio of $Ca^{2+} + Mg^{2+}$ and $HCO_3 + SO_4^{2-}$ compared with each other. This result around 28% and shows a lower value of $Ca^{2+} + Mg^{2+}$ over $HCO_3^- + SO_4^{2-}$ and indicates the dissolution of silicates from volcanic sulphide rocks. The presence of sulphate ions in groundwater is very essential for the growth of plants. The higher value of >1000 mg/l increase the soil salinity which hinders the Ca^{2+} absorption in plants and high Na^+ input (Amiri et al., 2021).

5.8.5 Potassium (K^+) & Sodium (Na^+)

In groundwater of study area, the cations (K^+ & Na^+) are most abundant. The lower value of K shows a good deal with tholeiitic pillow basalt (Naseem et al., 2010) and is resistant to the chemical weathering of Potassium feldspar ($K_2O\ Al_2O_3\ 6SiO_2$). The K^+ value ranges from 2-24 mg/l. The Na^+/Cl ratio is 0.97 on average in samples, very close to the seawater average of 0.55. The Na^+/Cl^- average ratio represents that NaCl may be imparted from the Arabian coast located in the west of study area. $Na^+/ Na^+ + Cl^-$ and $Ca^{2+} / Ca^{2+} + SO_4^{2-}$ molar ratio in Figure 5.63 used to build a genetic association sample cluster fall (US, UI, UN, UG, UR, UD, UT, ST, SA, AM, BM, BT and KA) towards seawater intrusion.

The range of Na^+ is 120-896 mg/l a little higher than the allowable limit. The higher amount of Na^+ also impacts the soil and decreases permeability and infiltration speed (Banerjee & Prasad, 2020). Na^+ excess concentration directly impacts the plant leaf causing leaf burn (Syed et al., 2021). The rotated space diagram shows a close relationship of Na^+ with Cl^- (Figure 5.64). The Na^+ concentration is increased in groundwater as compared to this research which was 50-665 mg/l (Naseem et al., 2010).

The spatial distribution of Na^+ to demarcate the high-risk zone for a decline in permeability and negative impact on plants (Figure 5.65). A higher amount of Na^+ is found in the west and southwest of study area close to the Arabian sea.

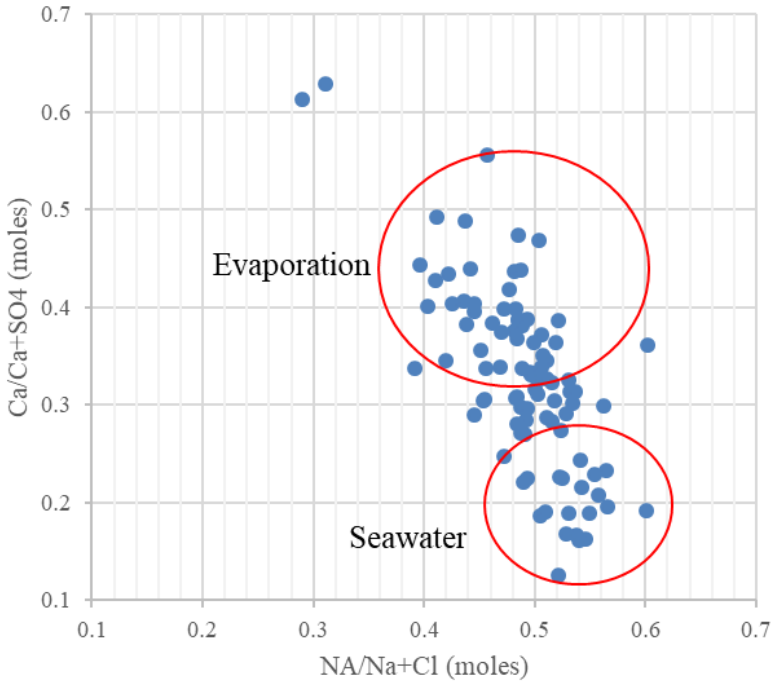

Figure 5.63 Na/Na+Cl and Ca/Ca+SO_4 molar ratio plotted for study are used to build a genetic association (Hounslow, 2018).

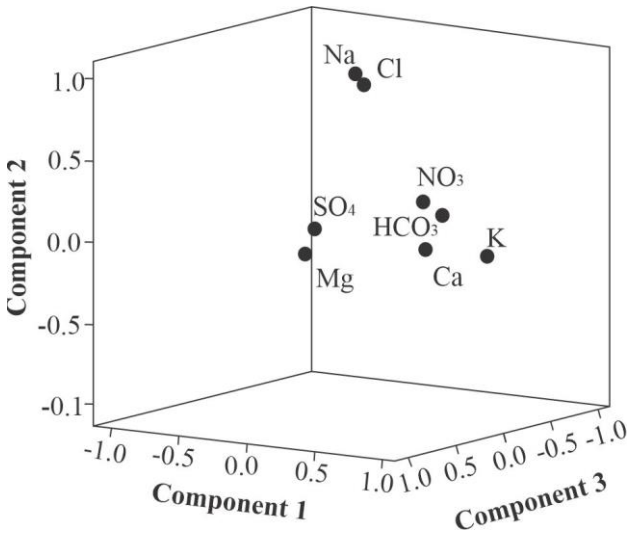

Figure 5.64 Rotated Space Diagram for chemical parameters association.

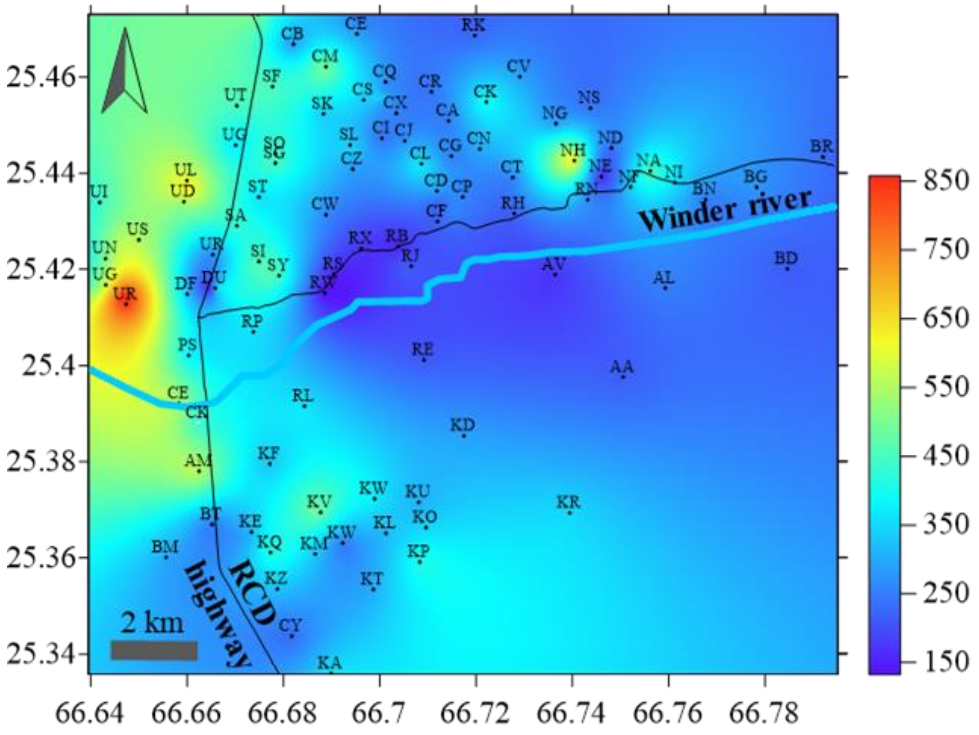

Figure 5.65 Spatial distribution of Na (mg/l) in 94 groundwater samples of Winder Balochistan.

5.8.6 Calcium (Ca^{2+}) and Magnesium (Mg^{2+})

The Ca^{2+} & Mg^{2+} ions also play a vital role to define seawater influence in groundwater. Magnesium is also a significant parameter in groundwater and may influence crop production such as by causing Ca^{2+} deficiency from higher Mg concentration in soil (Ayer & Westcot, 1985). The sample shows a low Ca^{2+}/Mg^{2+} ratio that is 0.6 and an average of 1.01, depicting seawater intrusion impact. The higher value of Ca^{2+}/Mg^{2+} in groundwater suggests that Ca^{2+} and Mg^{2+} are also driven from ophiolites weathering and carbonate rocks present in the north-east of the study area. The Mg^{2+}/ Ca^{2+} vs Na^{+} / Ca^{2+} relationship shows the variation in the composition of groundwater and also discriminates the source of ions from silicates and carbonate rocks. The study area sample also leans toward the igneous origin rocks present in the north-east of study area as shown in Figure 5.66.

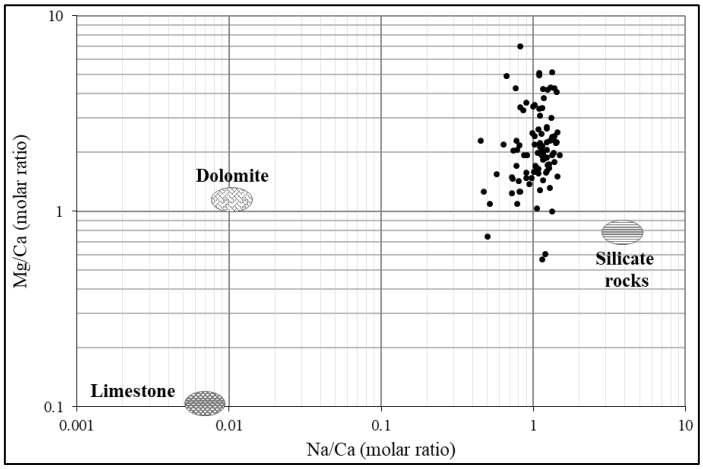

Figure 5.66 Mg^{2+}/Ca^{2+} vs Na^{+}/Ca^{2+} relationship shows the variation in the composition of groundwater.

The average Calcium 133 mg/l and average Magnesium 83 mg/l represent the 2nd and 3rd abundant ion present in water sample of study area. Calcium exhibits a strong relationship with Ca^{2+} +Mg^{2+} - HCO_3 in a sample where the range is 2.95-15.24 with an average of 7.55 (meq/l). It also indicates that Mg and Ca drive from ophiolites weathering along with carbonate rocks. Ca^{2+} and Mg^{2+} relation is variable between each other, supported by the correlation matrix. and it shows Ca^{2+} and Mg^{2+} are present in groundwater due to rock interaction in an arid climate.

The maximum value of analysis for selected parameters clearly shows the variation in the concentration of groundwater sample. The comparison with the previous research of 2010 used to evaluate the difference in measured parameters (Table 5.3). It can also assessed from graphical presentation where parameters such as Na^{+}, Ca^{2}, HCO_3^{-} and Cl^{-} maximum values exceeding the WHO 2021 standards (Figure 5.67). These maxim values are estimated in the west of study area. In case of TDS the average value of current study is also exceeding the upper permissible limit.

Table 5.3 The summary of physiochemical parameter minimum, maximum and average value of the present study compared with the average value of 2010 and World health organization standard 2021.

Parameter	min	max	avg. of current study	avg. value from previous 2010	(WHO, 2021)	
					HDL	MPL
Ca^{2+} (mg/l)	75.3	280	133.3	150	75	200
Mg^{2+} (mg/l)	30	152	83.8	92	30	150
Na^{+} (mg/l)	120	896	331.5	236	Nil	200
K^{+} (mg/l)	2	24	6.1	9.98	Nil	30
HCO_3^{-} (mg/l)	138	775	361.9	399	200	350
Cl^{-} (mg/l)	232	1270	522.2	388	250	400
SO_4^{2-} (mg/l)	119.7	555	306.9	372	200	400
NO_3^{-} (mg/l)	41	110	66	Nil	45	No Relaxation
pH (mg/l)	6.5	8.5	7.3	7.42	7	8.5
EC (dS/m)	1.5	4.6	2.7	2.79	Nil	1.5
TDS (mg/l)	493	5200	1872.2	2507	Nil	1000

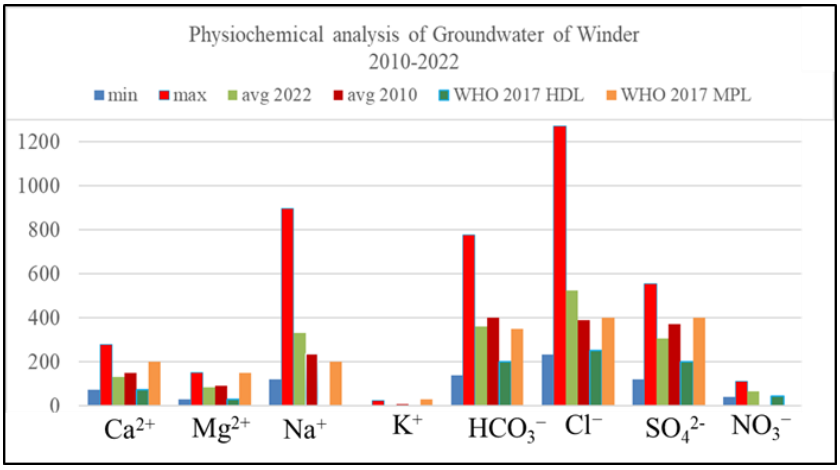

Figure 5.67 The comparative analysis of Physiochemical parameters of present study results from 2022, 2010 and World Health Organization standard 2021.

5.8.7 Chloro-Alkaline Indices (CAI)

Chloro-Alkaline Indices are important factors to evaluate changes in water composition during traveling into the subsurface (Jalees et al., 2021; Dhakate & Gurunadha, 2015). Infiltration of water into soil or rock exchange ions in two distinct indices as follows (Schoeller, 1977).

Both were determined by subsequent equation 5.2 and 5.3.

$$\mathrm{CAI}-1=\frac{[\mathrm{Cl}-(\mathrm{Na}+\mathrm{K})]}{\mathrm{Cl}} \qquad \ldots\ldots\ldots\ldots\ldots\ldots\ldots\ldots \qquad \text{eq. (5.2)}$$

$$\mathrm{CAI}-2=\frac{[\mathrm{Cl}-(\mathrm{Na}+\mathrm{K})]}{[\mathrm{SO_4}+\mathrm{HCO_3}]} \qquad \ldots\ldots\ldots\ldots\ldots\ldots\ldots\ldots \qquad \text{eq. (5.3)}$$

The estimated range of CAI-1 is -0.55-0.57 and the average value is 0.01. The CAI-2 ranges from -0.81-0.06 and the average value is -0.02. CAI positive value shows Na^+ & K^+ exchange from water and Mg^{2+} and Ca^{2+} from the soil. The CAI negative is found in the opposite situation where an exchange is going to be reversed. CAI-1 and CAI-2 statistics are presented that more than 75% of samples are positive and around 25% show a negative ratio. This concludes that groundwater in the study area experienced an exchange of ions between the alkali & alkaline earth metal.

The presence of major ions helped to understand the source of groundwater and its impact on the surrounding environment. The Schoeller graph delivers a suitable approach to exhibit groundwater chemical composition of a region (Naseem et al., 2010). A plot can be observed for average composition of groundwater in meq/l (Figure 5.68), shows that $Na^+>Ca^{2+}>Mg^{2+}>K^+$ (meq/l) for the cation and $Cl^->HCO_3^-> SO_4^{2-}$ (meq/l) for anions.

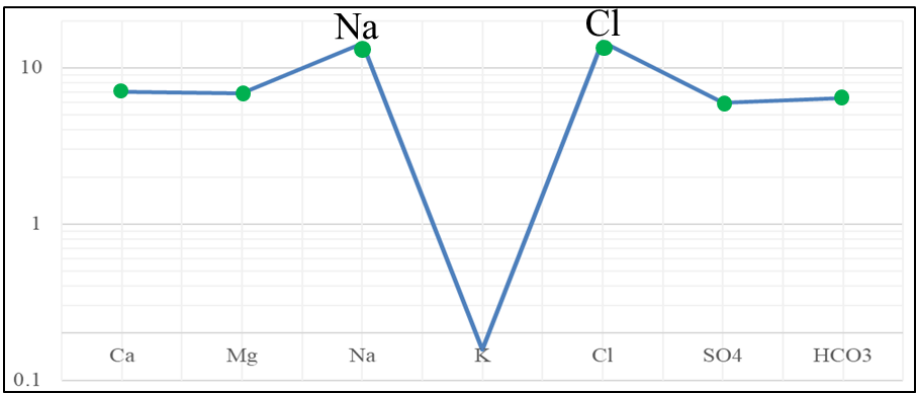

Figure 5.68 Schoeller graph represents an average composition for groundwater samples of Winder in (meq/l).

The Stiff diagram pattern identification is utilized for quick interpretation to evaluate hydrochemical facies. Seven hydrochemical facies can be classified i.e. Ca-Mg-SO_4-HCO_3, Mg/Ca-HCO_3, Ca-Mg-HCO_3-SO_4, Mg-Ca-HCO_3-SO_4, Na-Cl, Ca-Na-SO_4-Cl and Na-Ca-HCO_3-SO_4. To assemble the Stiff configuration, a polygon is designed using three parallel axes. The horizontal axis contains (meq/l) for anions and cations. On the right anions whereas cations were placed on left of the vertical zero axis.

The diagram was constructed for each sample in order to compare the concentration of certain anions and cations. The Stiff diagram shape analysis suggests dominant hydrochemical facies for the study area Na-Cl (72%), Ca-Cl (10%) and $MgSO_4$ (8%). The remaining 10% represent mix type i.e. Ca-HCO_3 and Na-Ca-HCO_3-SO_4 as shown in Figure 5.69 (a and b), thus indicating a varying condition for ions enrichment in the study area. Due to the high concentration of Na and Cl ions in groundwater samples of the study area near the coast (US, UI, UN, UG, UR, UD, UT, ST, SA, AM, BM, BT and KA) interpreted as Na-Cl type and impacted by intrusion.

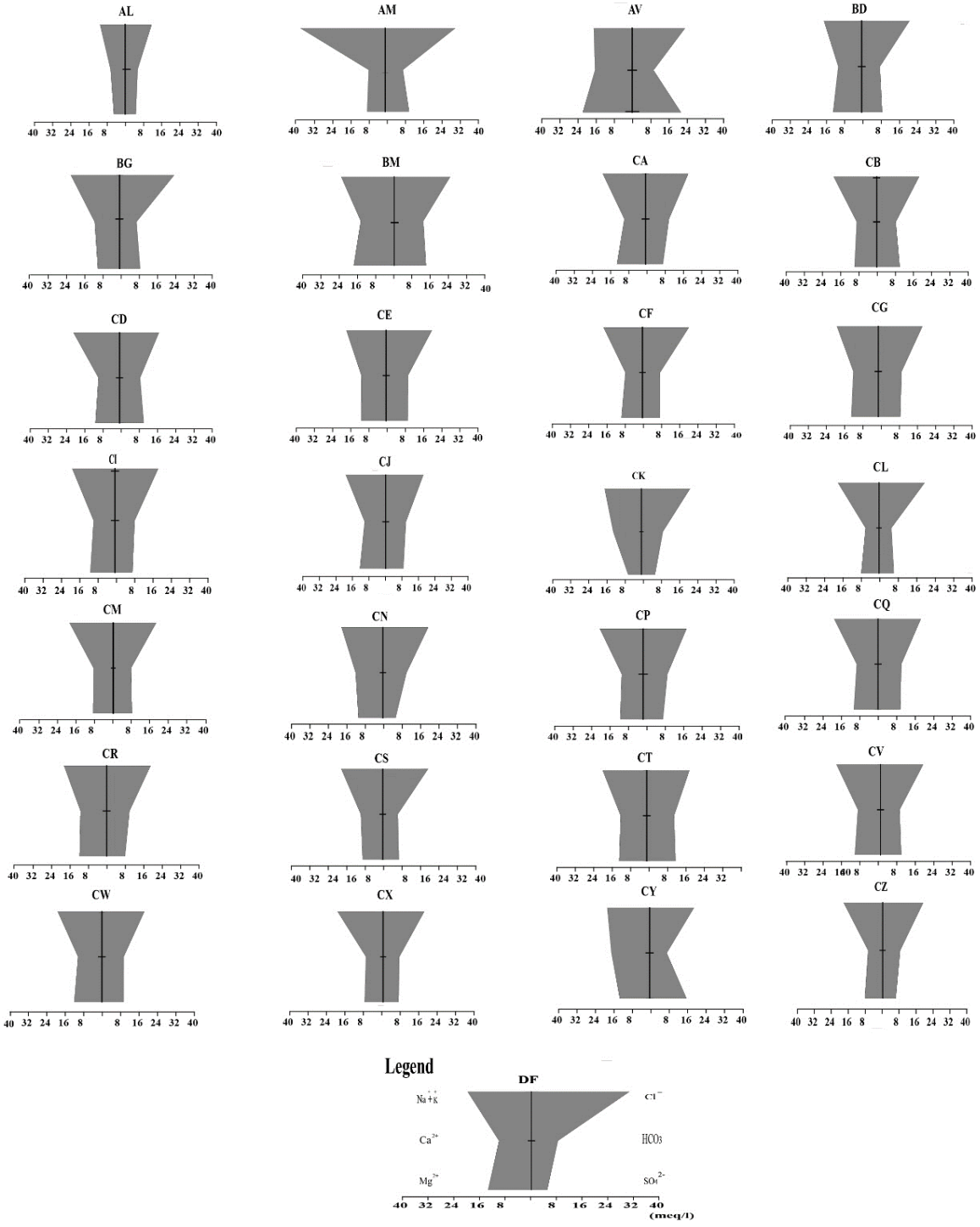

Figure 5.69 (a) Stiff diagram for groundwater samples of the study area.

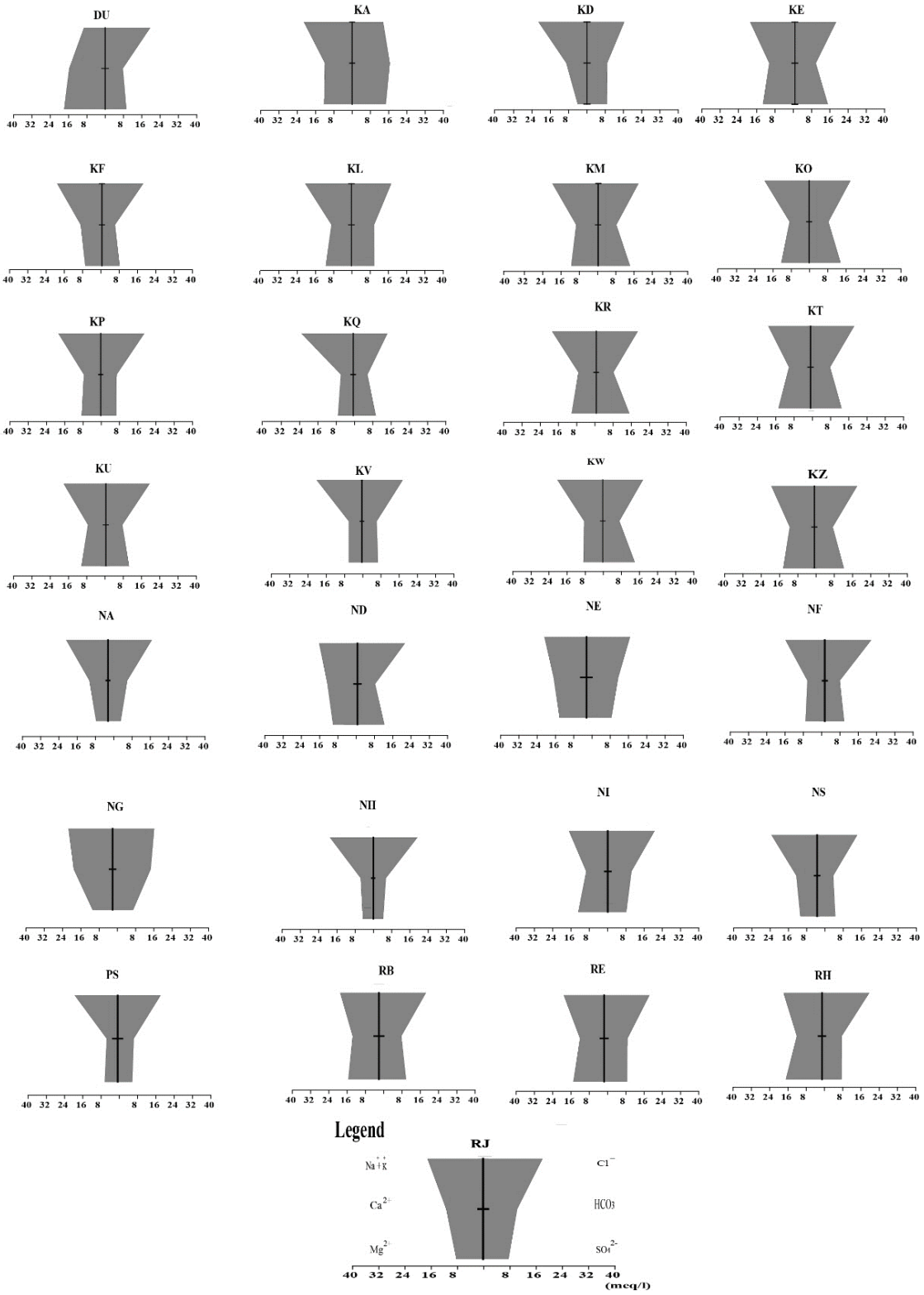

Figure 5.69 (b) Stiff diagram for groundwater samples of the study area.

5.9 Hydrofacies Analysis

The ionic composition of water, can be represented by a variety of trilinear diagrams also known as Piper diagram (Patil, 2023; Shyam et al., 2022). The trilinear diagram is extensively utilized to characterize the hydro-chemical parameter of groundwater. This was primarily used by Hill (1940) and further improved by Piper (1944) to define water chemistry (Piper, 1944; Hill, 1940). It comprised two triangles on right side for cations and on left side for anions. Both anion and cation are represented as a single plot within the central part of diamond shape region. This diagram is very useful to classify the type of water & hydro-geochemical facies (Merino et al., 2021; Gao et al., 2020). The hydrofacies illustrate genetic relationship of water and marked in diagram by the zones of distinctive concentration of anion and cation. The piper diagram can represent the ionic composition of samples in large numbers collected from study area. It also differentiates and visualized water mixed from multiple sources effectively (Bastianoni et al., 2021; Russoniello & Lautz, 2020).

Almost 73% of sample of groundwater demonstrate the mixed type of cations distribution, 24% of samples show Na-K type remaining sample impacted by Mg type water. For anions, 43% of samples plotted in mix type zone and 57% plotted toward Cl type. The hydrofacies evaluation of study area between the main anions, 56% of analysed samples on plot are found within the classification of mixed-type whereas 44% decline towards the Cl-type. The hydrofacies evaluation of study area shows that the origin of water is influenced by the salinity due to higher concentrations of Chlorine and mixed type represents the contribution from the rocks. Most of the data were plotted in middle to upper zone of a diamond-shaped area of diagram. The Piper diagram classifies the type of water into Class-1 NaCl, Class-2 $CaMgHCO_3$, Class-III $NaCaHCO_3$, Class-IV CaCl, Class-V $CaMgSO_4$ and Class-VI $NaHCO_3$. The plotted graph for the groundwater sample of Winder representing Class-1 NaCl, Class-IV CaCl and $CaMgSO_4$. Major cations in the sample show the presence of Na-type water and major anions illustrate the Chlorine type water (Figure 5.70). The groundwater exposure to sedimentary and basaltic composition aquifers also increases the ratio of ions. The samples of the current study show that the sample proximity is near a basaltic

rock in disparity to sedimentary rock. The hydrofacies have also been analyzed by using hydrodynamic facies model diagram also known as HFE-D (Gimenez-Forcada, 2010). The diagram not only provides the facies but also demarcate the seawater intrusion and freshwater interface of groundwater sample (Sadeghfam et al., 2022; Le et al., 2020). The HFE diagram takes into account the proportions of the four major ions and their interactions, resulting in sixteen hydrochemical facies or thirty-two if Mg^{2+} and SO_4^{2-} participate along with HCO_3 and Ca^{2+}. The word "Mix" is used to identify the facies when the percentage of the cation or anion is less than 50% but also higher than the percentage of any other cations or anions taken into consideration (Gimenez-Forcada, 2010).

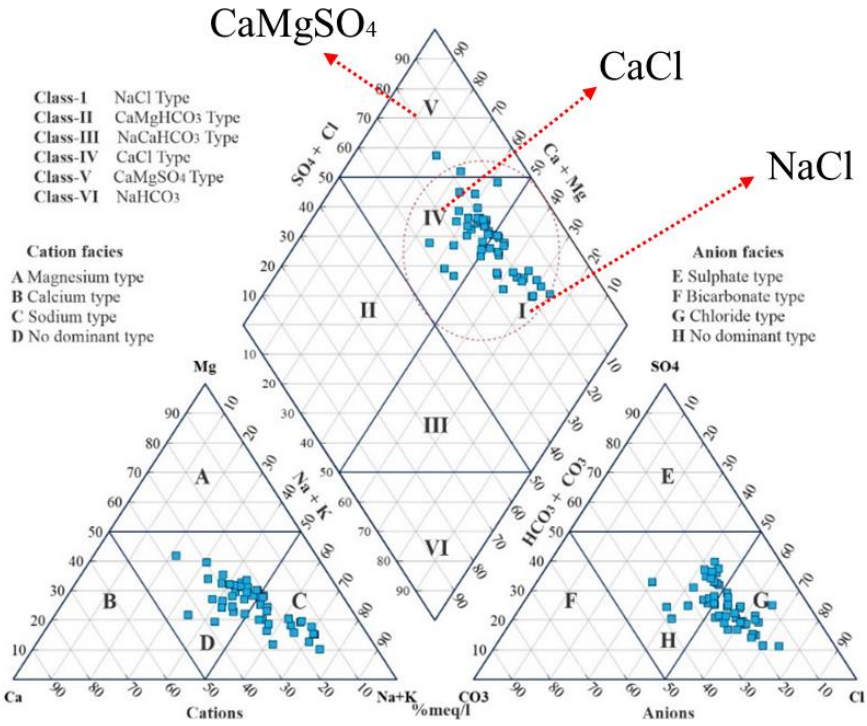

Figure 5.70 The groundwater hydrochemical analysis plotted on Piper diagram to evaluate the chemistry in Class I, Class II, Class III and Class IV.

Around 16 facies can be interpreted from the HFE-D i.e. NaHCO3, Na-MixHCO_3/MixSO_4, Na-MixCl, Na-Cl, MixNa-HCO_3/SO_4, MixNa-MixHCO_3/MixSO_4,

MixNa-MixCl, MixNa-Cl, MixCa-HCO_3/SO_4, MixCa-$MixHCO_3$-$MixSO_4$, MixCa-MixCl, MixCa-Cl, $CaHCO_3/SO_4$, Ca-$MixHCO_3/MixSO_4$, Ca-MixCl and Ca-Cl. The groundwater sample of study area cluster represents MixNa-MixCl, MixNa-Cl, MixCa-MixCl, MixCa-Cl, Na-Cl and MixNa-$MixHCO_3$ type hydrochemical facies (Figure 5.71). The groundwater sample of study area from the west and south-west BT, UG, UT, UR, CL, BS, RB, DU, BG and CN were impact by intrusion of seawater. The integration of Piper and HFE-D plots delineates same type of facies for groundwater of study area.

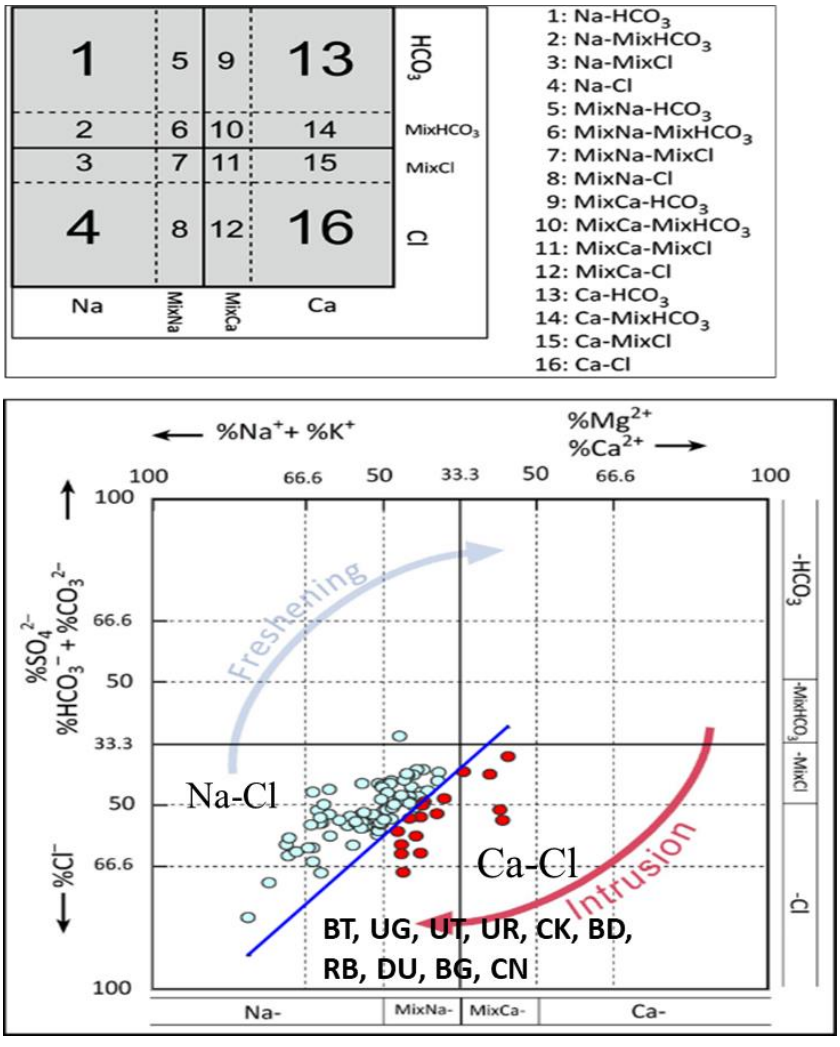

Figure 5.71 Hydrodynamic facies evolution, diagram (HFE-D) to investigate the water quality with respect to fresh and saline. This plot based on multi rectangular analysis of anions and cations.

5.10 Water Quality for Irrigation

The water quality for irrigation was assessed to demonstrate its suitability for fruit and crops (Maghraby & Bamousa, 2021; Naseem et al., 2010). The quality of groundwater not only impacts the crop but also has a great influence on soil (Bouaroudj et al., 2019; Minhas et al., 2019) The presence of salts is extremely injurious for agricultural land as they restrict the plant's growth. Basically, the growth of plants restricts due to alterations in metabolic processes and osmotic pressures (Shabbir et al., 2022; Safdar et al., 2019). The irrigation water quality was measured for irrigation using the following parameters i.e. Sodium (Na%), Residue sodium carbonate (RSC), Potential salinity (PS), Wilcox diagram, Magnesium absorption ratio (MAR), Sodium adsorption ratio (SAR), Kelley's ratio (KR) and Permeability index (PI) (Azhari et al., 2023; Chidambaram et al., 2022). These parameters were estimated to define the appropriateness of irrigation water as per the standard permissible limit (Table 5.4). The estimated maximum, minimum and average value of RSC, SAR, Na%, PI, PS, MAR and KR is summarized in Table 5.5.

Table 5.4 The standard ranges for EC. RSC. SAR and MAR for irrigation water quality.

Quality parameters	Range	Classification
EC (μS/cm) (Wilcox 1955)	<250	Excellent
	250–750	Good
	750–2250	Permissible
	>2250	Unsuitable
SAR (Ayers and Westcot 1994)	<10	Excellent
	10–18	Good
	18–26	Permissible
	>26	Unsuitable
RSC (Richards 1954)	<1.25	Good for irrigation
	1.25–2.5	Doubtful for irrigation
	>2.5	Unsuitable for irrigation
	25–75	Doubtful for irrigation
	<25	Unsuitable for irrigation
PI (Doneen 1964)	>75	Suitable
	75-25	Moderate
	<25	Not suitable
MH (%) (Szabolcs 1964)	<50	Suitable for irrigation
	>50	Unsuitable for irrigation

Table 5.5 The summary of groundwater analysis for irrigation water quality.

	min	max	avg	median	mode
RSC	-15.2	-2.6	-7.6	-7.4	-2.6
Na %	20.7	79.1	50.1	48.9	20.7
SAR	1.7	17.3	5.8	5.0	1.7
PS	8.4	38.6	18.0	16.7	8.4
PI	37.2	396.9	133.3	115.4	37.2
MAR	31.0	59.8	50.6	52.4	45.2
KR	0.3	3.8	1.2	1.0	0.3

5.10.1 Residue Sodium Carbonate (RSC)

Water containing high bicarbonate ions, increases the Mg and Ca presence in soil as result of the precipitation of water used for irrigation. In result, the relative amount of Na ions in form of sodium bicarbonate Na_2CO_3 increases in water which is referred to as RSC (Zaman et al., 2018). This factor is very significant for water suitability in irrigation (Murtaza et al., 2021). It is calculated from the given expression in equation 5.4 (Gupta, 1983).

$$\mathrm{RSC} = [(\mathrm{HCO_3}) + \mathrm{CO_3})] - [\mathrm{Ca} + \mathrm{Mg}] \qquad \text{……..} \qquad \text{eq. (5.4)}$$

The RSC range is between -15.2 to -2.6 (meq/l) showing good water quality for irrigation (Table 5.5). The high amount of RSC such as more than 2.5 (meq/l) groundwater used for irrigation causes salt build-up. It will resist the movement of air and water through clogged pore spaces in soil (Kurunc et al., 2020). A negative RSC value suggests that sodium build-up is not likely to occur whereas a positive value of RSC indicates that sodium build-up is possible in the soil. Therefore, water is unsuitable for irrigation if the value of RSC exceeds 2.5 (meq/l), whereas if the RSC value range between 1.25 and 2.5 (meq/l), then the water is defined as marginal quality and the water is reported as suitable for irrigation only if <1.25 (meq/l) is estimated in Table 5.4.

5.10.2 Sodium Percent (Na%)

Na is mostly referred as Na% in irrigation water and calculated by the following calculation in equation 5.5 (Kammoun et al., 2021; Aziane et al., 2020).

$$\% \text{ Na} = \frac{\text{Na}^{+}}{\text{Na}^{+}+\text{Ca}^{2+}+\text{Mg}^{2+}+\text{K}^{+}} \times 100 \quad \text{.....} \quad \text{eq. (5.5)}$$

Where, the concentration all parameters are expressed in (meq/l) and Na calculated in percentage.

The Na% & EC is a very important factors for classification of groundwater suitability for agriculture (Beyene et al., 2019; Rawy et al., 2019). The Na% classified the water quality into excellent if < 20 Na%, good if range is 20-40 Na%, permissible if range is 40-60 Na%, the doubtful range is 60-80 Na% and unsuitable where >80 Na% (Wilcox, 1955). The binary plot shows that 5% of samples are lies close to fair range and a majority of samples are poor to a very poor type of water. The EC versus Na% graph on log scale shows that few samples are non-saline alkaline type except a few samples and most of the samples are representing high values (Figure 5.72). The calculated Na% concentration of Winder agriculture farm and the surrounding area is 20.7-79.1 and an average of 50.1 (Table 5.5). It is the amount of salt that gradually accumulates in the soil during repetitive irrigation practice (Mohanavelu et al., 2021). A concentration of Na% > 60% resulted from accumulation of Na and probably soil deterioration with respect to infiltration and aeration (Zhao et al., 2021; Cox et al., 2018). The distribution map of Na% shows a higher value toward the western part of study area and a lower value along the Winder River (Figure 5.73).

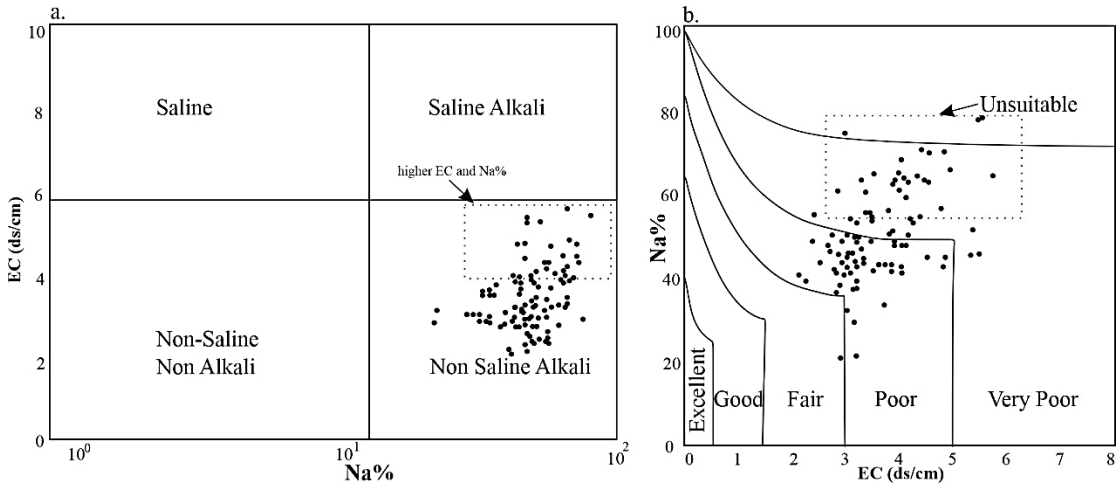

Figure 5.72 EC vs Na% relationship Wilcox classification and Na% vs EC United States, Salinity Laboratory (USSL) diagram (Gevera et al., 2020; Richards, 1954).

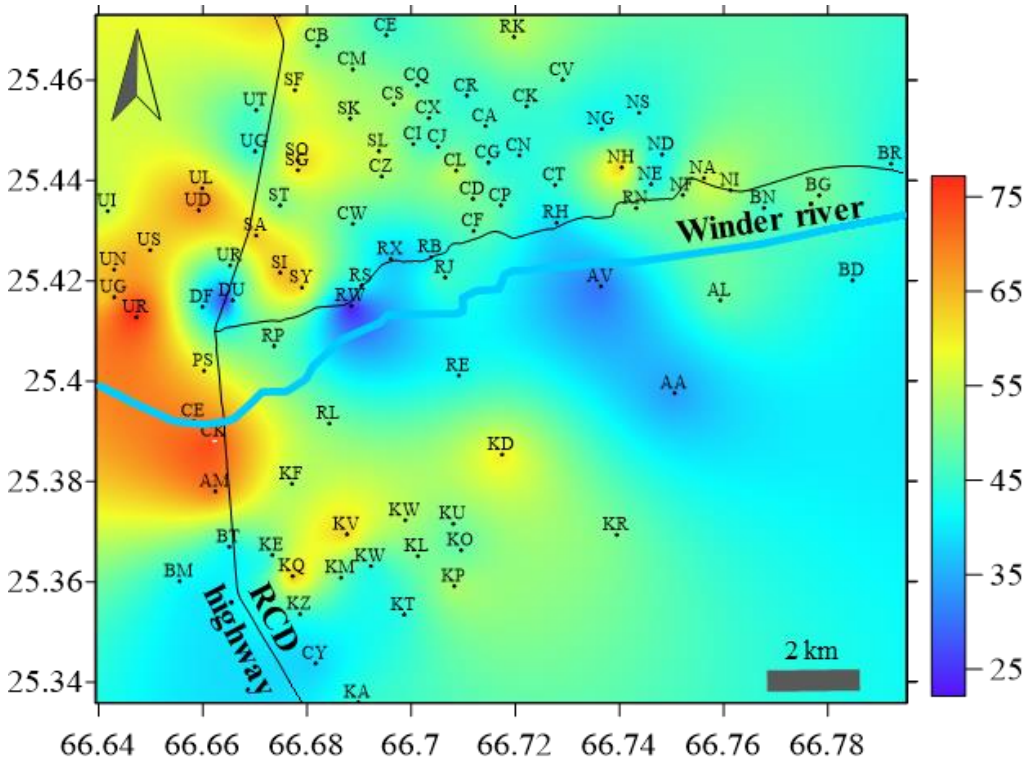

Figure 5.73 Spatial distribution of Na% in 94 groundwater samples of Winder Balochistan .

5.10.3 Potential Salinity (PS)

PS is the total amount of soluble salt which accumulates occur in the soil during repeated irrigation activity. This results an increase in the salinity of soil (Doneen, 1964). The high amount of PS is due to presence of salts mostly obtained from mineralization. PS amount was calculated from the sum of Cl^- & $SO_4^{2-}/2$ concentration (Abdulameer et al., 2021). The estimated PS of study area shows 8.4-38.6 and average of 18.0.

5.10.4 Sodium Absorption Ratio (SAR)

SAR is the determination of Na concentration relative to Ca^{2+} & Mg^{2+}, in water which impacts the soil and plants (Khalid, 2019). SAR causes a sodium risk from water used in irrigation. The relative content of Na^+, Mg^{2+} and Ca^{2+} in (meq/l) utilized to measure the Na hazard and represents the SAR. The SAR can be calculated from the given expression in equation 5.6 (Patterson, 1994).

$$SAR = \frac{Na^+}{\sqrt{\frac{Ca^{2+} + Mg^{2+}}{2}}} \quad \ldots\ldots\ldots\ldots\ldots\ldots\ldots \quad \text{eq. (5.6)}$$

The value of SAR <10 is excellent, SAR 10-28 are moderate and >28 are classified as hazardous groundwater samples for agriculture activity. In study area, the range of sample lies between 1.7-17.3 and an average value is 5.8. This indicates excellent to moderate quality of water and no hazards of SAR. This range represents the suitability of water for irrigation to grow fruit and crops in Winder area.

The plot of EC vs. SAR of current water sample shows no impact on infiltration. PRIME (2010) characterized the groundwater for water infiltration (relative rate) by the

salinity (EC) and SAR. The EC vs. SAR using Wilcox diagram was plotted and it is also referred as US Salinity Laboratory (USSL) plot of the acquired samples. It depicts no reduction in the rate of water infiltration due to medium to very high salinity hazards and low to medium sodium hazards (Figure 5.74). The value of SAR in the western part of the study area is very high due to the high salinity of water (Figure 5.75).

5.10.5 Wilcox Diagram

The Wilcox diagram is also used to evaluate the water quality for irrigation, it was designed by U.S. Department of Agriculture (Pivic et al., 2022). The salinity Hazard plotted on the x-axis is denoted by EC and SAR on the y-axis (Figure 5.74). The analysis shows that the majority of samples are in the zone of high salinity hazard due to EC where the study area average groundwater is still at a moderate level and water can be used for irrigation activities.

5.10.6 Magnesium Absorption Ratio (MAR)

Most of the groundwater generally shows an equilibrium stage for Ca^{2+} and Mg^{2+}. But water containing higher Mg badly impacts the production of the crop. MAR of water used in irrigation was introduced by Raghunath (1987) as given by:

$$\mathrm{MAR} = \frac{\mathrm{Mg}^{2+}}{(\mathrm{Ca}^{2+} + \mathrm{Mg}^{2+})} \times 100 \quad \ldots\ldots\ldots\ldots\ldots\ldots \quad \text{eq. (5.7)}$$

Where (meq/l) is the ionic concentrations of all parameters.

MAR >50 is referred as in appropriate and dangerous for irrigation as it may cause infiltration issues in soil (Ayer & Westcot, 1985). In study area the range of MAR

is 31-59.8 (Figure 5.76). The average value is 50.6. This range shows the groundwater is at the upper permissible limit and causes harm due to the presence of a higher concentration of Mg^{2+}. The high concentration of Mg^{2+} in the study area can be associated with the exposure of water with pillow basalt and rocks containing high Ca^{2+} & Mg^{2+}.

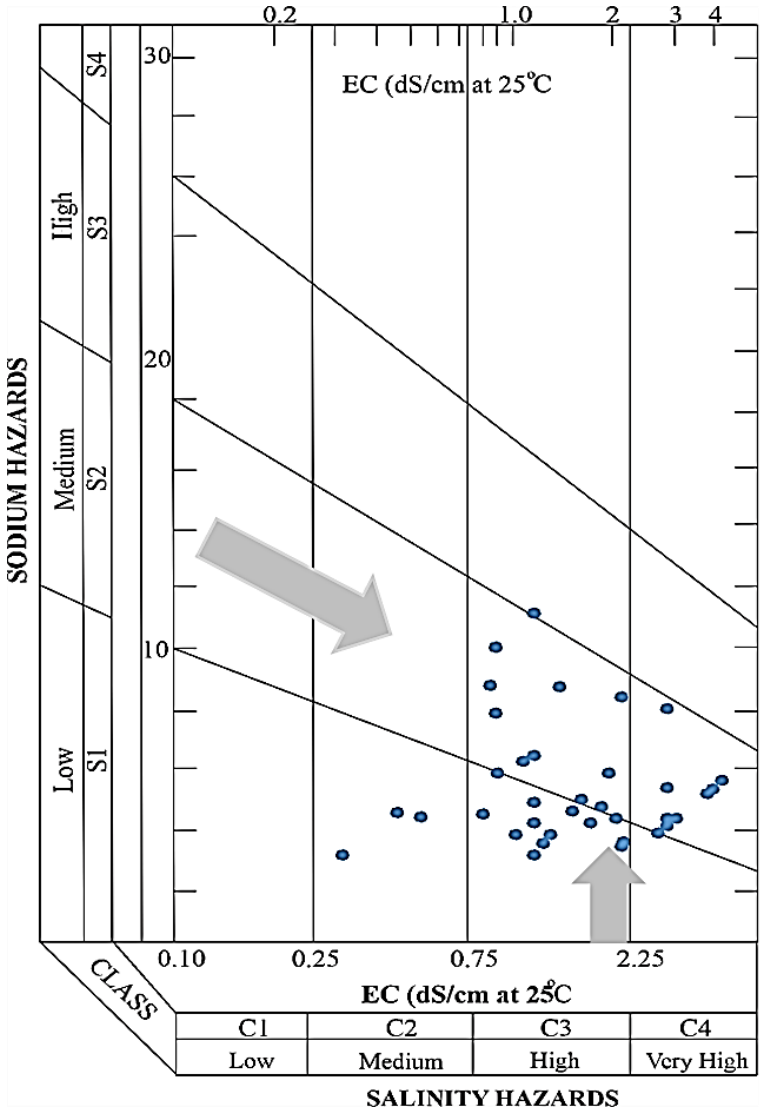

Figure 5.74 The graph characterizes the EC VS SAR relationship for the groundwater sample of Winder. The x-axis represents the EC from low to very high class and the y-axis for Sodium Hazard from low to high.

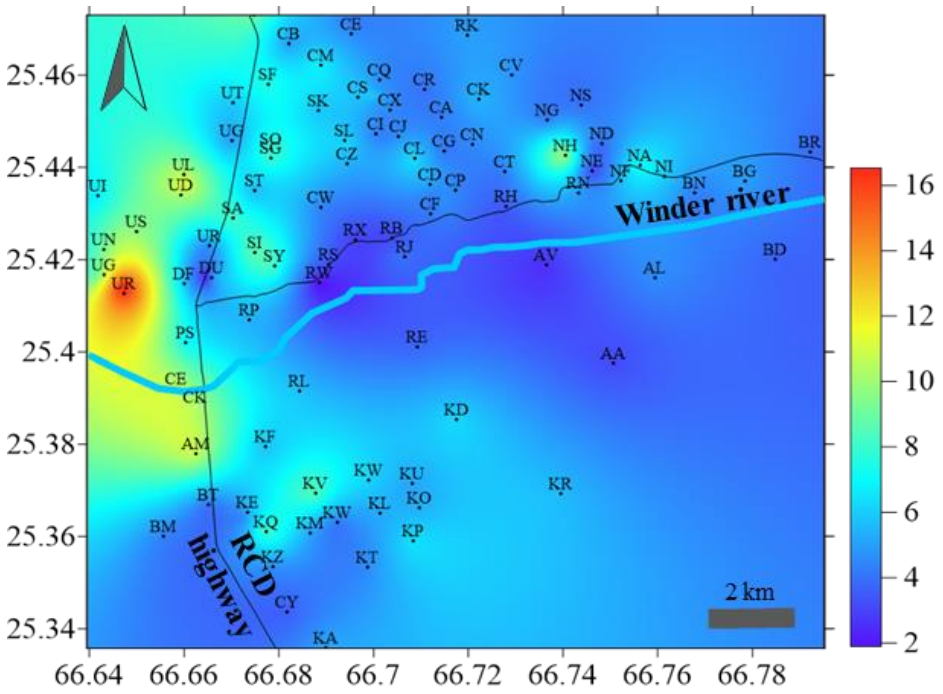

Figure 5.75 Spatial distribution of estimated SAR for 94 groundwater samples of Winder Balochistan.

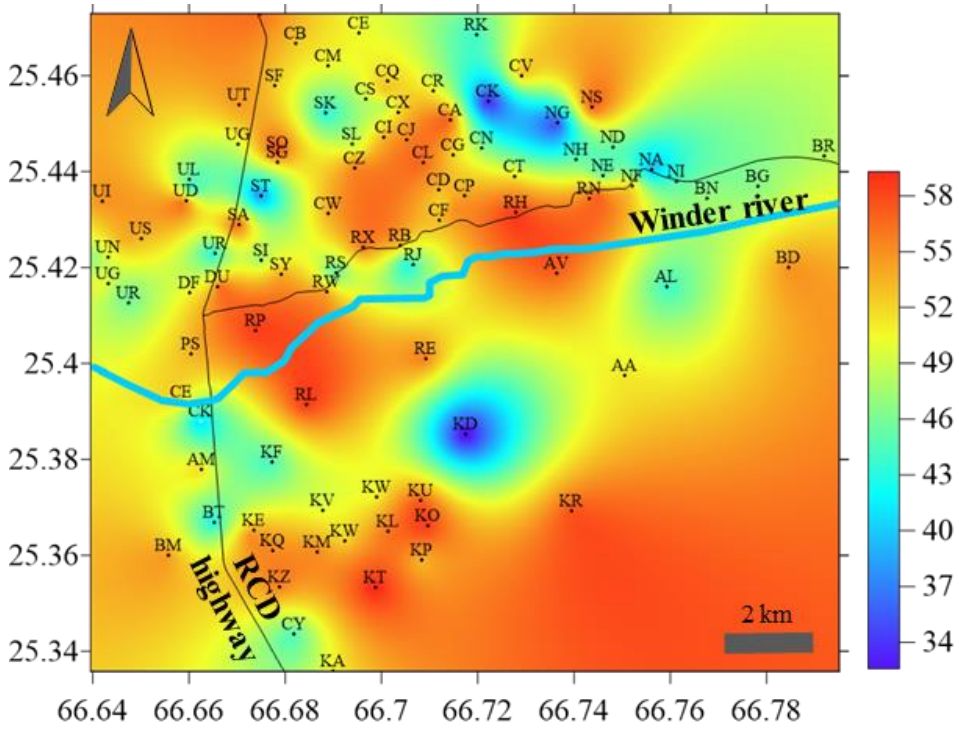

Figure 5.76 Spatial distribution of MAR higher and lower concentration plotted for study area.

5.10.7 Permeability index (PI)

The permeability index of groundwater used for irrigation created a concept of soil permeability which can be measured from the equation 5.8 (Doneen, 1964).

$$\mathrm{PI} = \frac{\mathrm{Na}+\sqrt{\mathrm{HCO_3}}}{\mathrm{Ca + Mg + Na}} \times 100 \ \text{(all parameter are in meq/l)} \qquad \ldots\ldots \quad \text{eq. (5.8)}$$

The long-term utilization of poor quality water for irrigation had a negative impact on soil permeability. It is based on the concentration of total dissolved salts, bicarbonate and sodium in water. There are four classes for irrigation water according to Permeability Index. Class I >75%, Class II range 75%-50%, Class III approximately 25%. Class I & II characterize as good for irrigation and Class III is not suitable for irrigation (Biswas et al., 2022). The sample of study area lies in Class I and II range 37-396 and is referred as suitable (Table 5.4).

5.10.8 Kelley's Ratio (KR)

The Kelley ratio is an important parameter introduced by (Kelley, 1963) to evaluate irrigation water quality. It is the level of Na^+ against the Ca^{2+} and Mg^{2+}. Kelley's ratio less than 1 shows that water is suitable for irrigation and greater than 1 consider as unsuitable (Goswami & Rai, 2022; Kouadra & Demdoum, 2020). In Winder, the range of ratio is 0.3-3.8 and the mean value is 1.20. The range reveals that study area has good-quality of water for irrigation. The value is >1 in 60% of samples (SI, SY, SO, SL, SG, SA, SF, UD, UP, UL, UL, UG, UI, CB, CX, CS, CL, KQ, KL, KV, KR and NA) represent unsuitable conditions. The value of Kelly's ratio was 0.2-2.3 with an average value of 0.72 (Naseem et al., 2010) which shows the increasing trend in ratio and deterioration of water quality for agriculture.

5.10.9 Lime Deposition Potential (LDP)

Water also controls the temperature in irrigation and cool the fruit plants, particularly in a hot climate. The warm climate damage the colour as well as the fruit tissue and finally burn the fruit (Marklein et al., 2020). The water provides hydro-cooling effect decrease the temperature. Therefore, the LDP is measured from a composition of cooling water (IFS, 1995). In higher LDP water. In this case, the water samples were also assessed for cooling of crops in which all parameters Ca^{2+}, pH, Na^{+}, Mg^{2+}, K^{+} and HCO_3^{-} parameters are converted to mg/l in to meq/l values. All parameter values were finally added to the given equation 5.9.

$$\mathrm{pHc} = \mathrm{p}\,(\mathrm{Ca} + \mathrm{Mg} + \mathrm{Na} + \mathrm{K}) + \mathrm{p}\,(\mathrm{Ca} + \mathrm{Mg}) + \mathrm{p}\,(\mathrm{HCO_3}) \quad \ldots. \quad \text{eq. (5.9)}$$

After the addition of value pHc was finally calculated. The pH value was subtracted from the calculated pHc. In case the value of pH is greater than the pHc, lime would precipitate. The average value of pHc, in the study area, is 5.55 which is lower than the measured pH of groundwater.

$$\text{Lime Deposition Potential} = \mathrm{pH} - \mathrm{pHc} \quad \ldots\ldots\ldots\ldots\ldots \quad \text{eq. (5.10)}$$

$$\text{Lime Deposition Potential} = 7.27 - 5.55 = 1.72$$

In conclusion, the sample has LDP value ranges of 1.09-2.8 and an average 1.81. In this case LDP value is higher than 1 and lime will deposit on fruit where a farmer is utilizing water LDP>1 for crops cooling. It leaves the spot (deposition of carbonates) on fruit a result it severely impacts the value of crop (Bhat et al., 2018). The increase in pH of water, high rate of evaporation in arid regions and loss of carbon dioxide are responsible for higher LDP. These environmental changes are the main factor that triggers the deposition of lime on fruits and plants (Flynn, 2009). Similarly, on pumping equipment and supply pipes of irrigation water.

The parameters average value for RSC, Na%, SAR, PS, PI, MAR and KR shows trend is moving toward the unsuitable condition and harmful (Table 5.6). The maximum values of these parameter for current study are already at stage of impact the soil and agriculture activity of study area as shown in Figure 5.77.

Table 5.6 The irrigation water quality parameters min, max and average value for the present reserearch and the average value of 2010-2011.

Irrigation quality	min	Max	Avg. 2022	Avg. 2010, 2011	Remarks
RSC	-15.2	-2.6	-7.6	-7.88	RSC 2.5 is not suitable for irrigation.
Na %	20.7	79.1	50.1	38	Irrigation water with Na% >60% may result in Na accumulation
SAR	1.7	17.3	5.8	3.76	SAR values <10 are classified as excellent for irrigation. Values 10-28 are moderate and >28 are hazardous. The average SAR value of the present study is 3.76
PS	8.4	38.6	18	14.82	PS >10 unsuitable (Subbarao & Reddy, 2018)
PI	37.2	396.9	133.3	50.7	Class I & II >75% good for irrigation while the third category (Class III) having 25% unsuitable.
MAR	31	59.8	50.6	49.89	MAR values exceeding 50 are considered harmful
KR	0.3	3.8	1.2	0.73	Kelley's ratio <1 is suitable for irrigation

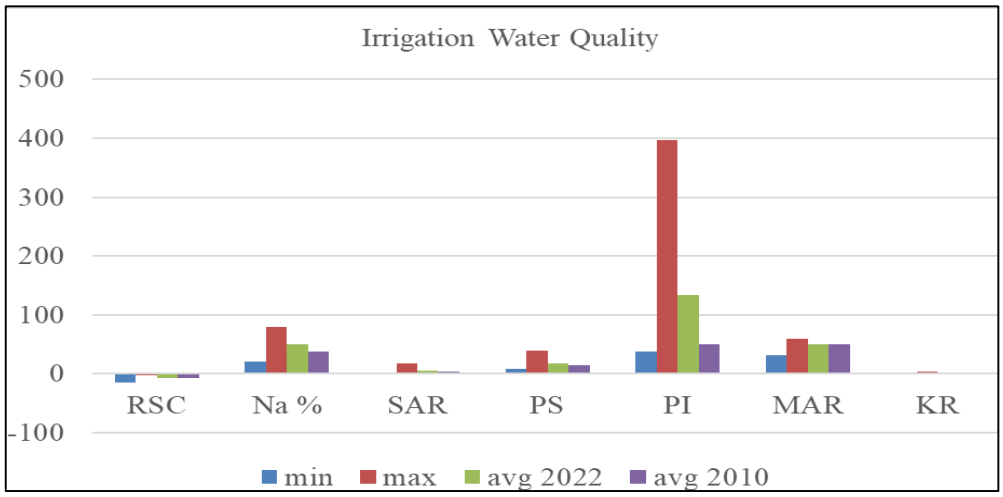

Figure 5.77 Comparative analysis of irrigation water quality parameters 2022 with the average irrigation water quality parameters of 2010.

5.11 Trace Elements

The aim of the study is to assess the irrigation quality of groundwater of Winder with the accumulation of trace elements. Groundwater samples of WR, NA, KA, KU, AA, AL, AM, DU, UG, UP, RW, RE, CM, CZ, CL, CN, UL, and ST was prepared to examine the trace elements and analysis with the help of an Atomic Absorption Spectrometer in lab. The location of samples is given in Figure 4.9. The concentration and quantity of trace elements in water may represent dual characteristics. The purpose of the study is to explicate the trace element geochemistry of the groundwater and its appropriateness for irrigation purposes along with the role of sedimentary and igneous rocks in the distribution of different trace elements. It is also advantageous to cultivators for irrigation planning and reducing environmental issues by identifying the influence of rocks on water quality. The collected samples indicate the presence of Zinc (Zn), Chromium (Cr), Nickel (Ni), Cadmium (Cd), Lead (Pb), Iron (Fe) and Cobalt (Co) as shown in Table 5.7.

The presence of trace elements is essential for the healthy growth of crops (Kaur et al., 2022). The high amount of trace elements become toxic for soil and crops and there are some elements which can be hazardous even at very low quantity (Sinduja et al., 2022). Due to agricultural activity on land, the water containing a high concentration of trace element enriches the soil gradually (Hussain et al., 2022). The accumulation of trace elements is absorbed by plants from water and soil, the higher amount of metals in crops becomes hazardous for human health (Shahid et al., 2020). The domestic and irrigation water needed proper assessment of the trace elements to provide mitigation measures for the protection of crops and human health in Winder (WWF, 2007). The following are the trace element estimation of Winder area is summarized and listed in (Table 5.7).

Table 5.7 Summary of Trace element analysis of groundwater sample of study area estimated in µg/l.

Station	Cd	Zn	Cu	Cr	Fe	Mn	Ni	Co	Pb
Min	1.00	7.00	12.70	11.00	30.50	14.00	20.00	1.00	30.00
Max	19.00	640.00	85.00	88.00	1524.00	97.00	302.00	19.10	117.00
Avg	5.69	92.07	49.63	46.47	440.79	38.31	89.75	6.13	67.53
WHO	10	2000	200	100	5000	200	200	50	5000

5.11.1 Zinc (Zn)

Zn has high mobility in water is high and comprises an average concertation of 20 µg/l in water. Sample collected from Winder represents a range from 7-640 and an average of 66.3 µg/l (Table 5.7). It is much higher than the average value of Zn in groundwater due to high mobility in water and close to the source. The extreme Zn concentration quantified in the groundwater of Winder is 640 µg/l, implying harmless conditions. The higher amount of Zn possibly came from MVT/Sedex mineralization and the ophiolites. The relationship between Zn vs. Cr, Cu and Mn displays a similar pattern as in Figure 5.78. It clearly indicates the input of source from Bela Ophiolite. Zn is a very essential element of different enzyme systems for energy production, growth control and protein synthesis (Awasthi et al., 2022). The approximate amount of Zn required for healthy growth is 20 mg/kg (Gurmani et al., 2012). The upper allowable limit of Zn is 2000 µg/l for groundwater used in irrigation (Ayers and Westcott, 1985). In study area sample range of zinc was 8-800 µg/l, with an average value of 76 µg/l (Naseem et al., 2013).

5.11.2 Copper (Cu)

The sample of study area depicts the range of Cu between 12.7-85 and an average value is 49.7 µg/l lies in safe condition (Table 5.7). The maximum recommended concentration according to WHO is 200µg/l. The value becomes toxic for plant when higher than 1000 µg/l (WHO, 2006). In comparison with the previous work the range of Copper was 14.0 – 107.0 µg/l (Naseem et al., 2013). Overall the concentration of Copper in a sample of the study area is in a safe zone. In case of a higher amount of Copper in water where > 1000 µg/l become highly toxic for plants. Copper show close association with Mn and Cr (Figure 5.78). In study area the source of copper in the groundwater is from ophiolites which are present in the north-eastern part of study area The concentration of Copper was observed in Acacia Arabica, Tamarix Aphylla and Salvadora Oleoides (Naseem et al., 2010).

5.11.3 Chromium (Cr)

The groundwater sample of Winder comprises a range of Cr 11-88 and an average value is 46.13 µg/I. The average is lower than the maximum allowable limit for irrigation use i.e. 100 µg/l. The higher concentration of Cr validates the presence and contribution of ophiolites in groundwater of the study area. Ultramafic rock usually contains high Cr (Maurizot et al., 2020). The natural source of Cr present is groundwater considered as safe as compared to industrial waste. Chromium VI is highly toxic and contaminate the aquifer from industrial waste and pollution (Camacho & Armienta, 2000).

5.11.4 Iron (Fe)

Generally, the abundance of Iron Fe in groundwater is highly effected by the pH (Xia et al., 2022). The range of Fe concentration is from 30-1524 in collected water samples. The maximum recommended Fe concentration is 5000 µg/l for crops and the measured value is very low in samples (Sataa et al., 2016). The lower concentration of Fe <100 µg/l causes blockage in the irrigation process. The higher concentration discolour the leaves and decreases photosynthesis and transpiration activity (Nyamangyoku & Bertin, 2013). In case of a higher abundance of Fe phosphate becomes precipitate and reduces the concentration of phosphorous in crops (Tiessen, 2008).

The concentration of Fe in the study area ranges from 32.0 -1840.0 µg/l and an average value was 411 µg/l. Fe comprises various geochemical characteristics and is one of the important parameters of the crust. It is present in a different section of ophiolites and is also found in sulphides. The ternary plot is very useful to suggest genetic affiliation. The genetic source is commonly indicated by linear plot of Fe-Cr-Cu in Figure 5.79 (b). The diverse geochemical behaviour reflected by plots of Fe-Cr-Mn in Figure 5.79 (c). The analysis shows the connection of element with the composition of the Bela Ophiolite.

The concentration of Mn in groundwater recorded ranges between 14-97 µg/l. It is lower than the recommended value of 200 µg/l for crop production. The widespread presence of Mn mineralization in the study area. The lower concentration of Mn was also observed in twigs of wild and fruit plants (Naseem et al., 2005b). It is an essential micronutrient and has a close relationship with function of Cu, Fe and Zn. This element is needed for respiration, photosynthesis and nitrate assimilation (Prusty et al., 2022). The deficiency of Mn directly impacts oxygen production (Varma & Jangra, 2021) and leads to the accumulation of citric acid and reduction in cellulose and sugar content of plants. The main reason for Mn low concentration is due to its insoluble nature in alkaline water (Zhang et al., 2021). The previous research represents a higher amount in Mn where the range was 15.0-102 µg/l (Naseem et al., 2013).

5.11.5 Nickel (Ni)

Water sampling from Winder shows variability in Ni range from 20-302 µg/l. The range displays good realtion with ophiolites composition in study area. Ni is linked with massive volcanic sulphides and chromite from different units (Kang et al., 2022). Ni vs. Mn & Cr diagram utilized to demonstrate the diverse character of Ni. It shows to a level according to the concentration (Figure 5.78). Ni higher values >300 µg/l are associated with the sample collected from KA and >100 µg/l DU, AM and CL. The study area sample shows very high average of Ni 142 µg/l as compared with the average concentration in water (Ayers & Westcot, 1985). According to the WHO 2006 standard permissible limit value is 10 µg/l for irrigation purposes which is much lower than the study area. Therefore high Ni observes in study area samples for irrigation use. This element is very harmful for a plant, Biogeochemically it is a lethal element (Magna et al., 2021).

5.11.6 Cobalt (Co)

The occurrence of Co in groundwater is very low. The average value is 5.69 µg/l. The range of Co is 1-19.1 µg/l. In most of the samples, the concentration is less than 10 µg/l except for some of the sample which shows higher amounts of RW & KA. According to the standard the permissible limit of Co recommended for irrigation use is 50 µg/l (Chen et al., 2021b), where the plant has a very minor toxic impact.

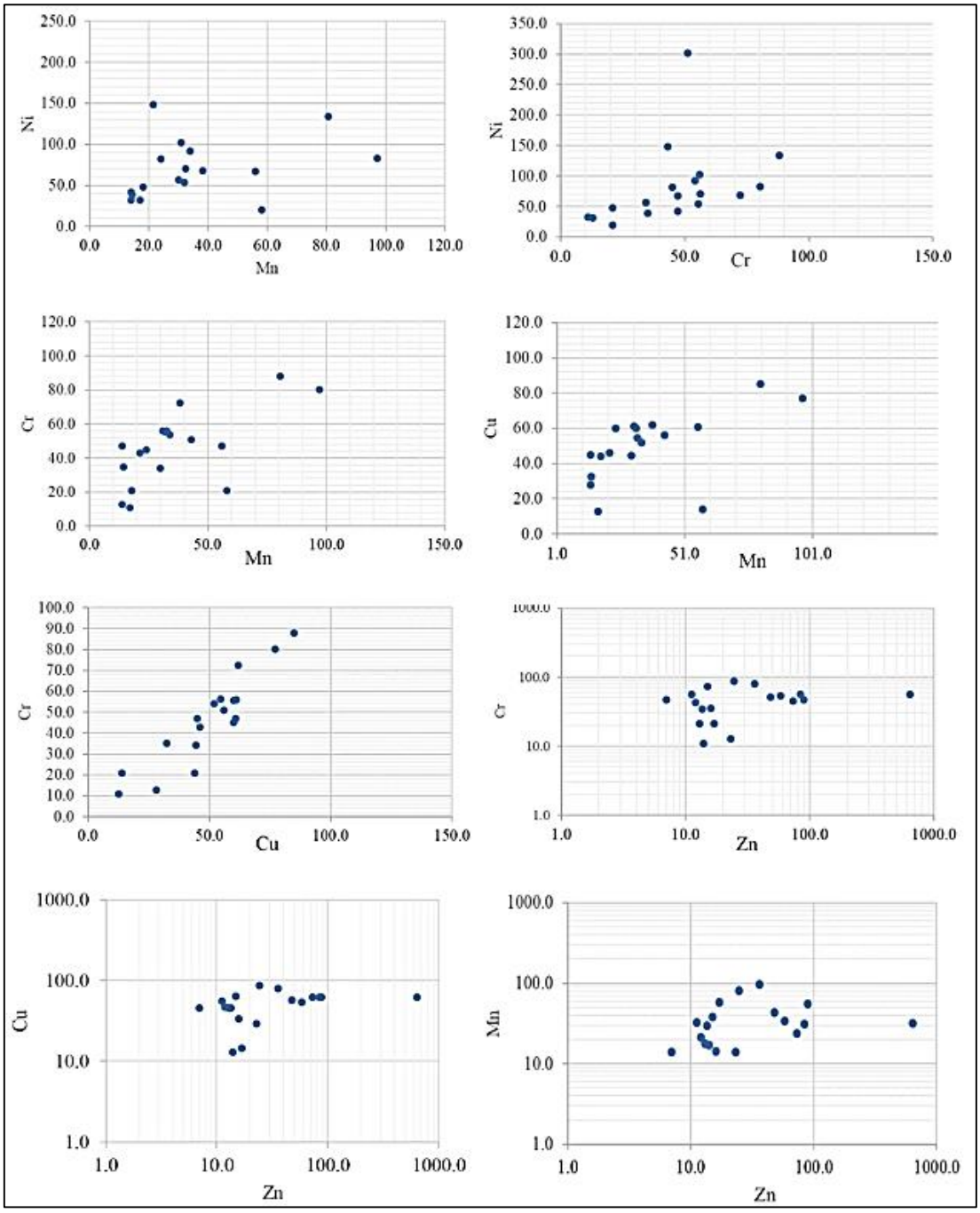

Figure 5.78 The graph represent the relationship between trace element of Winder area in µg/l. Magnese (Mn) -Chromium (Cr), Magnese (Mn) - Copper (Cu), Copper (Cu) - Chromium (Cr), Zinc (Zn) - Chromium (Cr), Zinc (Zn) - Copper (Cu) and Zinc (Zn) - Magnese (Mn).

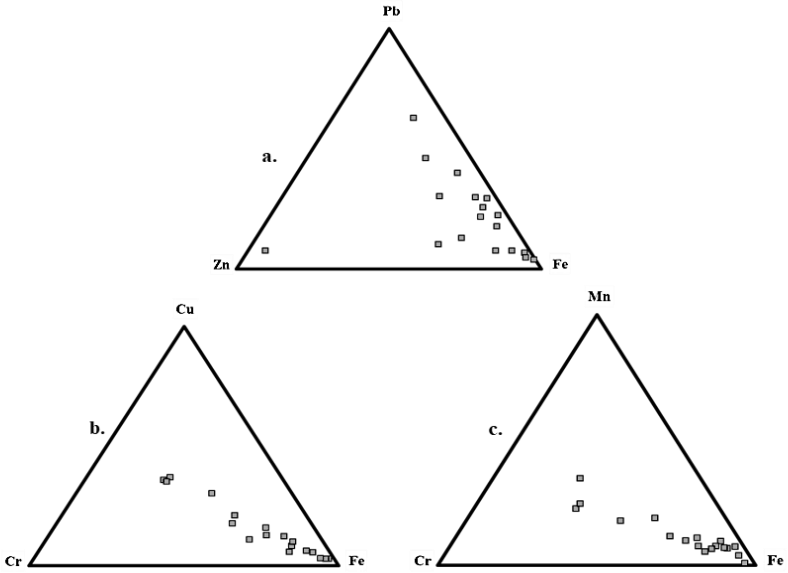

Figure 5.79 Ternary diagram representing the trace element variation in groundwater.

5.11.7 Lead (Pb)

It is a chalcophile element and is found in sulphide deposits. The abundance Pb in groundwater is 3 µg/l and has a very low mobility in water (Fouillac et al., 2009). The range in the Winder area is 30-117 and the mean value is 66.86 µg/l. The permissible limit in water used for irrigation is less than 200 µg/l. The water sample area is lower than the permissible limit.

5.11.8 Cadmium (Cd)

Cadmium is a soft metal, with a low melting point, which is usually present as different hydrothermal cluster compounds. Cd can leach out by dissolution and form aqueous complexes in groundwater (Dong et al., 2009). In study area samples there is

no contribution of anthropogenic activities and mainly linked with the sulphide of Bela Ophiolite. The presence of cadmium is a result due to chemical weathering as it is soluble and easy to move in water (Hoareau et al., 2022). pH value mainly controls the concentration in groundwater (Kubier et al., 2019).

The Cd in groundwater of Winder ranges from 1-19 and an average value is 5.2 µg/l. The average value is very high in comparison with river water i.e. 0.03 µg/l (Naseem et al., 2013). A high concentration of Cd greater than 10 µg/l had been observed in the samples toward the north-east, mainly near the Winder River, the concentration is decreasing as it moves away from the river and toward the coast due to higher pH value of water. It is very essential to see that high concentration of Cd is linked with Ni, indicating input from the lower sulphide of Ophiolite (Dilek & Yang, 2018). There is no major impact on human health from Cadmium. However, a low level can cause vomiting, nausea and diarrhoea. Nevertheless, long-term exposure to high amounts of Cd active heart diseases, fragile bones, kidney damage, cancer and high blood pressure (Suhani et al., 2021; Engwa et al., 2019).

5.12 Trace Element Discussion

The trace elements in study area are also found in the fruit and plant of Winder, Balochistan to provide the micronutrient through soil. The major influence of trace elements was reported in Manilkara Zapota P. Royen fruit. A higher concentration of Chromium, Copper and Nickel was observed in soil of the study area. The presence of Bela Ophiolite is considered the main source of trace elements in the soil of study area (Hamza et al., 2013).

The comparative study of present data analysis and previous research on groundwater composition of study area reveals that the trace element concentration decreased in groundwater (Figure 5.80). The reason for the decline in concentration is the assessment of pH range which can be utilized to evaluate the micronutrient

availability such as Mn, Fe, Cu, Zn, etc. Generally, lower pH increases the absorption of an element in water. The present study pH range in the study area shows unfavourable conditions due to higher values for the occurrence of trace elements. Besides this the presence of bicarbonate ions is high and they are not dangerous, but the combination with Mg or Ca precipitate in carbonate is risky. It might decrease the concentration of Zn & other metals (Ayer & Westcot, 1985).

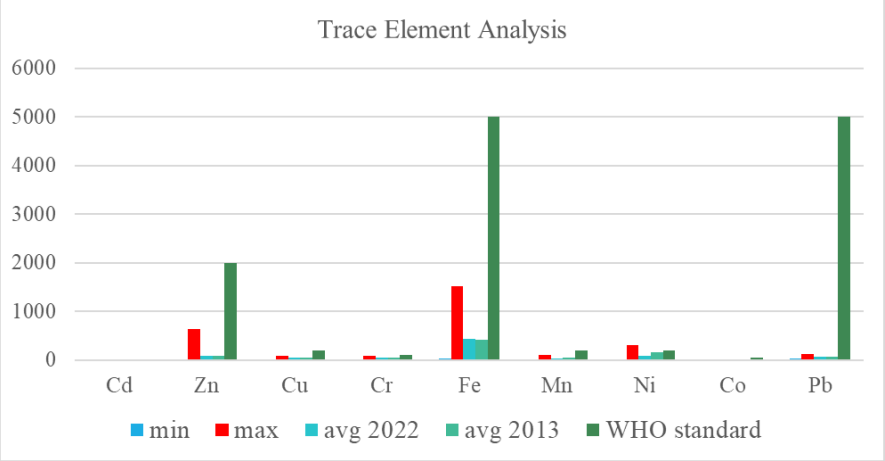

Figure 5.80 Trace element comparative analysis of present research in µg/l on (y-axis) and an average value of 2013, groundwater sample of Winder, Balochistan.

5.13 Integration of Geophysical and Hydrochemical analysis.

The integrated analysis was carried out using geophysical resistivity data, hydrogeological data and hydrochemical analysis of groundwater. The results from the geophysical analysis show that the water quality is at a vulnerable stage on the left side of the RCD highway or in the western side of study area. Moreover, the water table is at a deeper depth of more than 45 meters as moving away from Winder River.

The interpreted resistivity data was mapped for the distribution of resistivity for an aquifer and then pseudo-cross-section was also constructed to calibrate with the Dar-Zarrouk parameter results for validation (Figure 5.81). Finally, the deterioration of

water quality near to coast has resulted from seawater intrusion marked based on the integration where the resistivity results were correlated with the groundwater sample. Moreover, the water sample also shows higher TDS values, Na-Cl type water facies is dominant identified from the HEF-D diagram and Piper plot. The Gibbs diagram, EC vs SAR and other statistical analysis also describe the contribution of rock in the composition of groundwater and increase in salinity due to overexploitation. Figure 5.82 shows the integration of TDS, Sodium, Chlorine and Gibbs plot with the TDS map of area. The analysis shows that originally groundwater composition was controlled by the rock present in the north-east of study area. The fresh and high TDS zone are identified to explore the potential aquifer for domestic and irrigation purpose.

The irrigation water quality parameters average value for RSC, Na%, SAR, PS, PI, MAR and KR shows that average value trend is moving toward the unsuitable condition for irrigation. The estimation of Na%, SAR, and Salinity hazards from measured field parameter of study are already at the stage of impacting the soil and agriculture activity of Winder. The estimated results help to identify the fresh-saline boundary based on the integrated results of the water samples and resistivity mapping (Figure 5.81 & 5.82).

The tube wells UF, UG, UN, US, UD, UL, UR, UG, UT, UP, PS, KA, KZ, KT, KA and KQ located toward the west and show high salinity. Whereas moving toward the proximal or inland, the water quality becomes suitable. These points are close to the R-1, R-2, R-24, R-26, R25 and R-27 which also depict low resistivity values. The estimated values also correlated with the previous research conducted in the study area a decade ago which also highlight the drastic change in the water table and quality as discussed in for each parameter in hydrochemical analysis. The aquifer parameter integrated in Figure 5.81 & 5.82 support that the study area is effected by seawater intrusion. The lower values were observed in the south-east and toward the western part of the study area due to high conductance, effected by seawater intrusion. The co-efficient of anisotropy represent the homogeneous condition shows high permeability in sand and sandy gravel depicting the high vulnerability of seawater in the coastal aquifer of Winder.

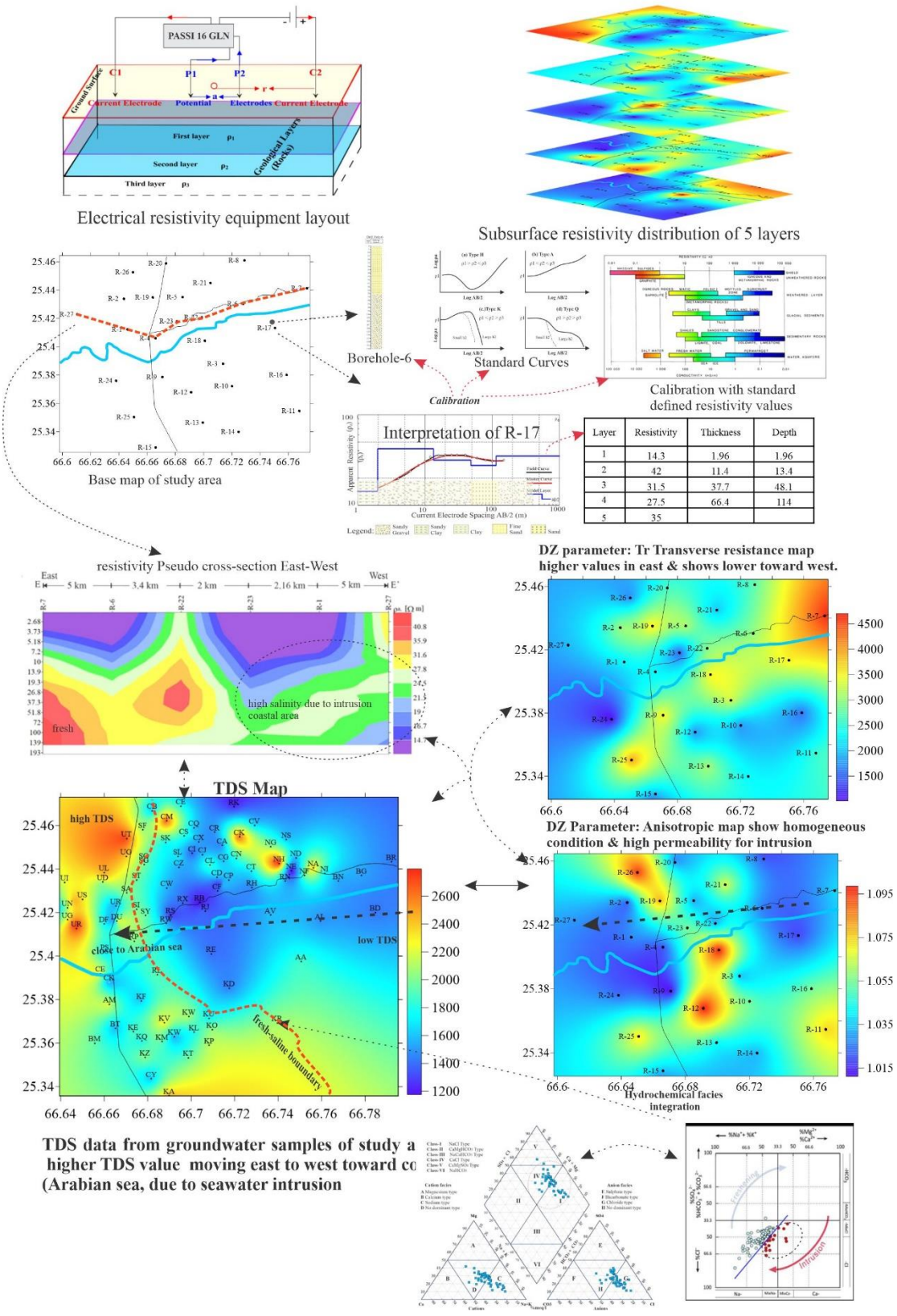

Figure 5.81 Integrated analysis of geophysical and hydrochemical results using geophysical results with groundwater concentration map and statistical analysis using piper plot and hydrodynamic facies diagram.

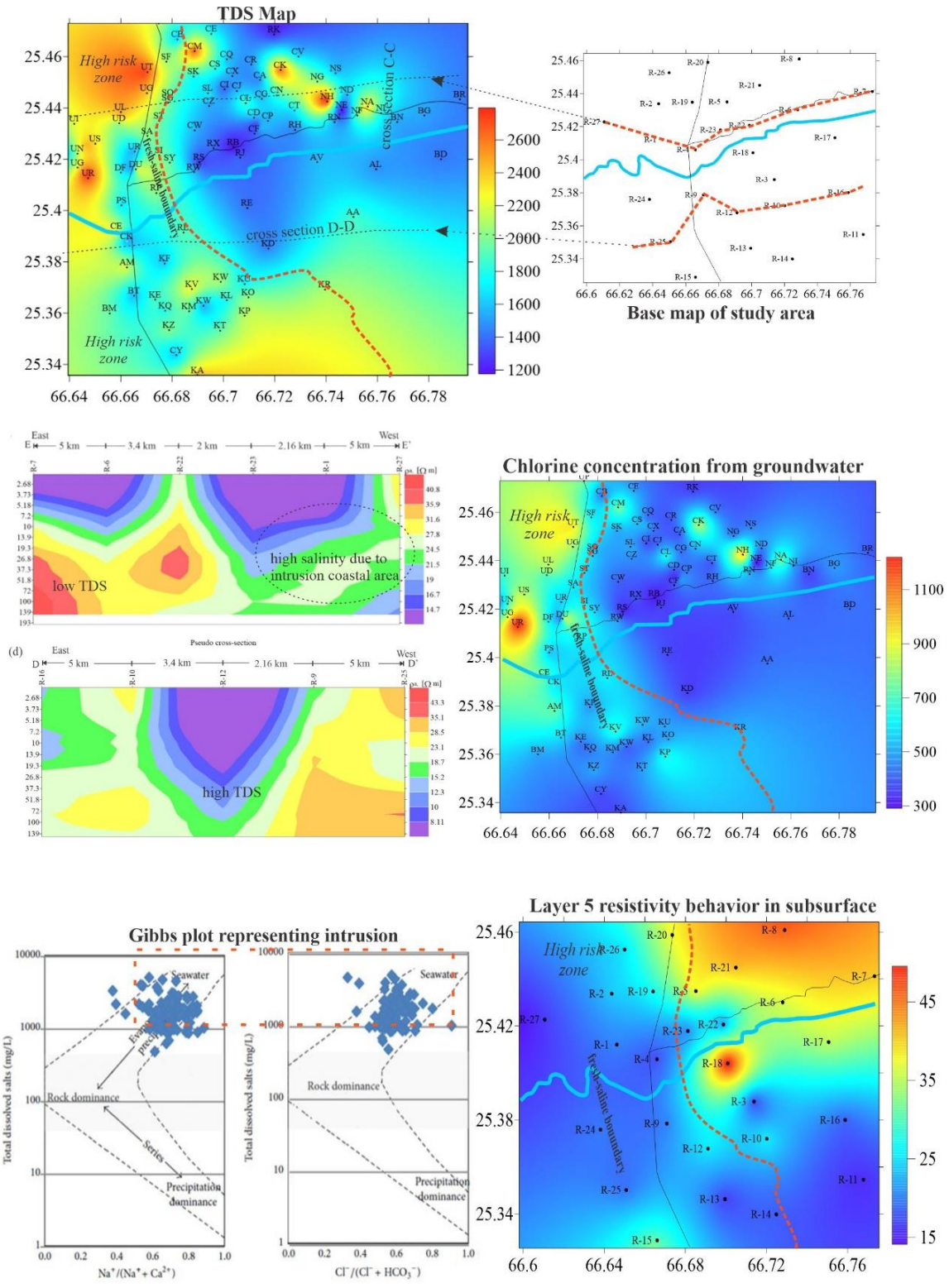

Figure 5.82 Spatial integration of groundwater sample TDS, Sodium concentration, chlorine concentration, seawater intrusion analysis using Gibbs plot with the geophysical electrical resistivity cross-section C-C', D-D'.

CHAPTER 6

CONCLUSION

Groundwater utilization has increased due to industrialization, urbanization and intensive irrigation activities around the world to overcome the demand of 21st Century. Water resources play a critical role in the regular function of ecosystems and geosystems. The increase in demand of groundwater resulted in the decline of water table and the deterioration of water quality. The United Nation 2030 Sustainable Development Goals (SDGs) address the issue of water resource protection in terms of quality and sustainable use. SDG-6 focus on the accessibility of water and its sustainable management. Moreover, SDG-11 focuses on ensuring the availability of fresh water for human consumption. The success of SDG 2030 goals depends on quantitative research which remains poor for this issue. But this can be overcome from the existing knowledge related to water resources, identifying gaps in sustainability, temporal and spatial data collection and monitoring of freshwater resources.

The following are the main conclusions summarized from this research work aligned with the objectives. Winder valley is geologically north-south trending valley, comprised Jurassic-Cretaceous rocks in Pab and Mor ranges. The rough topography

was drained by the Winder River and its tributaries. The surface geology of study area covered by the recent alluvial deposit, rich in minerals for agriculture activities.

Based on the information acquired from vertical electrical sounding and integration with hydrogeological data the plotted geo-electrical values for each VES station depict significant similarities in terms of resistivity and interpreted lithological layers. It provides the opportunity to map the shallow subsurface electro-stratigraphy and demarcate the presence of an aquifer having low salinity based on the resistivity and geometry of the aquifer. The study area aquifer is identified as unconfined and anisotropic based on data analysis. Layer 1 resistivity ranges from 2-38 Ωm and an average value is 17.5 Ωm. The apparent resistivity distribution for layer-1 shows that the resistivity is higher toward the west due to dry and unsaturated sand dunes deposits. The lower resistivity pattern toward the west and the central part of study area depicts the sandy clay and clay. Layer 2 resistivity ranges from 6.32-42 Ωm and an average value is 23 Ωm. The range of resistivity in layer-2 indicate the higher resistivity zone toward the north-east presence of sandy gravel whereas the south-west and north-west of study area depict the presence of sand. The layer 3 resistivity value ranges from 14-50.4 Ωm and average value is 29 Ωm. Layer 4 resistivity ranges from 13.5-51.6 Ωm and an average value is 31.5 Ωm. Layer 5 resistivity value ranges from 14.1-51.4 Ωm and an average value is 27.35 Ωm. Layer 3,4 and 5 show higher resistivity in the central and eastern parts of study area whereas the western side shows low resistivity zones. Layer 4 and 5 are saturated and low resistivity depict the brackish water condition toward the western side. The higher resistivity closure along the Winder River delineated as the high potential of freshwater zone. The thickness map of study area provides the distribution of Quaternary sediment deposited over the triangular-shaped Lasbela plain. The source of sediment is from the north-east of study area where maximum thickness of sediment was observed and sediment was also contributed from Bela Ophiolite, Mor and Pab ranges.

The interpreted subsurface geology and drilled log suggested that the depositional environment of deposited sediment are high-energy river and distributaries. The sand and sandy gravel deposited by river near to zone covered by sand dune deposits. The minimum thickness contour closures 50 meters observed in the

west near to Miani- Hor coastal area, south-east Kathore and north-west of study area and maximum value is 117 meters toward the north-east.

Darzarouk parameter concluded as where the lower values Tr < 2000 Ωm2 is observed in south-east and toward the western part of the study area due to high conductance, effected by seawater intrusion. The higher value of T also represents the presence of sandy gravel and sand whereas lower values indicate silt, sand and clay. The estimated value of Sc for 27 VES stations up to 150-meter depth shows high variation ranges from 1.27-7.29 mho for study area. The lower values of Longitudinal Conductance "Sc" < 2 mhos indicate the fresh zone, 2-4 interpreted as brackish water and higher values >4 identified as saline water. The lower values for longitudinal resistivity interpreted as saline toward the coastal belt of study area and higher values are identified as good quality water in the north-east and south-east. The value is in the range of 13.96-43.36 Ωm. The lower values for longitudinal resistivity interpreted as saline toward the coastal belt of study area and higher values identified as good quality water in north-east and south-east. The value of transverse resistivity is in the range of 15.8-46.2 Ωm. The anisotropy surface represents the homogenous and isotropic nature of the sand and sandy gravel aquifer distribution in the subsurface. The co-efficient of anisotropy values ranged from 1.007 to 1.09 λ. The homogeneous condition shows high permeability in sand and sandy gravel depicting the high vulnerability of seawater in the coastal aquifer of Winder.

The hydro-chemical analysis shows that precipitation is the main source of groundwater recharge in study area. The water aquifers are enriched in Na^{+}, K^{+}, Ca^{2+}, Mg^{2+}, HCO_3^{-}, Cl^{-}, SO_4^{2-}, NO_3^{-}. The graphical evaluation of chemical parameters of groundwater based on Piper's Trillinear, HFE-D, Stiff and Gibbs diagram pointed out the presence of Na^{+}, Cl^{-}, Ca^{2+}, Mg^{2+}, SO_4^{2-}, NO_3^{-} and HCO_3^{-} composition as dominant in water samples. The result of EC, SAR and Na% also suggest that groundwater of study area is fresh to brackish and poor to fair class for irrigation. As per WHO standards, TDS is very high for drinking and the locals are using it without any treatment. The higher salinity of groundwater is the result of over-pumping of water reserves in study area where in the last decade seawater is also contributing to recharge to increase the salinity. The current analysis concluded that at present conditions the

groundwater is fair to suitable for agriculture activity except on left of the RCD highway where the higher salinity hazard is observed. In comparison with the previous data, most of the parameters show that groundwater quality has deteriorated in last 10 years. If the rate of overexploitation will remain same without sustainable groundwater management the region will face a drastic impact on agriculture activity due to seawater intrusion. The results show the alkaline water type, pH value and salinity of study area are high. Therefore, the trace element concentration depicts decreasing trend in comparison with the previous research.

Finally, the recommendation suggest that the overall groundwater quality has been impacted due to overexploitation in Winder, causing water scarcity and shrinkage of water resources and seawater intrusion. It can be destabilizing the social stability, the productivity of crops, economic growth of area, public health issue, environmental impacts and countless socio-economic traits in future. The current research finding can be utilized for sustainable groundwater management of study area to address the current situation where over-pumping severely effects the water quality and causes seawater intrusion. The geophysical and hydrochemical parameter maps can be utilized to categorize the low-high risk zone for agriculture activities and domestic use of water. The pumping of groundwater should be stopped from tube wells near to the coast such as UF, UG, UN, US, UD, UL, UR, UG, UT, UP, PS, KA, KZ, KT, KA and KQ. These tube wells are close to the Arabian sea and decline in water table eventually covered by seawater intrusion.

The government should design a policy on the utilization of groundwater for agriculture. Instead of overstressing the aquifer to meet the demand and completely overlie on groundwater there must be alternatives. The artificial groundwater recharge tube wells would be an effective technique for study areas based on geophysical investigation in this research. The agriculture department should divert the farmer toward smart farming and drip irrigation. Once these recommendations are practically applied by the government then current research can also be utilized for temporal analysis and effectiveness of the implementation of recharge projects. The study also highlights the importance of geophysical investigation for estimating aquifer properties and its integration with hydro-chemical data.

REFERENCES

Abba, S., Benaafi, M., Usman, A., Ozsahin, D. U., Tawabini, B., & Aljundi, I. H. (2023). Mapping of groundwater salinization and modelling using meta-heuristic algorithms for the coastal aquifer of eastern Saudi Arabia. Science of the Total Environment, 858, 159697.

Abdulameer, A., Thabit, J., Kanoua, W., Wiche, O., & Merkel, B. (2021). Possible sources of salinity in the Upper Dibdibba Aquifer, Basrah, Iraq. . Water (13), 578.

Abidin, M. H. Z., Saad, R., Ahmad, F., Wijeyesekera, D. C., & Baharuddin, M. F. T. (2011). Application of geophysical methods in Civil engineering. Malaysian Technical Universities International Conference on Engineering and Technology,

Abrar, N., Khan, M. R., Hameed, F., Asghar, A., Bangash, A. A., Nisar, U. B., Niaz, J., Farooq, M., Khan, M. Y., & Awan, M. (2019). Application of electrical resistivity method in delineating aquifer properties along with vulnerability mapping in Gujrat District and surrounding areas of Punjab province, Pakistan. Journal of Himalayan Earth Sciences Volume, 52(2), 106-128.

Adamo, N., Al-Ansari, N., Sissakian, V., Laue, J., & Knutsson, S. (2021). Geophysical methods and their applications in dam safety monitoring. Journal of Earth Sciences and Geotechnical Engineering, 11(1), 291-345.

Adimalla, N. (2019). Groundwater quality for drinking and irrigation purposes and potential health risks assessment: a case study from semi-arid region of South India. Exposure and health, 11(2), 109-123.

Adimalla, N., Qian, H., & Nandan, M. (2020). Groundwater chemistry integrating the pollution index of groundwater and evaluation of potential human health risk: A case study from hard rock terrain of south India. Ecotoxicology and environmental safety, 206, 111-217.

Adimalla, N., Qian, H., & Tiwari, D. M. (2021). Groundwater chemistry, distribution and potential health risk appraisal of nitrate enriched groundwater: A case study from the semi-urban region of South India. Ecotoxicology and environmental safety, 111-207.

Adimalla, N., & Taloor, A. K. (2020). Hydrogeochemical investigation of groundwater quality in the hard rock terrain of South India using Geographic Information System (GIS) and groundwater quality index (GWQI) techniques. Groundwater for Sustainable Development, 10, 100-288.

Afolayan, J., Olorunfemi, M., & Afolabi, A. (2004). Geoelectric/electromagnetic VLF survey for groundwater development in a basement terrain–a case study. Ife Journal of Science, 6(1), 74-78.

Afridi, W. A. K. (2022). A study on Sustainable Water Management Systems in view of UN SDG 6 centering advanced ICTs.

Ahmed, R., Mahar, G. A., & Iqbal, M. J. (2013). Agricultural Potential in Winder Basin, Lasbela: An analysis based on Farmer's Perceptions. FUUAST Journal of Biology, 3(2), 63-68.

Ahmed, R., & Mahmood, K. (2007). Process of development and future prospects: A geographical analysis of Balochistan province. Pakistan Geographical Review, 62(1), 15-30.

Ahmed, Z. (1993). Leucocratic rocks from the Bela ophiolite, Khuzdar district, Pakistan. Geological Society, London, Special Publications, 74(1), 89-100.

Ahmed, Z., Ansari, M. T., Zahir, M., Shakir, U., & Subhan, M. (2020). Hydrogeophysical investigation for groundwater potential through Electrical Resistivity Survey in Islamabad, Pakistan.

Ahsan, S. N. (1995). Petrogenesis of Shirinab Formation, Lasbela-Khuzdar area, Balochistan, Pakistan. Ph. D. dissertation, Dept. Geol., Univ. Karachi.

Ahsan, S. N., & Mallick, K. A. (1999). Geology and genesis of barite deposits of Lasbela and Khuzdar Districts, Balochistan, Pakistan. Resource Geology, 49(2), 105-111.

Ahsanullah. (1971). Landform and Drainage Basins in Karachi Region. Master Plan for Karachi Metropolitan Region.

Aizebeokhai, A., Olayinka, A., Singh, V., & Uhuegbu, C. (2011). Effectiveness of 3D geoelectrical resistivity imaging using parallel 2D profiles. Current science, 1036-1052.

Aizebeokhai, A. P. (2010). 2D and 3D geoelectrical resistivity imaging: Theory and field design. Scientific Research and Essays, 5(23), 3592-3605.

Akbar, M., Khan, S. A., Dilawar, S., & Hassan, M. T. (2021). Water Crisis in Pakistan: Prospect and Implications IMPLICATIONS. PalArch's Journal of Archaeology of Egypt/Egyptology, 18(1), 4884-4892.

Akhtar, M. M., Mohammad, A. D., Ehsan, M., Akhtar, R., & Manzoor, Z. (2021). Water resources of Balochistan, Pakistan—a review. Arabian Journal of Geosciences, 14(4), 1-16.

Akhter, G., & Hasan, M. (2016). Determination of aquifer parameters using geoelectrical sounding and pumping test data in Khanewal District, Pakistan. Open Geosciences, 8(1), 630-638.

Akhter, M., & Masood, T. (1991). Geology of Sulaiman Range Geological Survey of Pakistan (Vol. 342).

Akram, M., Aslam, M., & Rasheed, H. (2007). Water quality status of Pakistan.

Ali, A., Farid, H. U., Khan, Z. M., Ahmad, I., Anjum, M. N., & Shahzad, H. (2022). Climate Explained Variability and Sensitivity of Groundwater Level. Available at SSRN 4210708.

Ali, A., Iqbal, M., & Waheed, A. (2021). Groundwater quality assessment near Nullah Lai stream of Pakistan. Central Asian Journal of Environmental Science and Technology Innovation, 2(2), 45-51.

Ali, S. (2005). Mountain Agriculture in Pakistan: Crop Combination and Food Sustainability. Journal Geographic, 10, 47-56.

Alizai, M. (1998). Unused agricultural land of Pakistan and its spatial distribution. Studies in Pakistan Geography, edited by Israr-ud-Din, Department of Geography, Urban and Regional Planning, University of Peshawar, Peshawar.

Allemann, F. (1979). Time of emplacement of the Zhob Valley ophiolite and Bela ophiolites, Balochistan. Geodynamics of Pakista, edited by A. Farah and KA De Jong, 215-242.

Almeida, A., Maciel, D. F., Sousa, K. F., Nascimento, C. T. C., & Koide, S. (2021). Vertical Electrical Sounding (VES) for Estimation of Hydraulic Parameters in the Porous Aquifer. Water, 13(2), 170.

Amiri, V., Bhattacharya, P., & Nakhaei, M. (2021). The hydrogeochemical evaluation of groundwater resources and their suitability for agricultural and industrial uses in an arid area of Iran. Groundwater for Sustainable Development, 12, 100-527.

Annan, A. (1997). Engineering and environmental geophysics: the future. Geological Society, London, Engineering Geology Special Publications, 12(1), 419-426.

Anoop, S., Ashwathi, C., Baburaj, V. H., & Pillai, R. S. (2021). Hydrogeochemical status and geoelectrical characteristics of the shallow aquifers of Kalanad Basin, Kasaragod, Kerala, India. Applied Water Science, 11(2), 1-16.

Anwar, M. (1991). Revised nomenclature and stratigraphy of Ferozabad, Alozai and Mona Jhal Groups of Balochistan (Axial Belt), Pakistan. Acta Mineral. Pakistan, 5, 46-61.

Arif, M., Jan, M., & Ahsan, S. (1997). Mineral chemistry of the chromite occurrences from the Bela ophiolite in Khuzdar, Balochistan, Western Pakistan. Proc. National Symposium on Economic geology of Pakistan, Islamabad,

Arulnangai, M. (2020). Interpretation of groundwater quality using Piper diagram in around Ariyalur District, Tamilnadu India. Journal of Natural Remedies, 21(8 (1)), 193-198.

Arulnangai, R., Sihabudeen, M. M., Vivekanand, P., & Kamaraj, P. (2021). Influence of physico chemical parameters on potability of ground water in ariyalur area of Tamil Nadu, India. Materials Today: Proceedings, 36, 923-928.

Asare, A., Appiah-Adjei, E. K., Ali, B., & Owusu-Nimo, F. (2021). Assessment of seawater intrusion using ionic ratios: the case of coastal communities along the Central Region of Ghana. Environmental Earth Sciences, 80(8), 1-14.

Ashraf, M. (2016). Groundwater management in Balochistan, Pakistan.

Ashraf, M., & Sheikh, A. A. (2017). Sustainable groundwater management in Balochistan. Pakistan Council of Research in Water Resources.

Auken, E., & Christiansen, A. V. (2004). Layered and laterally constrained 2D inversion of resistivity data. Geophysics, 69(3), 752-761.

Awan, M. (2019). Application of electrical resistivity method in delineating aquifer properties along with vulnerability mapping in Gujrat District and surrounding areas of Punjab province, Pakistan. Journal of Himalayan Earth Sciences Volume, 52(2), 106-128.

Awasthi, S., Chauhan, R., & Srivastava, S. (2022). The importance of beneficial and essential trace and ultratrace elements in plant nutrition, growth, and stress tolerance. In Plant Nutrition and Food Security in the Era of Climate Change (pp. 27-46). Elsevier.

Ayer, R., & Westcot, D. (1985). Water quality for agriculture, irrigation and drainage. Paper no, 29.

Ayers, R. S., & Westcot, D. W. (1985). Water quality for agriculture (Vol. 29). Food and Agriculture Organization of the United Nations Rome.

Azhari, H. E., Cherif, E. K., Sarti, O., Azzirgue, E. M., Dakak, H., Yachou, H., Esteves da Silva, J. C. G., & Salmoun, F. (2023). Assessment of surface water quality using the Water Quality Index (IWQ), Multivariate Statistical Analysis (MSA) and Geographic Information System (GIS) in Oued Laou Mediterranean Watershed, Morocco. Water, 15(1), 130.

Aziane, N., Khaddari, A., IbenTouhami, M., Zouahri, A., Nassali, H., & Elyoubi, M. S. (2020). Evaluation of groundwater suitability for irrigation in the coastal aquifer of Mnasra (Gharb, Morocco). Mediterranean Journal of Chemistry, 10(2), 197-212.

Bai, J., Zhao, Q., Wang, W., Wang, X., Jia, J., Cui, B., & Liu, X. (2019). Arsenic and heavy metals pollution along a salinity gradient in drained coastal wetland soils: Depth distributions, sources and toxic risks. Ecological indicators, 96, 91-98.

Baig, N., Khan, S., Bashir, I., & Ma, J. (2023). Does China Pakistan Economic Corridor become an avenue to achieve sustainable development goal no. 2 (food security) in Pakistan: Under the condition of COVID-19? PloS one, 18(1).

Banerjee, P., & Prasad, B. (2020). Determination of concentration of total sodium and potassium in surface and ground water using a flame photometer. Applied Water Science, 10(5), 1-7.

Bank, W. (2008). Balochistan Economic Report : From Periphery to Core, Volume 1. Summary Report. Washington, DC.

Bannert, D., Cheema, A., Ahmed, A., & Schäffer, U. (1995). The Structural Development of the Western Fold Belt,-Pakistan.

Bari, J. A., Vennila, G., & Karthikeyan, P. (2021). Appraisal of hydrogeochemical processes and groundwater quality in Bhavani taluk Erode district, Tamil Nadu, India. Arabian Journal of Geosciences, 14(13), 1-20.

Bartzas, G., Tinivella, F., Medini, L., Zaharaki, D., & Komnitsas, K. (2015). Assessment of groundwater contamination risk in an agricultural area in north Italy. Information Processing in Agriculture, 2(2), 109-129.

Bashir, E. (2008). Geology and geochemistry of magnesite ore deposits of Khuzdar area, Balochistan University of Karachi].

Bashir, E., Naseem, S., Nadeem, S., Sheikh, S. A., & Shirin, K. (2004). Petrography, Mineralogy And Geochemistry Of Baran Lak Magnesite And Associated Rocks, Khuzdar, Baluchistan, Pakistan. Journal Of Himalayan Earth Sciences, 37.

Bashir, E., Naseem, S., Sheikh, A., & Kaleem, M. (2009). Mineralogy of the Kraubath-type magnesite deposits of the Khuzdar area, Balochistan. Pakistan. Journal of the Earth Sciences Application and Research Centre of Hacettepe University. Yerbilimleri, 30(3), 169-180.

Bashir, E., Nasim, S., & Hamza, S. (2007). Hydrogeochemistry of the Winder River and adjoining tributaries, Balochistan, Pakistan. Chinese Journal of Geochemistry, 26(3), 259-266.

Bassey, P., Lawrence, O., & Ailego, J. (2019). Geo-electrical Resistivity Evaluation of Groundwater Potential at University Of Benin Ugbowo Campus, Benin-City, Edo State of Nigeria, Using the Schlumberger Array. Journal of Applied Sciences and Environmental Management, 23(9), 1761-1770.

Bastianoni, A., Guastaldi, E., Barbagli, A., Bernardinetti, S., Zirulia, A., Brancale, M., & Colonna, T. (2021). Multivariate analysis applied to aquifer hydrogeochemical evaluation: A case study in the Coastal significant subterranean water body between “Cecina River and San Vincenzo”, Tuscany (Italy). Applied Sciences, 11(16), 7595.

Bauder, T. A., Waskom, R., Sutherland, P., & Davis, J. (2011). Irrigation water quality criteria Colorado State University. Libraries].

Bayowa, O., Adagunodo, T., Akinluyi, F., & Hamzat, W. (2022). Geoelectrical exploration of the Coastal Plain Sands of Okitipupa area, southwestern Nigeria. International Journal of Environmental Science and Technology, 1-18.

Belhassan, K. (2021). Water scarcity management. In Water Safety, Security and Sustainability (pp. 443-462). Springer.

Beyene, G., Aberra, D., & Fufa, F. (2019). Evaluation of the suitability of groundwater for drinking and irrigation purposes in Jimma Zone of Oromia, Ethiopia. Groundwater for Sustainable Development, 9, 100216.

Bhagat, C., Puri, M., Mohapatra, P. K., & Kumar, M. (2021). Imprints of seawater intrusion on groundwater quality and evolution in the coastal districts of south Gujarat, India. Case Studies in Chemical and Environmental Engineering, 3, 100.

Bhat, M. A., Wani, S. A., Singh, V. K., Sahoo, J., Tomar, D., & Sanswal, R. (2018). Journal of Agricultural Science and Food Research.
Bhattacharya, B., & Patra, H. (1968). Direct methods in geoelectric sounding: Principle and interpretation. In: Elsevier Science Publ. Co. Inc.
Bhattacharya, P. (2012). Direct current geoelectric sounding: Principles and interpretation.
Biswas, G., Arshad, M., Saba, N. U., Arora, T., & Ahmed, S. (2022). Hydrogeochemical investigation and groundwater quality assessment toward 'smart city planning in a coastal aquifer, India. Water Practice and Technology.
Biswas, T., Pal, S. C., Saha, A., Ruidas, D., Islam, A. R. M. T., & Shit, M. (2023). Hydro-chemical assessment of groundwater pollutant and corresponding health risk in the Ganges delta, Indo-Bangladesh region. Journal of Cleaner Production, 382, 135-229.
Bobachev, C. (2002). IPI2Win: A windows software for an automatic interpretation of resistivity sounding data. Moscow State University, 320.
Bodmer, R., & Ward, S. H. (1968). Continuous sounding-profiling with a dipole-dipole resistivity array. Geophysics, 33(5), 838-842.
Bogardi, J. J., & Fekete, B. M. (2021). Water: a Unique Phenomenon and Resource. In Handbook of Water Resources Management: Discourses, Concepts and Examples (pp. 9-40). Springer.
Bortolotti, V., & Principi, G. (2005). Tethyan ophiolites and Pangea break-up. Island Arc, 14(4), 442-470.
Bouaroudj, S., Menad, A., Bounamous, A., Ali-Khodja, H., Gherib, A., Weigel, D. E., & Chenchouni, H. (2019). Assessment of water quality at the largest dam in Algeria (Beni Haroun Dam) and effects of irrigation on soil characteristics of agricultural lands. Chemosphere, 219, 76-88.
Braga, A. C. d. O., Malagutti Filho, W., & Dourado, J. C. (2006). Resistity (DC) method applied to aquifer protection studies. Revista Brasileira de Geofísica, 24, 573-581.
Bugica, K., Sterba-Boatwright, B., & Wetz, M. S. (2020). Water quality trends in Texas estuaries. Marine Pollution Bulletin, 152, 110-903.
BUITEMS, & UNDP. (2015). Drought risk assessment in the Province of Balochistan, Pakistan.
Burke, F., Hamza, S., Naseem, S., Nawaz-ul-Huda, S., Azam, M., & Khan, I. (2016). Impact of cadmium polluted groundwater on human health: winder, Balochistan. Sage Open, 6(1).
Burke, F., Huda, S., Hamza, S., & Azam, M. (2005). Disparities in agricultural productivity in Balochistan-A GIS perspective. Pakistan Geographical Review, 60(1), 27-34.
Byrne, D. E., Sykes, L. R., & Davis, D. M. (1992). Great thrust earthquakes and aseismic slip along the plate boundary of the Makran subduction zone. Journal of Geophysical Research: Solid Earth, 97(B1), 449-478.
Camacho, R., & Armienta, M. (2000). Natural chromium contamination of groundwater at Leon Valley, Mexico. Journal of Geochemical Exploration, 68(3), 167-181.
Cande, S. C., & Stegman, D. R. (2011). Indian and African plate motions driven by the push force of the Reunion plume head. Nature, 475(7354), 47-52.
Cangemi, M., Censi, V., Madonia, P., & Favara, R. (2021). Application of Geostatistical Tools to the Geochemical Characterization of the Peloritani Mts (Sicily, Italy) Aquifers. Water, 13(22), 3269.

Chardonnet, J. (1956). Spate (OHK)-India and Pakistan. A general and regional geography. Revue économique, 7(6), 1040-1041.
Chatterjee, S., Goswami, A., & Scotese, C. R. (2013). The longest voyage: tectonic, magmatic, and paleoclimatic evolution of the Indian plate during its northward flight from Gondwana to Asia. Gondwana Research, 23(1), 238-267.
Chebet, E. B., Kibet, J. K., & Mbui, D. (2020). The assessment of water quality in river Molo water basin, Kenya. Applied Water Science, 10(4), 1-10.
Chen, F., Khan, Z. I., Zafar, A., Ma, J., Nadeem, M., Ahmad, K., Mahpara, S., Wajid, K., Bashir, H., & Munir, M. (2021b). Evaluation of toxicity potential of cobalt in wheat irrigated with wastewater: health risk implications for public. Environmental Science and Pollution Research, 28(17), 21119-21131.
Chen, K., Sun, L., & Xu, J. (2021a). Statistical analyses of groundwater chemistry in the Qingdong coalmine, northern Anhui province, China: implications for water–rock interaction and water source identification. Applied Water Science, 11(2), 1-12.
Chen, L., Ma, T., Wang, Y., & Zheng, J. (2020). Health risks associated with multiple metal (loid) s in groundwater: A case study at Hetao Plain, northern China. Environmental Pollution, 263, 114-562.
Chidambaram, S., Prasanna, M., Venkatramanan, S., Nepolian, M., Pradeep, K., Panda, B., Thivya, C., & Thilagavathi, R. (2022). Groundwater quality assessment for irrigation by adopting new suitability plot and spatial analysis based on fuzzy logic technique. Environmental Research, 204, 111-729.
Christensen, N. (2000). Difficulties in determining electrical anisotropy in subsurface investigation. geophysical prospecting. Geophysical Prospecting, 48, 1-19.
Chukwuma, E., Orakwe, L., Anizoba, D., Amaefule, D., Odoh, C., & Nzediegwu, C. (2015). Geo-electric groundwater vulnerability assessment of overburden aquifers at Awka in Anambra State, south-eastern Nigeria. European journal of Biotechnology and Bioscience, 3(1), 29-34.
Claeson, F. (2021). Responses in river water quality during summers with extreme weather periods in Europe. Student thesis series INES.
Cobourn, K., Elbakidze, L., & Ghosh, S. (2017). Conjunctive water management in hydraulically connected regions in the Western United States. In Competition for Water Resources (pp. 278-297). Elsevier.
Coker, J. O. (2012). Vertical electrical sounding (VES) methods to delineate potential groundwater aquifers in Akobo area, Ibadan, South-western, Nigeria. Journal of Geology and Mining Research, 4(2), 35-42.
Coleman, R. G. (1977). What is an Ophiolite? In Ophiolites (pp. 1-7). Springer.
Condie, K. (1989). Plate tectonics and crustal evolution [MI. In: Oxford, Pergamon Press, 476p.
Condie, K. C. (1997). Butterworth Heinemann, Plate Tectonics and Crustal Evolution. In: Oxford, Amsterdam, Boston, London, New York, Paris, San Diego, San Francisco ….
Copley, A., Avouac, J. P., & Royer, J. Y. (2010). India-Asia collision and the Cenozoic slowdown of the Indian plate: Implications for the forces driving plate motions. Journal of Geophysical Research: Solid Earth, 115(B3).
Cox, C., Jin, L., Ganjegunte, G., Borrok, D., Lougheed, V., & Ma, L. (2018). Soil quality changes due to flood irrigation in agricultural fields along the Rio Grande in western Texas. Applied Geochemistry, 90, 87-100.

Cox, J., & Cox, J. S. (2000). Subduction-obduction related petrogenetic and metamorphic evolution of the Semail ophiolite sole in Oman and the United Arab Emirates University of Oxford].
Dangar, S., Asoka, A., & Mishra, V. (2021). Causes and implications of groundwater depletion in India: A review. Journal of Hydrology, 126103.
Daniels, J. (1988). Locating caves, tunnels and mines. The leading edge, 7(3), 32-52.
Danoff, B. J. A. (2000). The Terrestrial influence: Geology and soils. Earth Institute Center for Environmental Sustainability.
DAWN. (2007). Plan to revamp Balochistan's agriculture system.
DeJong, K. A., & Subhani, A. (1979). Note on the Bela ophiolites with special reference to the Kanar area. Geodynamics of Pakistan, 263-269.
Delisle, G. (2004). The mud volcanoes of Pakistan. Environmental Geology, 46(8), 1024-1029.
Dhakate, R., & Gurunadha, R. (2015). Hydrochemical assessment of groundwater in alluvial aquifer region, Jalandhar District, Punjab, India. Environmental Earth Sciences, 73(12), 8145-8153.
Dilek, Y. (2003). Ophiolite pulses, mantle plumes and orogeny. Geological Society, London, Special Publications, 218(1), 9-19.
Dilek, Y. (2006). Collision tectonics of the Mediterranean region: causes and consequences. Special papers- Geological Society of America, 409, 1.
Dilek, Y., & Furnes, H. (2014). Ophiolites and their origins. Elements, 10(2), 93-100.
Dilek, Y., & Furnes, H. (2019). Tethyan ophiolites and Tethyan seaways. Journal of the Geological Society, 176(5), 899-912.
Dilek, Y., Furnes, H., & Shallo, M. (2007). Suprasubduction zone ophiolite formation along the periphery of Mesozoic Gondwana. Gondwana Research, 11(4), 453-475.
Dilek, Y., & Newcomb, S. (2003). Ophiolite concept and its evolution. Special Papers-Geological Society of America, 1-16.
Dilek, Y., & Yang, J. (2018). Ophiolites, diamonds, and ultrahigh-pressure minerals: new discoveries and concepts on upper mantle petrogenesis. Lithosphere, 10(1), 3-13.
Ding, L., Qasim, M., Jadoon, I. A., Khan, M. A., Xu, Q., Cai, F., Wang, H., Baral, U., & Yue, Y. (2016). The India–Asia collision in north Pakistan: Insight from the U–Pb detrital zircon provenance of Cenozoic foreland basin. Earth and Planetary Science Letters, 455, 49-61.
Dobenecker, B., Reese, S., & Herbst, S. (2021). Effects of dietary phosphates from organic and inorganic sources on parameters of phosphorus homeostasis in healthy adult dogs. PloS one, 16(2), e0246950.
Doneen, L. (1964). Water quality in agriculture. Department of Water Sciences and Engineering, University of California, Davis.
Dong, D., Zhao, X., Hua, X., Liu, J., & Gao, M. (2009). Investigation of the potential mobility of Pb, Cd and Cr (VI) from moderately contaminated farmland soil to groundwater in Northeast, China. Journal of Hazardous Materials, 162(2-3), 1261-1268.
Dor, N., Syafalni, S., Abustan, I., Rahman, M. T. A., Nazri, M. A. A., Mostafa, R., & Mejus, L. (2011). Verification of surface-groundwater connectivity in an irrigation canal using geophysical, water balance and stable isotope approaches. Water resources management, 25(11), 2837-2853.

Egbai, J., & Iserhien-Emekeme, R. (2015). Aquifer transmissivity Dar Zarrouk parameters and groundwater flow direction in Abudu, Edo State, Nigeria. Int. J. Sci. Env. Tech, 4(3), 628-640.

Egbueri, J. C., Mgbenu, C. N., Digwo, D. C., & Nnyigide, C. S. (2021). A multi-criteria water quality evaluation for human consumption, irrigation and industrial purposes in Umunya area, southeastern Nigeria. International Journal of Environmental Analytical Chemistry, 1-25.

Ekwule, O., Simeon, A., & Amer, M. (2022). Coupling Hydrochemical Characterization with Geospatial Analysis to Understand Groundwater Quality Parameters In North Central Nigeria.

Elawadi, E., El-Qady, G., Salem, A., & Ushijima, K. (2001). Detection of cavities using pole-dipole resistivity technique. Memoirs- Faculy of Enginering Kyushu University., 61(4), 101-112.

Eliopoulos, G. D., Eliopoulos, I.-P. D., Tsioubri, M., & Economou-Eliopoulos, M. (2020). Distribution of Selenium in the Soil–Plant–Groundwater System: Factors Controlling Its Bio-Accumulation. Minerals, 10(9), 795.

Engwa, G. A., Ferdinand, P. U., Nwalo, F. N., & Unachukwu, M. N. (2019). Mechanism and health effects of heavy metal toxicity in humans. Poisoning in the modern world-new tricks for an old dog, 10, 70-90.

Essefi, E., & Hajji, S. (2023). Water Crisis in Tunisia During the Anthropocene and Great Acceleration Wetlands as Key Sites of Hydrogeological Modifications. In Climatic and Environmental Significance of Wetlands: Case Studies from Eurasia and North Africa (pp. 97-116). IGI Global.

Fahim, A. K. F., Kamal, A. M., & Shahid, S. (2023). Spatiotemporal change in groundwater sustainability of Bangladesh and its major causes. Stochastic Environmental Research and Risk Assessment, 37(2), 665-680.

Fajana, A. O. (2020). Groundwater aquifer potential using electrical resistivity method and porosity calculation: a case study. NRIAG Journal of Astronomy and Geophysics, 9(1), 168-175.

Farah, A., Lawrence, R., & DeJong, K. (1984). An overview of the tectonics of Pakistan. Marine geology and oceanography of Arabian Sea and Coastal Pakistan. Van Nostrand Reinhold Company, New York, 161-176.

Fatmi, A. (1977). Mesozoic 29-56. Stratigraphy of Pakistan, GSP Memoirs, 12.

Fatmi, A., Haidri, I., Anwar, M., & Mengal, J. (1986). Stratigraphy of Ziddi Formation (Ferozabad Group) and Parh Group (Mona Jhal Group), Khuzdar District, Balochistan. Pakistan. Geol. Surv. Pakistan, Record LXXV.

Fatmi, A., Hyderi, I., Anwar, M., Mengal, J., Hafeez, M., & Khan, M. (1999). Stratigraphy of Mesozoic rocks of southern Balochistan, Pakistan. GSP, Rec, 85(1).

Flynn, R. (2009). Irrigation Water Analysis and Interpretation. NM State University, Cooperative Extension Service.

Flynn, R., McVeigh, C., Mackin, F., & Wilson, F. R. (2021). Sources of stream base flow in blanket peat covered catchments. Journal of Hydrology, 603, 126965.

Fouillac, A. M., Grath, J., Ward, R., & Quevauviller, P. (2009). Groundwater Monitoring. Wiley.

Fowler, J., Graham, R., Sassi, W., Smewing, J., & Warburton, J. (2004). Two-dimensional kinematic modeling of the southern Kirthar fold belt, Pakistan.

Freeze, R. A., & Cherry, J. A. (1979). Groundwater Prentice-Hall Inc. Eaglewood Cliffs, NJ.

Gabr, M. E., Soussa, H., & Fattouh, E. (2021). Groundwater quality evaluation for drinking and irrigation uses in Dayrout city Upper Egypt. Ain Shams Engineering Journal, 12(1), 327-340.
Gaffney, C. F., Gater, J., & Ovenden, S. (2002). The use of geophysical techniques in archaeological evaluations.
Gao, Y., Qian, H., Ren, W., Wang, H., Liu, F., & Yang, F. (2020). Hydrogeochemical characterization and quality assessment of groundwater based on integrated-weight water quality index in a concentrated urban area. Journal of Cleaner Production, 260, 121006.
Gass, I. (1980). The Troodos massif: Its role in the unravelling of the ophiolite problem and its significance in the understanding of constructive plate margin processes.
Gazal, O. M. D. N. M. (2021). Groundwater deterioration in arid agricultural area under the pressure of climate change and high refugee inflow. Case study: Jordan. International Journal of Hydrology Science and Technology, 12(3), 253-315.
Georgaki, I., Soupios, P., Sakkas, N., Ververidis, F., Trantas, E., Vallianatos, F., & Manios, T. (2008). Evaluating the use of electrical resistivity imaging technique for improving CH_4 and CO_2 emission rate estimations in landfills. Science of the Total Environment, 389(2-3), 522-531.
George, N. J. (2021). Modelling the trends of resistivity gradient in hydrogeological units: a case study of alluvial environment. Modeling Earth Systems and Environment, 7(1), 95-104.
Gevera, P. K., Cave, M., Dowling, K., Gikuma-Njuru, P., & Mouri, H. (2020). Naturally occurring potentially harmful elements in groundwater in Makueni County, south-eastern Kenya: Effects on drinking water quality and agriculture. Geosciences, 10(2), 62.
Gibbs, R. J. (1970). Mechanisms controlling world water chemistry. Science, 170(3962), 1088-1090.
Gimenez-Forcada, E. (2010). Dynamic of sea water interface using hydrochemical facies evolution diagram. Groundwater, 48(2), 212-216.
Gnos, E., Immenhauser, A., & Peters, T. (1997). Late Cretaceous/early Tertiary convergence between the Indian and Arabian plates recorded in ophiolites and related sediments. Tectonophysics, 271(1-2), 1-19.
Gnos, E., Khan, M., Mahmood, K., Khan, A. S., Shafique, N. A., & Villa, I. M. (1998). Bela oceanic lithosphere assemblage and its relation to the Reunion hotspot. Terra Nova-Oxford, 10(2), 90-95.
GoP. (2011). Pakistan Statistical Yearbook Statistical Division, Federal Bureau of Statistics, Islamabad.
GoP. (2012). Economic survey 2011–2012. In: Govt. of Pakistan, Economic Advisor's Wing, Finance Division Islamabad.
Goswami, S., & Rai, A. K. (2022). Estimating suitability of groundwater for drinking and irrigation, in Odisha (India) by statistical and WQI methods. Environmental monitoring and assessment, 194(7), 1-18.
Gupta, S. (1983). Variations of water table in Yamuna drainage basin of Haryana-implications and management strategies. Seminar on Strategies for Irrigation Water Management, Patna,
Gurmani, A. R., Khan, S. U., Andaleep, R., Waseem, K., & Khan, A. (2012). Soil Application of Zinc Improves Growth and Yield of Tomato. International Journal of Agriculture & Biology, 14(1).
Habberjam, G. (1972). The effects of anisotropy on square array resistivity measurements. Geophysical Prospecting, 20(2), 249-266.

Habib, M. A., Islam, A. R. M. T., Bodrud-Doza, M., Mukta, F. A., Khan, R., Siddique, M. A. B., Phoungthong, K., & Techato, K. (2020). Simultaneous appraisals of pathway and probable health risk associated with trace metals contamination in groundwater from Barapukuria coal basin, Bangladesh. Chemosphere, 242, 125183.

Habib, Z. (2021). Water availability, use and challenges in Pakistan-Water sector challenges in the Indus Basin and impact of climate change. Food & Agriculture Org.

Hakim, M., Juraimi, A., Begum, M., Hasanuzzaman, M., Uddin, M., & Islam, M. (2009). Suitability evaluation of groundwater for irrigation, drinking and industrial purposes. American Journal of Environmental Sciences, 5(3), 413-419.

Halcrow. (2007). Supporting Public Resource Management in Balochistan. Basin-wide Water Resources Availability and Use. Asian Development Bank: Supporting Public Resource Management in Balochistan

Hamam, I., Zhang, N., Liu, A., Johnson, M., & Dahn, J. (2020). Study of the reactions between Ni-rich positive electrode materials and aqueous solutions and their relation to the failure of Li-ion cells. Journal of The Electrochemical Society, 167(13), 130-521.

Hamza, S., Naseem, S., Bashir, E., Rizwani, G. H., & Hina, B. (2013). Trace element geochemistry of Manilkara zapota (L.) P. Royen, fruit from winder, Balochistan, Pakistan in perspective of medical geology. Pakistan journal of pharmaceutical sciences, 26(4), 805-811.

Hamza, S., Naseem, S., Nawaz-ul-Huda, S., Burke, F., & Bashir, E. (2014). Application of Multivariate Analyses Techniques (PCA and CA) for Evaluation of Trace Elements in the Selected Fruits of Winder Area. Asia Pacific Journal of Education, Arts and Sciences, 1.

Han, D., & Currell, M. J. (2022). Review of drivers and threats to coastal groundwater quality in China. Science of the Total Environment, 806, 150-913.

Hasan, M., Shang, Y., Akhter, G., & Jin, W. (2020c). Delineation of contaminated aquifers using integrated geophysical methods in Northeast Punjab, Pakistan. Environmental monitoring and assessment, 192(1), 1-15.

Hasan, M., Shang, Y., Jin, W., Shao, P., Yi, X., & Akhter, G. (2020a). Geophysical Assessment of Seawater Intrusion into Coastal Aquifers of Bela Plain, Pakistan. Water, 12(12), 3408.

Hasan, M., Shang, Y., Metwaly, M., Jin, W., Khan, M., & Gao, Q. (2020b). Assessment of groundwater resources in coastal areas of Pakistan for sustainable water quality management using joint Geophysical and Geochemical approach: A case sudy. Sustainability, 12(22), 9730.

Hasan, Z., & Tewari, D. (2020d). Characteristics of groundwater quality in the aquifer of Indo-Nepal Border of Balrampur City. INTERNATIONAL JOURNAL OF PLANT AND ENVIRONMENT, 6(02), 146-151.

Hassan, E., Rai, J. K., & Anekwe, U. O. (2017). Geoelectrical survey of ground water in some parts of Kebbi State Nigeria, a case study of Federal Polytechnic Bye-Pass Birnin Kebbi and Magoro Primary Health Center Fakai Local Government. Geosciences, 7(5), 141-149.

Hassan, W., Mostafa, M. M., Fujimaki, H., & Inoue, M. (2009). Irrigation improvement assessment from the water quality and human health perspective in the Nile Delta. Journal of Food, Agriculture & Environment, 7(3&4), 815-822.
Hatch, M., & Street, G. (2021). Environmental geophysics. Preview, 2021(211), 29-30.
He, H., Li, Y., Wang, S., Ma, Q., & Pan, Y. (2020). A high precision method for calcium determination in seawater using ion chromatography. Frontiers in Marine Science, 7, 231.
Heaney, M. B. (2017). Electrical conductivity and resistivity. In Measurement, instrumentation, and sensors handbook (pp. 26-21-26-16). CRC Press.
Hedley, R., Warburton, J., & Smewing, J. (2001). Sequence stratigraphy and tectonics in the Kirthar Foldbelt, Pakistan. Geology and climate of the Arabian Sea region, Geol Society London.
Hem, J. D. (1985). Study and interpretation of the chemical characteristics of natural water (Vol. 2254). Department of the Interior, US Geological Survey.
Henriet, J. (1976). Direct applications of the Dar Zarrouk parameters in ground water surveys. Geophysical Prospecting, 24(2), 344-353.
Hilbich, C., Marescot, L., Hauck, C., Loke, M., & Mäusbacher, R. (2009). Applicability of electrical resistivity tomography monitoring to coarse blocky and ice-rich permafrost landforms. Permafrost and Periglacial Processes, 20(3), 269-284.
Hill, R. A. (1940). Geochemical patterns in Coachella valley. Eos, Transactions American Geophysical Union, 21(1), 46-53.
Hinsch, R., Asmar, C., Nasim, M., Abbas, M. A., & Sultan, S. (2019). Linked thick-to thin-skinned inversion in the central Kirthar Fold Belt of Pakistan. Solid Earth, 10(2), 425-446.
Hinze, W. J. (1990). The role of gravity and magnetic methods in engineering and environmental studies. In Geotechnical an Environmental Geophysics: Volume I: Review and Tutorial (pp. 75-126). Society of Exploration Geophysicists.
Hoareau, C. E., Hadibarata, T., & Yılmaz, M. (2022). Occurrence of cadmium in groundwater in China: a review. Arabian Journal of Geosciences, 15(17), 1-13.
Hora, T. (2022). Addressing groundwater over-extraction in India: assessments, monitoring methods and interventions.
Hossain, M., & Patra, P. K. (2020). Contamination zoning and health risk assessment of trace elements in groundwater through geostatistical modelling. Ecotoxicology and environmental safety, 189, 110038.
Hounslow, A. W. (2018). Water quality data: analysis and interpretation. CRC press.
HSC. (1960). Hunting Survey Cooperation Reconnaissance geology of part of west Paksitan
Huerta, A. J., Callejas-Jiménez, M., Carrillo, L., & Castillo, M. (2019). Dam implications on salt-water intrusion and land use within a tropical estuarine environment of the Gulf of Mexico. Science of the Total Environment, 652, 1102-1112.
Hussain, I., Afzal, S., Ashraf, M. A., Rasheed, R., Saleem, M. H., Alatawi, A., Ameen, F., & Fahad, S. (2022). Effect of metals or trace elements on wheat growth and its remediation in contaminated soil. Journal of Plant Growth Regulation, 1-25.
Ijumulana, J., Ligate, F., Bhattacharya, P., Mtalo, F., & Zhang, C. (2020). Spatial analysis and GIS mapping of regional hotspots and potential health risk of fluoride concentrations in groundwater of northern Tanzania. Science of the Total Environment, 735, 139584.
Iqbal, M., & Shah, S. (1980). A guide to the stratigraphy of Pakistan: Geological Survey of Pakistan. Quetta, Pakistan, 53, 37.

Ishiwatari, A. (1994). Circum-Pacific Phanerozoic multiple ophiolite belts. " Circum-Pacific Ophiolites" Proceedings of the 29th International Geological Congress, Part D.,

Jalees, M. I., Farooq, M. U., Anis, M., Hussain, G., Iqbal, A., & Saleem, S. (2021). Hydrochemistry modelling: evaluation of groundwater quality deterioration due to anthropogenic activities in Lahore, Pakistan. Environment, Development and Sustainability, 23(3), 3062-3076.

Jan, A., Baez-Villanueva, O. M., & Ribbe, L. (2022). Spatio-temporal Evaluation of Gridded Precipitation and Evapotranspiration Products Over Balochistan Province in Pakistan.

Janjua, S., Hassan, I., Muhammad, S., Ahmed, S., & Afzaal, M. (2021). Water management in Pakistan's Indus Basin: challenges and opportunities. Water Policy.

Jayarajan, S. K. P., & Kuriachan, L. (2021). Exposure and health risk assessment of nitrate contamination in groundwater in Coimbatore and Tirupur districts in Tamil Nadu, South India. Environmental Science and Pollution Research, 28(8), 10248-10261.

Jhorar, R., Smit, A., & Roest, C. (2009). Assessment of alternative water management options for irrigated agriculture. Agricultural Water Management, 96(6), 975-981.

Kadam, A., Wagh, V., Jacobs, J., Patil, S., Pawar, N., Umrikar, B., Sankhua, R., & Kumar, S. (2021). Integrated approach for the evaluation of groundwater quality through hydro geochemistry and human health risk from Shivganga river basin, Pune, Maharashtra, India. Environmental Science and Pollution Research, 1-23.

Kadri, I. (1995). Petroleum Geology of Pakistan: Pakistan Petroleum Limited. Karachi, Pakistan.

Kaleem, M., Naseem, S., Bashir, E., Shahab, B., & Mansha, M. (2019). Impact of water-rocks interaction on groundwater geochemistry of southern Mor Range, Balochistan, Pakistan and its appraisal for drinking water quality. Journal of the Chemical Society of Pakistan, 41(2), 368-368.

Kammoun, S., Trabelsi, R., Re, V., & Zouari, K. (2021). Coastal aquifer salinization in semi-arid regions: the case of grombalia (Tunisia). Water, 13(2), 129.

Kang, J., Chen, L.-M., Yu, S.-Y., Zheng, W.-Q., Dai, Z.-H., Zhou, S.-H., & Ai, Q.-X. (2022). Chromite geochemistry of the Jinchuan Ni-Cu sulfide-bearing ultramafic intrusion (NW China) and its petrogenetic implications. Ore Geology Reviews, 141, 104644.

Karunanidhi, D., Aravinthasamy, P., Subramani, T., Kumar, D., & Setia, R. (2021). Investigation of health risks related with multipath entry of groundwater nitrate using Sobol sensitivity indicators in an urban-industrial sector of south India. Environmental Research, 200, 111726.

Katz, B. G., & Collins, J. J. (1998). Evaluation of chemical data from selected sites in the surface-water ambient monitoring program (SWAMP) in Florida.

Kaur, G., Kumar, R., Mittal, S., Sahoo, P. K., & Vaid, U. (2021). Ground/drinking water contaminants and cancer incidence: A case study of rural areas of South West Punjab, India. Human and ecological risk assessment: an international journal, 27(1), 205-226.

Kaur, H., Kaur, H., Kaur, H., & Srivastava, S. (2022). The beneficial roles of trace and ultratrace elements in plants. Plant Growth Regulation, 1-18.

Kaur, L., Rishi, M. S., & Siddiqui, A. U. (2020). Deterministic and probabilistic health risk assessment techniques to evaluate non-carcinogenic human health risk

(NHHR) due to fluoride and nitrate in groundwater of Panipat, Haryana, India. Environmental Pollution, 259, 113711.
Kaveh, A., Mohammadi, A., Gorum, T., Sarıkaya, M. A., Alizadeh, H., Akbaş, A., & Mirarabi, A. (2022). Main drivers of drainage pattern development in onshore Makran Accretionary Wedge, SE Iran. International Journal of Earth Sciences, 1-21.
Kazmi, A. H., & Abbasi, I. A. (2008). Stratigraphy and Historical Geology of Pakistan Department and National Centre of Excellence in Geology, University of Peshawar, Pakistan, 524p.
Kazmi, A. H., & Jan, M. Q. (1997). Geology and tectonics of Pakistan. Graphic publishers.
Kearey, P., Brooks, M., & Hill, I. (2002). An introduction to geophysical exploration (Vol. 4). John Wiley & Sons.
Kearey, P., Klepeis, K. A., & Vine, F. J. (2009). Global tectonics. John Wiley & Sons.
Keller, G., & Frischknecht, F. (1966). Electrical Methods In Geophysical Prospecting Pergamon Press Inc. In: Oxford.
Kelley, W. (1963). Use of saline irrigation water. Soil Science, 95(6), 385-391.
Khalid, S. (2019). An assessment of groundwater quality for irrigation and drinking purposes around brick kilns in three districts of Balochistan province, Pakistan, through water quality index and multivariate statistical approaches. Journal of Geochemical Exploration, 197, 14-26.
Khan, F., & Dhanani, M. R. (1998). The role of 'Reported'Cultivated Area in Green Revolution in Pakistan. Studies in Pakistan Geography, edited by Israr-ud-Din, Department of Geography, Urban and Regional Planning, University of Peshawar, Peshawar.
Khan, J. A. (1993). The climate of Pakistan. Rehbar Publishers.
Khan, M. (1998). Petrological and structural studies of the igneous rock of the Baran Lak area, Bela-Khuzdar, Districts, Balochistan University of Balochistan Quetta].
Khan, M., Gnos, E., Mahmood, K., & Khan, A. (1999). The metamorphic rocks associated with the Bela Ophiolite. Acta Mineralogica Pakistanica, 10, 37-44.
Khan, M., Kerr, A. C., & Mahmood, K. (2007a). Formation and tectonic evolution of the Cretaceous–Jurassic Muslim Bagh ophiolitic complex, Pakistan: Implications for the composite tectonic setting of ophiolites. Journal of Asian Earth Sciences, 31(2), 112-127.
Khan, M., Khan, M. J., Kakar, M. I., & Mehmud, K. (2018). Geology and tectonic detting of Nal Ophiolite, District Khuzdar, Balochistan, Pakistan. American Journal of Earth and Environmental Sciences, 1(3), 115-123.
Khan, M., Raza, H. A., & Alam, S. (1991). Petroleum geology of the Makran region: implications for hydrocarbon occurrence in cool basins. Journal of Petroleum Geology, 14(1), 5-18.
Khan, S. R., Jan, M. Q., Khan, T., & Khan, M. A. (2007b). Petrology of the dykes from the Waziristan Ophiolite, NW Pakistan. Journal of Asian Earth Sciences, 29(2-3), 369-377.
Knoll, L., Breuer, L., & Bach, M. (2019). Large scale prediction of groundwater nitrate concentrations from spatial data using machine learning. Science of the Total Environment, 668, 1317-1327.
Koefoed, O. (1979). Resistivity sounding on an earth model containing transition layers with linear change of resistivity with depth. Geophysical Prospecting, 27(4), 862-868.

Koefoed, O., & Principles, G. (1979). Resistivity soundings measurements. Geosounding principles, 1.
Kokinou, E., & Sarris, A. (2011). Detection of the near surface structure through a multidisciplinary geophysical approach. Open Geosciences, 3(4), 349-357.
Korres, N. E., Varanasi, V. K., Slaton, N. A., Price, A. J., & Bararpour, T. (2019). Effects of salinity on rice and rice weeds: short-and long-term adaptation strategies and weed management. In Advances in Rice Research for Abiotic Stress Tolerance (pp. 159-176). Elsevier.
Kouadra, R., & Demdoum, A. (2020). Hydrogeochemical characteristics of groundwater and quality assessment for the purposes of drinking and irrigation in Bougaa area, Northeastern Algeria. Acta Geochimica, 39(5), 642-654.
Kozheshkurt, V., Ivanov, I., Antonenko, Y., Katrich, V., Bozhkov, A., & Gromovoy, T. (2021). Devising an express method for estimating the quality of colostrum and its components based on electrical conductivity. Eastern-European Journal of Enterprise Technologies, 1(11), 109.
Kubier, A., Wilkin, R. T., & Pichler, T. (2019). Cadmium in soils and groundwater: a review. Applied Geochemistry, 108, 104388.
Kumar, P., Mahajan, A. K., & Kumar, A. (2020). Groundwater geochemical facie: implications of rock-water interaction at the Chamba city (HP), northwest Himalaya, India. Environmental Science and Pollution Research, 27(9), 9012-9026.
Kumar, P., Yuan, X., Kumar, M. R., Kind, R., Li, X., & Chadha, R. (2007). The rapid drift of the Indian tectonic plate. Nature, 449(7164), 894-897.
Kumar, R., & Mathur, S. (2022). Natural Reserves of Water on Earth. In Handbook of Research on Water Sciences and Society (pp. 699-721). IGI Global.
Kumari, M., & Rai, S. (2020). Hydrogeochemical evaluation of groundwater quality for drinking and irrigation purposes using water quality index in semi arid region of India. Journal of the Geological Society of India, 95(2), 159-168.
Kurtz, D. B., Schellberg, J., & Braun, M. (2010). Ground and satellite based assessment of rangeland management in sub-tropical Argentina. Applied Geography, 30(2), 210-220.
Kurunc, A., Aslan, G. E., Karaca, C., Tezcan, A., Turgut, K., Karhan, M., & Kaplan, B. (2020). Effects of salt source and irrigation water salinity on growth, yield and quality parameters of Stevia rebaudiana Bertoni. Scientia Horticulturae, 270, 109458.
Kushawaha, J., & Aithani, D. (2021). Geogenic Pollutants in Groundwater and Their Removal Techniques. Groundwater Geochemistry: Pollution and Remediation Methods, 1-21.
Langridge, P. (2022). Micronutrient Toxicity and Deficiency. In Wheat Improvement (pp. 433-449). Springer.
Lanjwani, M. F., Khuhawar, M. Y., Khuhawar, T. M. J., Samtio, M. S., & Memon, S. Q. (2021). Spatial variability and hydrogeochemical characterisation of groundwaters in Larkana of Sindh, Pakistan. Groundwater for Sustainable Development, 14, 100632.
Lawrence, R., Yeats, R., Khan, S., Farah, A., & DeJong, K. (1981). Thrust and strike slip fault interaction along the Chaman transform zone, Pakistan. Geological Society, London, Special Publications, 9(1), 363-370.
Le, T. T. V., Lertsirivorakul, R., Bui, T. V., & Schulmeister, M. K. (2020). An Application of HFE-D for Evaluating Sea Water Intrusion in Coastal Aquifers of Southern Vietnam. Groundwater, 58(6), 1012-1022.

Lech, M., Skutnik, Z., Bajda, M., & Markowska-Lech, K. (2020). Applications of electrical resistivity surveys in solving selected geotechnical and environmental problems. Applied Sciences, 10(7), 2263.

Lee, J. Y., & Song, S. H. (2007). Evaluation of groundwater quality in coastal areas: implications for sustainable agriculture. Environmental Geology, 52(7), 1231-1242.

Lekshmi, S., & Kani, M. K. (2017). Assessment of seawater intrusion using chemical indicators. Int. J. Eng. Adv. Technol, 7, 100-108.

Li, D., Zhai, Y., Lei, Y., Li, J., Teng, Y., Lu, H., Xia, X., Yue, W., & Yang, J. (2021). Spatiotemporal evolution of groundwater nitrate nitrogen levels and potential human health risks in the Songnen Plain, Northeast China. Ecotoxicology and environmental safety, 208, 111524.

Li, X., Peterson, J., Liu, G.-J., & Qian, L. (2001). Assessing regional sustainability: the case of land use and land cover change in the middle Yiluo catchment of the Yellow River basin, China. Applied Geography, 21(1), 87-106.

Lino, Y., Pranjal, K., Priyansh, S., Jagath, C., Udayashankar, H. N., Babu, D. S., & Balakrishna, K. (2023). Submarine Groundwater Discharge (SGD): Impacts, challenges, limitations, and management recommendations. Groundwater for Sustainable Development, 100903.

Loke, M. H., Rucker, D., Chambers, J., Wilkinson, P., & Kuras, O. (2020). Electrical resistivity surveys and data interpretation. In Encyclopedia of solid earth geophysics (pp. 1-6). Springer.

Lowry, T., & Shive, P. N. (1990). An evaluation of Bristow's method for the detection of subsurface cavities. Geophysics, 55(5), 514-520.

Lu, J., Wu, J., Zhang, C., & Zhang, Y. (2020). Possible effect of submarine groundwater discharge on the pollution of coastal water: Occurrence, source, and risks of endocrine disrupting chemicals in coastal groundwater and adjacent seawater influenced by reclaimed water irrigation. Chemosphere, 250, 126323.

Ma, C., Li, Y., Li, X., & Gao, L. (2020). Evaluation of groundwater sustainable development considering seawater intrusion in Beihai City, China. Environmental Science and Pollution Research, 27(5), 4927-4943.

Maghraby, E. M., & Bamousa, A. O. (2021). Evaluation of groundwater quality for drinking and irrigation purposes using physicochemical parameters at Salilah area, Madinah Munawarah District, Saudi Arabia. Journal of Taibah University for Science, 15(1), 695-709.

Magna, E. K., Koranteng, S. S., Donkor, A., & Gordon, C. (2021). Health Risk Assessment and Levels of Heavy Metals in Farmed Nile Tilapia (Oreochromis niloticus) from the Volta Basin of Ghana. Journal of Chemistry, 2021.

Mahar, G. A., Ahmed, R., & Iqbal, M. J. (2013). Temporal change assessment of agricultural land by Satellite Remote Sensing (SRS) technique.

Mahboob, S. S., Liu, G., Yang, Q., Casazza, M., Agostinho, F., & Giannetti, B. F. (2021). Sustainability assessment of agriculture production systems in Pakistan: A provincial-scale energy-based evaluation. Ecological Modelling, 455, 109654.

Mahlet, G. (2022). Quality assesment of tap water on sub cities of arada and Gulele

Mahmood, K., Boudier, F., Gnos, E., Monié, P., & Nicolas, A. (1995). 40Ar/39Ar dating of the emplacement of the Muslim Bagh ophiolite, Pakistan. Tectonophysics, 250(1-3), 169-181.

Mahoney, J. J. (1988). Deccan traps. In Continental flood basalts (pp. 151-194). Springer.

Maillet, R. (1947). The fundamental equations of electrical prospecting. Geophysics, 12(4), 529-556.
Makhfuza, I. (2022). Soil Ecology and Functions Barqarorlik vayetakchi yadqiqotlaronlayn Ilmiy Jurnali 2(9), 177-181.
Mallick, J., Kumar, A., Almesfer, M. K., Alsubih, M., Singh, C. K., Ahmed, M., & Khan, R. A. (2021). An index-based approach to assess groundwater quality for drinking and irrigation in Asir region of Saudi Arabia. Arabian Journal of Geosciences, 14(3), 1-17.
Manisalidis, I., Stavropoulou, E., Stavropoulos, A., & Bezirtzoglou, E. (2020). Environmental and health impacts of air pollution: a review. Frontiers in public health, 8, 14.
Marklein, A., Elias, E., Nico, P., & Steenwerth, K. (2020). Projected temperature increases may require shifts in the growing season of cool-season crops and the growing locations of warm-season crops. Science of the Total Environment, 746, 140918.
Martínez, T. J. A., Mora, A., Mahlknecht, J., Daesslé, L. W., Cervantes-Avilés, P. A., & Ledesma-Ruiz, R. (2021). Estimation of nitrate pollution sources and transformations in groundwater of an intensive livestock-agricultural area (Comarca Lagunera), combining major ions, stable isotopes and MixSIAR model. Environmental Pollution, 269, 115445.
Maurizot, P., Sevin, B., Lesimple, S., Bailly, L., Iseppi, M., & Robineau, B. (2020). Mineral resources and prospectivity of the ultramafic rocks of New Caledonia. Geological Society, London, Memoirs, 51(1), 247-277.
Mebarki, S., Kharroubi, B., & Kendouci, M. A. (2021). Physicochemical evolution and evaluation of groundwater quality in Mougheul area (Southwest of Algeria). Applied Water Science, 11(2), 1-14.
Megaw, P. K., Barton, M. D., & Falce, J. I. (1996). Carbonate-hosted lead-zinc (Ag, Cu, Au) deposits of northern Chihuahua, Mexico.
Mehri, A. (2020). Trace elements in human nutrition (II)–an update. International journal of preventive medicine, 11.
Merino, L. M., Aguilera, H., González-Jiménez, M., & Díaz-Losada, E. (2021). D-Piper, a modified piper diagram to represent big sets of hydrochemical analyses. Environmental Modelling & Software, 138, 104979.
Metwaly, M., El-Qady, G., Massoud, U., El-Kenawy, A., Matsushima, J., & Al-Arifi, N. (2010). Integrated geoelectrical survey for groundwater and shallow subsurface evaluation: case study at Siliyin spring, El-Fayoum, Egypt. International Journal of Earth Sciences, 99(6), 1427-1436.
Mikhailova, E. A., Zurqani, H. A., Post, C. J., Schlautman, M. A., & Post, G. C. (2021). Soil diversity (pedodiversity) and ecosystem services. Land, 10(3), 288.
Miller, T. S. (2000). Simulation of ground-water flow in an unconfined sand and gravel aquifer at Marathon, Cortland County, New York. US Department of the Interior, US Geological Survey.
Minhas, P. S., Qadir, M., & Yadav, R. K. (2019). Groundwater irrigation induced soil sodification and response options. Agricultural Water Management, 215, 74-85.
Mitchell, A. H. G., & Garson, M. S. (1981). Mineral deposits and global tectonic settings. Academic Press.
Modi, A., Khatri, N., Tyagi, S., & Jha, A. (2021). Analysis of Contaminants in Sewage and Groundwater: Future Impact on Human and Animal Health. Environmental Claims Journal, 1-14.

Mohammad, A. D., & Rind, R. F. (2020). An application of WQI and correlation matrix to evaluate groundwater quality around Brick Kilns of Loralai District Balochistan. Journal of Asian Scientific Research, 10(2), 88-95.

Mohanavelu, A., Naganna, S. R., & Al-Ansari, N. (2021). Irrigation induced salinity and sodicity hazards on soil and groundwater: An overview of its causes, impacts and mitigation strategies. Agriculture, 11(10), 983.

Mokoena, P., Kanyerere, T., & van Bever Donker, J. (2020). Hydrogeochemical characteristics and evaluation of groundwater quality for domestic and irrigation purposes: a case study of the Heuningnes Catchment, Western Cape Province, South Africa. SN Applied Sciences, 2(9), 1-12.

Moore, J., & Walsh, J. (2021). Quantitative analysis of Cenozoic faults and fractures and their impact on groundwater flow in the bedrock aquifers of Ireland. Hydrogeology Journal, 1-20.

Moores, E. (1982). Origin and emplacement of ophiolites. Reviews of Geophysics, 20(4), 735-760.

Mukherjee, I., & Singh, U. K. (2022). Hydrogeochemical characterizations and quality evaluation of groundwater in the major river basins of a geologically and anthropogenically driven semi-arid tract of India. Science of the Total Environment, 805, 150323.

Müller, R. D., Cannon, J., Qin, X., Watson, R. J., Gurnis, M., Williams, S., Pfaffelmoser, T., Seton, M., Russell, S. H., & Zahirovic, S. (2018). GPlates: building a virtual Earth through deep time. Geochemistry, Geophysics, Geosystems, 19(7), 2243-2261.

Munir, M. U., Ahmad, A., Hopmans, J. W., Belgacem, A. O., & Baig, M. B. (2021). Water scarcity threats to National Food Security of Pakistan—Issues, implications, and way forward. In Emerging Challenges to Food Production and Security in Asia, Middle East, and Africa (pp. 241-266). Springer.

Murtaza, G., Rehman, M., Qadir, M., Shehzad, M., Zeeshan, N., Ahmad, H., Farooqi, Z., & Naidu, R. (2021). High residual sodium carbonate water in the Indian subcontinent: concerns, challenges and remediation. International Journal of Environmental Science and Technology, 1-16.

Mushtaq, S., Reardon-Smith, K., Stone, R., & Khair, S. M. (2013). A blueprint for sustainable groundwater management in Balochistan, Pakistan.

Nadiri, A. A., Moghaddam, A. A., Tsai, F. T., & Fijani, E. (2013). Hydrogeochemical analysis for Tasuj plain aquifer, Iran. Journal of earth system science, 122(4), 1091-1105.

Naseem, S., Hamza, S., & Bashir, E. (2010). Groundwater geochemistry of Winder agricultural farms, Balochistan, Pakistan and assessment for irrigation water quality. European water, 31, 21-32.

Naseem, S., Hamza, S., & Bashir, E. (2012). Assessment of geochemistry of soils for agriculture at Winder, Balochistan, Pakistan. Water quality, soil and managing irrigation of crops, InTech-Open Access Publisher, Croatia, 73-94.

Naseem, S., Hamza, S., Bashir, E., & Ahmed, S. (2005b). Distribution of Mn in the fruits and wild flora of Winder area, Balochistan, Pakistan and its impact on Human Health. Editorial Advisory Board e, 18(4), 689-699.

Naseem, S., Hamza, S., Bashir, E., Pirzada, T., & Talpur, M. M. A. (2013). Trace element geochemistry of groundwater of Winder, Balochistan, Pakistan and its appraisal for irrigation water quality. British Journal of Applied Science & Technology, 3(1), 182.

Naseem, S., Hamza, S., Nawaz-ul-Huda, S., & Bashir, E. (2014). Geochemistry of Cd in groundwater of Winder, Balochistan and suspected health problems. Environmental Earth Sciences, 71(4), 1683-1690.

Naseem, S., Naseem, S., & Sheikh, S. A. (2005c). Geochemical Evaluation of Depositional Environment of Parh Limestone, Southern Pab Range, Balochistan, Pakistan. SPE/PAPG Annual Technical Conference,

Naseem, S., & Sheikh, S. A. (2002). Biogeochemical prospecting of sulphide minerals in Winder Valley, Balochistan, Pakistan. Resource Geology, 52(1), 59-66.

Naseem, S., Sheikh, S. A., Qadeeruddin, M., & Shirin, K. (2002a). Geochemical stream sediment survey in Winder Valley, Balochistan, Pakistan. Journal of Geochemical Exploration, 76(1), 1-12.

Newell, D. B., & Tiesinga, E. (2019). The international system of units (SI). NIST Special Publication, 330, 1-138.

Niamatullah, M. (1997). Geometry and tectonic of the Ornach–Nal Fault, A southern extension of the Chaman Transform zone, Pakistan. Acta Mineralogica Pakistanica, 8, 1-8.

Niamatullah, M. (1998). Anomalous orientation of the Khude Range Fold Belt and enigma of Khuzdar Syntaxis in Southern Kirthar Fold Belt, Pakistan. Acta Mineralogica Pakistanica, 9, 73-84.

Niaz, A., Bibi, T., Qureshi, J. A., Rahim, S., Hameed, F., & Shedayi, A. A. (2021). A Comparison Between Schlumberger and Wenner Configurations in Delineating Subsurface Water Bearing Zones: A Case Study of Rawalakot Azad Jammu and Kashmir, Pakistan. International Journal of Economic and Environmental Geology, 12(3), 25-31.

Nicolas, A. (2012). Structures of ophiolites and dynamics of oceanic lithosphere (Vol. 4). Springer Science & Business Media.

Noble, A., Tuit, C., Maney, J., & Wait, A. (2020). A review of marine water sampling methods for trace metals. Environmental Forensics, 21(3-4), 267-290.

Noetling, F. (1903). übergang zwischen Kreide und Eocaen in Baluchistan. Zentbl. Miner. Geol. Paläont., 1903, 514-523.

Noori, A. R., & Singh, S. (2021). Status of groundwater resource potential and its quality at Kabul, Afghanistan: a review. Environmental Earth Sciences, 80, 1-13.

Ntarlagiannis, D., Robinson, J., Soupios, P., & Slater, L. (2016). Field-scale electrical geophysics over an olive oil mill waste deposition site: evaluating the information content of resistivity versus induced polarization (IP) images for delineating the spatial extent of organic contamination. Journal of Applied Geophysics, 135, 418-426.

Nugraha, G. U., Nur, A. A., Pranantya, P. A., Lubis, R. F., & Bakti, H. (2022). Analysis of groundwater potential zones using Dar-Zarrouk parameters in Pangkalpinang city, Indonesia. Environment, Development and Sustainability, 1-23.

Nyamangyoku, I. O., & Bertin, P. (2013). Mechanisms of resistance to ferrous iron toxicity in cutivated rices: Oryza sativa L., Oryza glaberrima Steud. and interspecific hybrids. Int. J. Agron. Plant Prod, 4, 2570-2591.

Okpoli, C. C. (2013). Sensitivity and resolution capacity of electrode configurations. International Journal of Geophysics, 2013.

Olasehinde, P., & Bayewu, O. (2011). Evaluation of electrical resistivity anisotropy in geological mapping: A case study of Odo Ara, West Central Nigeria. African Journal of Environmental Science and Technology, 5(7), 553-566.

Olayinka, A. (1992). Geophysical siting of boreholes in crystalline basement areas of Africa. Journal of African Earth Sciences (and the Middle East), 14(2), 197-207.

Oldenburg, D. W., Kang, S., Heagy, L. J., & Maxwell, M. (2022). Direct current resistivity methods. In Engineering Geophysics (pp. 67-75). CRC Press.

Oliver, H., & Raj, S. (2012). Estimation of conductance anomalies in subsurface through Dar-Zarrouk parameters by resistivity inversion method. International Journal of Physical and Mathematical Sciences, 3(1).

Osiakwan, G. M., Appiah-Adjei, E. K., Kabo-Bah, A. T., Gibrilla, A., & Anornu, G. (2021). Assessment of groundwater quality and the controlling factors in coastal aquifers of Ghana: An integrated statistical, geostatistical and hydrogeochemical approach. Journal of African Earth Sciences, 184, 104371.

Oster, J. L., Covey, A. K., Lawrence, C. R., Giannetta, M. G., & Druhan, J. L. (2021). A reactive transport approach to modeling cave seepage water chemistry II: Elemental signatures. Geochimica et Cosmochimica Acta, 311, 353-373.

Ouhamdouch, S., Bahir, M., & Ouazar, D. (2021). Seawater intrusion into coastal aquifers from semi-arid environments, Case of the alluvial aquifer of Essaouira basin (Morocco). Carbonates and Evaporites, 36(1), 1-12.

Ouzerbane, Z., Essahlaoui, A., El Hmaidi, A., Najine, A., & El Ouali, A. (2022). Contribution to the study of water resources in the coastal region of Essaouira, using vertical electrical soundings (VES), electrical resistivity tomography (ERT) and GIS (Essaouira, Morocco).

Pakistan. (2012). Connecting Agriculture for Better Farming. In: Pakistan agriculture overview.

Pakistan, W. (2007). National surface water classification criteria and irrigation water quality guidelines for Pakistan. Proposed by WWF Pakistan through consultation with stakeholders, 1-9.

Palacky, G. (1987). Resistivity characteristics of geologic targets. Electromagnetic Methods Appl. Geophysics, 1, 1351pp.

Parasnis, D. S. (2012). Principles of applied geophysics. Springer Science & Business Media.

Parker, T. K., Jansen, J., Behroozmand, A. A., Halkjaer, M., & Thorn, P. (2022). Applied Geophysics for Managed Aquifer Recharge. Groundwater, 60(5), 606-618.

Parkhomenko, E. I. (2012). Electrical properties of rocks. Springer Science & Business Media.

Patil, S. (2023). Hydro-geo Chemical Analysis of Groundwater and Surface Water Near Bhima River Basin Jewargi Taluka Kalburgi, Karnataka. In Recent Trends in Construction Technology and Management (pp. 361-372). Springer.

Patil, S. N., & Prasad, S. R. (2020). An Impact of Nationwide Lockdown on Physico-chemical Parameters of Bhogavati River Water. ES Energy & Environment, 11, 28-39.

Patriat, P., & Achache, J. (1984). India–Eurasia collision chronology has implications for crustal shortening and driving mechanism of plates. Nature, 311(5987), 615-621.

Patterson, R. A. (1994). On-site treatment and disposal of septic tank effluent. University of New England.

Peters, T. (2000). Formation and evolution of the western Indian Ocean as evidence by the Masirah Ophiolite: A review.

Piper, A. M. (1944). A graphic procedure in the geochemical interpretation of water-analyses. Eos, Transactions American Geophysical Union, 25(6), 914-928.

Pivic, R., Maksimovic, J., Dinic, Z., Jaramaz, D., Majstorovic, H., Vidojevic, D., & Stanojkovic-Sebic, A. (2022). Hydrochemical Assessment of Water Used for Agricultural Soil Irrigation in the Water Area of the Three Morava Rivers in the Republic of Serbia. Agronomy, 12(5), 1177.

Pointet, T. (2022). The United Nations World Water Development Report 2022 on groundwater, a synthesis. LHB, 108(1), 2090867.

Power, C., Gerhard, J., Tsourlos, P., Soupios, P., Simyrdanis, K., & Karaoulis, M. (2014). Improved Time-lapse ERT Monitoring of Dense Non-aqueous phase Liquids (DNPLs) with Surface-to-horizontal Borehole Arrays. Near Surface Geoscience 2014-20th European Meeting of Environmental and Engineering Geophysics,

Priestley, K., Sobouti, F., Mokhtarzadeh, R., A Irandoust, M., Ghods, R., Motaghi, K., & Ho, T. (2022). New Constraints for the On-Shore Makran Subduction Zone Crustal Structure. Journal of Geophysical Research: Solid Earth, 127(1), e2021JB022942.

Princela, M. A., Jose, J. M. A., Gladis, E. E., Arthi, D., & Joseph, J. (2021). Regional assessment of groundwater quality for drinking purpose. Materials Today: Proceedings, 45, 2916-2920.

Prusty, S., Sahoo, R. K., Nayak, S., Poosapati, S., & Swain, D. M. (2022). Proteomic and Genomic Studies of micronutrient deficiency and toxicity in Ppants. Plants, 11(18), 2424.

Qasim, J. M., Asif Khan, M., & Sufyan Qazi, M. (1993). The Sapat mafic-ultramafic complex, Kohistan arc, North Pakistan.

Qasim, M., Ahmad, J., Ding, L., Tanoli, J. I., Sattar, M., Rehman, Q. U., Awais, M., Umar, M., Baral, U., & Khan, H. (2021). Integrated provenance and tectonic implications of the Cretaceous–Palaeocene clastic sequence, Changla Gali, Lesser Himalaya, Pakistan. Geological Journal, 56(9), 4747-4759.

Qureshi, A. S. (2015). Improving food security and livelihood resilience through groundwater management in Pakistan. Global Advanced Research Journal of Agricultural Science, 4(10), 687-710.

Qureshi, M., Tariq, M., & Abid, Q. (1993). Geological Survey of Pakistan. Geological Map of Pakistan.

Raghunath, H. M. (1987). Ground water: hydrogeology, ground water survey and pumping tests, rural water supply and irrigation systems. New Age International.

Rahaman, M. A., Rahman, M. M., & Nazimuzzaman, M. (2020). Impact of salinity on infectious disease outbreaks: Experiences from the global coastal region. Good Health and Well-Being, 415-424.

Rahman, I. U., Yian, C., Hussain, S., Ali, A., Qasim, M., Khan, I., & Khan, M. (2022). Geophysical Prospecting of Aquifer Hydrogeological Properties: Implications for Groundwater Resource Management in Parts of Indus Plain, Pakistan.

Raihan, F., & Alam, J. (2008). Assessment of groundwater quality in Sunamganj of Bangladesh.

Rajendra , P. D., Sadashivaiah, C., & Rangnna, G. (2009). Hydrochemical characteristics and evaluation of groundwater quality of Tumkur Amanikere Lake Watershed, Karnataka, India. E-Journal of Chemistry, 6(S1), S211-S218.

Raji, W., & Abdulkadir, K. (2020). Evaluation of groundwater potential of bedrock aquifers in Geological Sheet 223 Ilorin, Nigeria, using geo-electric sounding. Applied Water Science, 10(10), 1-12.

Rakib, M., Sasaki, J., Matsuda, H., Quraishi, S. B., Mahmud, M. J., Bodrud-Doza, M., Ullah, A. A., Fatema, K. J., Newaz, M. A., & Bhuiyan, M. A. (2020). Groundwater salinization and associated co-contamination risk increase severe drinking water vulnerabilities in the southwestern coast of Bangladesh. Chemosphere, 246, 125646.

Rao, A. S., Reddy, K. S., & Takkar, P. (1997). Malachite green method compared to ascorbic acid for estimating small amounts of phosphorus in water, 0.01 M calcium chloride, and Olsen soil extracts. Communications in Soil Science and Plant Analysis, 28(6-8), 589-601.

Rasool, A., Xiao, T., Farooqi, A., Shafeeque, M., Liu, Y., Kamran, M. A., Katsoyiannis, I. A., & Eqani, S. A. M. A. S. (2017). Quality of tube well water intended for irrigation and human consumption with special emphasis on arsenic contamination at the area of Punjab, Pakistan. Environmental geochemistry and health, 39(4), 847-863.

Rawy, A. M., Ismail, E., & Abdalla, O. (2019). Assessment of groundwater quality using GIS, hydrogeochemistry, and factor statistical analysis in Qena Governorate, Egypt. Desalination and Water Treatment, 162, 14-29.

Redwan, M., Moneim, A. A. A., & Amra, M. A. (2016). Effect of water–rock interaction processes on the hydrogeochemistry of groundwater west of Sohag area, Egypt. Arabian Journal of Geosciences, 9(2), 111.

Reissland, M. U. (1989). Electrical measurements: fundamentals, concepts, applications. bohem press.

Reynolds, J. M. (2011). An introduction to applied and environmental geophysics. John Wiley & Sons.

Rezaei, H., Jafari, A., Kamarehie, B., Fakhri, Y., Ghaderpoury, A., Karami, M. A., Ghaderpoori, M., Shams, M., Bidarpoor, F., & Salimi, M. (2019). Health-risk assessment related to the fluoride, nitrate, and nitrite in the drinking water in the Sanandaj, Kurdistan County, Iran. Human and ecological risk assessment: an international journal, 25(5), 1242-1250.

Rice, E. W., Baird, R. B., Eaton, A. D., & Clesceri, L. S. (2017). Standard methods for the examination of water and wastewater; American public health association (APHA), American water works association (AWWA) and water environment federation (WEF). Federation.

Richards, L. A. (1954). Diagnosis and improvement of saline and alkali soils (Vol. 78). LWW.

Rizvi, Y., Faridudin, M., & Seema, N. (1992). Preliminary petrology and micropaleontological studies of Cretaceous carbonate rocks in Ghoranji section Duddar quadrangle, Lasbela. GSP IR, 514.

Roshni, T., Choudhary, S., Jha, M. K., Ghorbani, M. A., & Wable, P. S. (2022). Management of groundwater drought risk by reliability theory and copula model in Sina basin, India. Sustainable Water Resources Management, 8(1), 1-17.

Roy, B., Pramanik, M., & Manna, A. K. (2023). Hydrogeochemistry and quality evaluation of groundwater and its impact on human health in North Tripura, India. Environmental monitoring and assessment, 195(1), 1-29.

Russoniello, C. J., & Lautz, L. K. (2020). Pay the PIED Piper: Guidelines to Visualize Large Geochemical Datasets on Piper Diagrams. Groundwater, 58(3), 464-469.

Sabale, R., Venkatesh, B., & Jose, M. (2023). Sustainable water resource management through conjunctive use of groundwater and surface water: a review. Innovative Infrastructure Solutions, 8(1), 1-12.

Sadeghfam, S., Bagheri, A., Razzagh, S., Nadiri, A. A., Vadiati, M., Senapathi, V., & Sekar, S. (2022). Hydrochemical analysis of seawater intrusion by graphical techniques in coastal aquifers to delineate vulnerable areas. In Groundwater Contamination in Coastal Aquifers (pp. 91-104). Elsevier.

Sadeqi, D. (2023). An integrated approach to address the temporal variation of geochemistry in groundwater of an arid region. Environmental monitoring and assessment, 195(1), 1-22.

Safdar, H., Amin, A., Shafiq, Y., Ali, A., Yasin, R., Shoukat, A., Hussan, M. U., & Sarwar, M. I. (2019). A review: Impact of salinity on plant growth. Nat. Sci, 17(1), 34-40.

Saha, N., & Rahman, M. S. (2020). Groundwater hydrogeochemistry and probabilistic health risk assessment through exposure to arsenic-contaminated groundwater of Meghna floodplain, central-east Bangladesh. Ecotoxicology and environmental safety, 206, 111349.

Saleh, H., & Samsudin, A. R. (2013). Application of vertical electrical sounding (VES) in subsurface geological investigation for potential aquifer in Lahad Datu, Sabah. AIP Conference Proceedings,

Salman, A. M., Abed, A. M., & Thabit, J. M. (2020). Comparison between Dipole-dipole and Pole-dipole arrays in delineation of subsurface weak zones using 2d electrical imaging technique in Al-Anbar University, Western Iraq. Iraqi Journal of Science, 567-576.

Samouelian, A., Cousin, I., Tabbagh, A., Bruand, A., & Richard, G. (2005). Electrical resistivity survey in soil science: a review. Soil and Tillage research, 83(2), 173-193.

Sarris, A., Papadopoulos, N., Agapiou, A., Salvi, M. C., Hadjimitsis, D. G., Parkinson, W. A., Yerkes, R. W., Gyucha, A., & Duffy, P. R. (2013). Integration of geophysical surveys, ground hyperspectral measurements, aerial and satellite imagery for archaeological prospection of prehistoric sites: the case study of Vésztő-Mágor Tell, Hungary. Journal of Archaeological Science, 40(3), 1454-1470.

Sarwar, G. (1981). Geology of the Bela ophiolites in the Wayaro area, Las Bela District, south central Pakistan. University of Cincinnati.

Sarwar, G. (1982). Bela Ophiolites, South Central Pakistan-a Cretaceous plate boundary transform complex. Geol. Sot. Am., Abstr. with Progams, 14(7), 608.

Sarwar, G. (1992). Tectonic setting of the Bela Ophiolites, southern Pakistan. Tectonophysics, 207(3-4), 359-381.

Sarwar, G. (2004). Earthquakes and the neo-tectonic framework of the Kutch-Hyderabad-Karachi triple junction area, Indo-Pakistan. Pakistan Journal of Hydrocarbon Research, 14, 35-40.

Sarwar, G., & DeJong, K. (1979). Arcs, oroclines, syntaxes: The curvatures of mountain belts in Pakistan, Geodynamics of Pakistan A. Farah, K. DeJong, 341-349.

Sarwar, G., & DeJong, K. A. (1984). Composition and origin of the Kanar Melange, southern Pakistan. Melanges: Their Nature, Origin, and Significance: Geological Society of America Special Paper, 198, 127-137.

Sataa, A.-B., Albakeri, S., & Salih, M. M. (2016). Evaluation The Quality of Wells Water in Greenbelt Area North of AL-Najaf Al Ashraf City. Eng. Technol. J, 34(14 Part).
Sayal, E. A. (2015). Water Management Issues of Pakistan. In: Doctoral), University of the Punjab, Lahore, Pakistan.
Schoeller, H. (1977). Geochemistry of groundwater. Groundwater studies, an international guide for research and practice, UNESCO, Paris, 1-18.
Schwartz, F. W., Liu, G., & Yu, Z. (2020). HESS Opinions: The myth of groundwater sustainability in Asia. Hydrology and Earth System Sciences, 24(1), 489-500.
Seladji, S., Cosenza, P., Tabbagh, A., Ranger, J., & Richard, G. (2010). The effect of compaction on soil electrical resistivity: a laboratory investigation. European journal of soil science, 61(6), 1043-1055.
Seton, M., Müller, R. D., Zahirovic, S., Gaina, C., Torsvik, T., Shephard, G., Talsma, A., Gurnis, M., Turner, M., & Maus, S. (2012). Global continental and ocean basin reconstructions since 200 Ma. Earth-Science Reviews, 113(3-4), 212-270.
Shabbir, R., Singhal, R. K., Mishra, U. N., Chauhan, J., Javed, T., Hussain, S., Kumar, S., Anuragi, H., Lal, D., & Chen, P. (2022). Combined abiotic stresses: challenges and potential for crop improvement. Agronomy, 12(11), 2795.
Shah, S. (2002). Lithostratigraphic units of the Sulaiman and Kirthar Provinces, lower Indus basin, Pakistan. GSP, Rec, 107.
Shah, S. (2009). Stratigraphy of Pakistan (memoirs of the geological survey of Pakistan). The Geological Survey of Pakistan, 22.
Shah, S. I. (1977). Stratigraphy of Pakistan.
Shah, S. T., Özacar, A. A., & Gülerce, Z. (2021). Fault-based probabilistic seismic hazard assessment of the eastern Makran subduction and the Chaman transform fault, Pakistan: Emphasis on the source characterization of megathrust. Journal of Asian Earth Sciences, 205, 104604.
Shahid, M., Niazi, N. K., Rinklebe, J., Bundschuh, J., Dumat, C., & Pinelli, E. (2020). Trace elements-induced phytohormesis: A critical review and mechanistic interpretation. Critical Reviews in Environmental Science and Technology, 50(19), 1984-2015.
Shammi, M., Rahman, M., Bondad, S. E., & Bodrud-Doza, M. (2019). Impacts of salinity intrusion in community health: a review of experiences on drinking water sodium from coastal areas of Bangladesh. Healthcare,
Shariah, M. I. A., & Shariah, S. K. (2019). Application of Electrical Resistivity Tomography Synthetic Modeling. Electronic Journal of Geotechnical Engineering, 24.
Sharma, P. V. (1997). Environmental and engineering geophysics. Cambridge university press.
Shervais, J. W. (2001). Birth, death, and resurrection: The life cycle of suprasubduction zone ophiolites. Geochemistry, Geophysics, Geosystems, 2(1).
Shervais, J. W., Kimbrough, D. L., Renne, P., Hanan, B. B., Murchey, B., Snow, C. A., Zoglman Schuman, M. M., & Beaman, J. (2004). Multi-stage origin of the Coast Range ophiolite, California: implications for the life cycle of supra-subduction zone ophiolites. International Geology Review, 46(4), 289-315.
Sheth, H. C. (2008). Do major oxide tectonic discrimination diagrams work? Evaluating new log-ratio and discriminant-analysis-based diagrams with Indian Ocean mafic volcanics and Asian ophiolites. Terra Nova, 20(3), 229-236.

Shrestha, A. K., & Basnet, N. (2018). The correlation and regression analysis of physicochemical parameters of river water for the evaluation of percentage contribution to electrical conductivity. Journal of Chemistry, 2018.

Shunmugam, K. (2022). Hydrogeochemistry and ionic ratios for identification of salinity sources in parts of Coromandel Coast of Pondicherry, South India. In Groundwater Contamination in Coastal Aquifers (pp. 245-260). Elsevier.

Shyam, R., Krishan, G., Kheraj, & Kumar, A. (2022). Evaluation of groundwater quality for life-supporting activities: a case study of Haryana, India. International Journal of River Basin Management, 1-12.

Siddiqui, H., Singh, P., Arif, Y., Sami, F., Naaz, R., & Hayat, S. (2022). Role of micronutrients in providing abiotic stress tolerance. In Microbial biofertilizers and micronutrient availability (pp. 115-136). Springer.

Sikandar, P., Bakhsh, A., Arshad, M., & Rana, T. (2010). The use of vertical electrical sounding resistivity method for the location of low salinity groundwater for irrigation in Chaj and Rachna Doabs. Environmental Earth Sciences, 60(5), 1113-1129.

Sinduja, M., Sathya, V., Maheswari, M., Dhevagi, P., Kalpana, P., Dinesh, G., & Prasad, S. (2022). Evaluation and speciation of heavy metals in the soil of the Sub Urban Region of Southern India. Soil and Sediment Contamination: An International Journal, 1-20.

Singh, P., Raj, A., & Yadav, B. (2022). Impacts of agriculture-based contaminants on groundwater quality. In Sustainability of Water Resources: Impacts and Management (pp. 249-261). Springer.

Singh, S., Gautam, P. K., Kumar, P., Biswas, A., & Sarkar, T. (2021). Delineating the characteristics of saline water intrusion in the coastal aquifers of Tamil Nadu, India by analysing the Dar-Zarrouk parameters. Contributions to Geophysics and Geodesy, 51(2), 141-163.

Singh, U., Das, R., & Hodlur, G. (2004). Significance of Dar-Zarrouk parameters in the exploration of quality affected coastal aquifer systems. Environmental Geology, 45(5), 696-702.

Slater, L. (2007). Near surface electrical characterization of hydraulic conductivity: From petrophysical properties to aquifer geometries—A review. Surveys in Geophysics, 28(2), 169-197.

Smewing, J. D., Warburton, J., & Cernuschi, A. (2002). Structural Inheritance in the Southern Kirthar Fold Belt. Proc. PAPG-SPE Annual Tech. Conf. Islamabad, Sp. Pub,

Smith, D. (1996). Sedimentary basins and the origin of intrusion-related carbonate-hosted Zn-Pb-Ag deposits.

Smith, D. L. (1986). Application of the pole-dipole resistivity technique to the detection of solution cavities beneath highways. Geophysics, 51(3), 833-837.

Snousy, M. G., Morsi, M. S., Elewa, A. M., Ahmed, S. A. E.-f., & El-Sayed, E. (2020). Groundwater vulnerability and trace element dispersion in the Quaternary aquifers along middle Upper Egypt. Environmental monitoring and assessment, 192(3), 1-36.

Solangi, G. S., Siyal, A. A., & Siyal, P. (2023). Indication of subsurface seawater intrusion into the Indus delta, Sindh, Pakistan. Mehran University Research Journal of Engineering and Technology, 42(1), 9-16.

Soupios, P., & Kokinou, E. (2016). Environmental geophysics: Techniques, advantages and limitations. Principles, applications and emerging technologies, 1.

Spate, O. H. K., & Learmonth, A. T. A. (2017). India and Pakistan: A general and regional geography. Routledge.
Spicer, R. A., Kelley, S. P., & Gilmour, I. (2003). The Cretaceous World. Cambridge University Press.
Srinivasa , S. G. (2004). Electrical resistivity surveys to delineate groundwater potential aquifers in Peddavanka watershed, Anantapur District, Andhra Pradesh, India. Environmental Geology, 46(1), 118-131.
Stampfli, G. M., & Borel, G. (2002). A plate tectonic model for the Paleozoic and Mesozoic constrained by dynamic plate boundaries and restored synthetic oceanic isochrons. Earth and Planetary Science Letters, 196(1-2), 17-33.
Stampfli, G. M., & Hochard, C. (2009). Plate tectonics of the Alpine realm. Geological Society, London, Special Publications, 327(1), 89-111.
Steenbergen, F. V., Kaisarani, A. B., Khan, N. U., & Gohar, M. S. (2015). A case of groundwater depletion in Balochistan, Pakistan: Enter into the void. Journal of Hydrology: Regional Studies, 4, 36-47.
Styles, P. (2012). Environmental Geophysics: Everything you ever wanted (needed!) to know but were afraid to ask! European Association of Geoscientists & Engineers.
Suhani, I., Sahab, S., Srivastava, V., & Singh, R. P. (2021). Impact of cadmium pollution on food safety and human health. Current Opinion in Toxicology, 27, 1-7.
Sultan, M., Khan, M., Khan, H., & Ahmad, B. (2022). Pathways to strengthening capabilities: A case for the adoption of climate-smart agriculture in Pakistan. APN Science Bulletin, 12(1), 171-183.
Syed, A., Sarwar, G., Shah, S. H., & Muhammad, S. (2021). Soil salinity research in 21st century in Pakistan: its impact on availability of plant nutrients, growth and yield of crops. Communications in Soil Science and Plant Analysis, 52(3), 183-200.
Tang, C., Godskesen, B., Aktor, H., Rijn, M. v., Kristensen, J. B., Rosshaug, P. S., Albrechtsen, H.-J., & Rygaard, M. (2021). Procedure for Calculating the Calcium Carbonate Precipitation Potential (CCPP) in Drinking Water Supply: Importance of Temperature, Ionic Species and Open/Closed System. Water, 13(1), 42.
Telahigue, F., Mejri, H., Mansouri, B., Souid, F., Agoubi, B., Chahlaoui, A., & Kharroubi, A. (2020). Assessing seawater intrusion in arid and semi-arid Mediterranean coastal aquifers using geochemical approaches. Physics and Chemistry of the Earth, Parts A/B/C, 115, 102811.
Telford, W., Geldart, L., Sheriff, R., & Keys, D. (1976). Applied geophysics: Cambridge Univ. Press, NY, 1-860.
Telford, W. M., Telford, W., Geldart, L., & Sheriff, R. E. (1990). Applied geophysics. Cambridge university press.
Thakur, V., & Wesnousky, S. (2002). Seismotectonics of 26 January 2001 Bhuj earthquake-affected region. Current science, 82(4), 396-399.
Tiessen, H. (2008). Phosphorus in the global environment. In The ecophysiology of plant-phosphorus interactions (pp. 1-7). Springer.
Timotewos, M. T., & Reddythota, D. (2000). Kulfo River Stream Impact on the Sustainability of Aquatic Life in Chamo Lake at Arba Minch. Journal of Water Resources and Ocean Science, 9(2), 48-55.
Toto, E. A., Kerrouri, C., Zouhri, L., Basri, M. E., Ibenbrahim, A., Mohamad, H., & Benammi, M. (2008). Geoelectrical exploration for groundwater in Al Maha

Forest, Ain Jouhra, Morocco. Hydrological Processes: An International Journal, 22(11), 1675-1686.
Tran, D. A., Tsujimura, M., Loc, H. H., Dang, D. H., Le Vo, P., Ha, D. T., Trang, N. T. T., Thuc, P. T. B., Dang, T. D., & Batdelger, O. (2021). Groundwater quality evaluation and health risk assessment in coastal lowland areas of the Mekong Delta, Vietnam. Groundwater for Sustainable Development, 15, 100679.
Tran, T. H. M., & Nguyen, K. G. (2018). Metal and metalloid concentrations in soil, surface water, and vegetables and the potential ecological and human health risks in the northeastern area of Hanoi, Vietnam. Environmental monitoring and assessment, 190(11), 1-14.
Troudi, N., Hamzaoui-Azaza, F., Tzoraki, O., Melki, F., & Zammouri, M. (2020). Assessment of groundwater quality for drinking purpose with special emphasis on salinity and nitrate contamination in the shallow aquifer of Guenniche (Northern Tunisia). Environmental monitoring and assessment, 192(10), 1-19.
Tsourlos, P. (1995). Modelling, interpretation and inversion of multielectrode resistivity survey data University of York].
Tumanski, S. (2006). Principles of electrical measurement. CRC press.
Tung, C. C., & Lim, S. C. (2017). Performance of electrical grounding system in soil at low moisture content condition at various compression levels. Journal of Engineering Science and Technology, 12(1), 27-47.
Uchenna, U. P., Lancia, M., Viaroli, S., Ugbaja, A. N., Galluzzi, M., & Zheng, C. (2023). Groundwater sustainability in African Metropolises: Case study from Calabar, Nigeria. Journal of Hydrology: Regional Studies, 45, 101-314.
Varma, S., & Jangra, M. (2021). Heavy metals stress and defense strategies in plants: An overview. Journal of Pharmacognosy and Phytochemistry, 10(1), 608-614.
Virkutyte, J., Sillanpää, M., & Latostenmaa, P. (2002). Electrokinetic soil remediation—critical overview. Science of the Total Environment, 289(1-3), 97-121.
Vredenburg, E. W. (1909). Report on the Geology of Sarawan, Jhalawan, Mekran and the State of Las Bela, Considered Principally from the Point of View of Economic Development. Geological survey of India.
Walker, L. (2020). TDS, Conductivity, and Salinity differences in Golf-course Ponds.
Wang, G., Shi, R., Mi, L., & Hu, J. (2022). Agricultural Eco-Efficiency: Challenges and Progress. Sustainability, 14(3), 1051.
Wang, Q., Dong, S., Wang, H., Yang, J., Huang, H., Dong, X., & Yu, B. (2020). Hydrogeochemical processes and groundwater quality assessment for different aquifers in the Caojiatan coal mine of Ordos Basin, northwestern China. Environmental Earth Sciences, 79(9), 1-15.
Wantasen, S., Luntungan, J., Tarore, A., Lumingkewas, A., & Ogie, T. (2021). Study on the quality of irrigation water in the talawaan irrigation channel using the Sodium Adsorption Ratio (SAR) Method. Journal of Physics: Conference Series,
Ward, M. H., Jones, R. R., Brender, J. D., De Kok, T. M., Weyer, P. J., Nolan, B. T., Villanueva, C. M., & Van Breda, S. G. (2018). Drinking water nitrate and human health: an updated review. International journal of environmental research and public health, 15(7), 1557.
Watson, K. A., & Barker, R. D. (1999). Differentiating anisotropy and lateral effects using azimuthal resistivity offset Wenner soundings. Geophysics, 64(3), 739-745.
Weather, W. (2022). www.worldweatheronline.com

Wei, X., Hao, M., Shao, M., & Gale, W. J. (2006). Changes in soil properties and the availability of soil micronutrients after 18 years of cropping and fertilization. Soil and Tillage research, 91(1-2), 120-130.
White, R. S., & Louden, K. E. (1982). The Makran continental margin: structure of a thickly sedimented convergent plate boundary: convergent margins: field investigations of margin structure and stratigraphy.
WHO. (2021). A global overview of national regulations and standards for drinking-water quality (924002364X).
Wiedicke, M., Neben, S., & Spiess, V. (2001). Mud volcanoes at the front of the Makran accretionary complex, Pakistan. Marine Geology, 172(1-2), 57-73.
Wightman, W., Jalinoos, F., Hanna, K., & Sirles, P. (2003). Application of geophysical methods to highway related problems.
Wilcox, L. (1955). Classification and use of irrigation waters. US Department of Agriculture.
Williams, M. (1959). 19. Stratigraphy of the Lower Indus Basin, West Pakistan. 5th World petroleum congress,
Wilson, S., Ingham, M., & McConchie, J. (2006). The applicability of earth resistivity methods for saline interface definition. Journal of Hydrology, 316(1-4), 301-312.
Worthington, S. R. (2022). Estimating effective porosity in bedrock aquifers. Groundwater, 60(2), 169-179.
Wu, J., Lu, J., Wen, X., Zhang, Z., & Lin, Y. (2019). Severe nitrate pollution and health risks of coastal aquifer simultaneously influenced by saltwater intrusion and intensive anthropogenic activities. Archives of environmental contamination and toxicology, 77(1), 79-87.
Xi, L., Chen, K., Huang, X., Gan, H., Xia, Z., & Tan, X. (2021). Hydrogeochemistry and origin of groundwater in the south coast of Hainan. Geological Bulletin of China, 40(2-3), 350-363.
Xia, X., Teng, Y., & Zhai, Y. (2022). Biogeochemistry of Iron Enrichment in Groundwater: An Indicator of Environmental Pollution and Its Management. Sustainability, 14(12), 7059.
Yaghi, M. M., Mohammed, M. Y., Towier, N. A., & Elsherif, K. M. (2020). Analysis of Potato Chips: Evaluation of Sodium, Potassium and Chloride Contents.
Yakubchuk, A., Nikishin, A., & Ishiwatari, A. (1994). A late Proterozoic ophiolite pulse. Proc. 29th Int'l. Geol. Congr., Part D,
Yeboah-Forson, A., & Whitman, D. (2014). Electrical resistivity characterization of anisotropy in the Biscayne Aquifer. Groundwater, 52(5), 728-736.
Yin, S., Xiao, Y., Han, P., Hao, Q., Gu, X., Men, B., & Huang, L. (2020). Investigation of groundwater contamination and health implications in a typical semiarid basin of North China. Water, 12(4), 1137.
Yiran, Z., Xuanlong, M., Haoli, Q., Hesheng, Z., & Yufeng, C. (2022). Research on Environmental Geophysical Methods in Geological Hazards Monitoring. International Journal of Environmental Protection and Policy, 10(4), 92.
Yonis, A. Y. (2022). Groundwater Investigation Using Vertical Electrical Sounding and Gis: a Case Study of Five Districts in Mogadishu, Banadir Region, Somalia University of Nairobi].
Yoshida, M., & Santosh, M. (2018). Voyage of the Indian subcontinent since Pangea breakup and driving force of supercontinent cycles: Insights on dynamics from numerical modeling. Geoscience Frontiers, 9(5), 1279-1292.

Yoshida, M., Zaman, H., Khadim, I., Ahmad, H., & Akram, H. (1997). Paleoposition of the Himalaya-Karakoram Belt and Surrounding Terranes since Cretaceous: Paleomagnetic Reconstruction of the Three Phase Collision History. Paleomagnetism of collision belts, 1.

Yusuf, M., & Abiye, T. (2019). Risks of groundwater pollution in the coastal areas of Lagos, southwestern Nigeria Groundwater Sustain. In: Dev.

Zaman, M., Shahid, S. A., & Heng, L. (2018). Irrigation water quality. In Guideline for salinity assessment, mitigation and adaptation using nuclear and related techniques (pp. 113-131). Springer.

Zeynolabedin, A., Ghiassi, R., & Dolatshahi Pirooz, M. (2021). Seawater intrusion vulnerability evaluation and prediction: a case study of Qeshm Island, Iran. Journal of Water and Climate Change, 12(1), 265-277.

Zhang, S., Tian, Y., Guo, Y., Shan, J., & Liu, R. (2021). Manganese release from corrosion products of cast iron pipes in drinking water distribution systems: Effect of water temperature, pH, alkalinity, SO_4^{2-} concentration and disinfectants. Chemosphere, 262, 127904.

Zhang, Z., Melo, L., Jansonius, R. P., Habibzadeh, F., Grant, E. R., & Berlinguette, C. P. (2020). pH matters when reducing CO_2 in an electrochemical flow cell. ACS Energy Letters, 5(10), 3101-3107.

Zhao, X., Guo, H., Wang, Y., Wang, G., Wang, H., Zang, X., & Zhu, J. (2021). Groundwater hydrogeochemical characteristics and quality suitability assessment for irrigation and drinking purposes in an agricultural region of the North China plain. Environmental Earth Sciences, 80(4), 1-22.

Zhu, M., Kong, F., Li, Y., Li, M., Zhang, J., & Xi, M. (2020). Effects of moisture and salinity on soil dissolved organic matter and ecological risk of coastal wetland. Environmental Research, 187, 109659.

Zohdy, A. A. (1965). The auxiliary point method of electrical sounding interpretation, and its relationship to the Dar Zarrouk parameters. Geophysics, 30(4), 644-660.

Zohdy, A. A. (1989). A new method for the automatic interpretation of Schlumberger and Wenner sounding curves. Geophysics, 54(2), 245-253.

Zohdy, A. A., Eaton, C., & Mabey, D. (1974). Application of surface geophysics to ground water investigation, Tech. Wat. Res. Inv., USGS Book, 2.

Zolekar, R. B., Todmal, R. S., Bhagat, V. S., Bhailume, S. A., Korade, M. S., & Das, S. (2021). Hydro-chemical characterization and geospatial analysis of groundwater for drinking and agricultural usage in Nashik district in Maharashtra, India. Environment, Development and Sustainability, 23, 4433-4452.

APPENDIX A

Questionnaire Survey:

1. Is there any research conducted using geophysical method in study area before to demarcate the groundwater table and aquifer thickness? Yes/No
2. What is the source of water for domestic and irrigation activity?
   -Tube well -Dug well -Government Supply
3. Is there any monitoring authority for the tube wells drilled for irrigation/domestic purpose in study area for Static water table, Abstraction and Quality? Yes/No
4. Is tube well owners and drilling companies require to obtain permission for drilling a borehole in area? Yes/No
5. Do you know the total number of tube wells?
6. How may gallons per day groundwater pump from each well?
7. Do you monitor the static and dynamic water table of well?
8. What is the total depth for drilling a new tube well?
9. What was the depth of drilled tube well before 10 years?
10. What is the pumping depth of groundwater from tube well?
11. How do you pump water from tube well? Electric Pump; Solar Pump; Diesel
12. What is the current water table of tube well?
13. Do you know the reason of declination of groundwater table in your area?
14. What is the problem related to the groundwater quantity and quality faced by locals?
15. Is there any impact of pumping from tube well on groundwater table in last 2 decades?
16. Is there any impact on quality of groundwater due to overexploitation of tube wells?
17. Is the present quality of water being match with the WHO standards and recent trends?
18. Are there specific groundwater quality issues / problems in your town? Yes/No
19. Is there any filtration plant to purify the groundwater for drinking purpose?
20. Do you have any suggestion and required steps to improve the groundwater management in your area?

APPENDIX B

Groundwater Management Awareness:

APPENDIX C

Groundwater Sampling, field measurement and tube-well information from local farmer and tubwell owner.

APPENDIX D

Awareness Seminar Organized On 8 January 2021 Local Farmers, Agriculture Department, Union Council, Government Official of Balochistan, Dunya News, and Student Bahria University Participated and editor Mustafa Habib published this article in Dunya newspaper.

بلوچستان

قدرتی وسائل سے مالا مال، پھر بھی مسائل کا شکار

وندر میں ڈیم بنائے جائیں، بورنگ سے پانی کی سطح کم اور فصلیں تباہ ہو رہی ہیں، عبدالعزیز

چٹانوں سے پانی میں کیڈمیم بڑھ رہی ہے، گردوں کے امراض میں اضافہ ہو رہا ہے، ڈاکٹر سلمیٰ

پنجاب پانی سے زراعت میں کماتا ہے، یہاں 15 گھنٹے کی لوڈ شیڈنگ ہے، غلام حیدر انگاریہ

خوبصورت پہاڑ، میدان اور معدنیات، بحریہ یونیورسٹی شعبہ ارتھ اینڈ انوائرمینٹل سائنسز کیساتھ وندر میں دنیا فورم

APPENDIX E

Geophysical data acquisition by using PASSI GLN-16 Electrical Resistivity equipment, on field data plotting.








APPENDIX F

Resistivity data of 27 VES station acquired from Winder Balochistan

Resistivity data of 27 VES station acquired from Winder Balochistan: AB/2 current electrode spacing, MN potential electrode spacing and R is resistance value from PASSI 16 GLN resistivity meter											
Station	**AB/2**	**MN**	**R**	**Station**	**AB/2**	**MN**	**R**	**Station**	**AB/2**	**MN**	**R**
R-1	2	1	0.921	R-2	2	1	1.273	R-3	2	1	1.613
R-1	4	1	0.240	R-2	4	1	0.222	R-3	4	1	0.364
R-1	6	1	0.112	R-2	6	1	0.125	R-3	6	1	0.142
R-1	8	1	0.070	R-2	8	1	0.075	R-3	8	1	0.082
R-1	10	2	0.116	R-2	10	2	0.154	R-3	10	2	0.116
R-1	15	2	0.059	R-2	15	2	0.051	R-3	15	2	0.054
R-1	20	2	0.036	R-2	20	2	0.041	R-3	20	2	0.035
R-1	25	2	0.027	R-2	25	2	0.029	R-3	25	2	0.023
R-1	30	10	0.089	R-2	30	10	0.091	R-3	30	10	0.085
R-1	35	10	0.062	R-2	35	10	0.061	R-3	35	10	0.069
R-1	40	10	0.048	R-2	40	10	0.051	R-3	40	10	0.051
R-1	45	10	0.045	R-2	45	10	0.041	R-3	45	10	0.041
R-1	50	20	0.062	R-2	50	20	0.074	R-3	50	20	0.072
R-1	60	20	0.045	R-2	60	20	0.049	R-3	60	20	0.053
R-1	70	20	0.031	R-2	70	20	0.034	R-3	70	20	0.037
R-1	80	20	0.024	R-2	80	20	0.027	R-3	80	20	0.028
R-1	90	20	0.022	R-2	90	20	0.021	R-3	90	20	0.021
R-1	100	50	0.036	R-2	100	50	0.048	R-3	100	50	0.049
R-1	150	50	0.019	R-2	150	50	0.023	R-3	150	50	0.020
R-4	2	1	1.868	R-5	2	1	0.756	R-6	2	1	0.874
R-4	4	1	0.505	R-5	4	1	0.222	R-6	4	1	0.255
R-4	6	1	0.276	R-5	6	1	0.110	R-6	6	1	0.128
R-4	8	1	0.165	R-5	8	1	0.072	R-6	8	1	0.085
R-4	10	2	0.219	R-5	10	2	0.102	R-6	10	2	0.118
R-4	15	2	0.098	R-5	15	2	0.043	R-6	15	2	0.059
R-4	20	2	0.067	R-5	20	2	0.037	R-6	20	2	0.040
R-4	25	2	0.042	R-5	25	2	0.024	R-6	25	2	0.028
R-4	30	10	0.148	R-5	30	10	0.095	R-6	30	10	0.100
R-4	35	10	0.106	R-5	35	10	0.070	R-6	35	10	0.074
R-4	40	10	0.079	R-5	40	10	0.055	R-6	40	10	0.059
R-4	45	10	0.062	R-5	45	10	0.043	R-6	45	10	0.046
R-4	50	20	0.098	R-5	50	20	0.072	R-6	50	20	0.079
R-4	60	20	0.064	R-5	60	20	0.051	R-6	60	20	0.054
R-4	70	20	0.044	R-5	70	20	0.038	R-6	70	20	0.040
R-4	80	20	0.032	R-5	80	20	0.030	R-6	80	20	0.030
R-4	90	20	0.022	R-5	90	20	0.023	R-6	90	20	0.024
R-4	100	50	0.049	R-5	100	50	0.051	R-6	100	50	0.052
R-4	150	50	0.017	R-5	150	50	0.023	R-6	150	50	0.023
R-7	2	1	0.866	R-8	2	1	2.725	R-9	2	1	1.452
R-7	4	1	0.317	R-8	4	1	0.546	R-9	4	1	0.406

Station	AB/2	MN	R	Station	AB/2	MN	R	Station	AB/2	MN	R
R-7	8	1	0.120	R-8	8	1	0.124	R-9	8	1	0.149
R-7	10	2	0.176	R-8	10	2	0.154	R-9	10	2	0.160
R-7	15	2	0.083	R-8	15	2	0.068	R-9	15	2	0.076
R-7	20	2	0.048	R-8	20	2	0.037	R-9	20	2	0.046
R-7	25	2	0.033	R-8	25	2	0.023	R-9	25	2	0.031
R-7	30	10	0.133	R-8	30	10	0.082	R-9	30	10	0.116
R-7	35	10	0.101	R-8	35	10	0.060	R-9	35	10	0.086
R-7	40	10	0.078	R-8	40	10	0.047	R-9	40	10	0.066
R-7	45	10	0.065	R-8	45	10	0.037	R-9	45	10	0.053
R-7	50	20	0.107	R-8	50	20	0.064	R-9	50	20	0.089
R-7	60	20	0.074	R-8	60	20	0.045	R-9	60	20	0.062
R-7	70	20	0.057	R-8	70	20	0.032	R-9	70	20	0.045
R-7	80	20	0.044	R-8	80	20	0.026	R-9	80	20	0.035
R-7	90	20	0.034	R-8	90	20	0.021	R-9	90	20	0.026
R-7	100	50	0.077	R-8	100	50	0.047	R-9	100	50	0.056
R-7	150	50	0.033	R-8	150	50	0.023	R-9	150	50	0.024
R-10	2	1	2.241	R-11	2	1	2.250	R-12	2	1	0.204
R-10	4	1	0.475	R-11	4	1	0.475	R-12	4	1	0.056
R-10	6	1	0.183	R-11	6	1	0.182	R-12	6	1	0.030
R-10	8	1	0.099	R-11	8	1	0.098	R-12	8	1	0.021
R-10	10	2	0.131	R-11	10	2	0.133	R-12	10	2	0.032
R-10	15	2	0.056	R-11	15	2	0.057	R-12	15	2	0.016
R-10	20	2	0.032	R-11	20	2	0.032	R-12	20	2	0.010
R-10	25	2	0.022	R-11	25	2	0.022	R-12	25	2	0.008
R-10	30	10	0.081	R-11	30	10	0.081	R-12	30	10	0.033
R-10	35	10	0.069	R-11	35	10	0.062	R-12	35	10	0.025
R-10	40	10	0.049	R-11	40	10	0.049	R-12	40	10	0.021
R-10	45	10	0.041	R-11	45	10	0.041	R-12	45	10	0.018
R-10	50	20	0.072	R-11	50	20	0.072	R-12	50	20	0.030
R-10	60	20	0.049	R-11	60	20	0.050	R-12	60	20	0.021
R-10	70	20	0.035	R-11	70	20	0.034	R-12	70	20	0.016
R-10	80	20	0.026	R-11	80	20	0.027	R-12	80	20	0.013
R-10	90	20	0.021	R-11	90	20	0.020	R-12	90	20	0.012
R-10	100	50	0.043	R-11	100	50	0.043	R-12	100	50	0.027
R-10	150	50	0.016	R-11	150	50	0.016	R-12	150	50	0.013
R-13	2	1	0.823	R-14	2	1	1.638	R-15	2	1	2.581
R-13	4	1	0.238	R-14	4	1	0.465	R-15	4	1	0.566
R-13	6	1	0.117	R-14	6	1	0.266	R-15	6	1	0.219
R-13	8	1	0.071	R-14	8	1	0.154	R-15	8	1	0.116
R-13	10	2	0.105	R-14	10	2	0.203	R-15	10	2	0.143
R-13	15	2	0.048	R-14	15	2	0.093	R-15	15	2	0.065
R-13	20	2	0.032	R-14	20	2	0.051	R-15	20	2	0.036
R-13	25	2	0.024	R-14	25	2	0.033	R-15	25	2	0.023
R-13	30	10	0.092	R-14	30	10	0.127	R-15	30	10	0.081
R-13	35	10	0.069	R-14	35	10	0.098	R-15	35	10	0.058

Station	AB/2	MN	R	Station	AB/2	MN	R	Station	AB/2	MN	R
R-13	40	10	0.056	R-14	40	10	0.080	R-15	40	10	0.043
R-13	45	10	0.045	R-14	45	10	0.063	R-15	45	10	0.034
R-13	50	20	0.080	R-14	50	20	0.108	R-15	50	20	0.056
R-13	60	20	0.057	R-14	60	20	0.072	R-15	60	20	0.038
R-13	70	20	0.042	R-14	70	20	0.048	R-15	70	20	0.027
R-13	80	20	0.032	R-14	80	20	0.035	R-15	80	20	0.021
R-13	90	20	0.025	R-14	90	20	0.025	R-15	90	20	0.017
R-13	100	50	0.056	R-14	100	50	0.054	R-15	100	50	0.037
R-13	150	50	0.023	R-14	150	50	0.021	R-15	150	50	0.015
R-16	2	1	1.256	R-19	2	1	0.416	R-20	2	1	1.418
R-16	4	1	0.311	R-19	4	1	0.146	R-20	4	1	0.420
R-16	6	1	0.139	R-19	6	1	0.085	R-20	6	1	0.219
R-16	8	1	0.070	R-19	8	1	0.056	R-20	8	1	0.142
R-16	10	2	0.091	R-19	10	2	0.084	R-20	10	2	0.197
R-16	15	2	0.040	R-19	15	2	0.044	R-20	15	2	0.090
R-16	20	2	0.029	R-19	20	2	0.031	R-20	20	2	0.052
R-16	25	2	0.020	R-19	25	2	0.022	R-20	25	2	0.032
R-16	30	10	0.071	R-19	30	10	0.084	R-20	30	10	0.113
R-16	35	10	0.053	R-19	35	10	0.064	R-20	35	10	0.082
R-16	40	10	0.042	R-19	40	10	0.050	R-20	40	10	0.062
R-16	45	10	0.034	R-19	45	10	0.040	R-20	45	10	0.046
R-16	50	20	0.056	R-19	50	20	0.075	R-20	50	20	0.076
R-16	60	20	0.039	R-19	60	20	0.053	R-20	60	20	0.051
R-16	70	20	0.029	R-19	70	20	0.040	R-20	70	20	0.037
R-16	80	20	0.023	R-19	80	20	0.032	R-20	80	20	0.028
R-16	90	20	0.018	R-19	90	20	0.025	R-20	90	20	0.023
R-16	100	50	0.038	R-19	100	50	0.056	R-20	100	50	0.050
R-16	150	50	0.016	R-19	150	50	0.023	R-20	150	50	0.021
R-17	2	1	1.316	R-18	2	1	0.332	R-21	2	1	0.806
R-17	4	1	0.402	R-18	4	1	0.132	R-21	4	1	0.222
R-17	6	1	0.208	R-18	6	1	0.075	R-21	6	1	0.102
R-17	8	1	0.137	R-18	8	1	0.054	R-21	8	1	0.063
R-17	10	2	0.196	R-18	10	2	0.080	R-21	10	2	0.087
R-17	15	2	0.097	R-18	15	2	0.047	R-21	15	2	0.039
R-17	20	2	0.057	R-18	20	2	0.030	R-21	20	2	0.025
R-17	25	2	0.037	R-18	25	2	0.024	R-21	25	2	0.017
R-17	30	10	0.130	R-18	30	10	0.096	R-21	30	10	0.062
R-17	35	10	0.095	R-18	35	10	0.072	R-21	35	10	0.046
R-17	40	10	0.073	R-18	40	10	0.060	R-21	40	10	0.036
R-17	45	10	0.056	R-18	45	10	0.048	R-21	45	10	0.029
R-17	50	20	0.090	R-18	50	20	0.083	R-21	50	20	0.053
R-17	60	20	0.060	R-18	60	20	0.056	R-21	60	20	0.037
R-17	70	20	0.042	R-18	70	20	0.041	R-21	70	20	0.028
R-17	80	20	0.032	R-18	80	20	0.033	R-21	80	20	0.023
R-17	90	20	0.025	R-18	90	20	0.026	R-21	90	20	0.018

Station	AB/2	MN	R	Station	AB/2	MN	R	Station	AB/2	MN	R
R-17	100	50	0.052	R-18	100	50	0.056	R-21	100	50	0.042
R-17	150	50	0.023	R-18	150	50	0.027	R-21	150	50	0.021
R-22	2	1	2.292	R-23	2	1	0.688	R-24	2	1	2.037
R-22	4	1	0.562	R-23	4	1	0.198	R-24	4	1	0.475
R-22	6	1	0.263	R-23	6	1	0.107	R-24	6	1	0.192
R-22	8	1	0.154	R-23	8	1	0.066	R-24	8	1	0.100
R-22	10	2	0.210	R-23	10	2	0.091	R-24	10	2	0.122
R-22	15	2	0.100	R-23	15	2	0.043	R-24	15	2	0.052
R-22	20	2	0.059	R-23	20	2	0.028	R-24	20	2	0.029
R-22	25	2	0.040	R-23	25	2	0.020	R-24	25	2	0.018
R-22	30	10	0.143	R-23	30	10	0.072	R-24	30	10	0.065
R-22	35	10	0.103	R-23	35	10	0.053	R-24	35	10	0.045
R-22	40	10	0.078	R-23	40	10	0.041	R-24	40	10	0.033
R-22	45	10	0.059	R-23	45	10	0.033	R-24	45	10	0.027
R-22	50	20	0.097	R-23	50	20	0.058	R-24	50	20	0.046
R-22	60	20	0.062	R-23	60	20	0.041	R-24	60	20	0.031
R-22	70	20	0.042	R-23	70	20	0.031	R-24	70	20	0.023
R-22	80	20	0.032	R-23	80	20	0.024	R-24	80	20	0.018
R-22	90	20	0.023	R-23	90	20	0.019	R-24	90	20	0.014
R-22	100	50	0.049	R-23	100	50	0.042	R-24	100	50	0.031
R-22	150	50	0.019	R-23	150	50	0.017	R-24	150	50	0.013
R-25	2	1	2.971	R-26	2	1	2.334	R-27	2	1	3.048
R-25	4	1	0.620	R-26	4	1	0.546	R-27	4	1	0.794
R-25	6	1	0.242	R-26	6	1	0.226	R-27	6	1	0.373
R-25	8	1	0.123	R-26	8	1	0.111	R-27	8	1	0.226
R-25	10	2	0.141	R-26	10	2	0.123	R-27	10	2	0.287
R-25	15	2	0.060	R-26	15	2	0.051	R-27	15	2	0.130
R-25	20	2	0.033	R-26	20	2	0.029	R-27	20	2	0.071
R-25	25	2	0.021	R-26	25	2	0.020	R-27	25	2	0.038
R-25	30	10	0.083	R-26	30	10	0.083	R-27	30	10	0.115
R-25	35	10	0.061	R-26	35	10	0.061	R-27	35	10	0.082
R-25	40	10	0.057	R-26	40	10	0.054	R-27	40	10	0.059
R-25	45	10	0.046	R-26	45	10	0.043	R-27	45	10	0.046
R-25	50	20	0.084	R-26	50	20	0.072	R-27	50	20	0.069
R-25	60	20	0.062	R-26	60	20	0.051	R-27	60	20	0.043
R-25	70	20	0.046	R-26	70	20	0.038	R-27	70	20	0.028
R-25	80	20	0.036	R-26	80	20	0.029	R-27	80	20	0.021
R-25	90	20	0.028	R-26	90	20	0.022	R-27	90	20	0.016
R-25	100	50	0.059	R-26	100	50	0.048	R-27	100	50	0.032
R-25	150	50	0.023	R-26	150	50	0.020	R-27	150	50	0.012

APPENDIX G

Groundwater samples coordinate and estimated parameters from lab in mg/l.

Physiochemical composition of groundwater sample of study area (mg/l)								
Station	**Ca**	**Mg**	**Na**	**K**	**HCO_3**	**Cl**	**SO_4**	**NO_3**
NA	182.0	70.0	460.0	13.0	570.0	755.0	295.0	110.0
NS	116.8	97.0	239.4	4.3	391.0	450.0	241.0	68.0
ND	146.8	72.3	212.0	4.8	264.0	412.0	317.1	79.0
NE	98.6	49.0	143.0	3.6	291.0	232.0	179.1	80.0
NF	131.0	88.0	336.0	8.0	345.0	621.0	351.0	62.0
NG	224.0	70.0	280.0	20.0	670.0	425.0	285.0	62.0
NH	170.0	85.0	665.0	9.0	520.0	1055.0	320.0	48.0
NI	143.0	70.0	358.0	3.0	336.0	487.0	298.0	54.0
KA	184.0	115.0	362.0	20.0	775.0	370.0	545.0	71.0
KF	137.0	65.0	325.0	9.5	256.0	471.0	275.0	71.0
KD	110.0	30.0	290.0	9.0	325.0	349.0	251.0	76.0
KU	115.0	95.0	305.0	9.0	320.0	495.0	354.9	44.0
KR	125.0	104.0	348.0	12.0	365.0	515.0	555.0	65.0
KP	143.0	98.0	410.0	4.0	412.0	654.0	314.0	88.0
KW	134.0	88.0	241.0	5.0	331.0	395.0	269.0	65.0
KV	126.0	76.0	495.0	4.0	430.0	691.0	369.0	94.0
KL	119.0	93.0	313.0	5.0	412.0	420.0	328.0	81.0
KQ	88.0	66.0	422.0	4.0	309.0	432.0	387.0	65.0
KE	148.0	112.0	294.0	4.0	368.0	421.0	457.0	75.0
KZ	163.0	125.0	324.0	5.0	369.0	501.0	467.0	72.0
KW	135.0	84.0	374.0	5.0	365.0	515.0	555.0	68.0
KM	143.0	106.0	338.0	4.0	359.0	462.0	496.0	57.0
KT	134.0	121.0	298.0	6.0	371.0	481.0	464.0	62.0
KO	133.0	115.0	345.0	5.0	398.0	496.0	512.0	49.0
AA	180.0	115.0	214.0	5.0	370.0	424.0	510.0	51.0
AL	128.0	60.0	251.0	3.0	336.0	413.0	225.0	63.0
AV	146.0	118.0	167.0	10.0	255.0	368.0	460.0	59.0
AM	98.0	65.0	574.0	5.0	319.0	735.0	340.0	79.0
BM	165.0	121.0	298.0	3.0	436.0	488.0	376.0	68.0
BT	170.8	75.1	242.9	5.5	145.0	570.0	296.9	60.0
DU	185.0	128.0	120.0	9.0	276.0	410.0	261.0	72.0
CY	179.2	85.4	224.7	5.9	244.0	368.0	414.0	68.0
CE	98.4	65.0	560.0	6.5	421.0	741.0	325.0	66.0
CK	75.3	30.5	426.0	4.7	202.0	587.0	119.7	66.0
PS	98.0	68.0	381.0	6.9	314.0	536.0	221.0	70.0
DF	168.0	136.0	375.0	6.7	418.0	897.0	197.0	65.0
UT	208.0	152.0	448.0	7.3	524.0	954.0	388.0	58.0
UL	133.8	62.3	653.0	4.5	425.0	825.0	264.2	60.0
UR	154.0	68.0	259.0	4.1	289.6	540.0	156.0	62.0

Station	Ca	Mg	Na	K	HCO_3	Cl	SO_4	NO_3
UG	210.0	124.0	358.0	2.0	485.0	815.0	356.0	74.0
UD	89.0	72.0	526.0	4.0	294.0	691.0	278.0	69.0
UP	101.0	80.0	497.0	12.0	334.0	750.0	320.0	77.0
RN	86.0	69.0	238.0	6.0	297.0	457.0	172.0	63.0
RK	85.0	40.0	224.0	14.0	275.0	355.0	165.0	62.0
RB	92.0	65.0	152.0	6.5	239.0	292.0	227.9	68.0
RX	114.0	89.0	173.0	4.4	324.0	384.0	268.0	56.0
RS	94.5	46.0	155.0	5.8	236.0	309.0	345.0	71.0
RP	140.0	120.0	360.0	5.0	435.0	595.0	312.0	61.0
RW	187.0	136.0	130.0	10.0	337.0	491.0	256.0	63.0
RJ	125.0	55.0	215.0	2.0	350.0	354.6	205.0	62.0
RL	125.0	109.0	365.0	5.5	355.0	600.0	291.0	70.0
RE	110.0	85.0	210.0	2.0	324.0	365.0	251.0	57.0
RH	124.0	108.0	215.0	4.0	295.0	412.0	231.0	65.0
BG	125.0	66.0	277.0	6.0	258.0	484.0	248.0	63.0
BN	137.0	75.0	247.0	5.0	345.0	349.0	311.0	60.0
BD	116.0	86.0	213.0	3.0	277.0	421.0	245.0	59.0
BR	142.0	81.0	224.0	4.0	271.0	378.0	257.0	62.0
CF	103.0	77.0	267.0	5.0	324.0	497.0	253.0	60.0
CD	118.0	82.0	292.0	6.0	349.0	389.0	324.0	61.0
CK	280.0	80.0	405.0	24.0	650.0	855.0	325.0	58.0
CM	200.0	124.0	505.0	6.5	550.0	770.0	455.0	87.0
CZ	95.0	71.0	290.0	5.5	350.0	470.0	207.0	67.0
CL	110.0	88.0	380.0	5.3	305.0	655.0	290.0	60.0
CP	85.0	55.0	195.0	3.3	295.0	305.0	189.0	76.0
CG	131.0	86.0	248.0	3.0	374.0	411.0	278.0	60.0
CT	131.0	84.0	251.0	4.0	416.0	377.0	345.0	72.0
CJ	122.0	91.0	263.0	5.0	360.0	388.0	247.0	60.0
CI	103.0	72.0	234.0	4.0	287.0	367.0	201.0	79.0
CS	125.0	69.0	278.0	6.0	315.0	512.0	264.0	86.0
CQ	115.0	79.0	269.0	4.0	381.0	407.0	287.0	65.0
CR	129.0	81.0	238.0	5.0	345.0	384.0	218.0	71.0
CA	106.0	87.0	243.0	4.0	358.0	379.0	209.0	66.0
CN	175.0	95.0	297.0	12.0	460.0	512.0	194.0	68.0
CV	132.0	91.0	293.0	4.0	341.0	441.0	292.0	60.0
CX	121.0	79.0	365.0	5.0	348.0	512.0	260.0	58.0
CE	139.0	85.0	254.0	4.0	374.0	456.0	292.0	67.0
CB	113.0	76.0	277.0	5.0	331.0	426.0	314.0	63.0
CW	125.0	88.0	264.0	4.0	351.0	396.0	275.0	66.0
UI	140.0	104.0	432.0	2.0	412.0	691.0	364.0	62.0
UR	112.0	56.0	896.0	3.2	138.0	1270.0	265.0	63.0
US	118.0	83.0	574.0	5.0	470.0	852.0	314.0	60.0
UG	123.0	76.0	496.0	4.9	327.0	798.0	194.0	71.0
UN	105.0	55.0	396.0	3.0	355.0	471.0	200.0	65.0
SF	129.0	87.0	458.0	3.0	411.0	598.0	321.0	67.0

Station	Ca	Mg	Na	K	HCO_3	Cl	SO_4	NO_3
SA	88.0	73.5	431.0	6.0	426.0	587.0	377.0	62.0
SG	118.0	78.0	453.0	5.0	382.0	561.0	342.0	68.0
SK	143.0	64.0	335.0	5.0	329.0	495.0	310.0	72.0
SL	119.0	71.0	344.0	4.0	299.0	498.0	283.0	68.0
SO	94.0	81.0	441.0	3.0	321.0	521.0	414.0	64.0
SY	105.0	75.0	458.0	3.0	386.0	559.0	321.0	57.0
SI	112.0	61.0	463.0	5.0	356.0	603.0	341.0	60.0
ST	200.0	70.0	356.0	10.0	402.0	565.0	295.0	64.0
WR	185	56	158	19	491	290	251	57
RV	146	98	214	4	394	355	357	41

APPENDIX H

Groundwater samples coordinate and estimated parameters from lab in (meq/l).

Physiochemical composition of groundwater sample of study area ((meq/l))								
Station	**Ca**	**Mg**	**Na**	**K**	**HCO_3**	**Cl**	**SO_4**	**NO_3**
NA	9.08	5.76	20.01	0.33	9.34	21.30	6.14	1.77
NS	5.83	7.98	10.41	0.11	6.41	12.69	5.02	1.10
ND	7.32	5.95	9.22	0.12	4.33	11.62	6.60	1.27
NE	4.92	4.03	6.22	0.09	4.77	6.54	3.73	1.29
NF	6.54	7.24	14.62	0.20	5.65	17.52	7.31	1.00
NG	11.18	5.76	12.18	0.51	10.98	11.99	5.93	1.00
NH	8.48	6.99	28.93	0.23	8.52	29.76	6.66	0.77
NI	7.14	5.76	15.57	0.08	5.51	13.74	6.20	0.87
KA	9.18	9.46	15.75	0.51	12.70	10.44	11.35	1.15
KF	6.84	5.35	14.14	0.24	4.20	13.29	5.73	1.15
KD	5.49	2.47	12.61	0.23	5.33	9.84	5.23	1.23
KU	5.74	7.82	13.27	0.23	5.24	13.96	7.39	0.71
KR	6.24	8.56	15.14	0.31	5.98	14.53	11.56	1.05
KP	7.14	8.06	17.83	0.10	6.75	18.45	6.54	1.42
KW	6.69	7.24	10.48	0.13	5.42	11.14	5.60	1.05
KV	6.29	6.25	21.53	0.10	7.05	19.49	7.68	1.52
KL	5.94	7.65	13.61	0.13	6.75	11.85	6.83	1.31
KQ	4.39	5.43	18.36	0.10	5.06	12.19	8.06	1.05
KE	7.39	9.21	12.79	0.10	6.03	11.87	9.51	1.21
KZ	8.13	10.28	14.09	0.13	6.05	14.13	9.72	1.16
KW	6.74	6.91	16.27	0.13	5.98	14.53	11.56	1.10
KM	7.14	8.72	14.70	0.10	5.88	13.03	10.33	0.92
KT	6.69	9.95	12.96	0.15	6.08	13.57	9.66	1.00
KO	6.64	9.46	15.01	0.13	6.52	13.99	10.66	0.79
AA	8.98	9.46	9.30	0.13	6.06	11.96	10.62	0.82
AL	6.39	4.94	10.91	0.08	5.51	11.65	4.68	1.02
AV	7.29	9.71	7.26	0.26	4.18	10.38	9.58	0.95
AM	4.89	5.35	24.96	0.13	5.23	20.73	7.08	1.27
BM	8.23	9.95	12.96	0.08	7.15	13.76	7.83	1.10
BT	8.52	6.18	10.56	0.14	2.38	16.08	6.18	0.97
DU	9.23	10.53	5.22	0.23	4.52	11.56	5.43	1.16
CY	8.94	7.02	9.77	0.15	4.00	10.38	8.62	1.10
CE	4.91	5.35	24.35	0.17	6.90	20.90	6.77	1.06
CK	3.76	2.51	18.52	0.12	3.31	16.56	2.49	1.06
PS	4.89	5.59	16.57	0.18	5.15	15.12	4.60	1.13
DF	8.38	11.19	16.30	0.17	6.85	25.30	4.10	1.05
UT	10.38	12.50	19.48	0.19	8.59	26.91	8.08	0.94
UL	6.68	5.12	28.39	0.12	6.96	23.27	5.50	0.97
UR	7.68	5.59	11.26	0.10	4.75	15.23	3.25	1.00

Station	Ca	Mg	Na	K	HCO_3	Cl	SO_4	NO_3
UG	10.48	10.20	15.57	0.05	7.95	22.99	7.41	1.19
UD	4.44	5.92	22.87	0.10	4.82	19.49	5.79	1.11
UP	5.04	6.58	21.61	0.31	5.47	21.15	6.66	1.24
RN	4.29	5.68	10.35	0.15	4.87	12.89	3.58	1.02
RK	4.24	3.29	9.74	0.36	4.51	10.01	3.44	1.00
RB	4.59	5.35	6.61	0.17	3.92	8.24	4.74	1.10
RX	5.69	7.32	7.52	0.11	5.31	10.83	5.58	0.90
RS	4.72	3.78	6.74	0.15	3.87	8.72	7.18	1.15
RP	6.99	9.87	15.65	0.13	7.13	16.78	6.50	0.98
RW	9.33	11.19	5.65	0.26	5.52	13.85	5.33	1.02
RJ	6.24	4.52	9.35	0.05	5.74	10.00	4.27	1.00
RL	6.24	8.97	15.87	0.14	5.82	16.92	6.06	1.13
RE	5.49	6.99	9.13	0.05	5.31	10.30	5.23	0.92
RH	6.19	8.88	9.35	0.10	4.83	11.62	4.81	1.05
BG	6.24	5.43	12.04	0.15	4.23	13.65	5.16	1.02
BN	6.84	6.17	10.74	0.13	5.65	9.84	6.48	0.97
BD	5.79	7.07	9.26	0.08	4.54	11.87	5.10	0.95
BR	7.09	6.66	9.74	0.10	4.44	10.66	5.35	1.00
CF	5.14	6.33	11.61	0.13	5.31	14.02	5.27	0.97
CD	5.89	6.75	12.70	0.15	5.72	10.97	6.75	0.98
CK	13.97	6.58	17.61	0.61	10.65	24.12	6.77	0.94
CM	9.98	10.20	21.96	0.17	9.01	21.72	9.47	1.40
CZ	4.74	5.84	12.61	0.14	5.74	13.26	4.31	1.08
CL	5.49	7.24	16.52	0.13	5.00	18.48	6.04	0.97
CP	4.24	4.52	8.48	0.08	4.83	8.60	3.94	1.23
CG	6.54	7.07	10.78	0.08	6.13	11.59	5.79	0.97
CT	6.54	6.91	10.91	0.10	6.82	10.63	7.18	1.16
CJ	6.09	7.49	11.43	0.13	5.90	10.94	5.14	0.97
CI	5.14	5.92	10.17	0.10	4.70	10.35	4.18	1.27
CS	6.24	5.68	12.09	0.15	5.16	14.44	5.50	1.39
CQ	5.74	6.50	11.70	0.10	6.24	11.48	5.98	1.05
CR	6.44	6.66	10.35	0.13	5.65	10.83	4.54	1.15
CA	5.29	7.16	10.57	0.10	5.87	10.69	4.35	1.06
CN	8.73	7.82	12.91	0.31	7.54	14.44	4.04	1.10
CV	6.59	7.49	12.74	0.10	5.59	12.44	6.08	0.97
CX	6.04	6.50	15.87	0.13	5.70	14.44	5.41	0.94
CE	6.94	6.99	11.04	0.10	6.13	12.86	6.08	1.08
CB	5.64	6.25	12.04	0.13	5.42	12.02	6.54	1.02
CW	6.24	7.24	11.48	0.10	5.75	11.17	5.73	1.06
UI	6.99	8.56	18.78	0.05	6.75	19.49	7.58	1.00
UR	5.59	4.61	38.96	0.08	2.26	35.82	5.52	1.02
US	5.89	6.83	24.96	0.13	7.70	24.03	6.54	0.97
UG	6.14	6.25	21.57	0.12	5.36	22.51	4.04	1.15
UN	5.24	4.52	17.22	0.08	5.82	13.29	4.16	1.05
SF	6.44	7.16	19.91	0.08	6.74	16.87	6.68	1.08

Station	Ca	Mg	Na	K	HCO_3	Cl	SO_4	NO_3
SA	4.39	6.05	18.74	0.15	6.98	16.56	7.85	1.00
SG	5.89	6.42	19.70	0.13	6.26	15.82	7.12	1.10
SK	7.14	5.26	14.57	0.13	5.39	13.96	6.45	1.16
SL	5.94	5.84	14.96	0.10	4.90	14.05	5.89	1.10
SO	4.69	6.66	19.17	0.08	5.26	14.70	8.62	1.03
SY	5.24	6.17	19.91	0.08	6.33	15.77	6.68	0.92
SI	5.59	5.02	20.13	0.13	5.83	17.01	7.10	0.97
ST	9.98	5.76	15.48	0.26	6.59	15.94	6.14	1.03
WR	9.2315	4.6068	6.873	0.486	8.047	8.18	5.23	0.919
RV	7.2854	8.0619	9.308	0.102	6.457	10.01	7.43	0.661

APPENDIX I

Groundwater irrigation water quality parameters.

Irrigation water quality parameters									
Station	**Na %**	**SAR**	**PS**	**PI**	**MAR**	**KR**	**CAI-1**	**CAI- 2**	**RSC**
NA	56.87	7.35	24.37	155.42	38.80	1.35	0.04	-0.06	-5.50
NS	42.80	3.96	15.20	93.74	57.78	0.75	0.17	-0.19	-7.40
ND	40.76	3.58	14.92	85.12	44.82	0.69	0.20	-0.21	-8.95
NE	40.74	2.94	8.41	93.86	45.03	0.69	0.04	-0.03	-4.18
NF	51.11	5.57	21.17	123.35	52.55	1.06	0.15	-0.21	-8.12
NG	41.11	4.19	14.95	91.48	34.00	0.72	-0.06	0.04	-5.96
NH	64.81	10.40	33.09	205.78	45.18	1.87	0.02	-0.04	-6.95
NI	54.56	6.13	16.84	138.97	44.66	1.21	-0.14	0.16	-7.39
KA	45.12	5.16	16.11	103.58	50.75	0.84	-0.56	0.24	-5.94
KF	53.22	5.73	16.15	132.84	43.89	1.16	-0.08	0.11	-7.99
KD	60.64	6.32	12.46	187.54	31.02	1.59	-0.30	0.28	-2.63
KU	49.04	5.10	17.66	114.78	57.66	0.98	0.03	-0.04	-8.31
KR	50.06	5.57	20.30	118.86	57.83	1.02	-0.06	0.05	-8.81
KP	53.82	6.47	21.72	134.44	53.05	1.17	0.03	-0.04	-8.45
KW	42.72	3.97	13.94	92.00	51.98	0.75	0.05	-0.05	-8.50
KV	63.01	8.60	23.33	192.88	49.86	1.72	-0.11	0.15	-5.49
KL	49.81	5.22	15.26	119.31	56.30	1.00	-0.16	0.14	-6.84
KQ	64.91	8.28	16.21	209.83	55.29	1.87	-0.51	0.48	-4.76
KE	43.37	4.44	16.63	91.84	55.51	0.77	-0.09	0.07	-10.57
KZ	43.18	4.64	18.99	89.88	55.84	0.77	-0.01	0.01	-12.37
KW	54.15	6.23	20.30	137.13	50.64	1.19	-0.13	0.11	-7.66
KM	47.95	5.22	18.19	108.02	55.00	0.93	-0.14	0.11	-9.97
KT	43.56	4.49	18.40	92.71	59.82	0.78	0.03	-0.03	-10.56
KO	48.05	5.29	19.32	109.09	58.77	0.93	-0.08	0.07	-9.57
AA	33.38	3.06	17.27	63.80	51.30	0.50	0.21	-0.15	-12.38
AL	48.91	4.59	13.99	117.10	43.59	0.96	0.06	-0.06	-5.82
AV	29.63	2.49	15.17	54.76	57.13	0.43	0.28	-0.21	-12.81
AM	70.65	11.03	24.27	266.11	52.23	2.44	-0.21	0.35	-5.01
BM	41.50	4.30	17.68	85.94	54.73	0.71	0.05	-0.05	-11.04
BT	41.57	3.90	19.17	82.33	42.01	0.72	0.33	-0.63	-12.32
DU	20.70	1.66	14.28	37.16	53.28	0.26	0.53	-0.61	-15.24
CY	37.74	3.46	14.69	73.71	44.00	0.61	0.04	-0.04	-11.97
CE	70.03	10.75	24.28	263.04	52.14	2.37	-0.17	0.26	-3.36
CK	74.36	10.46	17.80	324.68	40.01	2.96	-0.13	0.36	-2.95
PS	60.84	7.24	17.42	179.64	53.36	1.58	-0.11	0.17	-5.34
DF	45.23	5.21	27.35	96.68	57.17	0.83	0.35	-0.81	-12.72
UT	45.78	5.76	30.95	97.93	54.64	0.85	0.27	-0.43	-14.30
UL	70.44	11.69	26.02	263.06	43.41	2.41	-0.23	0.42	-4.83

Station	Na %	SAR	PS	PI	MAR	KR	CAI-1	CAI- 2	RSC
UR	45.69	4.37	16.86	101.21	42.13	0.85	0.25	-0.48	-8.53
UG	42.88	4.84	26.69	88.90	49.33	0.75	0.32	-0.48	-12.73
UD	68.60	10.05	22.38	241.84	57.15	2.21	-0.18	0.33	-5.55
UP	64.43	8.96	24.49	206.08	56.63	1.86	-0.04	0.06	-6.15
RN	50.55	4.64	14.68	125.95	56.95	1.04	0.19	-0.28	-5.10
RK	55.24	5.02	11.73	157.49	43.69	1.29	-0.01	0.01	-3.03
RB	39.54	2.96	10.61	86.41	53.81	0.66	0.18	-0.17	-6.02
RX	36.43	2.95	13.62	75.53	56.28	0.58	0.30	-0.29	-7.70
RS	43.80	3.27	12.31	102.41	44.52	0.79	0.21	-0.17	-4.63
RP	47.96	5.39	20.03	108.69	58.56	0.93	0.06	-0.07	-9.73
RW	21.39	1.76	16.51	39.00	54.52	0.28	0.57	-0.73	-15.00
RJ	46.37	4.03	12.14	109.11	42.04	0.87	0.06	-0.06	-5.03
RL	50.84	5.76	19.95	120.24	58.98	1.04	0.05	-0.08	-9.39
RE	42.15	3.65	12.91	91.61	56.02	0.73	0.11	-0.11	-7.17
RH	38.12	3.41	14.03	76.61	58.95	0.62	0.19	-0.23	-10.24
BG	50.47	4.99	16.23	120.85	46.54	1.03	0.11	-0.15	-7.44
BN	44.98	4.21	13.08	100.85	47.44	0.83	-0.10	0.08	-7.35
BD	41.71	3.65	14.43	88.56	55.00	0.72	0.21	-0.26	-8.32
BR	41.28	3.71	13.34	86.16	48.46	0.71	0.08	-0.08	-9.31
CF	50.01	4.85	16.65	121.26	55.21	1.01	0.16	-0.22	-6.16
CD	49.82	5.05	14.35	119.42	53.39	1.00	-0.17	0.15	-6.91
CK	45.41	5.49	27.50	101.55	32.02	0.86	0.24	-0.34	-9.90
CM	51.90	6.91	26.46	123.68	50.55	1.09	-0.02	0.02	-11.17
CZ	54.04	5.48	15.41	141.79	55.20	1.19	0.04	-0.05	-4.85
CL	56.23	6.55	21.49	147.37	56.88	1.30	0.10	-0.16	-7.73
CP	48.93	4.05	10.57	121.80	51.61	0.97	0.00	0.00	-3.93
CG	44.06	4.13	14.49	97.40	51.98	0.79	0.06	-0.06	-7.48
CT	44.61	4.21	14.23	100.57	51.39	0.81	-0.04	0.03	-6.63
CJ	45.49	4.39	13.52	102.14	55.15	0.84	-0.06	0.06	-7.67
CI	47.68	4.33	12.44	111.57	53.54	0.92	0.01	-0.01	-6.36
CS	50.04	4.95	17.19	120.52	47.64	1.01	0.15	-0.21	-6.75
CQ	48.66	4.73	14.47	115.99	53.11	0.96	-0.03	0.03	-5.99
CR	43.89	4.04	13.10	97.14	50.86	0.79	0.03	-0.03	-7.45
CA	45.71	4.24	12.87	104.35	57.50	0.85	0.00	0.00	-6.58
CN	43.38	4.49	16.46	94.63	47.23	0.78	0.08	-0.11	-9.01
CV	47.33	4.80	15.48	107.32	53.19	0.91	-0.03	0.03	-8.48
CX	55.62	6.34	17.15	145.63	51.84	1.27	-0.11	0.14	-6.83
CE	44.04	4.18	15.90	97.06	50.20	0.79	0.13	-0.14	-7.80
CB	50.05	4.94	15.28	120.87	52.58	1.01	-0.01	0.01	-6.47
CW	45.81	4.42	14.03	102.97	53.72	0.85	-0.04	0.04	-7.72
UI	54.64	6.74	23.28	137.57	55.05	1.21	0.03	-0.05	-8.79
UR	79.13	17.25	38.58	396.95	45.18	3.82	-0.09	0.41	-7.90
US	66.02	9.90	27.30	218.08	53.69	1.96	-0.04	0.07	-5.01
UG	63.28	8.66	24.53	192.74	50.46	1.74	0.04	-0.09	-7.03
UN	63.63	7.79	15.37	201.04	46.34	1.76	-0.30	0.40	-3.95

Station	Na %	SAR	PS	PI	MAR	KR	CAI-1	CAI- 2	RSC
SF	59.29	7.64	20.21	165.57	52.65	1.46	-0.19	0.23	-6.86
SA	63.89	8.20	20.48	204.85	57.93	1.80	-0.14	0.16	-3.46
SG	61.30	7.94	19.38	180.40	52.15	1.60	-0.25	0.30	-6.04
SK	53.76	5.85	17.19	136.18	42.46	1.17	-0.05	0.06	-7.01
SL	55.73	6.16	16.99	145.77	49.59	1.27	-0.07	0.09	-6.88
SO	62.65	8.05	19.01	189.07	58.69	1.69	-0.31	0.33	-6.09
SY	63.42	8.34	19.11	196.58	54.08	1.75	-0.27	0.32	-5.08
SI	65.22	8.74	20.56	212.56	47.31	1.90	-0.19	0.25	-4.77
ST	49.18	5.52	19.01	114.65	36.59	0.98	0.01	-0.02	-9.15
WR	32.42	2.61	10.79	46.88	33.29	0.50	0.10	-0.06	-5.79
RV	37.60	3.36	13.73	77.21	52.53	0.61	0.06	-0.04	-8.89

APPENDIX G

Station	S.No	Lat	Long
NA	**1**	25° 26.426' N	66° 45.353' E
NS	**2**	25° 27.209' N	66° 44.607' E
ND	**3**	25° 26.650' N	66° 44.825' E
NE	**4**	25° 26.353' N	66° 44.744' E
NF	**5**	25° 26.223' N	66° 45.109' E
NG	**6**	25° 27.014' N	66° 44.177' E
NH	**7**	25° 26.554' N	66° 44.407' E
NI	**8**	25° 26.280' N	66° 45.660' E
KA	**9**	25° 20.149' N	66° 41.375' E
KF	**10**	25° 22.766' N	66° 40.612' E
KD	**11**	25° 23.117' N	66° 43.030' E
KU	**12**	25° 22.287' N	66° 42.468' E
KR	**13**	25° 22.155' N	66° 44.350' E
KP	**14**	25° 21.540' N	66° 42.480' E
KW	**15**	25° 21.780' N	66° 41.520' E
KV	**16**	25° 22.161' N	66° 41.245' E
KL	**17**	25° 21.900'N	66° 42.060' E
KQ	**18**	25° 21.660' N	66° 40.620' E
KE	**19**	25° 21.838' N	66° 40.347' E
KZ	**20**	25° 21.205' N	66° 40.705' E
KW	**21**	25° 22.330' N	66° 41.917' E
KM	**22**	25° 21.701' N	66° 41.198' E
KT	**23**	25° 21.198' N	66° 41.903' E
KO	**24**	25° 21.971' N	66° 42.558' E
AA	**25**	25° 23.851' N	66° 45.015' E
AL	**26**	25° 24.963' N	66° 45.541' E
AV	**27**	25° 25.130' N	66° 44.167' E
AM	**28**	25° 22.675' N	66° 39.730' E
BM	**29**	25° 21.600'N	66° 39.318' E
BT	**30**	25° 22.011' N	66° 39.890' E
DU	**31**	25° 24.962' N	66° 39.931' E
CY	**32**	25° 20.615' N	66° 40.884' E
CE	**33**	25° 23.520' N	66° 39.480' E
CK	**34**	25° 23.280' N	66° 39.720' E
PS	**35**	25° 24.120' N	66° 39.600' E
DF	**36**	25° 24.960' N	66° 39.960' E
UT	**37**	25° 27.240' N	66° 40.200' E
UL	**38**	25° 26.160' N	66° 39.600' E
UR	**39**	25° 25.380' N	66° 39.900' E
UG	**40**	25° 26.746' N	66° 40.187' E
UD	**41**	25° 26.040' N	66° 39.540' E
UP	**42**	25° 28.380' N	66° 40.465' E
RN	**43**	25° 26.150' N	66° 44.697' E
RK	**44**	25° 28.116' N	66° 43.167' E
RB	**45**	25° 25.480' N	66° 42.212' E
RX	**46**	25° 25.456' N	66° 41.750' E
RS	**47**	25° 25.137' N	66° 41.412' E

Station	S.No	Lat	Long
RP	**48**	25° 24.415'N	66° 40.406'E
RW	**49**	25° 24.900'N	66° 41.295'E
RJ	**50**	25° 25.252'N	66° 42.290'E
RL	**51**	25° 23.488'N	66° 41.042'E
RE	**52**	25° 24.063'N	66° 42.532'E
RH	**53**	25° 25.892'N	66° 43.657'E
BG	**54**	25° 26.220'N	66° 46.680'E
BN	**55**	25° 26.068'N	66° 46.043'E
BD	**56**	25° 25.202'N	66° 47.062'E
BR	**57**	25° 26.593'N	66° 47.705'E
CF	**58**	25° 25.962'N	66° 42.846'E
CD	**59**	25° 26.176'N	66° 42.694'E
CK	**60**	25° 27.285'N	66° 43.311'E
CM	**61**	25° 27.727'N	66° 41.311'E
CZ	**62**	25° 26.520'N	66° 41.660'E
CL	**63**	25° 26.515'N	66° 42.501'E
CP	**64**	25° 26.001'N	66° 42.772'E
CG	**65**	25° 26.611'N	66° 42.873'E
CT	**66**	25° 26.343'N	66° 43.640'E
CJ	**67**	25° 26.794'N	66° 42.213'E
CI	**68**	25° 26.833'N	66° 42.008'E
CS	**69**	25° 27.266'N	66° 42.019'E
CQ	**70**	25° 27.446'N	66° 42.047'E
CR	**71**	25° 27.413'N	66° 42.625'E
CA	**72**	25° 27.050'N	66° 42.839'E
CN	**73**	25° 26.698'N	66° 43.229'E
CV	**74**	25° 27.601'N	66° 43.727'E
CX	**75**	25° 27.336'N	66° 42.012'E
CE	**76**	25° 28.304'N	66° 41.697'E
CB	**77**	25° 28.008'N	66° 40.907'E
CW	**78**	25° 25.879'N	66° 41.312'E
UI	**79**	25° 26.031'N	66° 38.491'E
UR	**80**	25° 24.840'N	66° 38.820'E
US	**81**	25° 25.521'N	66° 38.786'E
UG	**82**	25° 24.991'N	66° 38.486'E
UN	**83**	25° 25.329'N	66° 38.372'E
SF	**84**	25° 27.479'N	66° 40.645'E
SA	**85**	25° 25.740'N	66° 40.200'E
SG	**86**	25° 26.520'N	66° 40.680'E
SK	**87**	25° 27.138'N	66° 41.281'E
SL	**88**	25° 26.677'N	66° 41.684'E
SO	**89**	25° 26.640'N	66° 40.680'E
SY	**90**	25° 25.117'N	66° 40.727'E
SI	**91**	25° 25.292'N	66° 40.476'E
ST	**92**	25° 26.098'N	66° 40.475'E
WR	**93**	25° 26.900'N	66° 50.742'E
RV	**94**	25° 26.998'N	66° 50.793'E